FLUENT 6.3 Validation Guide

September 2006

Copyright © 2006 by Fluent Inc.
All Rights Reserved. No part of this document may be reproduced or otherwise used in any form without express written permission from Fluent Inc.

Airpak, FIDAP, FLUENT, FLUENT for CATIA V5, FloWizard, GAMBIT, Icemax, Icepak, Icepro, Icewave, Icechip, MixSim, and POLYFLOW are registered trademarks of Fluent Inc. All other products or name brands are trademarks of their respective holders.

CHEMKIN is a registered trademark of Reaction Design Inc.

Portions of this program include material copyrighted by PathScale Corporation 2003-2004.

Fluent Inc.
Centerra Resource Park
10 Cavendish Court
Lebanon, NH 03766

Contents

Introduction **Introduction-1**

1 Flow in a Rotating Cavity **1-1**

1.1 Purpose 1-1

1.2 Problem Description 1-1

1.3 References 1-1

1.4 Results 1-3

1.4.1 Validation-Specific Information 1-3

1.4.2 Plot Data 1-4

2 Natural Convection in an Annulus **2-1**

2.1 Purpose 2-1

2.2 Problem Description 2-1

2.3 References 2-2

2.4 Results 2-2

2.4.1 Validation-Specific Information 2-3

2.4.2 Plot Data 2-4

3 Flow in a 90° Planar Tee-Junction **3-1**

3.1 Purpose 3-1

3.2 Problem Description 3-1

3.3 References 3-1

3.4 Results 3-3

3.4.1 Validation-Specific Information 3-3

3.4.2 Plot Data 3-4

© Fluent Inc. August 8, 2006

4 Flows in Driven Cavities **4-1**

4.1 Purpose 4-1

4.2 Problem Description 4-1

4.3 References 4-1

4.4 Results 4-1

4.4.1 Trapezoidal Cavity 4-1

4.4.2 Triangular Cavity 4-1

4.4.3 Validation-Specific Information 4-3

4.4.4 Plot Data 4-4

5 Periodic Flow in a Wavy Channel **5-1**

5.1 Purpose 5-1

5.2 Problem Description 5-1

5.3 References 5-1

5.4 Results 5-2

5.4.1 Validation-Specific Information 5-2

5.4.2 Plot Data 5-3

6 Heat Transfer in a Pipe Expansion **6-1**

6.1 Purpose 6-1

6.2 Problem Description 6-1

6.3 References 6-2

6.4 Results 6-2

6.4.1 Validation-Specific Information 6-3

6.4.2 Plot Data 6-4

© Fluent Inc. August 8, 2006

7 Propane Jet in a Coaxial Air Flow **7-1**

7.1 Purpose 7-1

7.2 Problem Description 7-1

7.3 References 7-1

7.4 Results 7-3

7.4.1 Validation-Specific Information 7-3

7.4.2 Plot Data 7-4

8 Non-Premixed Hydrogen/Air Flame **8-1**

8.1 Purpose 8-1

8.2 Problem Description 8-1

8.3 References 8-2

8.4 Results 8-2

8.4.1 Validation-Specific Information 8-2

8.4.2 Plot Data 8-3

9 Flow through an Engine Inlet Valve **9-1**

9.1 Purpose 9-1

9.2 Problem Description 9-1

9.3 References 9-2

9.4 Results 9-2

9.4.1 Validation-Specific Information 9-2

9.4.2 Plot Data 9-3

© Fluent Inc. August 8, 2006

10 Turbulent Flow in a Transition Duct **10-1**

10.1 Purpose 10-1

10.2 Problem Description 10-1

10.3 References 10-1

10.4 Results 10-3

10.4.1 Validation-Specific Information 10-3

10.4.2 Plot Data 10-4

11 Transonic Flow Over an RAE 2822 Airfoil **11-1**

11.1 Purpose 11-1

11.2 Problem Description 11-1

11.3 References 11-3

11.4 Results 11-3

11.4.1 Validation-Specific Information 11-4

11.4.2 Plot Data 11-5

12 Mid-Span Flow Over a Goldman Stator Blade **12-1**

12.1 Purpose 12-1

12.2 Problem Description 12-1

12.3 References 12-1

12.4 Results 12-3

12.4.1 Validation-Specific Information 12-3

12.4.2 Plot Data 12-4

© Fluent Inc. August 8, 2006

13 Compressible Turbulent Mixing Layer **13-1**

13.1 Purpose 13-1

13.2 Problem Description 13-1

13.3 References 13-2

13.4 Results 13-2

13.4.1 Validation-Specific Information 13-2

13.4.2 Plot Data 13-3

14 Reflecting Shock Waves **14-1**

14.1 Purpose 14-1

14.2 Problem Description 14-1

14.3 References 14-2

14.4 Results 14-2

14.4.1 Validation-Specific Information 14-3

14.4.2 Plot Data 14-3

15 Turbulent Bubbly Flows **15-1**

15.1 Purpose 15-1

15.2 Problem Description 15-1

15.3 References 15-2

15.4 Results 15-2

15.4.1 Validation-Specific Information 15-2

15.4.2 Plot Data 15-3

© Fluent Inc. August 8, 2006

16 Adiabatic Compression and Expansion Inside an Idealized 2D In-Cylinder Engine **16-1**

16.1 Purpose 16-1

16.2 Problem Description 16-1

16.3 Results 16-2

16.3.1 Validation-Specific Information 16-3

16.3.2 Plot Data 16-3

17 Cavitation Over a Sharp-Edged Orifice **17-1**

17.1 Purpose 17-1

17.2 Problem Description 17-1

17.3 References 17-2

17.4 Results 17-2

17.4.1 Validation-Specific Information 17-2

17.4.2 Plot Data 17-3

18 Oscillating Laminar Flow Around a Circular Cylinder **18-1**

18.1 Purpose 18-1

18.2 Problem Description 18-1

18.3 References 18-2

18.4 Results 18-2

18.4.1 Validation-Specific Information 18-3

18.4.2 Plot Data 18-4

© Fluent Inc. August 8, 2006

19 Rotation of Two Immiscible Liquids **19-1**

19.1 Purpose 19-1

19.2 Problem Description 19-1

19.3 References 19-1

19.4 Results 19-3

19.4.1 Validation-Specific Information 19-3

19.4.2 Plot Data 19-4

20 Polyhedral and Tetrahedral Mesh Accuracy **20-1**

20.1 Purpose 20-1

20.2 Problem Description 20-1

20.3 References 20-1

20.4 Results 20-1

20.4.1 Validation-Specific Information 20-2

20.4.2 Plot Data 20-3

© Fluent Inc. August 8, 2006

© Fluent Inc. August 8, 2006

Introduction

The Contents of This Manual

The FLUENT Validation Manual contains a number of validations that compare the results obtained with FLUENT against experimental data.

Each Validation is organized to present the purpose of the validation, the problem description, references, and results.

Where to Find the Solution Files for the Validations

Solution files are listed in the Validation-Specific Information section for each validation. These solution files can be used to determine the details of solution settings used for the validation.

Solution files for the validations are available for download from the Fluent Inc. User Services Center (`www.fluentusers.com`). Click on the Documentation link on the FLUENT product page, then on the Validation Solution Files link on the documentation page, and select the file to download. Unzip the file in a working directory and the solution files will be available to read into FLUENT.

© Fluent Inc. August 8, 2006

Validation 1. Flow in a Rotating Cavity

1.1 Purpose

The purpose of this validation is to compare numerical values of swirl and radial velocity in a rotating cavity with experimental data [1,2].

1.2 Problem Description

An enclosed cylindrical cavity of height $L = 1.0$ m and radius $R = 1.0$ m has a lid that spins at $\Omega = 1.0$ rad/s, as shown in Figure 1.2.1. The flow field is 2D axisymmetric, so only the region bounded by the dashed lines in Figure 1.2.1 needs to be modeled. The Reynolds number of the flow based on the cavity radius R and the tip-speed of the disk (ΩR) is 1800. The flow within the cavity is assumed to be laminar. The problem can be solved using either a stationary reference frame or a rotating reference frame. The second-order discretization scheme is chosen because the flow in the cavity is not aligned with the grid (it crosses the grid lines obliquely), and this scheme leads to more accurate results in these cases.

1.3 References

1. Sorensen, J.N. and Loc, T.P., Higher-Order Axisymmetric Navier-Stokes Code: Description and Evolution of Boundary Conditions, *International Journal For Numerical Methods in Fluids*, 9:1517–1537, 1989.

2. Michelsen, J. A., *Modeling of Laminar Incompressible Rotating Fluid Flow*, AFM 86-05, Ph.D. thesis, Department of Fluid Mechanics, Technical University of Denmark, 1986.

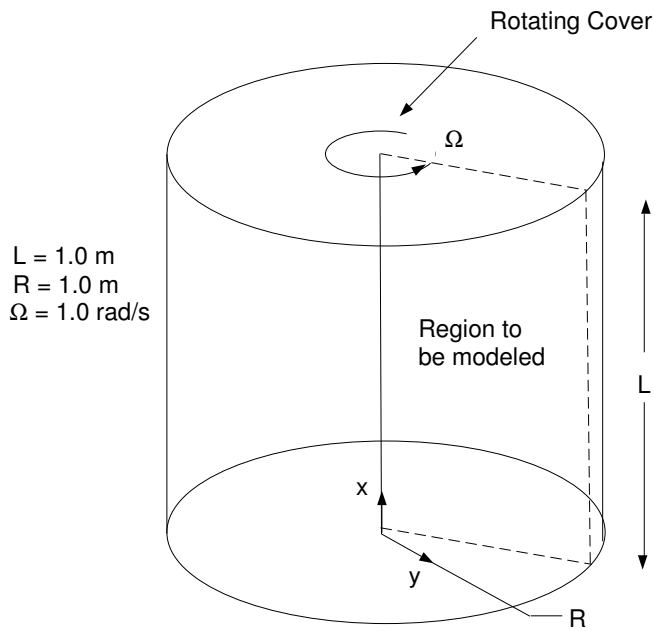

Figure 1.2.1: Problem Description

© Fluent Inc. August 8, 2006

1.4 Results

Figures 1.4.1 - 1.4.4 compare the computed swirl and radial velocity profiles with measured data at $y = 0.6$ m (for both the stationary and the rotating reference frame). Figures 1.4.5 - 1.4.8 compare the computed and measured velocities at $y = 0.9$ m. The computed velocities in the rotating frame were transformed to the stationary reference frame of the measured data. The results obtained with FLUENT match the measured velocity profiles and reproduce accurately the sharp gradients in swirl and radial velocity in the region of $x = 0.9$ m. The results show that the second-order discretization scheme produces good agreement with the data using a 41×41 non-uniform grid.

1.4.1 Validation-Specific Information

Solver:	FLUENT 2d, 2ddp
Version:	6.3.11
Solution Files:	1. `rotcv_r1.cas`, `rotcv_r1.dat`
	2. `rotcv_r2.cas`, `rotcv_r2.dat`

These solution files are available from the Fluent Inc. User Services Center as described in the Introduction.

1.4.2 Plot Data

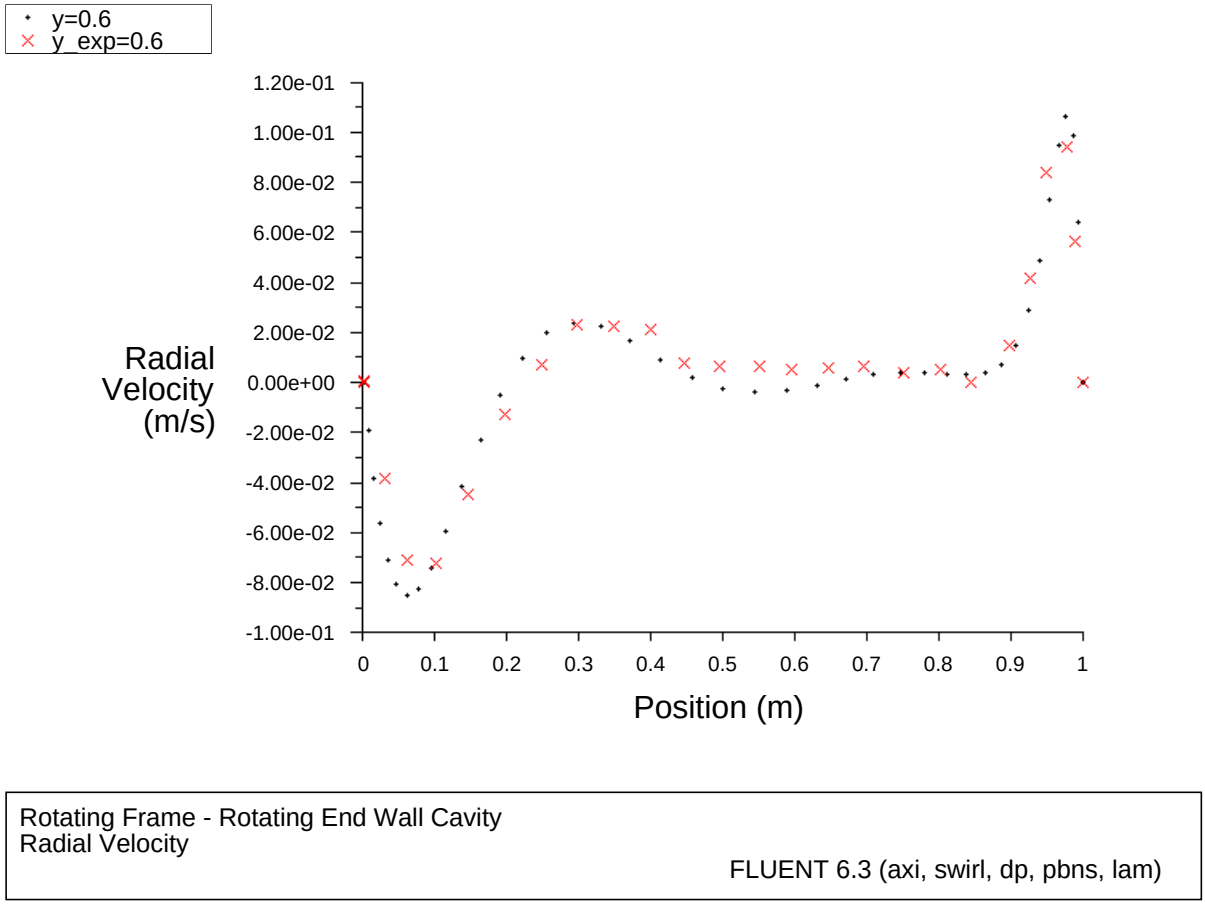

Figure 1.4.1: Comparison of Computed Radial Velocity Profile with Measured Data at $y = 0.6$ m (Rotating Reference Frame)

© Fluent Inc. August 8, 2006

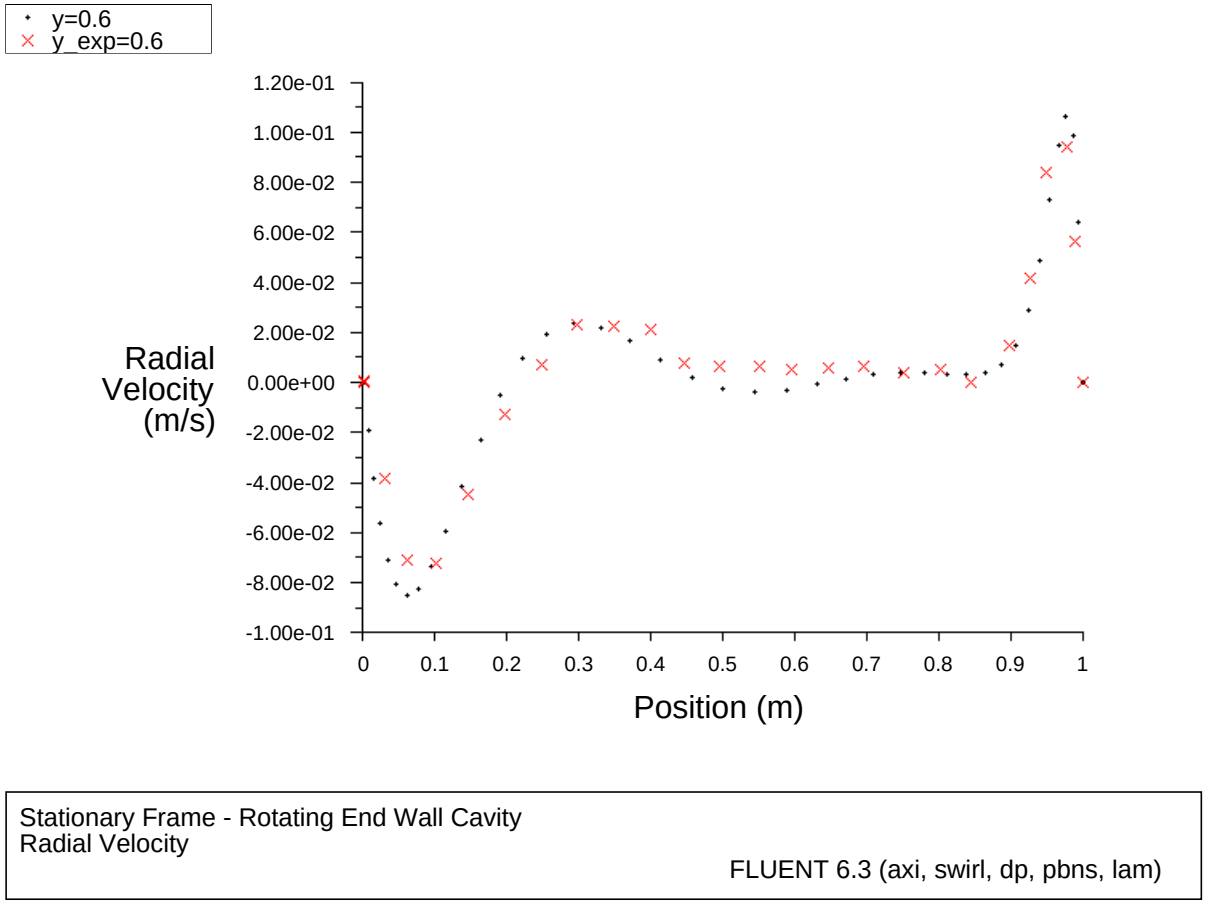

Figure 1.4.2: Comparison of Computed Radial Velocity Profile with Measured Data at $y = 0.6$ m (Stationary Reference Frame)

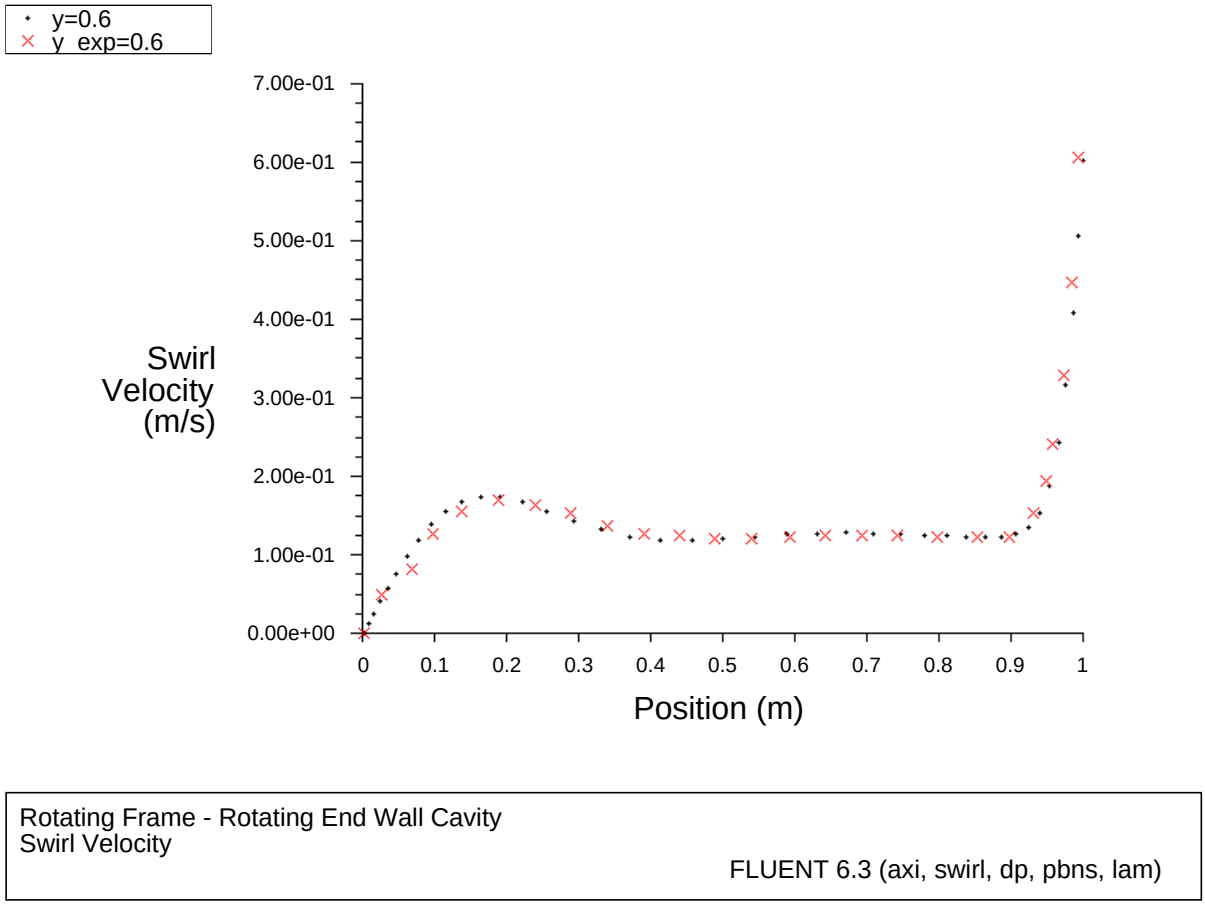

Figure 1.4.3: Comparison of Computed Swirl Velocity Profile with Measured Data at $y = 0.6$ m (Rotating Reference Frame)

© Fluent Inc. August 8, 2006

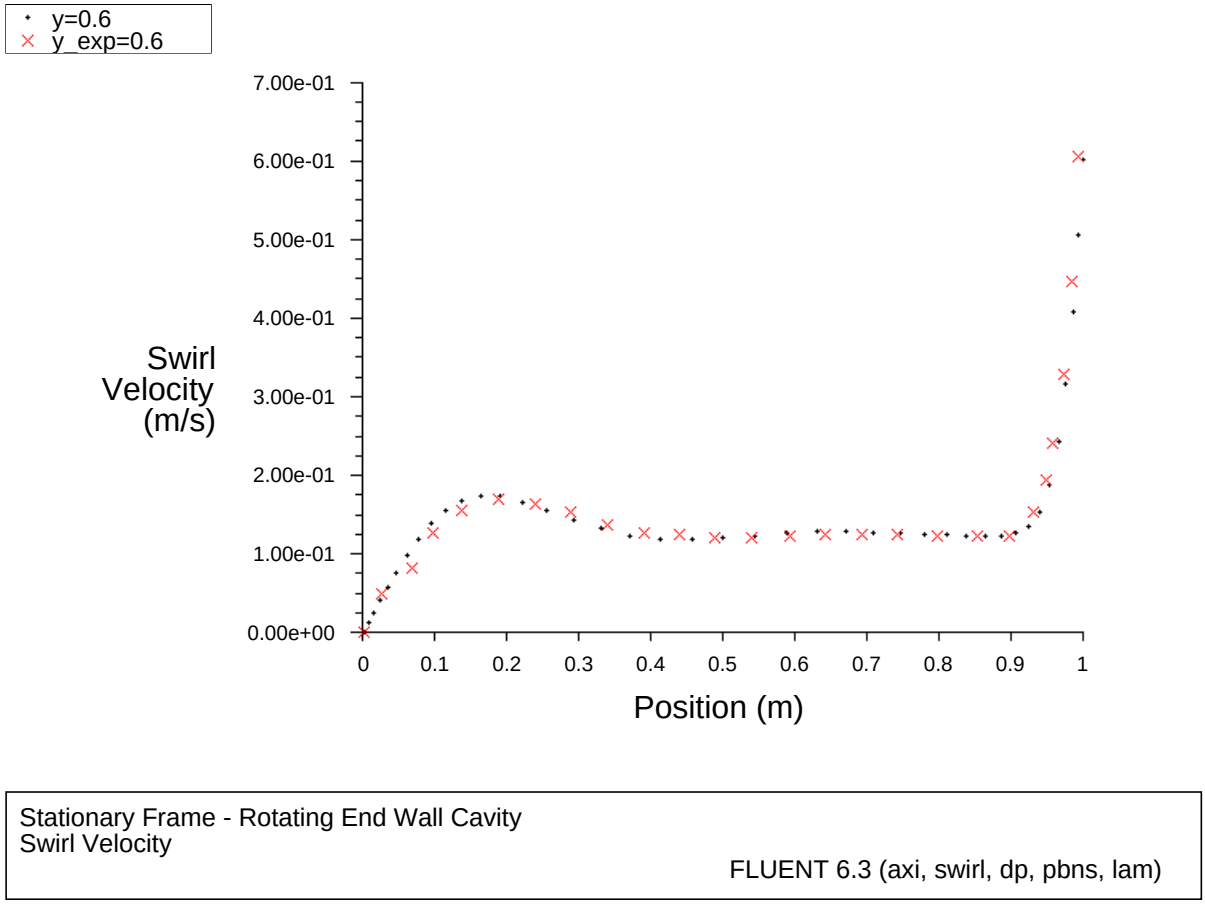

Figure 1.4.4: Comparison of Computed Swirl Velocity Profile with Measured Data at $y = 0.6$ m (Stationary Reference Frame)

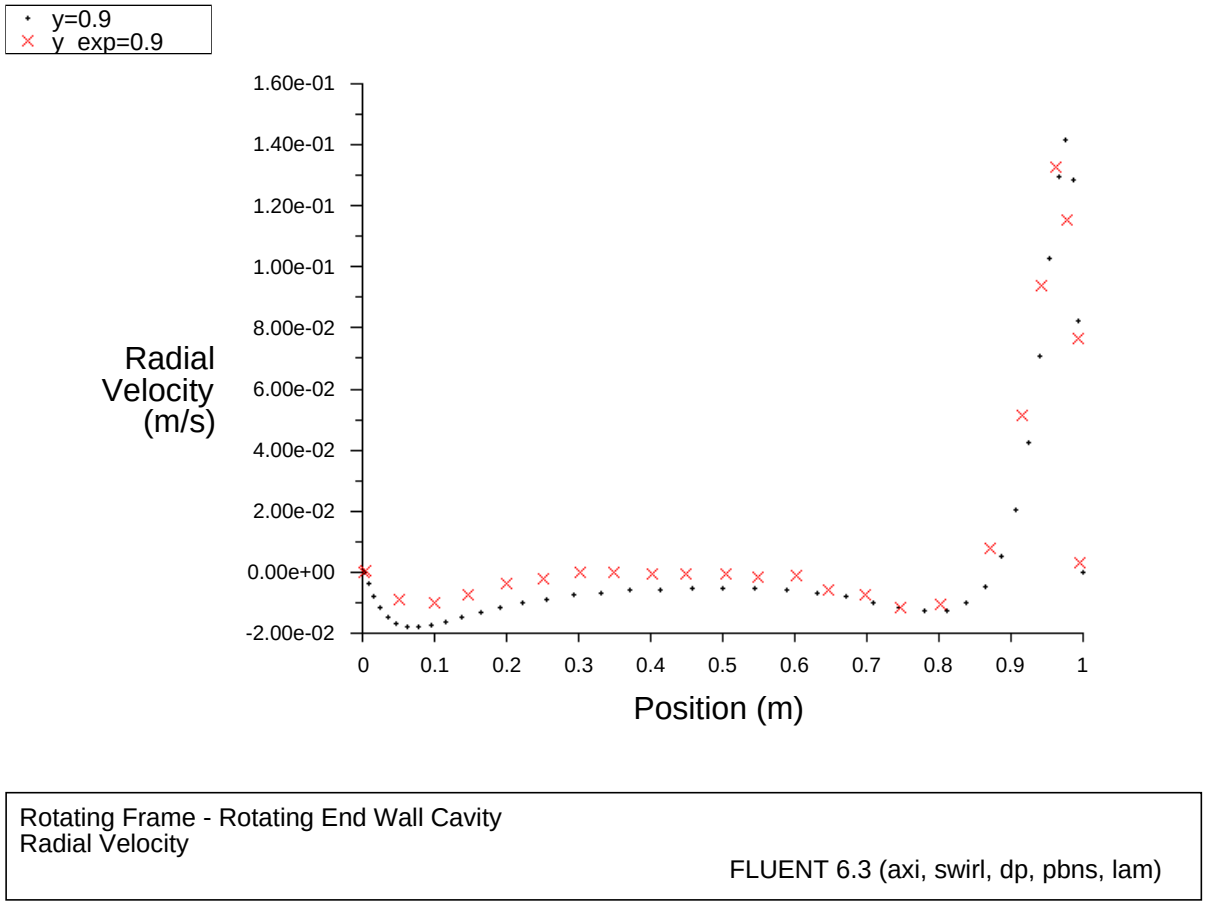

Figure 1.4.5: Comparison of Computed Radial Velocity Profile with Measured Data at $y = 0.9$ m (Rotating Reference Frame)

© Fluent Inc. August 8, 2006

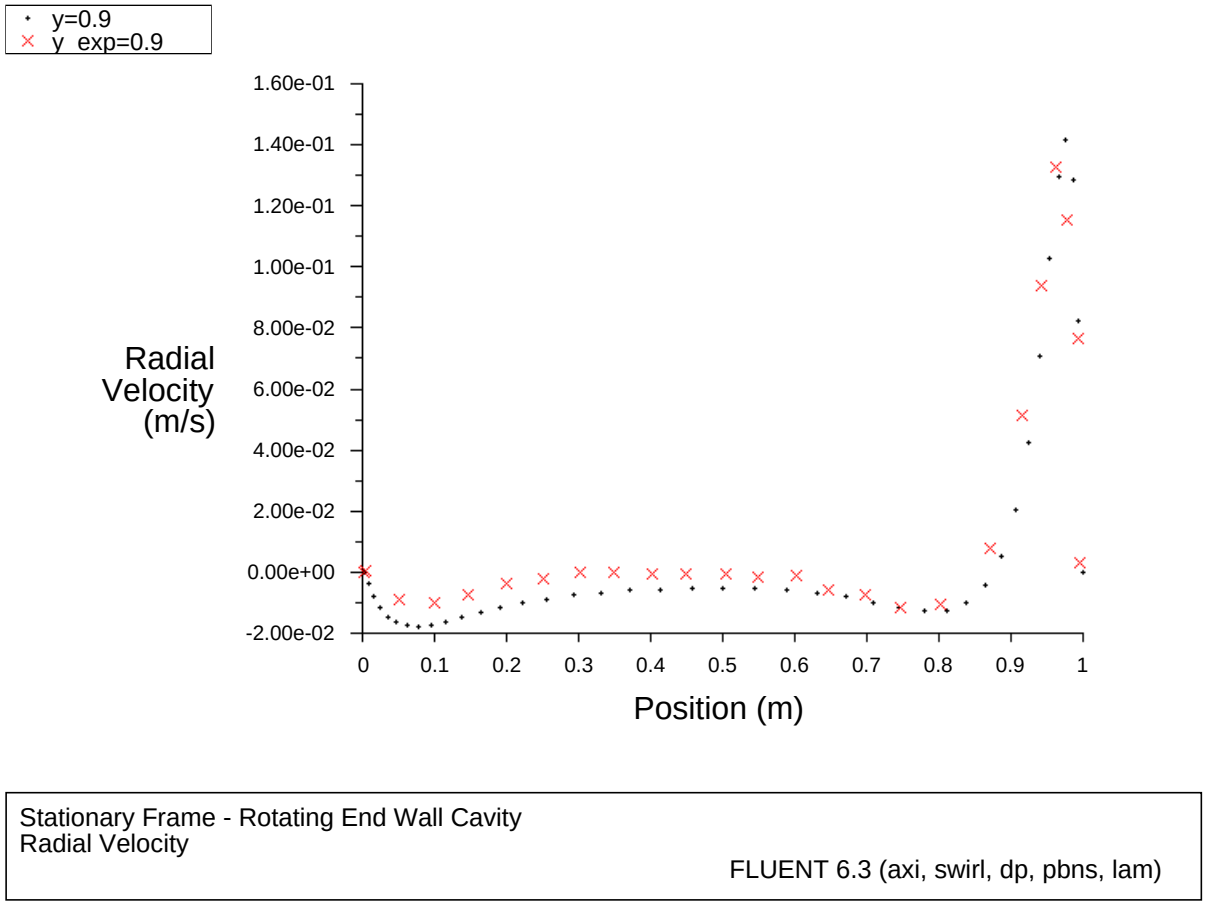

Figure 1.4.6: Comparison of Computed Radial Velocity Profile with Measured Data at $y = 0.9$ m (Stationary Reference Frame)

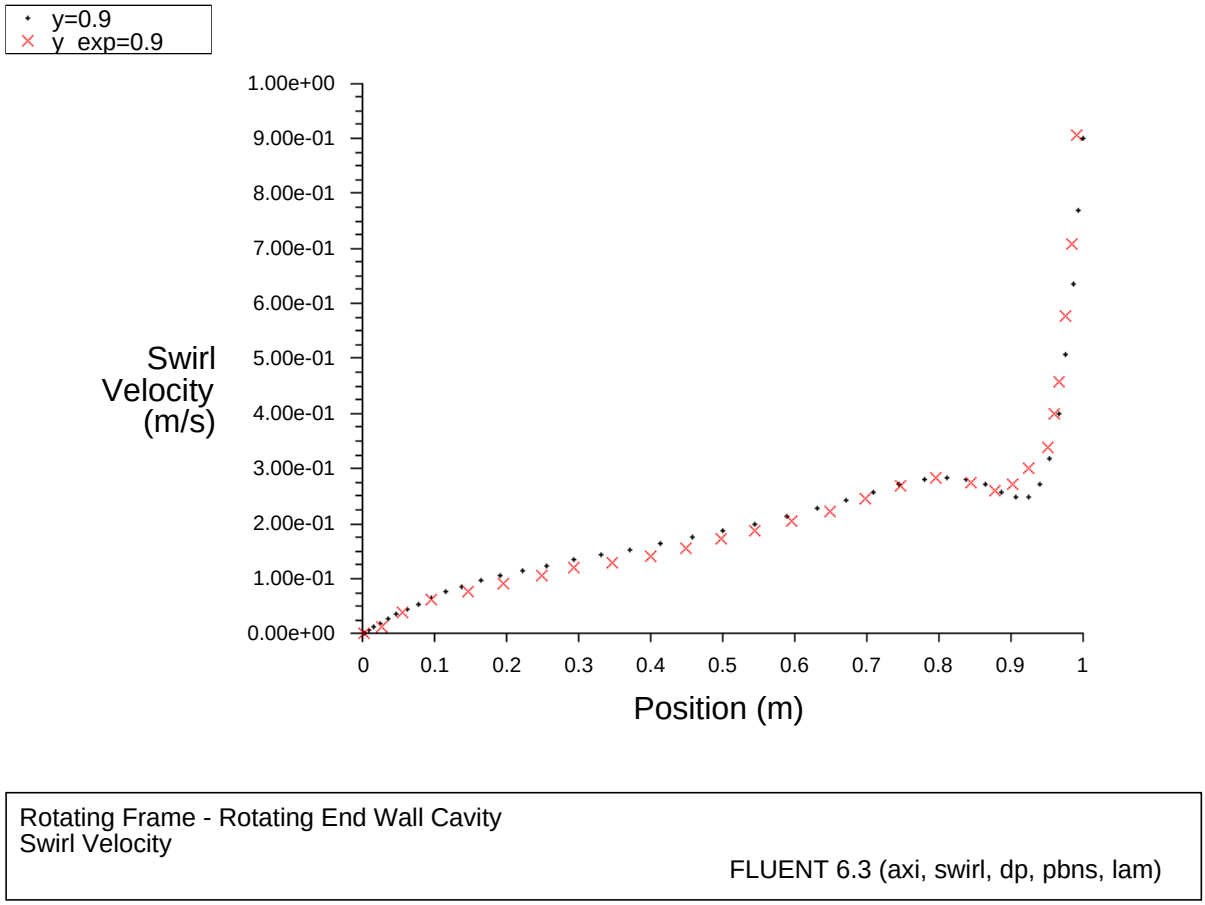

Figure 1.4.7: Comparison of Computed Swirl Velocity Profile with Measured Data at $y = 0.9$ m (Rotating Reference Frame)

© Fluent Inc. August 8, 2006

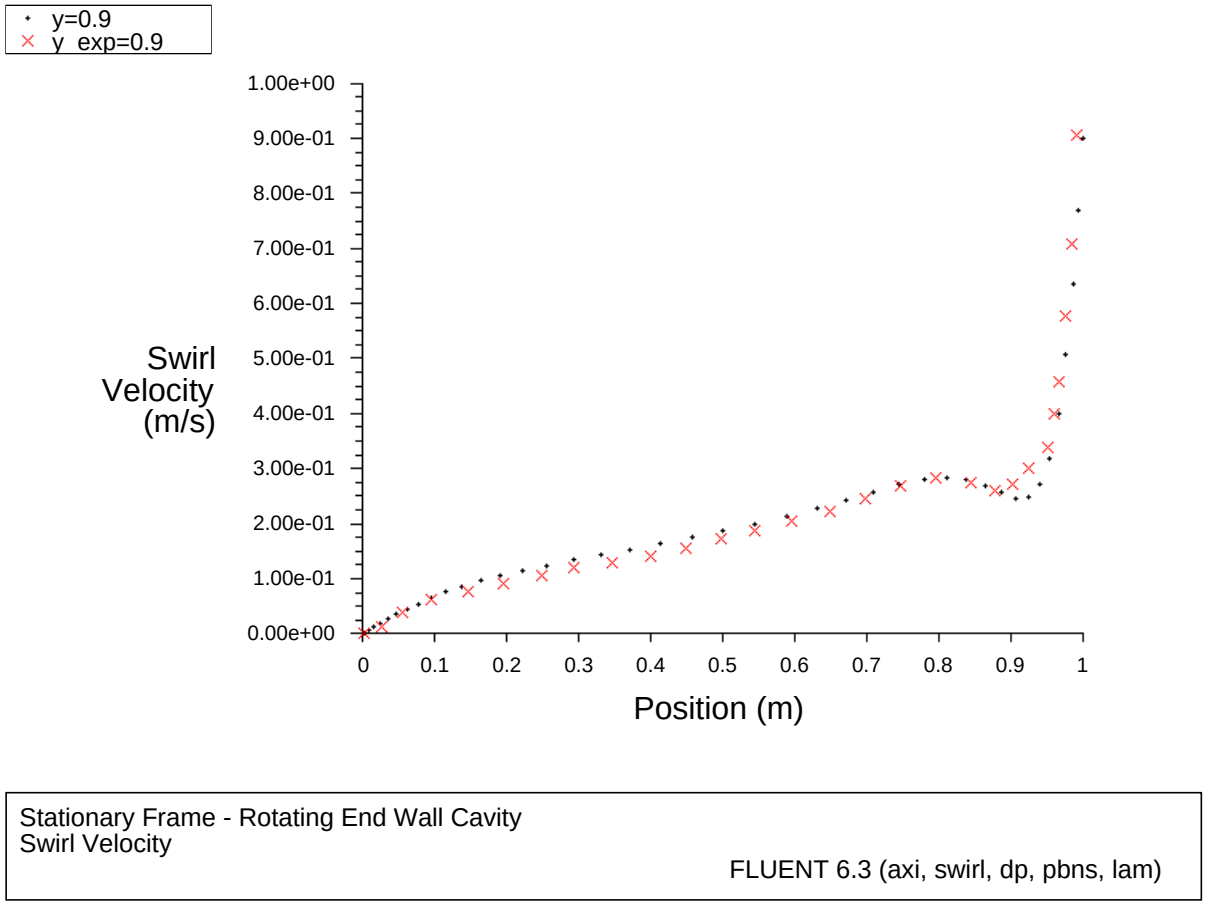

Figure 1.4.8: Comparison of Computed Swirl Velocity Profile with Measured Data at $y = 0.9$ m (Stationary Reference Frame)

© Fluent Inc. August 8, 2006

Validation 2. Natural Convection in an Annulus

2.1 Purpose

The purpose of this test is to compare the numerical prediction of temperature profiles along the symmetry lines with the experimental results of Kuehn and Goldstein [1,2] for the eccentric and concentric case. The test also compares the numerically predicted heat flux from the surface of the inner and outer cylinders for the eccentric and concentric cases with the experimental results.

2.2 Problem Description

A heated cylinder is placed inside another cylinder, trapping air in the resulting annular cavity. The inner cylinder is placed in two configurations, one in which the cylinders are concentric and the other in which the inner cylinder is displaced downwards. As the inner cylinder is hotter than the outer, a buoyancy-induced flow results and natural convection occurs. Only half of the domain needs to be modeled from symmetry considerations. The geometry of the problem is shown in Figure 2.2.1.

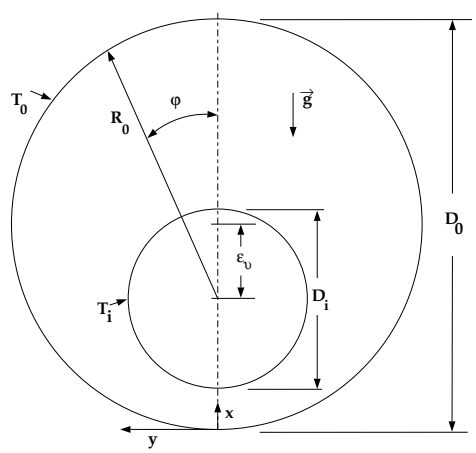

Figure 2.2.1: Problem Description

The radii of the outer and inner cylinders, respectively, are 46.3 mm and 17.8 mm. For the eccentric annulus case the eccentricity is $\epsilon = -0.6245$, which is very close to the value of -0.623 reported in the experiment. The eccentricity is the measure of the distance the inner cylinder is moved from the concentric position and is defined as

$$\epsilon = \epsilon_v / L \tag{2.2-1}$$

where

ϵ_v	=	the distance along the vertical axis the inner cylinder is moved from the concentric position (negative downwards)
	=	-17.8 mm
L	=	$\frac{D_o - D_i}{2}$
	=	28.5 mm
D_o	=	the diameter of the outer cylinder
	=	92.6 mm
D_i	=	the diameter of the inner cylinder
	=	35.6 mm

2.3 References

1. Kuehn, T.H. and Goldstein, R.J., An Experimental Study of Natural Convection Heat Transfer in Concentric and Eccentric Horizontal Cylindrical Annuli, *Journal of Heat Transfer*, 100:635–640, 1978.

2. Kuehn, T.H. and Goldstein, R.J., An Experimental and Theoretical Study of Natural Convection in the Annulus Between Horizontal Concentric Cylinders, *Journal of Fluid Mechanics*, 74:695–719, 1976.

2.4 Results

The temperature profiles along the symmetry lines for the eccentric and concentric cases are compared to the experimental data of Kuehn and Goldstein [1,2]. The agreement between the FLUENT predictions and the experimental data is very good.

The heat flux from the inner and outer cylinder surfaces for the eccentric and concentric cases is compared with the experimental data. FLUENT predictions of heat flux agree well with the benchmark experimental results, except for the outer wall heat flux prediction of the eccentric annulus. The relatively high grid skewness near the outer wall could be a possible reason for this marked deviation from the experimental data.

© Fluent Inc. August 8, 2006

2.4.1 Validation-Specific Information

Solver:	FLUENT 2d
Version:	6.3.11
Solution Files:	1. `concn_r1.cas`, `concn_r1.dat`
	2. `ecc_r2.cas`, `ecc_r2.dat`

These solution files are available from the Fluent Inc. User Services Center as described in the Introduction.

2.4.2 Plot Data

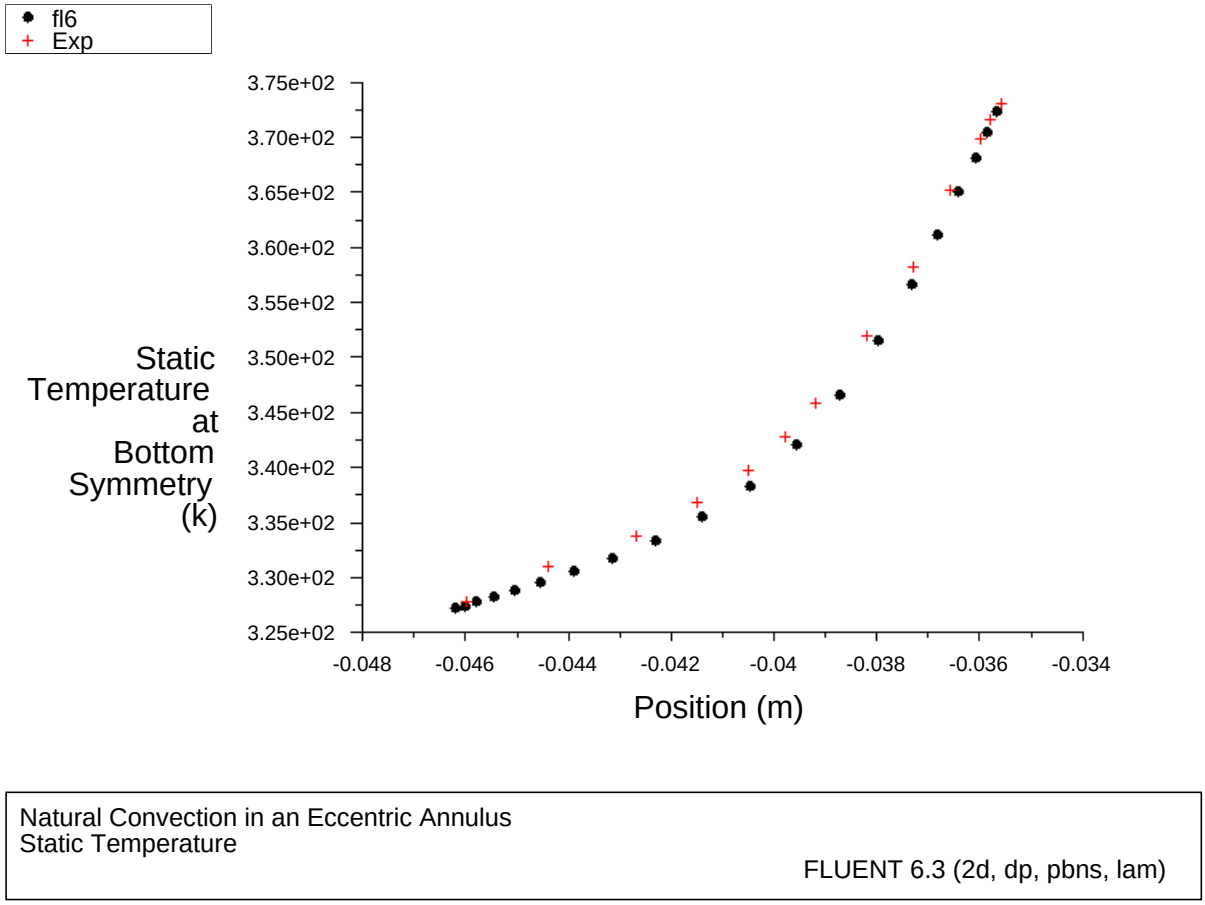

Figure 2.4.1: Temperature Profile Along the Bottom Symmetry Line for the Eccentric Case

© Fluent Inc. August 8, 2006

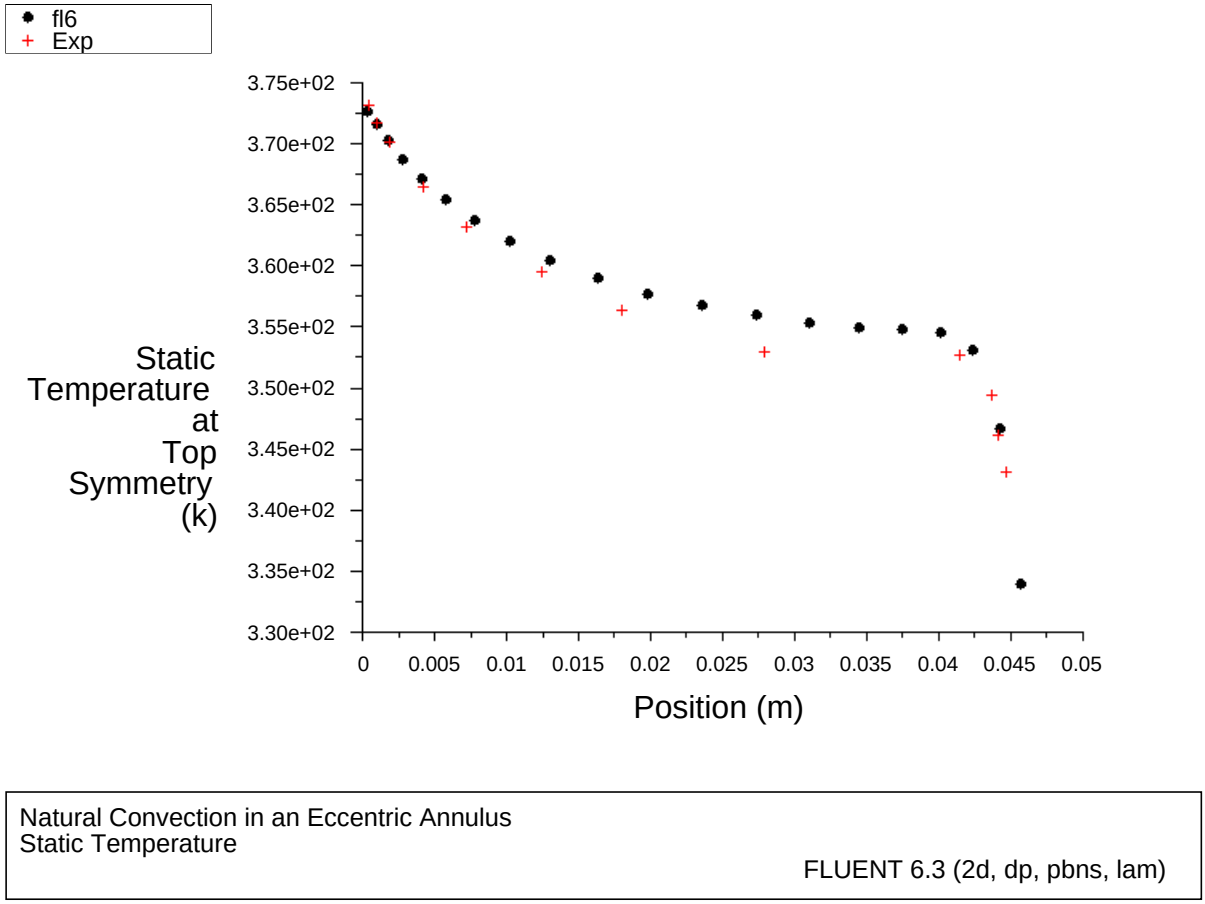

Figure 2.4.2: Temperature Profile Along the Top Symmetry Line for the Eccentric Case

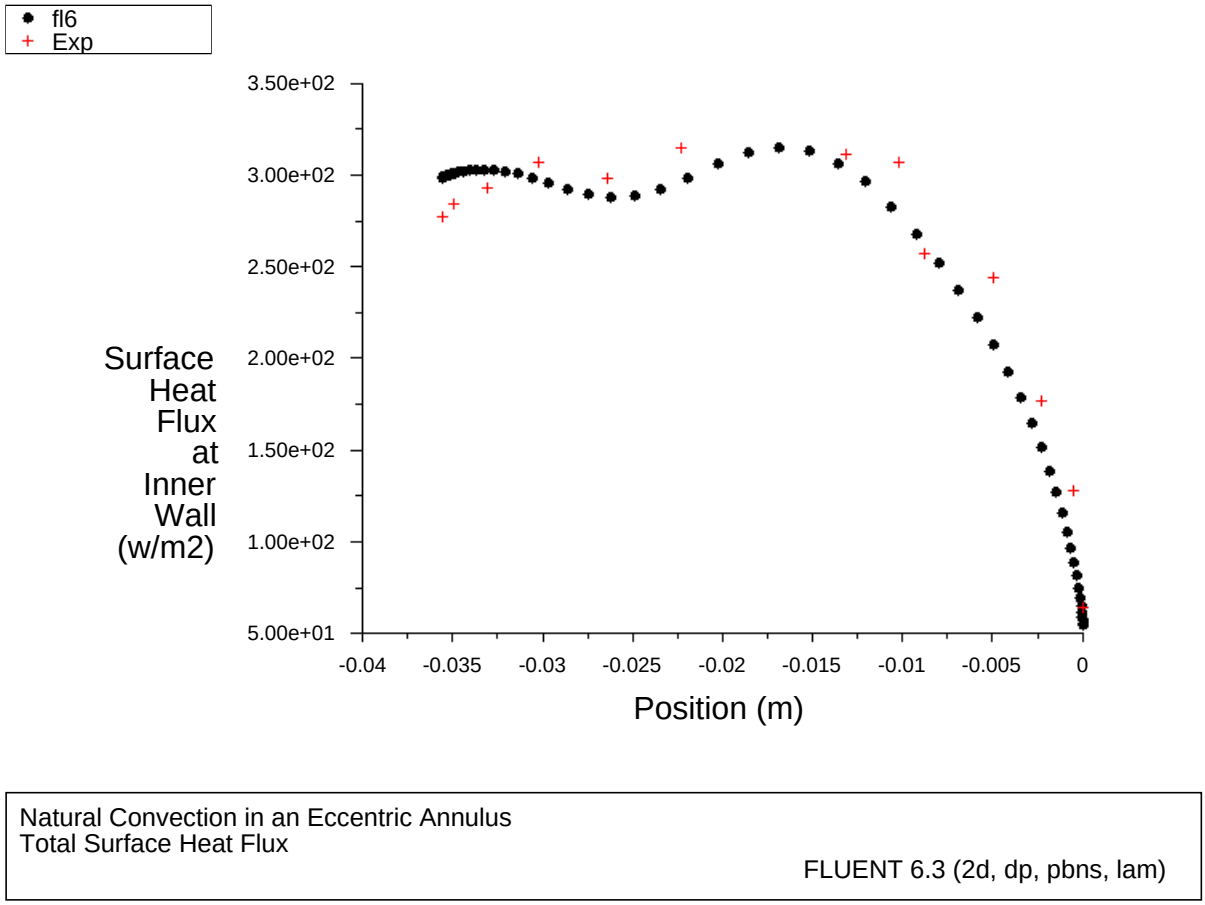

Figure 2.4.3: Comparison of Heat Flux from the Inner Cylinder Surface for the Eccentric Case

© Fluent Inc. August 8, 2006

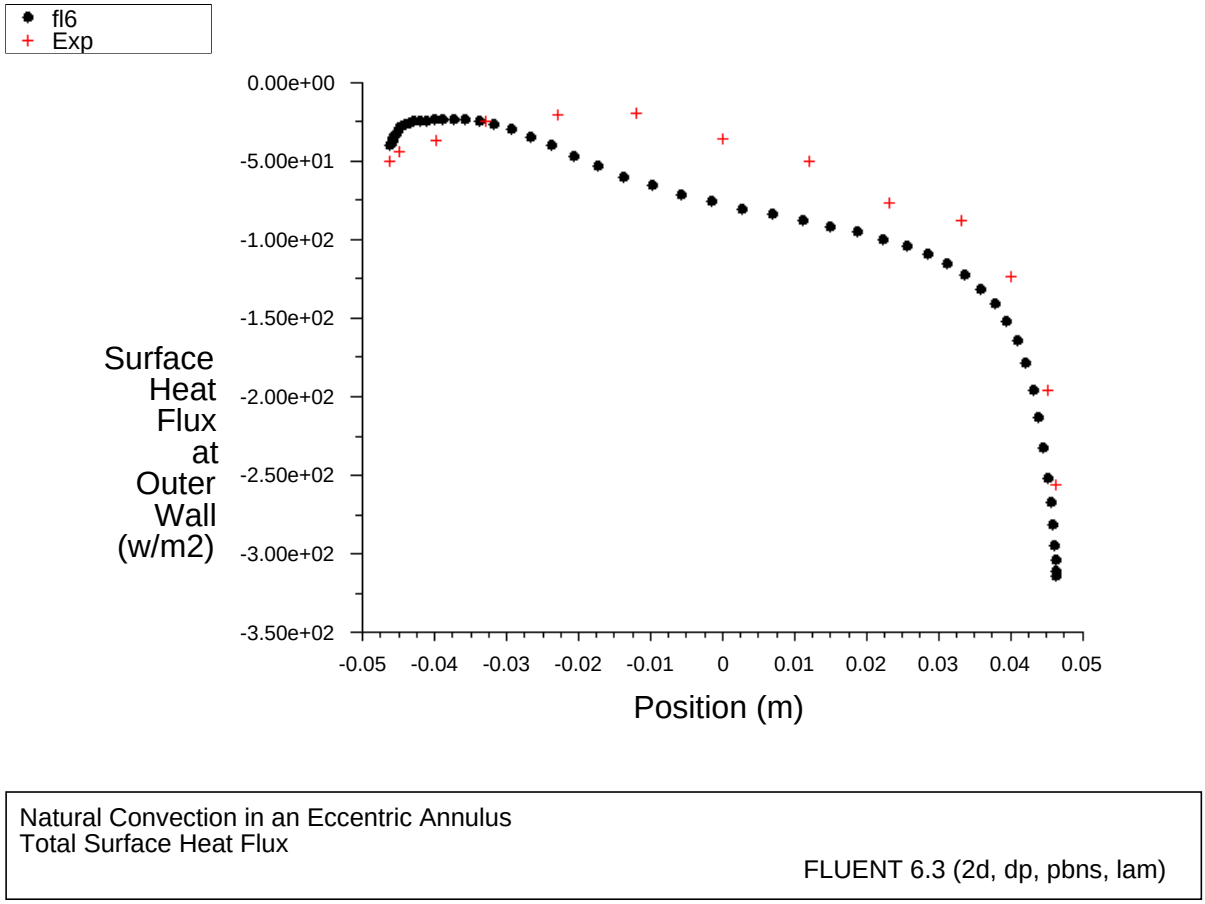

Figure 2.4.4: Comparison of Heat Flux from the Outer Cylinder Surface for the Eccentric Case

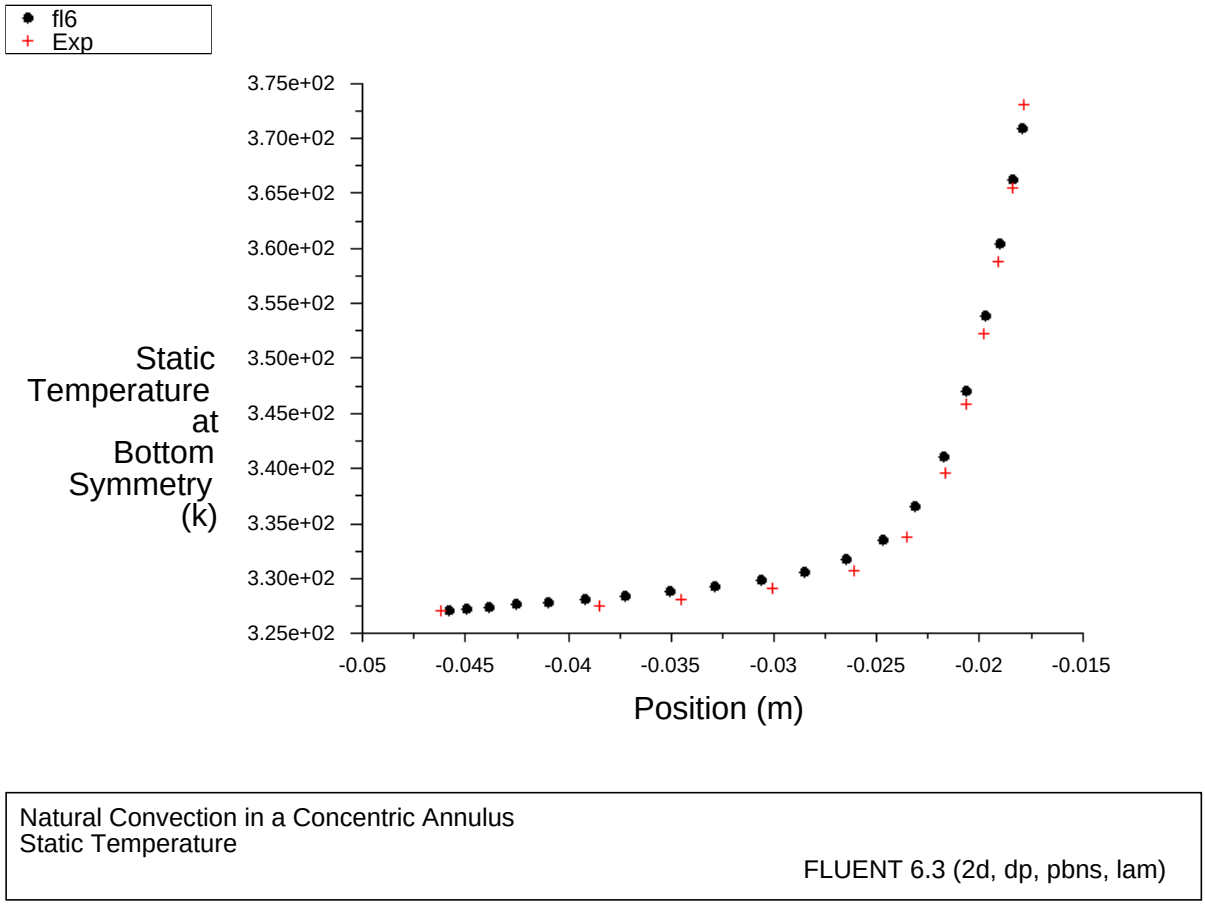

Figure 2.4.5: Temperature Profile Along the Bottom Symmetry Line for the Concentric Case

© Fluent Inc. August 8, 2006

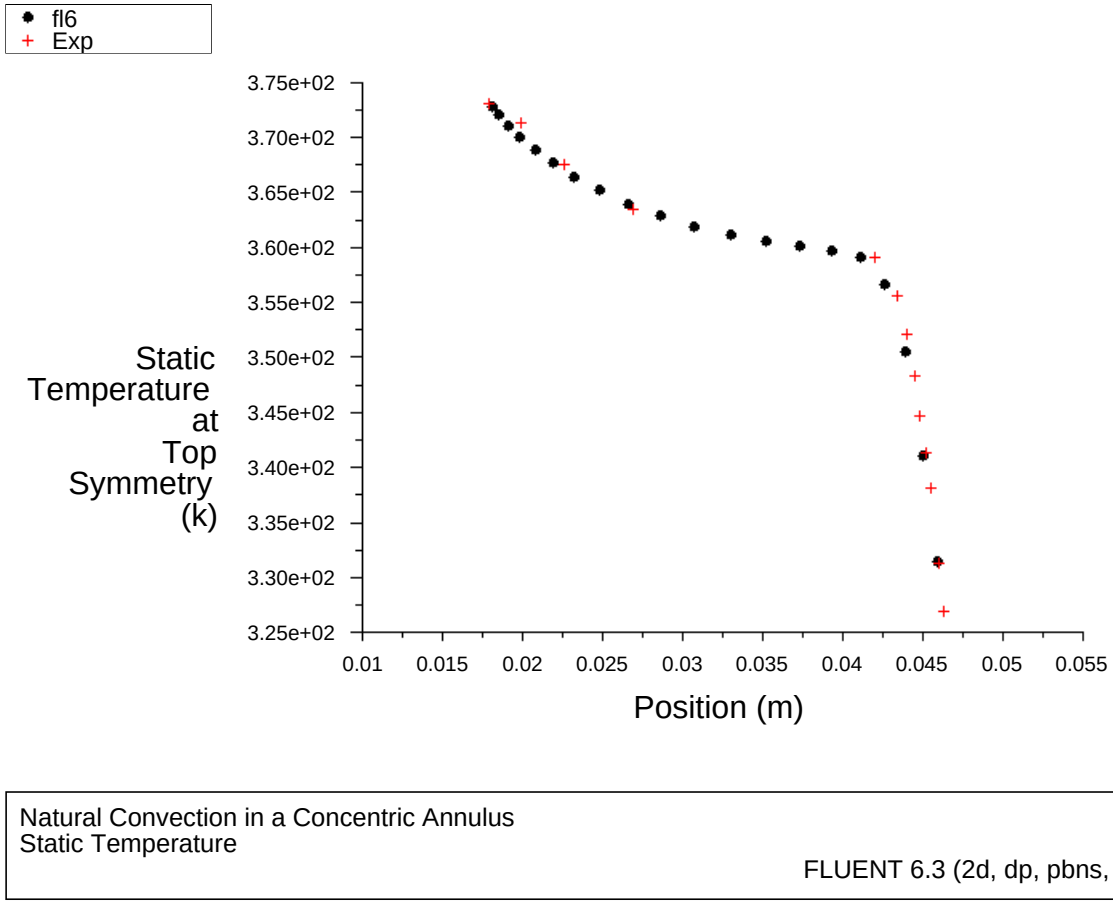

Figure 2.4.6: Temperature Profile Along the Top Symmetry Line for the Concentric Case

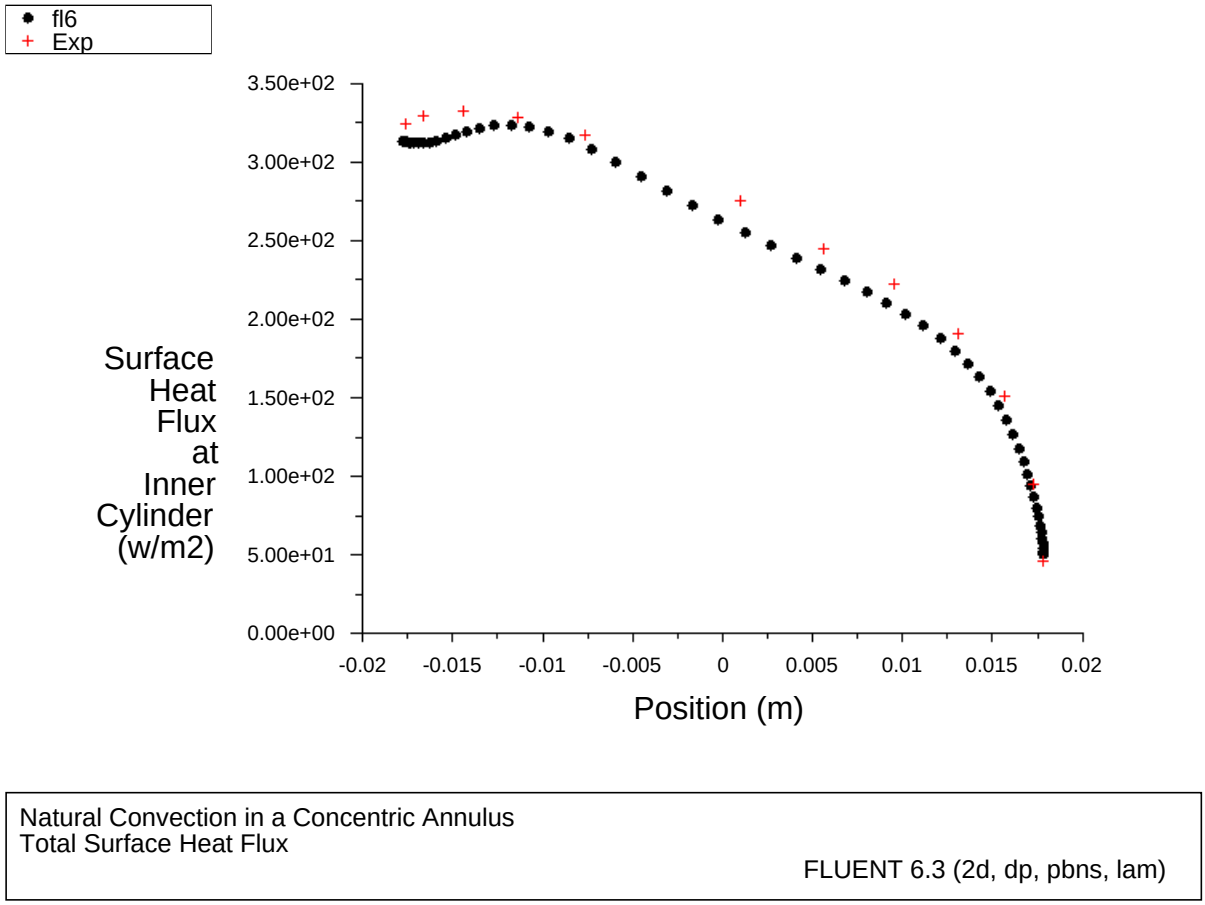

Figure 2.4.7: Comparison of Heat Flux from the Inner Cylinder Surface for the Concentric Case

© Fluent Inc. August 8, 2006

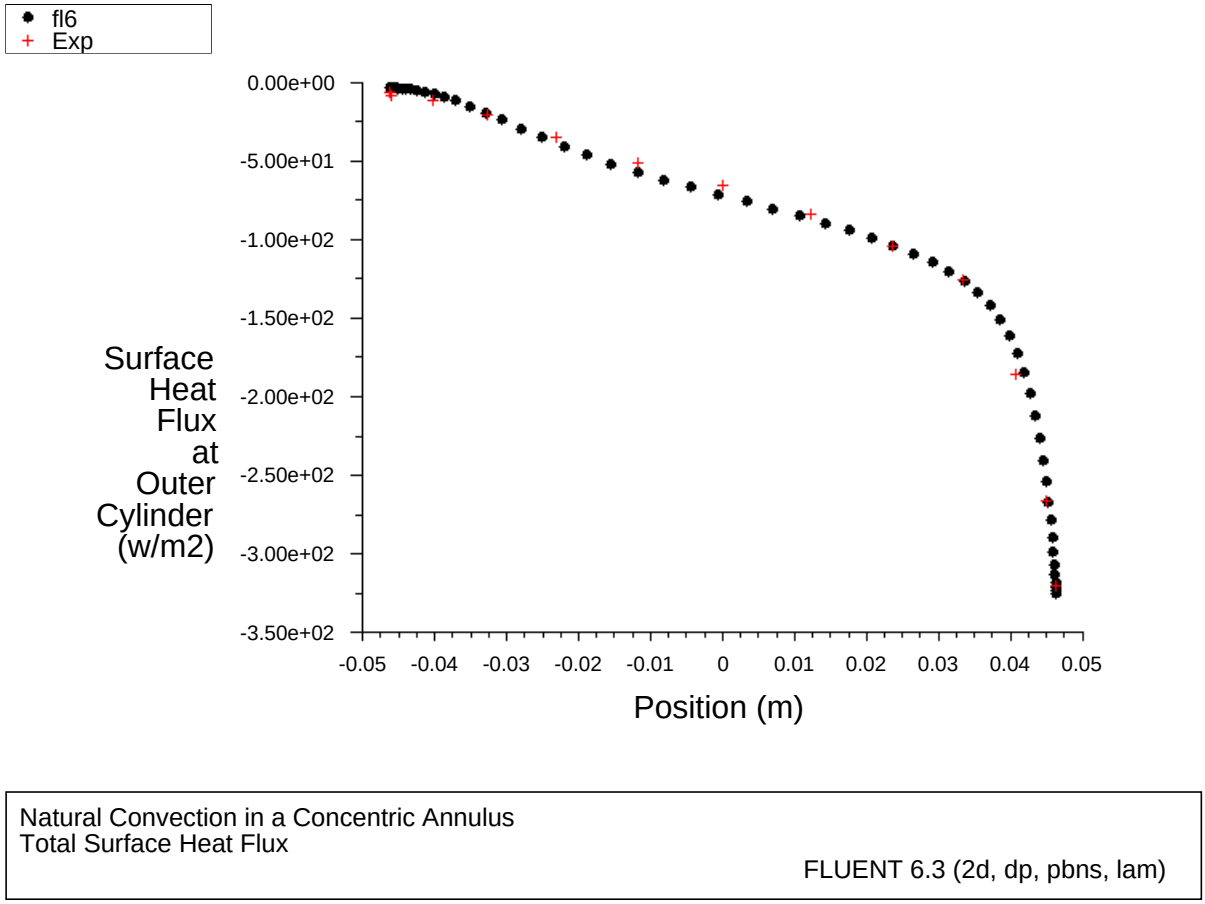

Figure 2.4.8: Comparison of Heat Flux from the Outer Cylinder Surface for the Concentric Case

© Fluent Inc. August 8, 2006

Validation 3. Flow in a 90° Planar Tee-Junction

3.1 Purpose

The purpose of this test is to compare FLUENT's prediction of the fractional flow in a dividing tee-junction with the experimental results of Hayes et al. [1].

3.2 Problem Description

The problem involves a planar 90° tee-junction as shown in Figure 3.2.1. The fluid enters through the bottom branch and divides into the two channels whose exit planes are held at the same static pressure.

The Reynolds number Re, based on the channel width and the centerline fluid velocity at the channel inlet, is given by

$$Re = \frac{\rho V_c W}{\mu} \tag{3.2-1}$$

where V_c is the inlet centerline velocity.

3.3 References

1. Hayes, R.E., Nandkumar, K., and Nasr-El-Din, H., Steady Laminar Flow in a 90 Degree Planar Branch, *Computers and Fluids*, 17(4): 537–553, 1989.

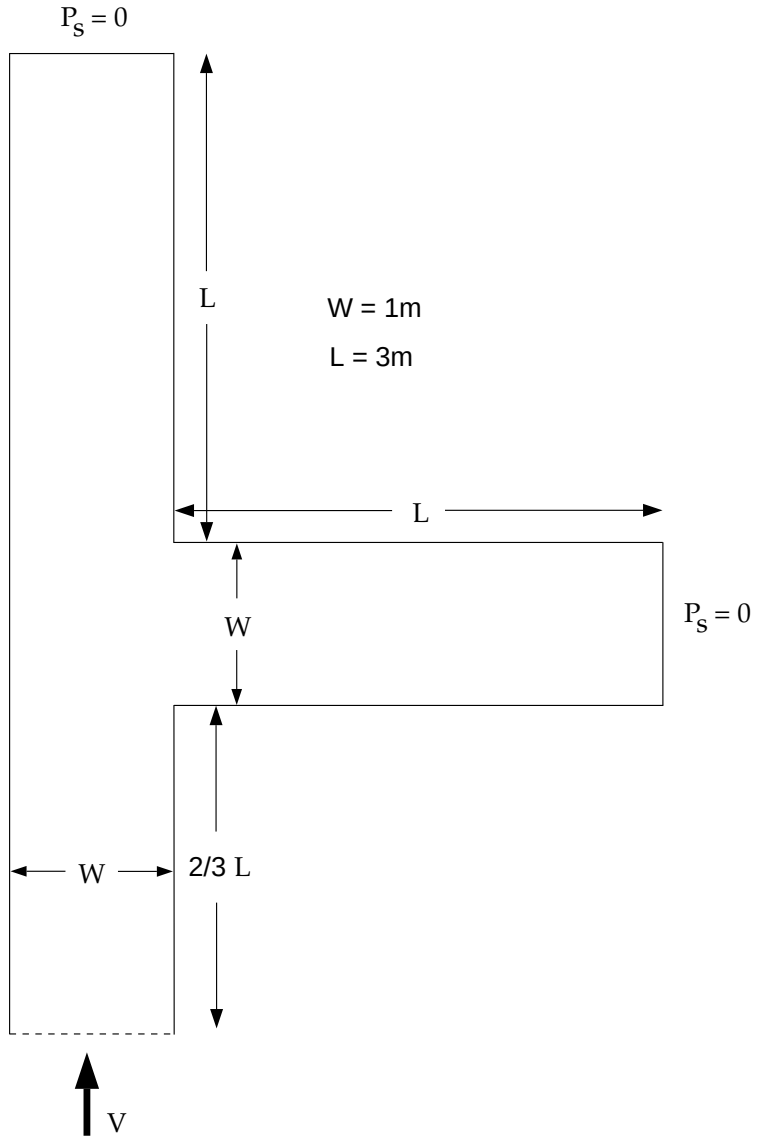

Figure 3.2.1: Problem Description

© Fluent Inc. August 8, 2006

3.4 Results

The test runs were made for five different Reynold numbers ($Re = 10$, $Re = 100$, $Re = 200$, $Re = 300$, and $Re = 400$). The FLUENT predictions are compared with the experimental results of Hayes et al.[1]. It is seen that with increasing flow rate in the main channel, less fluid escapes through the secondary (right) branch. The following table shows the fractional flow in the upper branch versus the Reynolds number. The FLUENT predictions of fractional flow versus Re agree very well with the experiment.

Table 3.4.1: Flow Split

Reynolds No., Re	10	100	200	300	400
Upper branch mass flow rate, kg/s	0.349	0.481	0.556	0.591	0.611
Right branch mass flow rate, kg/s	0.319	0.188	0.113	0.077	0.058
Total mass flow rate, kg/s	0.668	0.668	0.668	0.668	0.668
Flow split in the upper branch	0.523	0.719	0.832	0.885	0.914

3.4.1 Validation-Specific Information

Solver: FLUENT 2d
Version: 6.3.11
Solution Files:
1. `plarb_r1.cas`, `plarb_r1.dat` ($Re = 10$)
2. `plarb_r2.cas`, `plarb_r2.dat` ($Re = 100$)
3. `plarb_r3.cas`, `plarb_r3.dat` ($Re = 200$)
4. `plarb_r4.cas`, `plarb_r4.dat` ($Re = 300$)
5. `plarb_r5.cas`, `plarb_r5.dat` ($Re = 400$)

These solution files are available from the Fluent Inc. User Services Center as described in the Introduction.

3.4.2 Plot Data

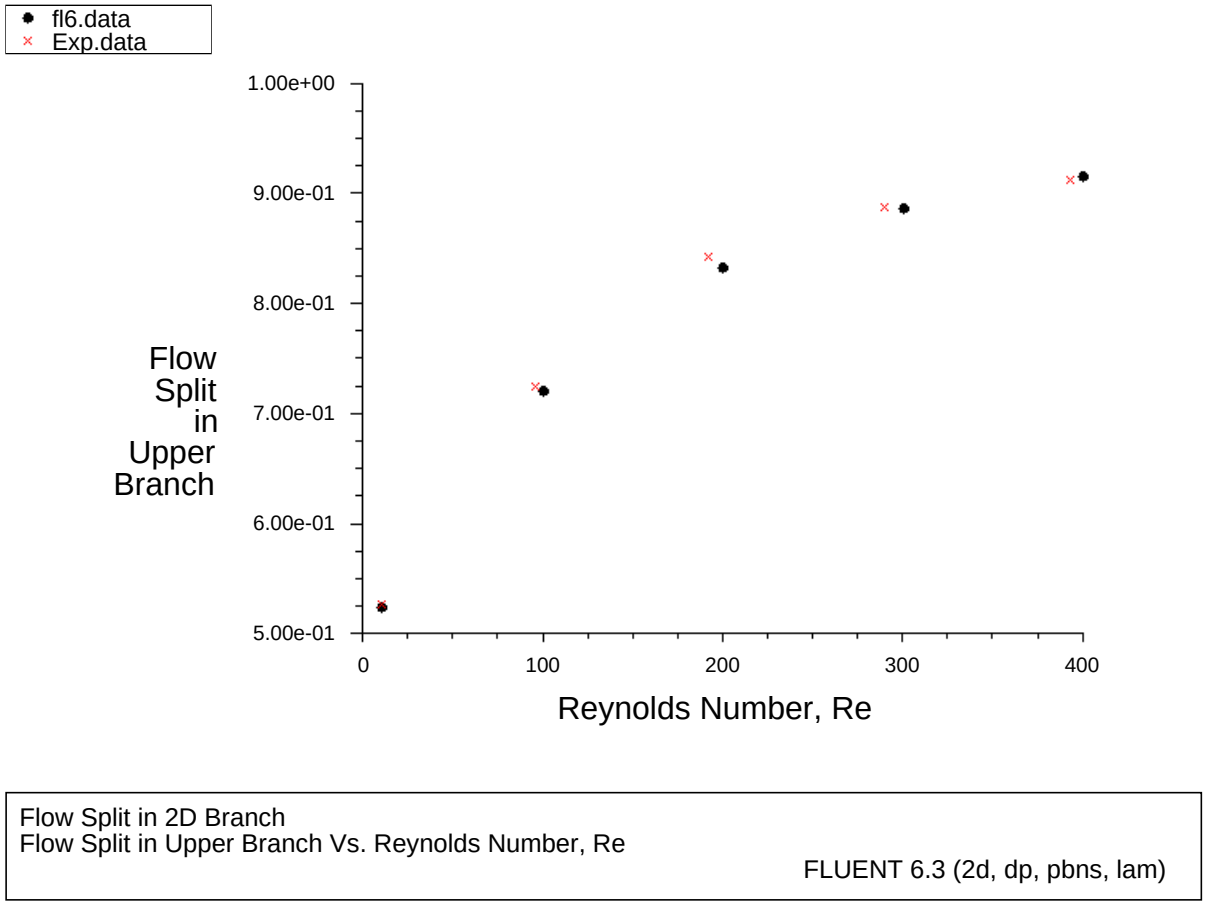

Figure 3.4.1: Flow Split in the Upper Branch vs. Reynolds Number

© Fluent Inc. August 8, 2006

Validation 4. Flows in Driven Cavities

4.1 Purpose

The purpose of this test is to compare the prediction of u and v velocity profiles in the 2D laminar driven trapezoidal cavity flow against the calculations by Darr and Vanka [1], and to compare u velocity profiles in the 2D laminar driven triangular cavity flow against the calculations of Jyotsna and Vanka [2].

4.2 Problem Description

Two types of cavities are considered. The first cavity is a trapezoidal cavity in which the top and bottom walls move but the side walls are stationary. The height of the cavity h is 1 m; the widths of the top and bottom walls are 1 m and 2 m, respectively (see Figure 4.2.1).

The second cavity is a triangular cavity with a driven top wall and stationary side walls. The height of the cavity h is 4 m; the width of the top wall is 2 m (see Figure 4.2.2).

4.3 References

1. Darr, J.H. and Vanka, S.P., Separated Flow in a Driven Trapezoidal Cavity, *Phys. Fluids A*, 3(3):385–392, March 1991.

2. Jyotsna, R. and Vanka, S.P., Multigrid Calculation of Steady, Viscous Flow in a Triangular Cavity, *J. Comp. Phys.*, 122:107–117, 1995.

4.4 Results

4.4.1 Trapezoidal Cavity

The u velocity profile at the vertical centerline of the cavity and the v velocity profile at the horizontal centerline of the cavity are compared to Darr and Vanka [1] results for both types of meshes.

4.4.2 Triangular Cavity

The normalized u velocity profiles at the vertical centerline of the cavity for the coarse and fine meshes are compared with Jyotsna and Vanka [2] data.

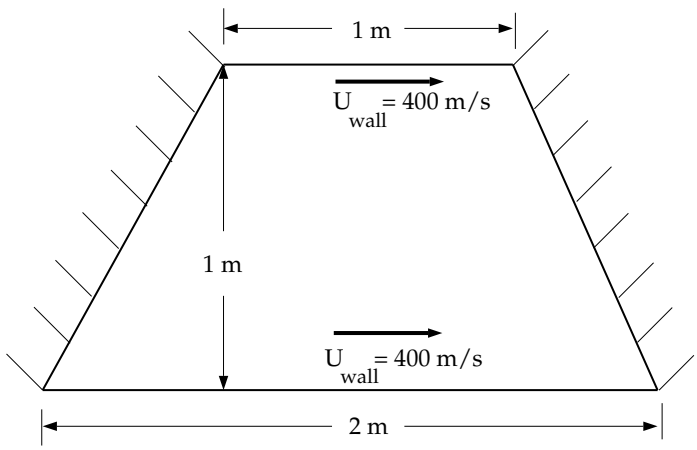

Figure 4.2.1: Problem Description: Trapezoidal Cavity

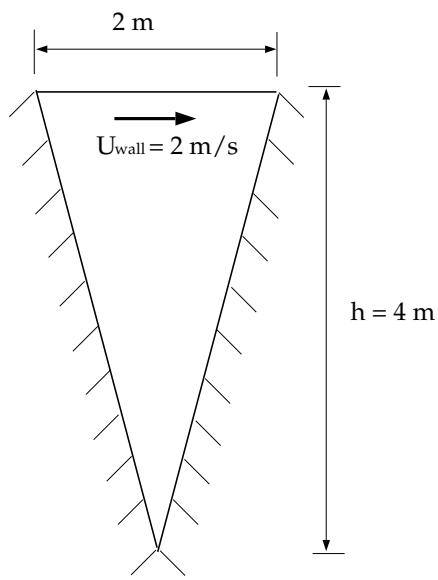

Figure 4.2.2: Problem Description: Triangular Cavity

© Fluent Inc. August 8, 2006

4.4.3 Validation-Specific Information

Solver:	FLUENT 2d
Version:	6.3.11
Solution Files:	1. `driv-trpz-tri_r1.cas`, `driv-trpz-tri_r1.dat`
	2. `driv-trpz-quad_r2.cas`, `driv-trpz-quad_r2.dat`
	3. `driv-tri-crs_r3.cas`, `driv-tri-crs_r3.dat`
	4. `driv-tri-fine_r3.cas`, `driv-tri-fine_r3.dat`

These solution files are available from the Fluent Inc. User Services Center as described in the Introduction.

4.4.4 Plot Data

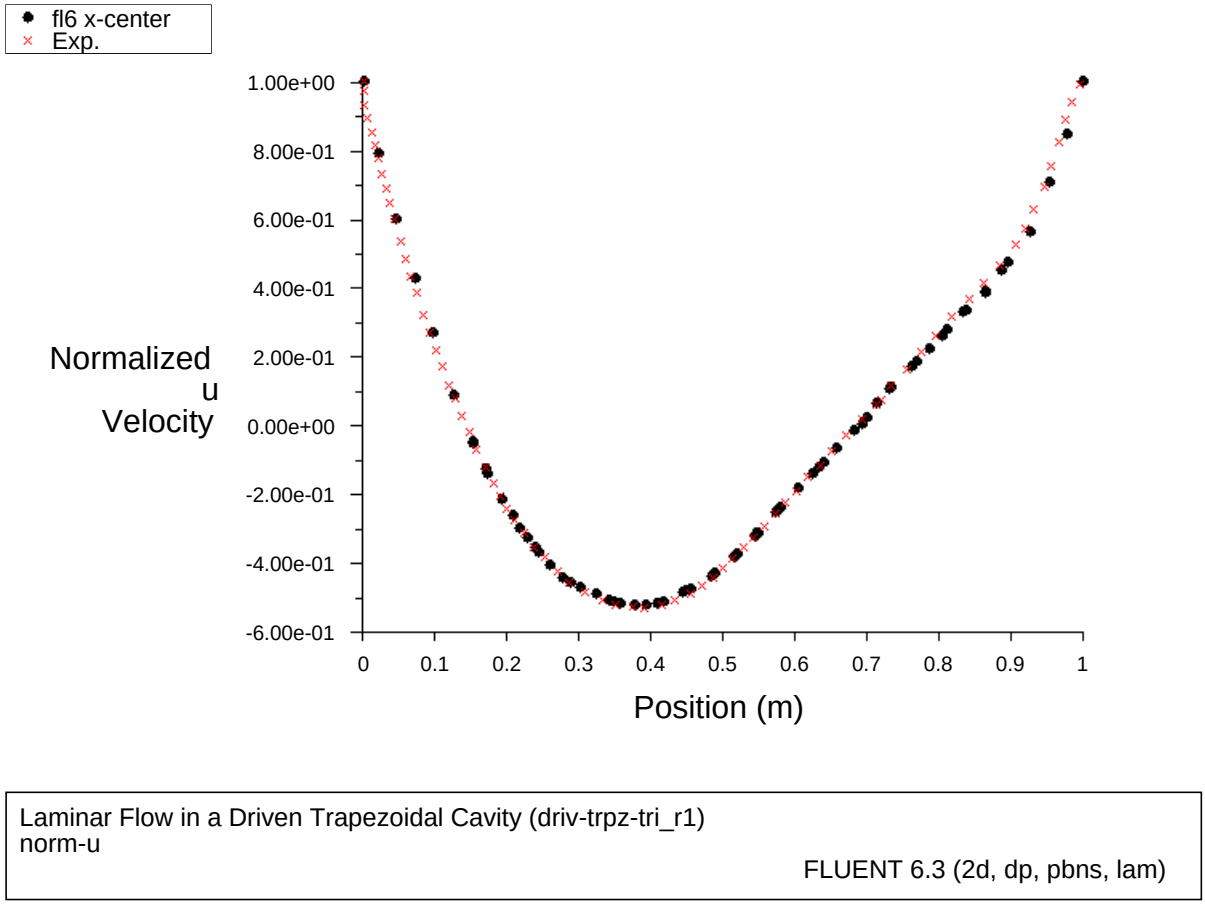

Figure 4.4.1: Normalized u Velocity at the Vertical Centerline of the Cavity (Triangular Mesh)

© Fluent Inc. August 8, 2006

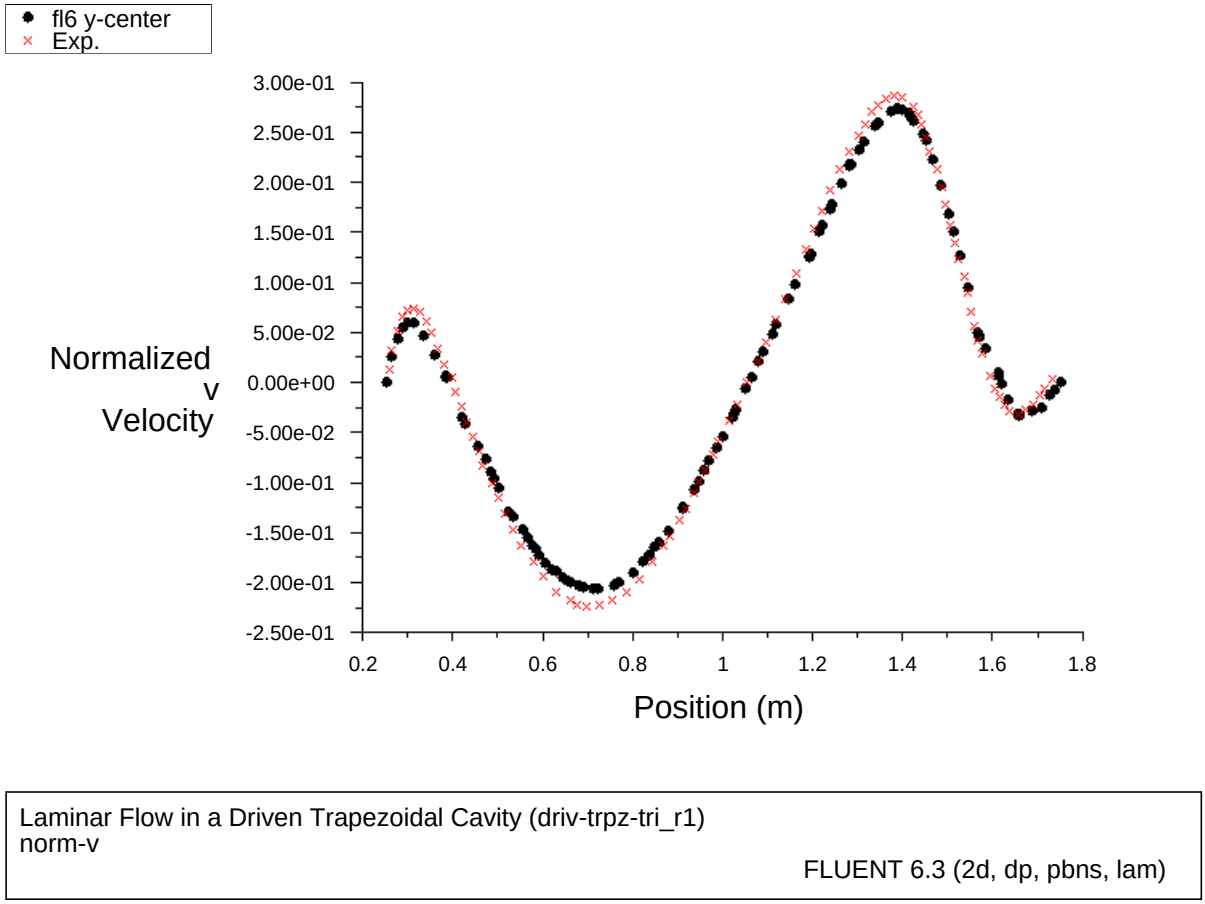

Figure 4.4.2: Normalized v Velocity at the Horizontal Centerline of the Cavity (Triangular Mesh)

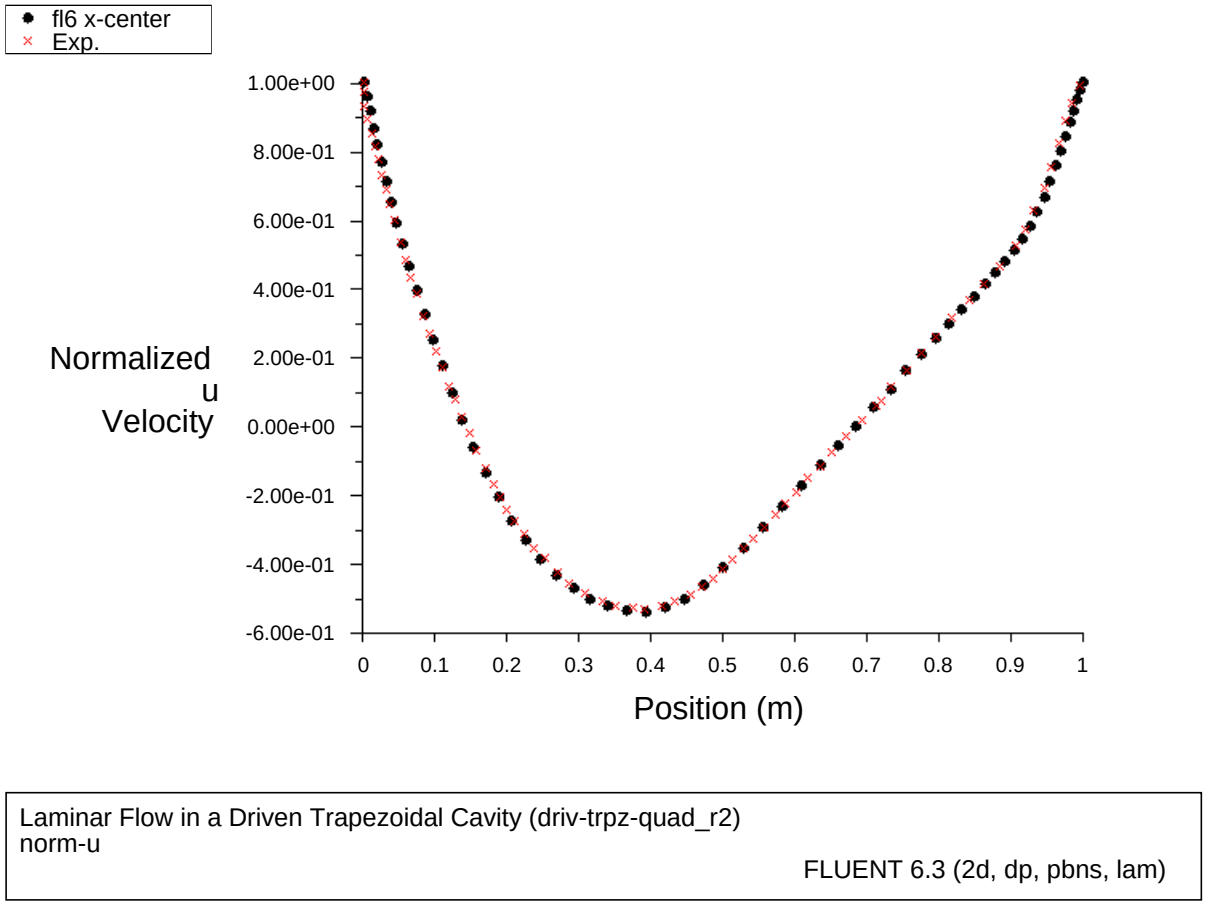

Figure 4.4.3: Normalized u Velocity at the Vertical Centerline of the Cavity (Quadrilateral Mesh)

© Fluent Inc. August 8, 2006

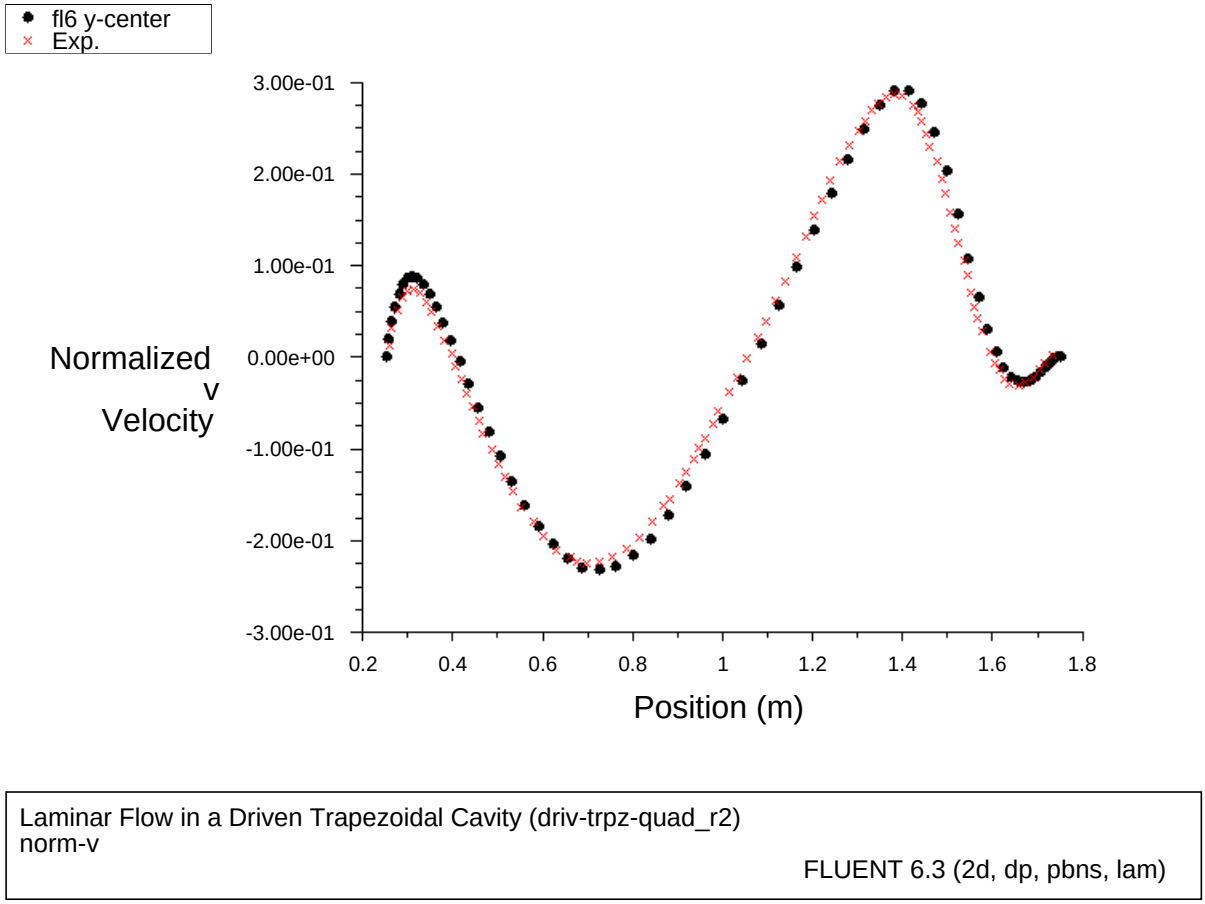

Figure 4.4.4: Normalized v Velocity at the Horizontal Centerline of the Cavity (Quadrilateral Mesh)

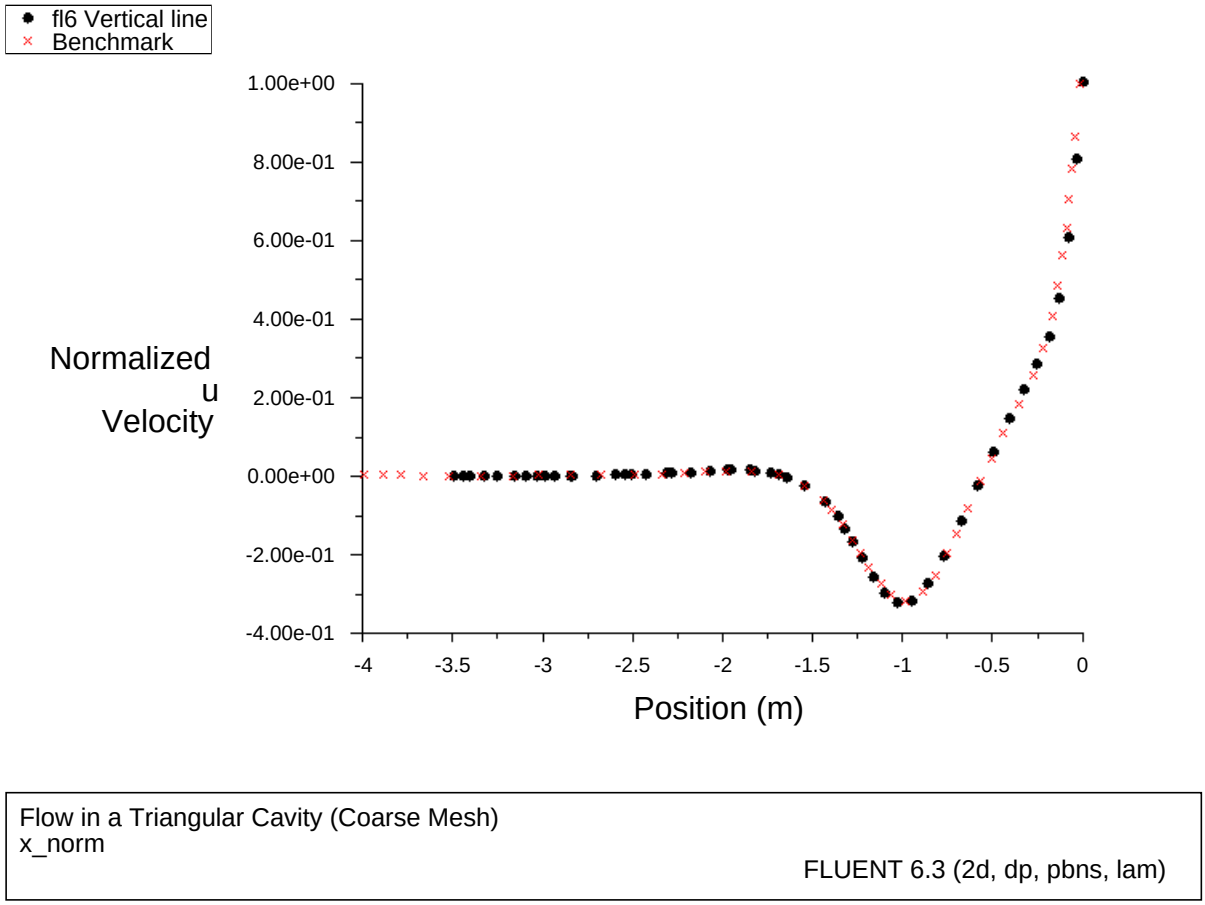

Figure 4.4.5: Normalized u Velocity at the Vertical Centerline of the Triangular Cavity (Mixed Coarse Mesh)

© Fluent Inc. August 8, 2006

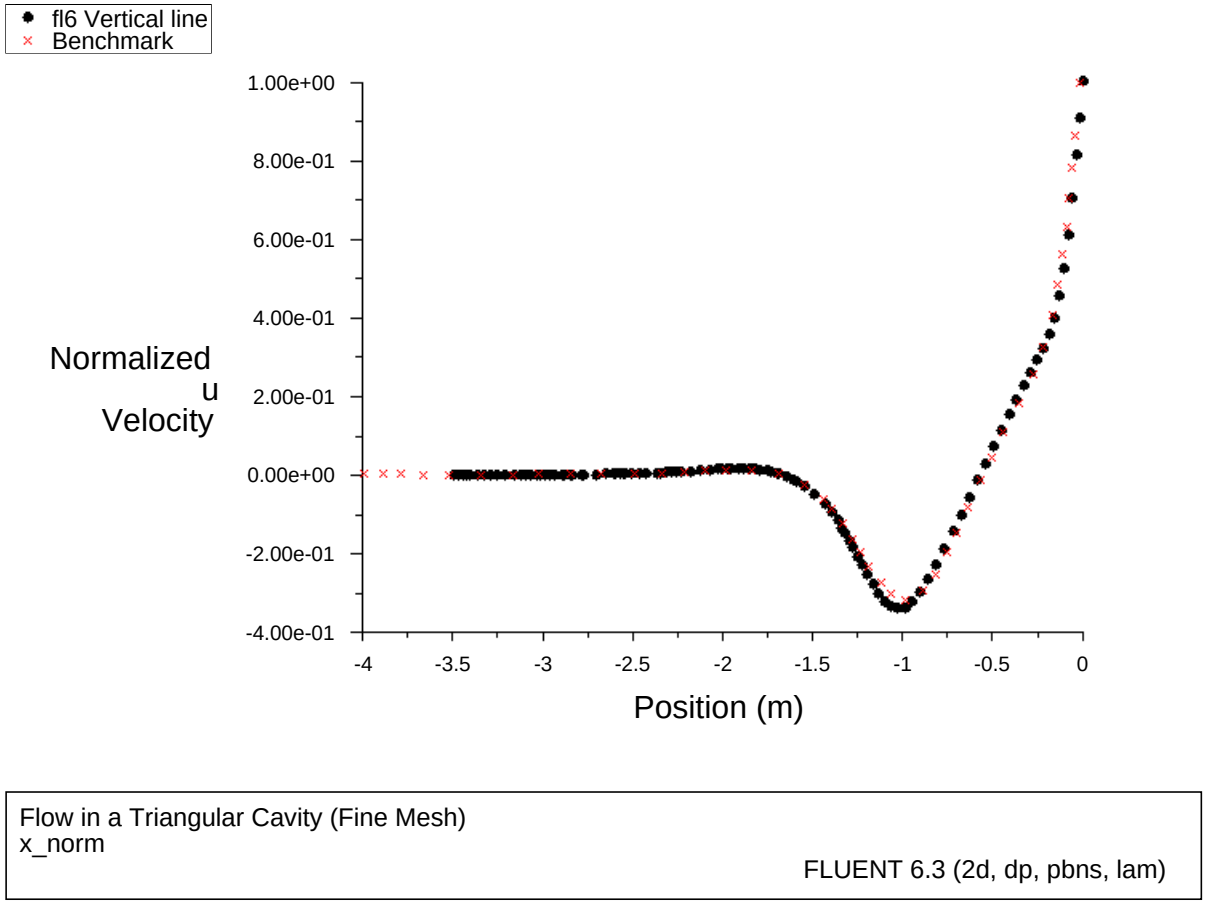

Figure 4.4.6: Normalized u Velocity at the Vertical Centerline of the Triangular Cavity (Mixed Fine Mesh)

© Fluent Inc. August 8, 2006

Validation 5. Periodic Flow in a Wavy Channel

5.1 Purpose

The purpose of this test is to compare the predictions of FLUENT's standard k-ε and RNG k-ε turbulence models against the experimental results of Kuzan [1] for the u velocity profiles.

5.2 Problem Description

The wavy bottom wall has a sinusoidal shape whose amplitude and wave length are 0.1 m and 1.0 m, respectively. Since the flow is periodic, the computational domain can be chosen to cover only one period of the wavy channel, as shown in Figure 5.2.1. The length of the periodic domain is 1 m.

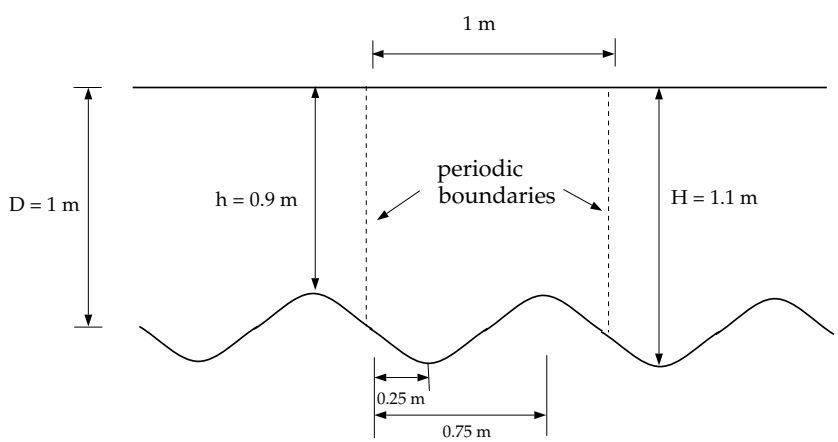

Figure 5.2.1: Problem Description

5.3 References

1. Kuzan, J.D., *Velocity Measurements for Turbulent Separated and Near-Separated Flows Over Solid Waves*, Ph.D. thesis, Dept. Chem. Eng., Univ. Illinois, Urbana, IL, 1986.

5.4 Results

Figures 5.4.1 - 5.4.4 compare the u velocity profiles at the wave crest and at the wave trough with Kuzan's [1] experimental results for both the standard k-ε and the RNG k-ε models. The u velocity is normalized by the average fluid velocity at the mean channel height, $U = 0.816$ m/s.

The velocity profiles at the wave trough confirm that the flow reversal occurs in the wave hollow, thus creating a recirculation zone. Near the top straight wall, velocity profiles remain attached to the wall. The predictions are in very close agreement with the experimental data.

5.4.1 Validation-Specific Information

Solver:	FLUENT 2d
Version:	6.3.11
Solution Files:	1. `std.cas`, `std.dat`
	2. `rng.cas`, `rng.dat`

These solution files are available from the Fluent Inc. User Services Center as described in the Introduction.

© Fluent Inc. August 8, 2006

5.4.2 Plot Data

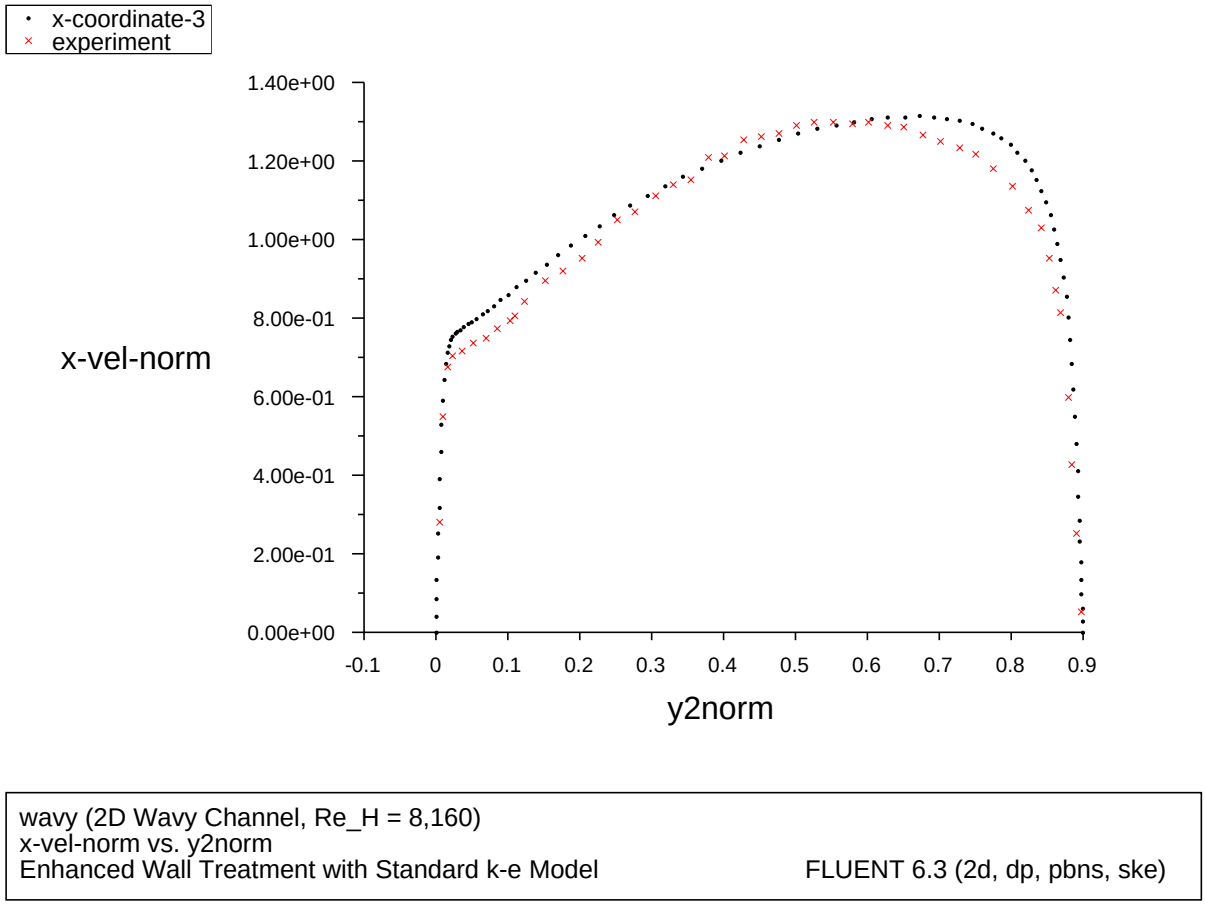

Figure 5.4.1: Normalized u Velocity at the Wave Crest (Standard k-ε Model)

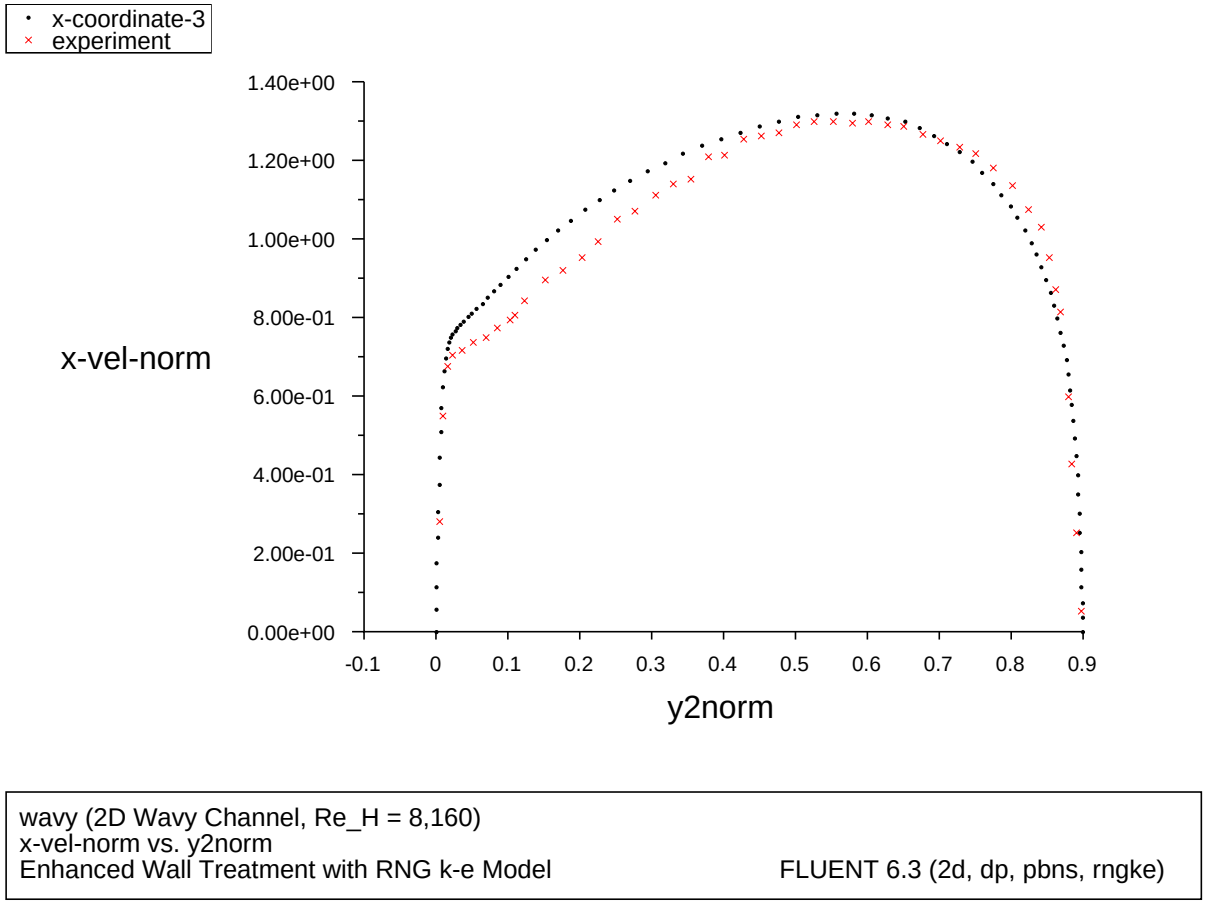

Figure 5.4.2: Normalized u Velocity at the Wave Crest (RNG k-ε Model)

© Fluent Inc. August 8, 2006

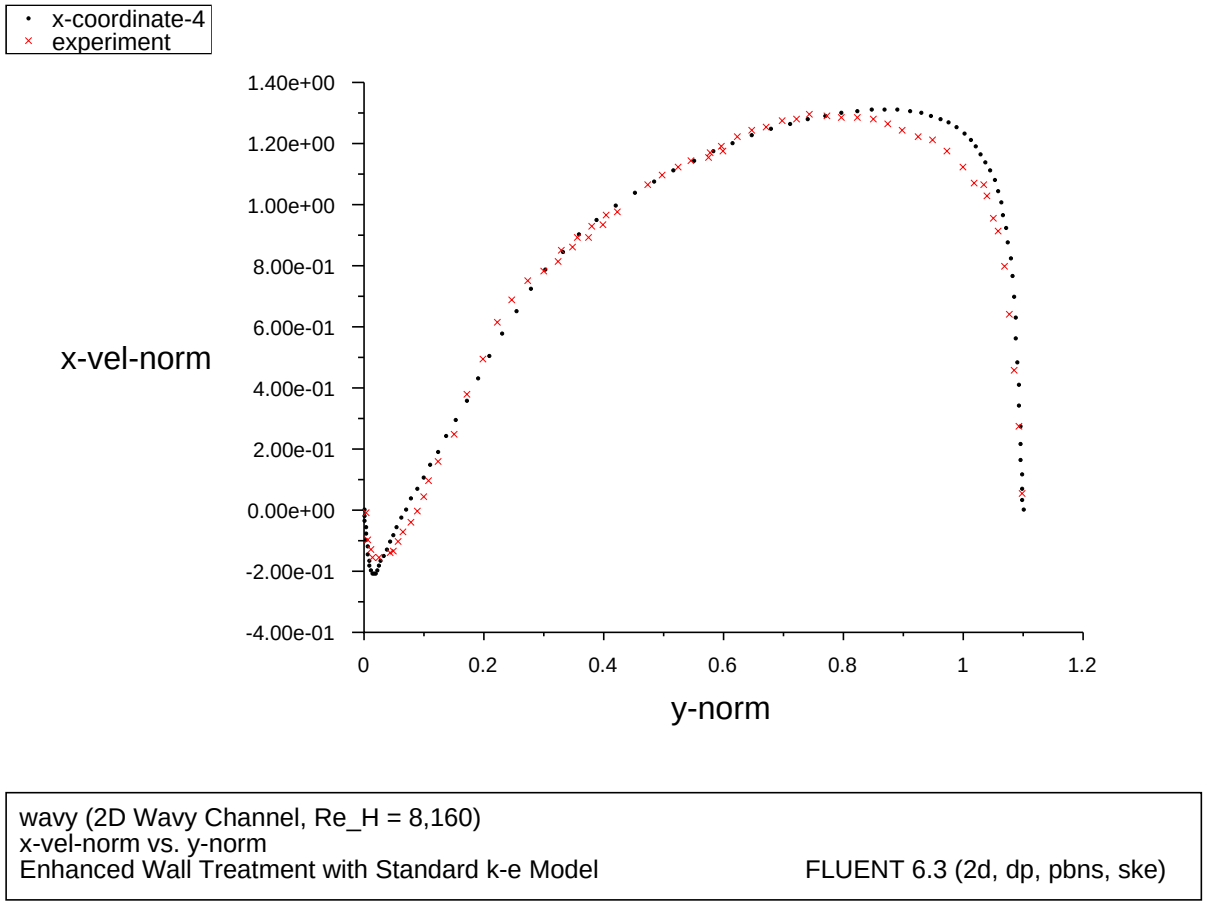

Figure 5.4.3: Normalized u Velocity at the Wave Trough (Standard k-ε Model)

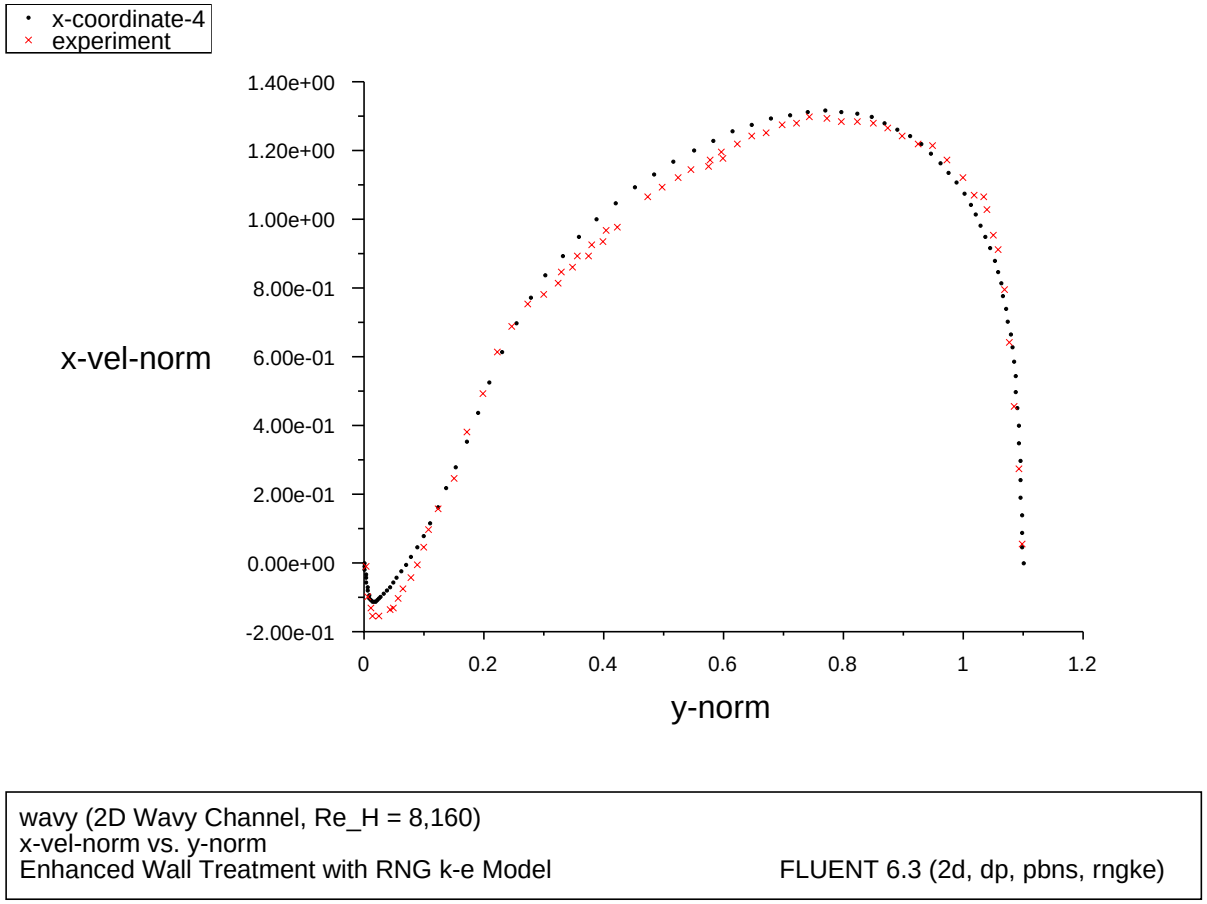

Figure 5.4.4: Normalized u Velocity at the Wave Trough (RNG k-ε Model)

© Fluent Inc. August 8, 2006

Validation 6. Heat Transfer in a Pipe Expansion

6.1 Purpose

The purpose of this test is to validate FLUENT's standard and non-equilibrium wall functions together with the standard k-ε and RNG k-ε turbulence models against the experimental data [1,2,3].

6.2 Problem Description

Figure 6.2.1 shows the geometry of the expansion considered. The inlet is placed $1H$ upstream of the step. The exit boundary is located $40H$ downstream of the step. The expansion ratio is $d/D = 0.400$, where $d = 1.33$ m is the inlet pipe diameter and $D = 3.33$ m is the downstream pipe diameter.

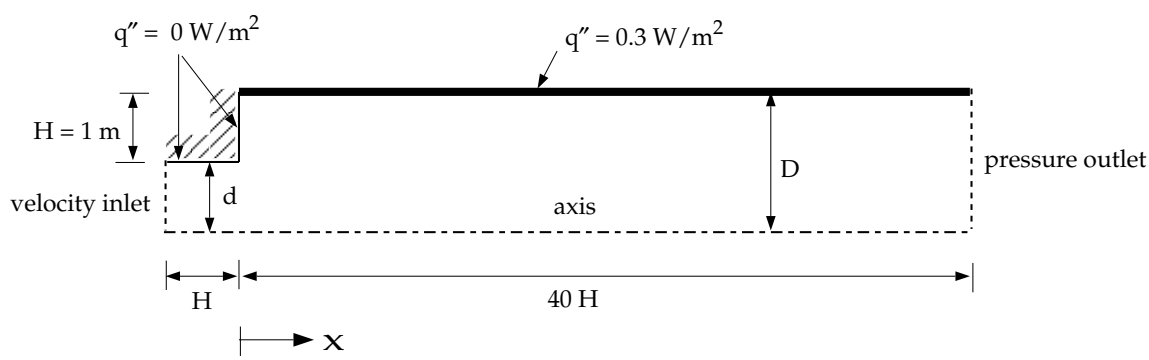

Figure 6.2.1: Problem Description

6.3 References

1. Baughn et al., Local Heat Transfer Downstream of an Abrupt Expansion in a Circular Channel With Constant Wall Heat Flux, *Journal of Heat Transfer*, 106:789–796, 1984.

2. Patel, C., Rodi, W., and Scheuerer, G., Turbulence Models for Near-Wall and Low-Reynolds-Number Flows: A Review, *AIAA Journal*, 23(9), 1984.

3. Schlichting, H., *Boundary-Layer Theory*, McGraw-Hill Series in Mechanical Engineering, 1979.

6.4 Results

The quantity of interest for comparison with the measurements of [1] is the Nusselt number, Nu, along the heated wall. The Nusselt number was calculated from the bulk temperature and the heat transfer coefficient. (See Figure 6.2.1 for the location of x.)

The bulk temperature is

$$T_B(x) = \frac{\dot{q}''(x)4x}{Re\mu c_p} + 273 \tag{6.4-1}$$

where $\dot{q}''(x)$ is the local heat flux (constant, in this case). The local heat transfer coefficient is

$$h(x) = \frac{\dot{q}''(x)}{T_{\text{wall}}(x) - T_B(x)} \tag{6.4-2}$$

Finally, the local Nusselt number is

$$Nu(x) = \frac{h(x)D}{k} \tag{6.4-3}$$

where D is the diameter of the pipe and k is the thermal conductivity of the fluid.

Data of [1] are in terms of Nu/Nu_{DB} where Nu_{DB} is the Nusselt number calculated with the Dittus-Boelter formula.

The variation of the ratio Nu/Nu_{DB} along the heated wall for the standard k-ε and RNG k-ε models with standard wall functions and non-equilibrium wall functions is presented here.

The FLUENT results are compared to the experimental results of [1]. The agreement is satisfactory for all cases. The use of the non-equilibrium wall functions slightly improves the results.

© Fluent Inc. August 8, 2006

6.4.1 Validation-Specific Information

Solver:	FLUENT 2d
Version:	6.3.11
Solution Files:	1. `std_swf.cas`, `std_swf.dat`
	2. `std_neqwf.cas`, `std_neqwf.dat`
	3. `rng_swf.cas`, `rng_swf.dat`
	4. `rng_neqwf.cas`, `rng_neqwf.dat`

These solution files are available from the Fluent Inc. User Services Center as described in the Introduction.

6.4.2 Plot Data

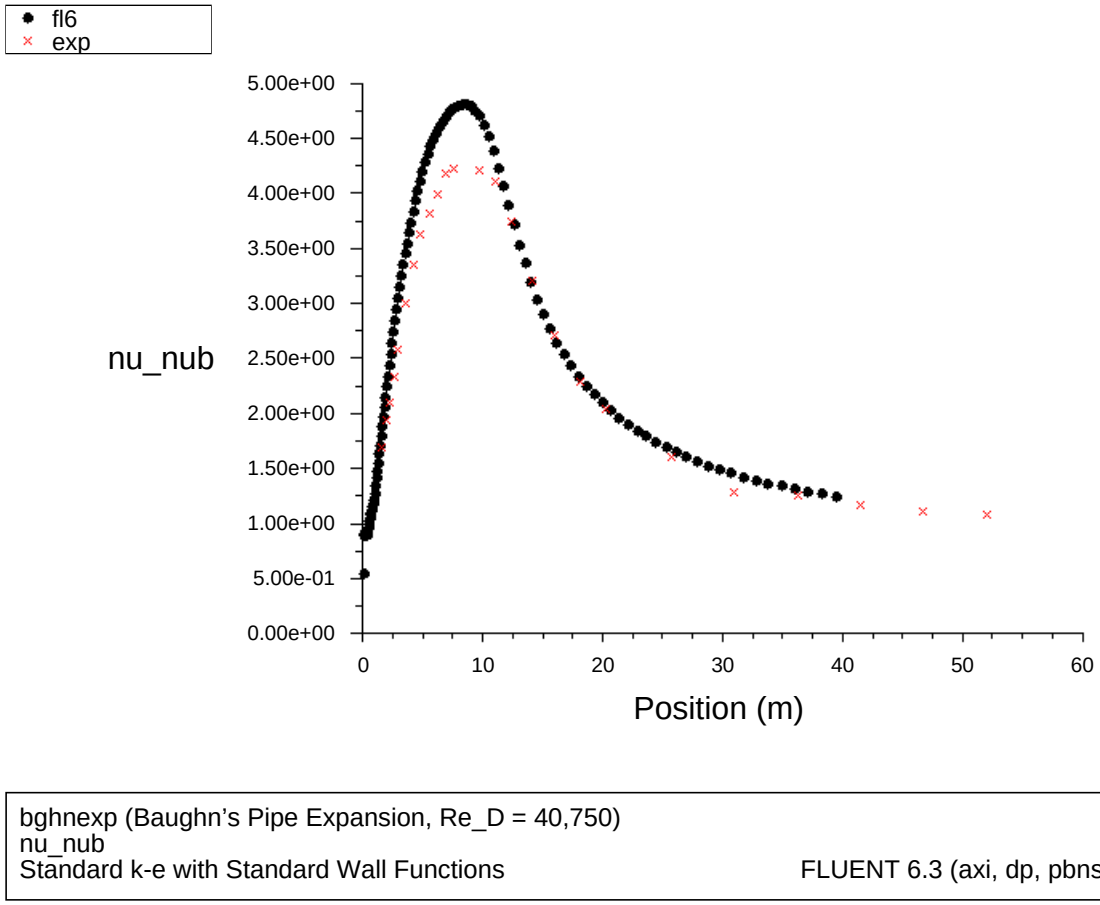

Figure 6.4.1: Nu/Nu_{DB} along the Downstream Pipe Wall (Standard k-ε Model, Standard Wall Functions)

© Fluent Inc. August 8, 2006

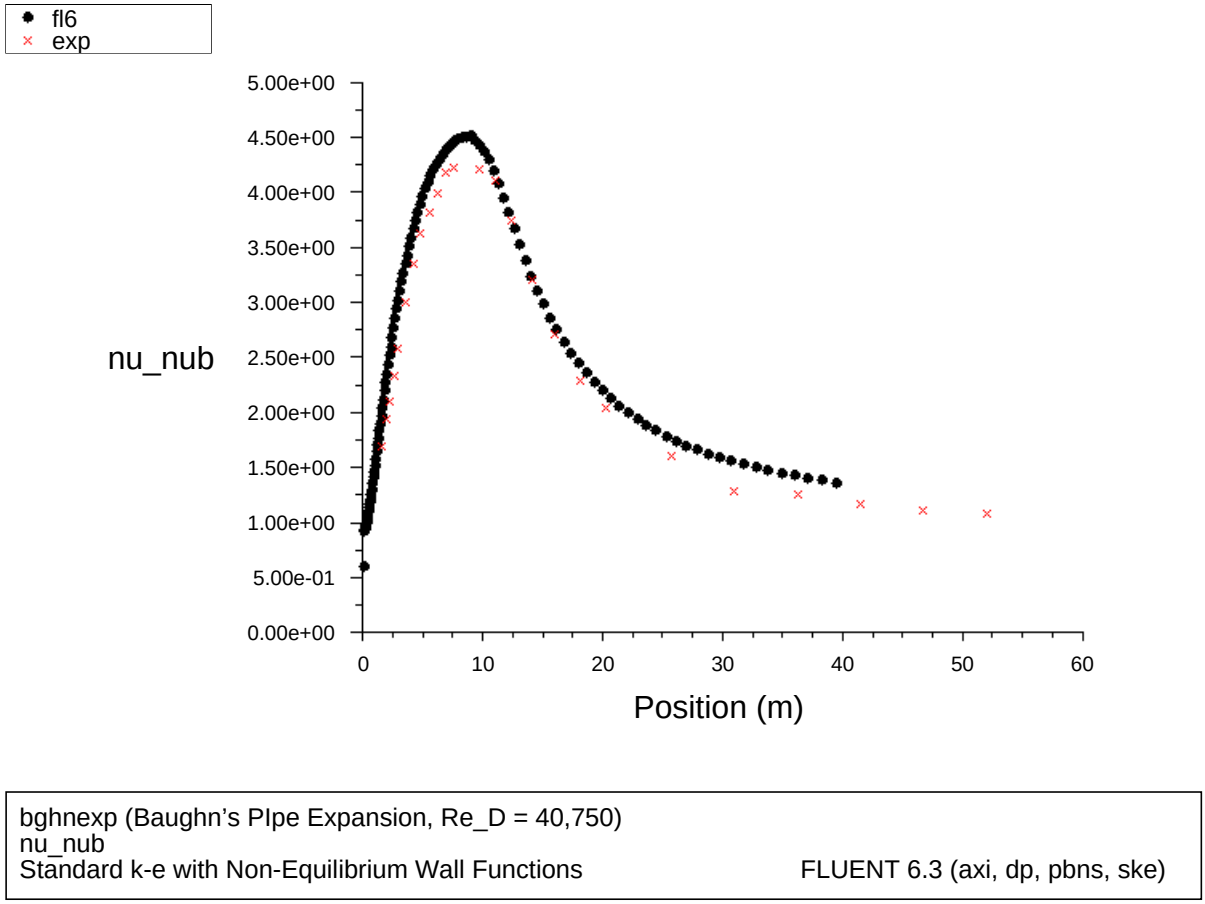

Figure 6.4.2: Nu/Nu_{DB} along the Downstream Pipe Wall (Standard k-ε Model, Non-Equilibrium Wall Functions)

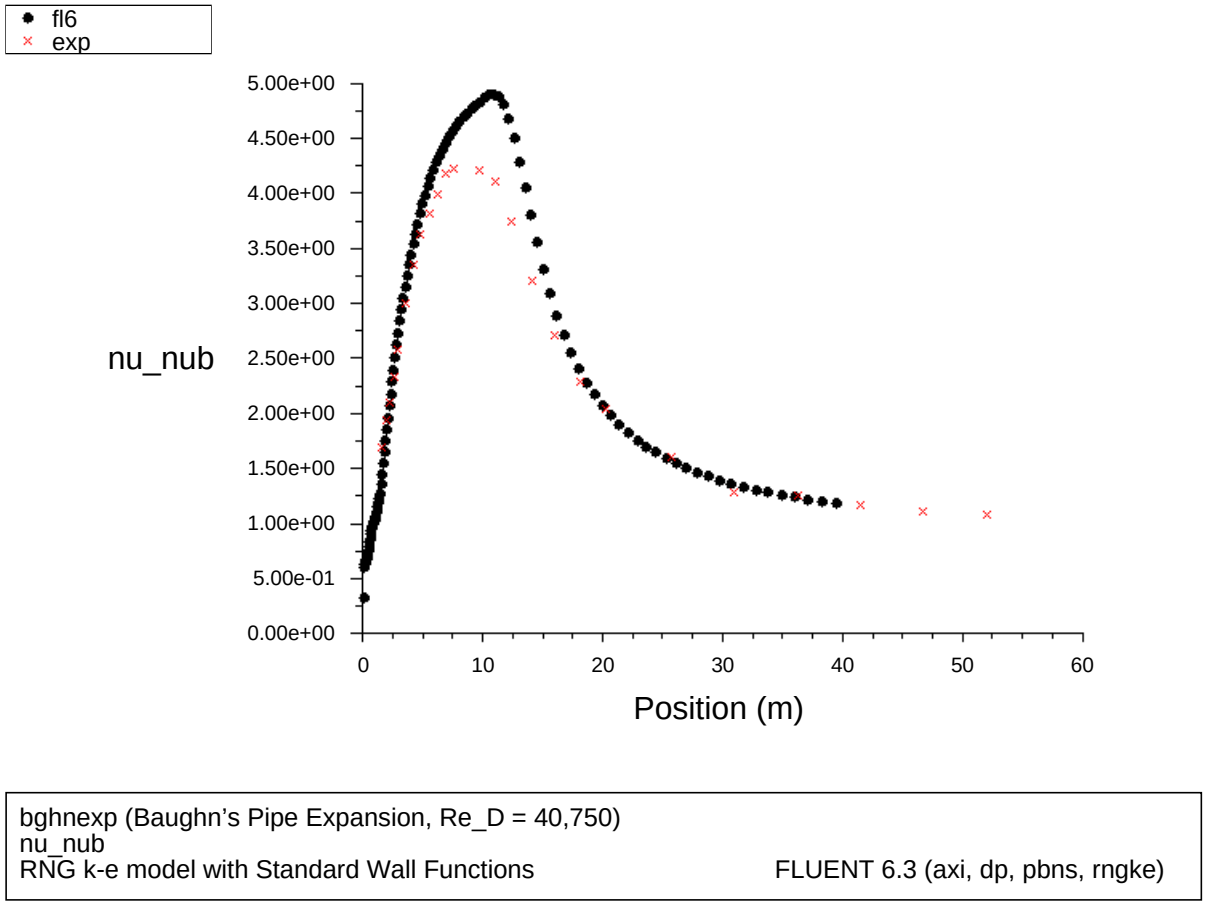

Figure 6.4.3: Nu/Nu_{DB} along the Downstream Pipe Wall (RNG k-ε Model, Standard Wall Functions)

© Fluent Inc. August 8, 2006

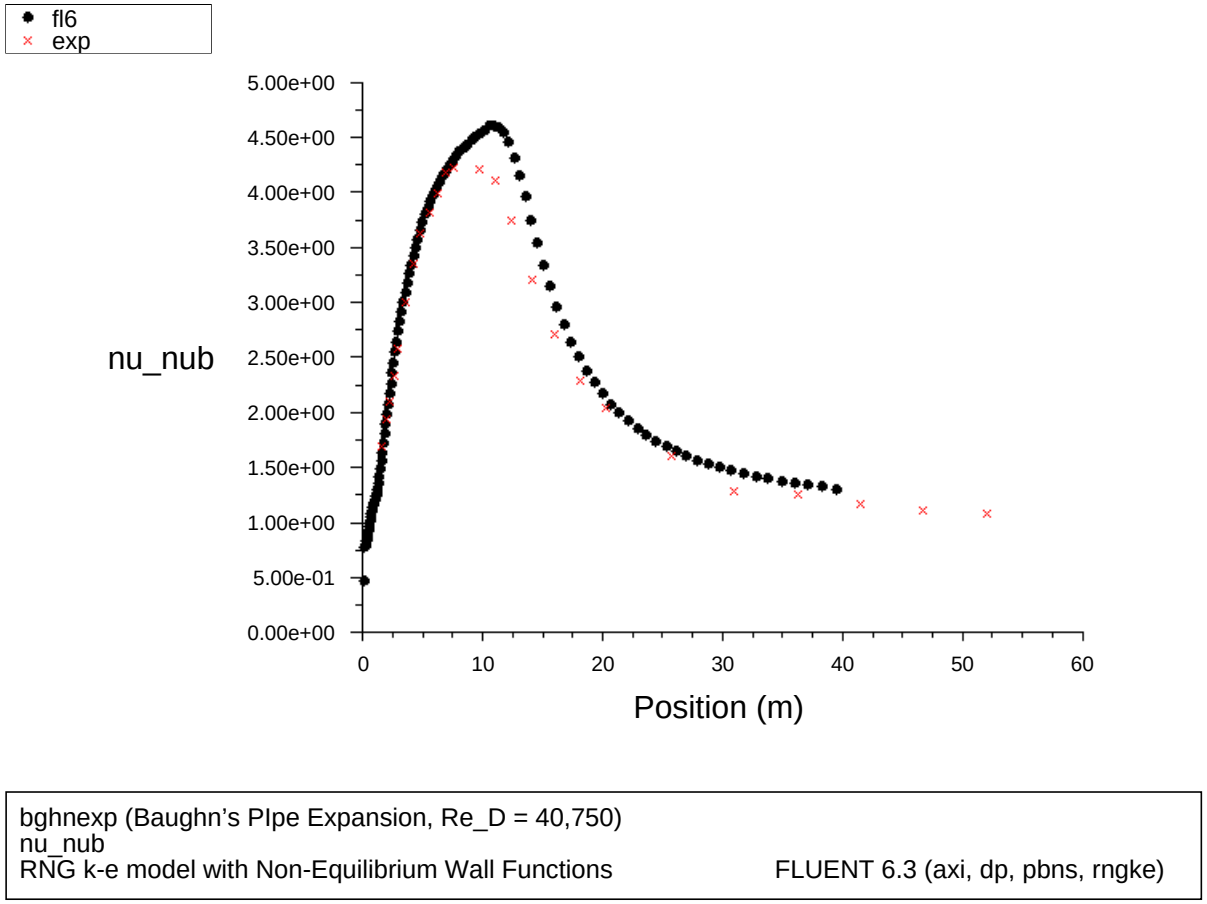

Figure 6.4.4: Nu/Nu_{DB} along the Downstream Pipe Wall (RNG k-ε Model, Non-Equilibrium Wall Functions)

© Fluent Inc. August 8, 2006

Validation 7. Propane Jet in a Coaxial Air Flow

7.1 Purpose

The aim of this validation is to compare FLUENT's predictions for the mean mixture fraction and the axial velocity along the jet axis with the experimental data [1,2,3]. The test was conducted using two methods: the non-reacting species transport model and the mixture fraction/PDF model. It also incorporated two types of meshes: a quadrilateral mesh and a triangular mesh.

7.2 Problem Description

The flow considered is a propane turbulent round jet in a coaxial air tunnel flow. The problem is axisymmetric. The tunnel has a length $L = 2$ m and a diameter $D = 0.3$ m. The inner diameter of the jet tube exit is $d = 5.2$ mm, and the outer diameter is $d' = 11$ mm. Figure 7.2.1 shows the geometry of the problem.

This problem involves three different species: propane (C_3H_8), oxygen (O_2), and nitrogen (N_2). The turbulent jet at the pipe exit contains only C_3H_8. The air that enters the tunnel is free of C_3H_8. There is no chemical reaction between species, and the flow is adiabatic.

7.3 References

1. Strahle, W.C., and Lekoudis, S.G., *Evaluation of Data on Simple Turbulent Reacting Flows*, AFOSR TR-85 0880, Chapter 2, School of Aerospace Engineering, Georgia Institute of Technology, Atlanta, GA.

2. Schefer, R.W., and Dibble, R.W., Simultaneous Measurements of Velocity and Density in a Turbulent Nonpremixed Flame, *AIAA Journal*, 23:1070–1078, 1985.

3. Schlichting, H., *Boundary-Layer Theory*, McGraw-Hill Series in Mechanical Engineering, 1979.

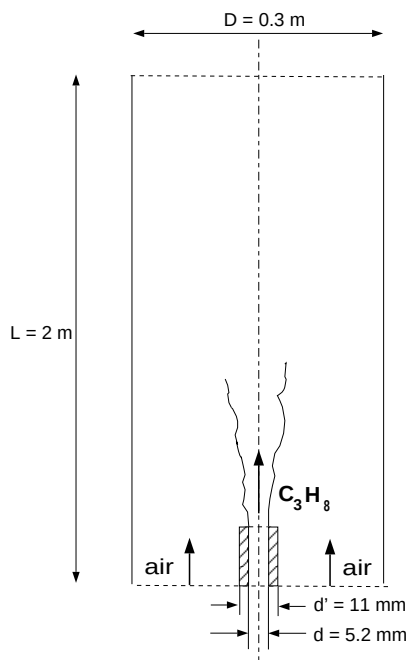

Figure 7.2.1: Problem Description

© Fluent Inc. August 8, 2006

7.4 Results

FLUENT's results for the four runs are compared to the data from [1] in Figures 7.4.1–7.4.7, as measured along the symmetry axis of the tunnel, downstream of the jet pipe exit. Figures 7.4.1–7.4.4 compare the propane mass fraction or the mean mixture fraction (for the nonreacting species transport model and the mixture fraction/PDF model). Figures 7.4.5–7.4.7 compare the axial velocities of the mixing flow.

Predictions of the mixture fraction or the propane mass fraction are very good for all the runs. The axial velocity distribution is in very close agreement with the benchmark.

7.4.1 Validation-Specific Information

Solver:	FLUENT 2ddp
Version:	6.3.11
Solution Files:	1. `mixing_quad.cas`, `mixing_quad.dat` (non-reacting species model) 2. `mixing_tri.cas`, `mixing_tri.dat` (non-reacting species model) 3. `mixing_pdf_quad.cas`, `mixing_pdf_quad.dat` (+ `mixing.pdf`) (mixture fraction/PDF model) 4. `mixing_pdf_tri.cas`, `mixing_pdf_tri.dat` (+ `mixing.pdf`) (mixture fraction/PDF model)

These solution files are available from the Fluent Inc. User Services Center as described in the Introduction.

7.4.2 Plot Data

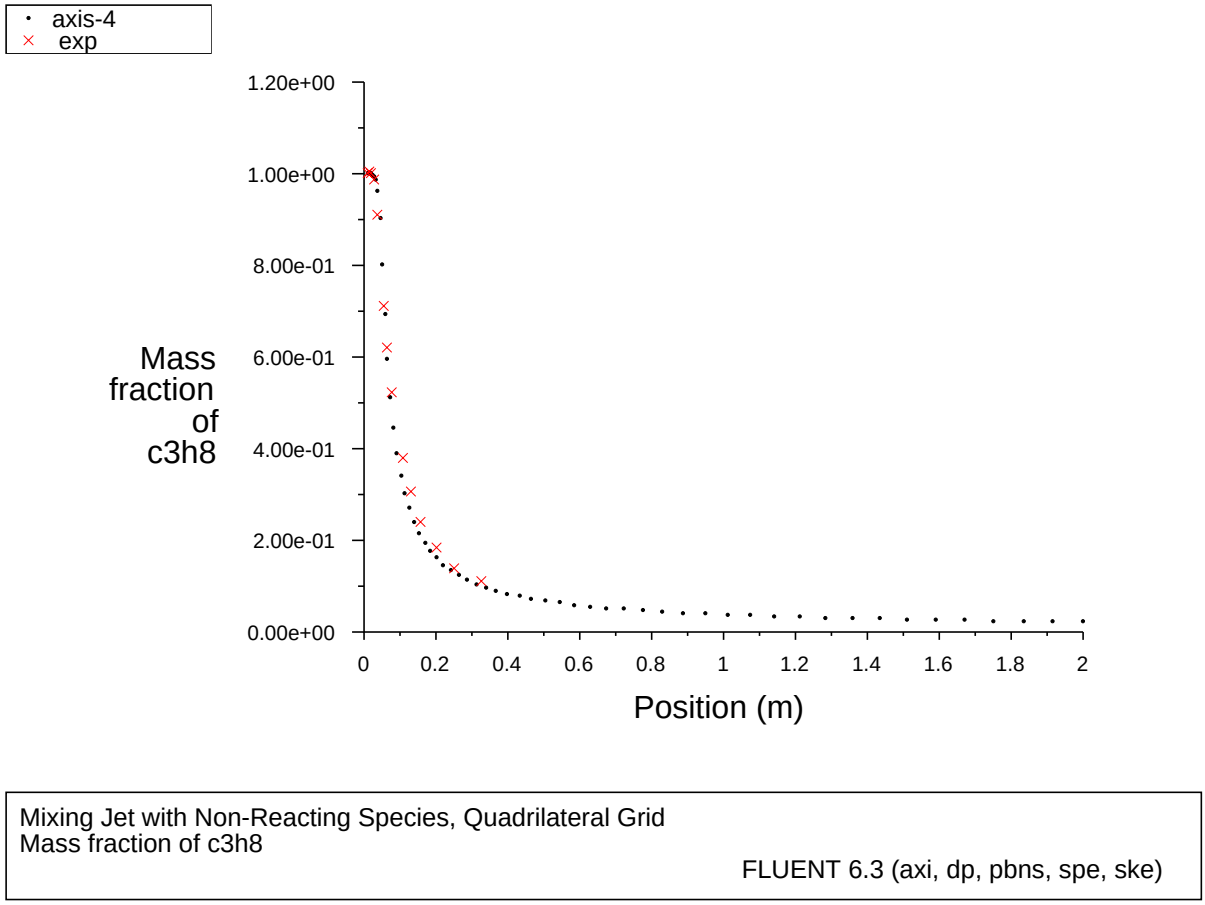

Figure 7.4.1: Propane Mass Fraction along the Symmetry Axis (Non-Reacting Species Transport Model, Quadrilateral Mesh)

© Fluent Inc. August 8, 2006

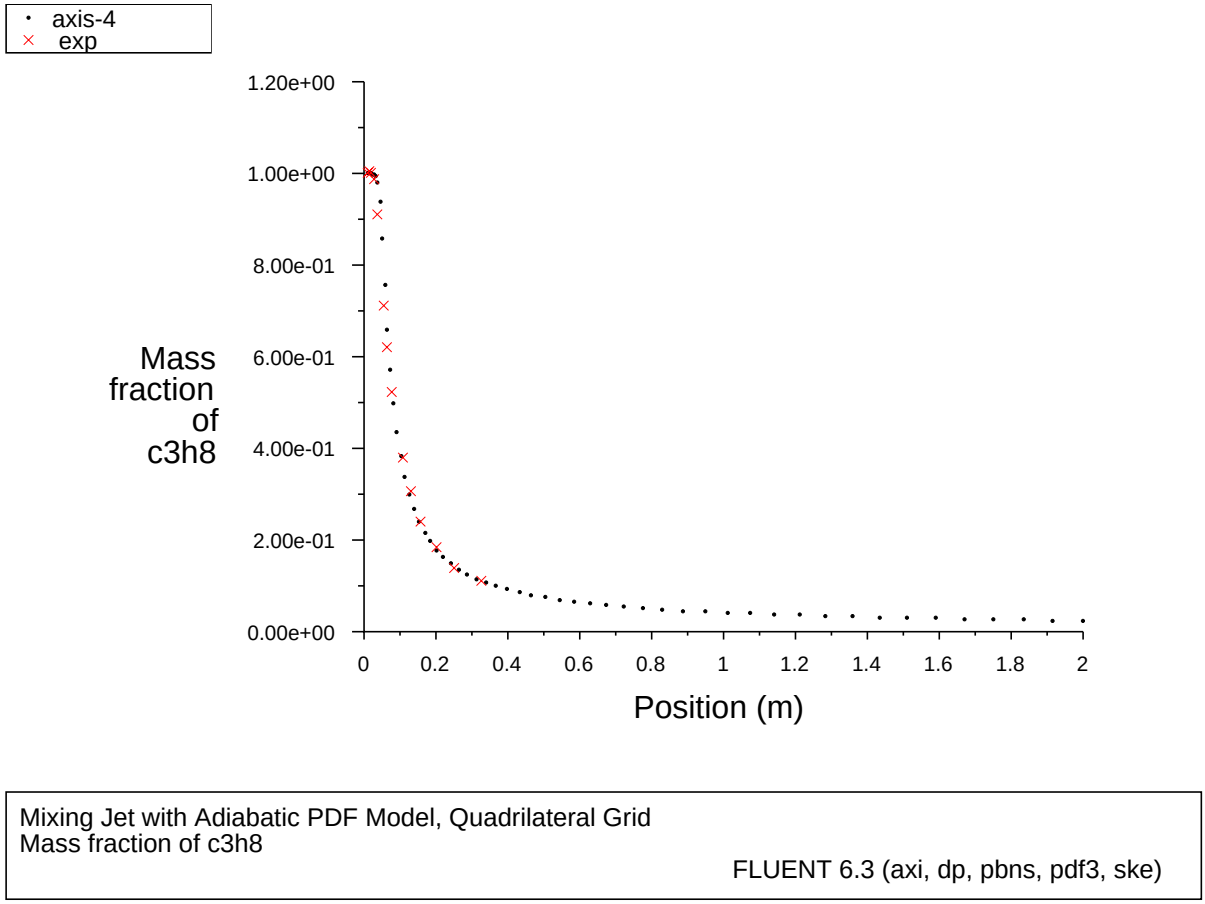

Figure 7.4.2: Propane Mass Fraction along the Symmetry Axis (Mixture Fraction/PDF Model, Quadrilateral Mesh)

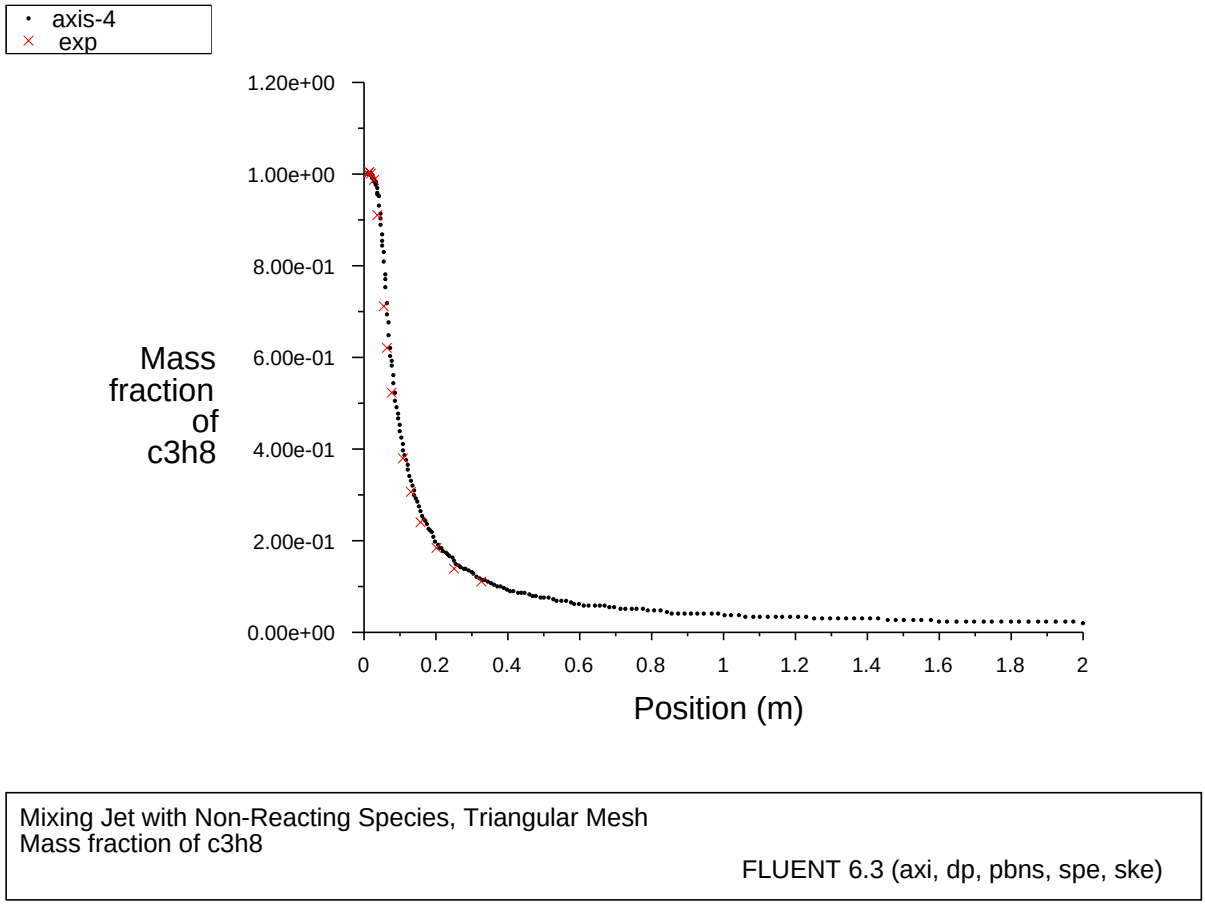

Figure 7.4.3: Mixture Fraction along the Symmetry Axis (Non-Reacting Species Transport Model, Triangular Mesh)

© Fluent Inc. August 8, 2006

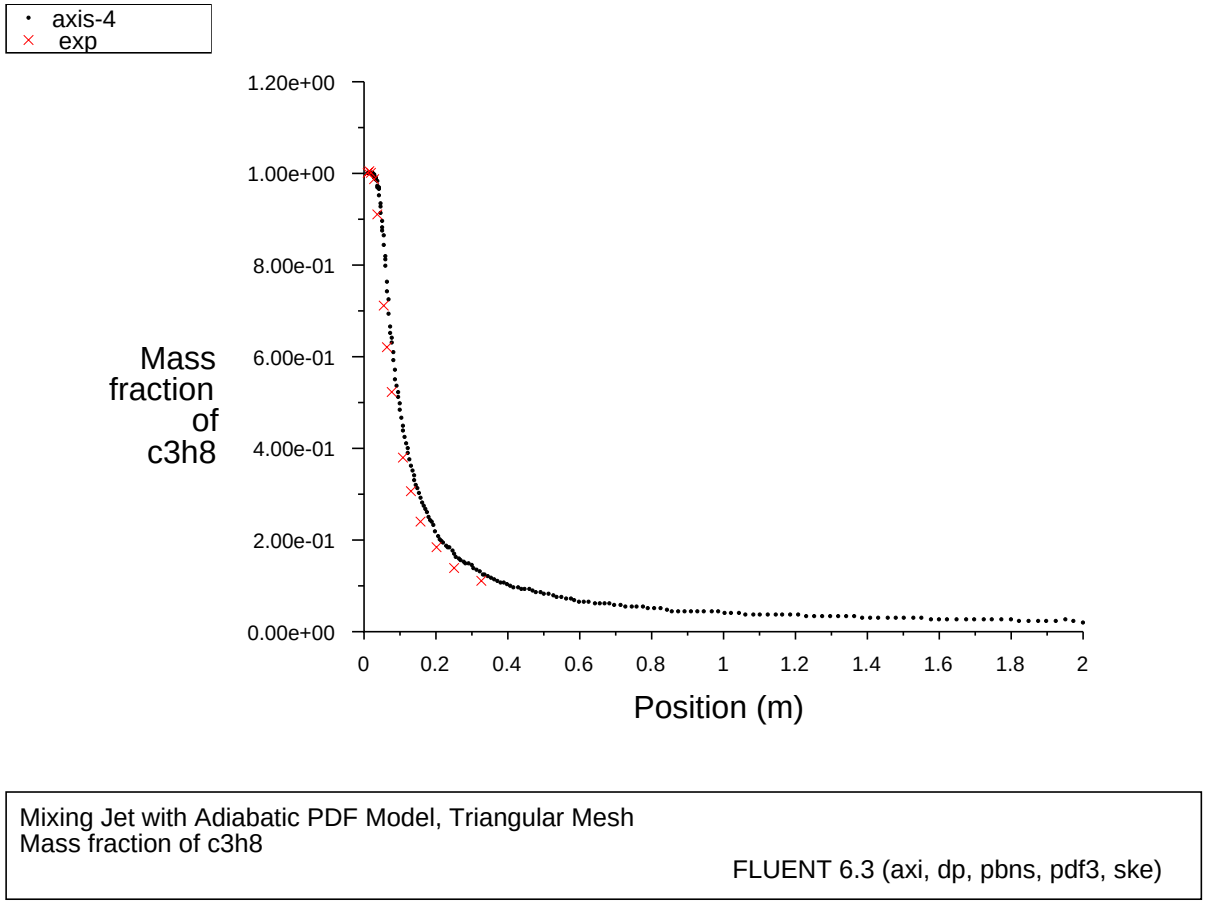

Figure 7.4.4: Mixture Fraction along the Symmetry Axis (Mixture Fraction/PDF Model, Triangular Mesh)

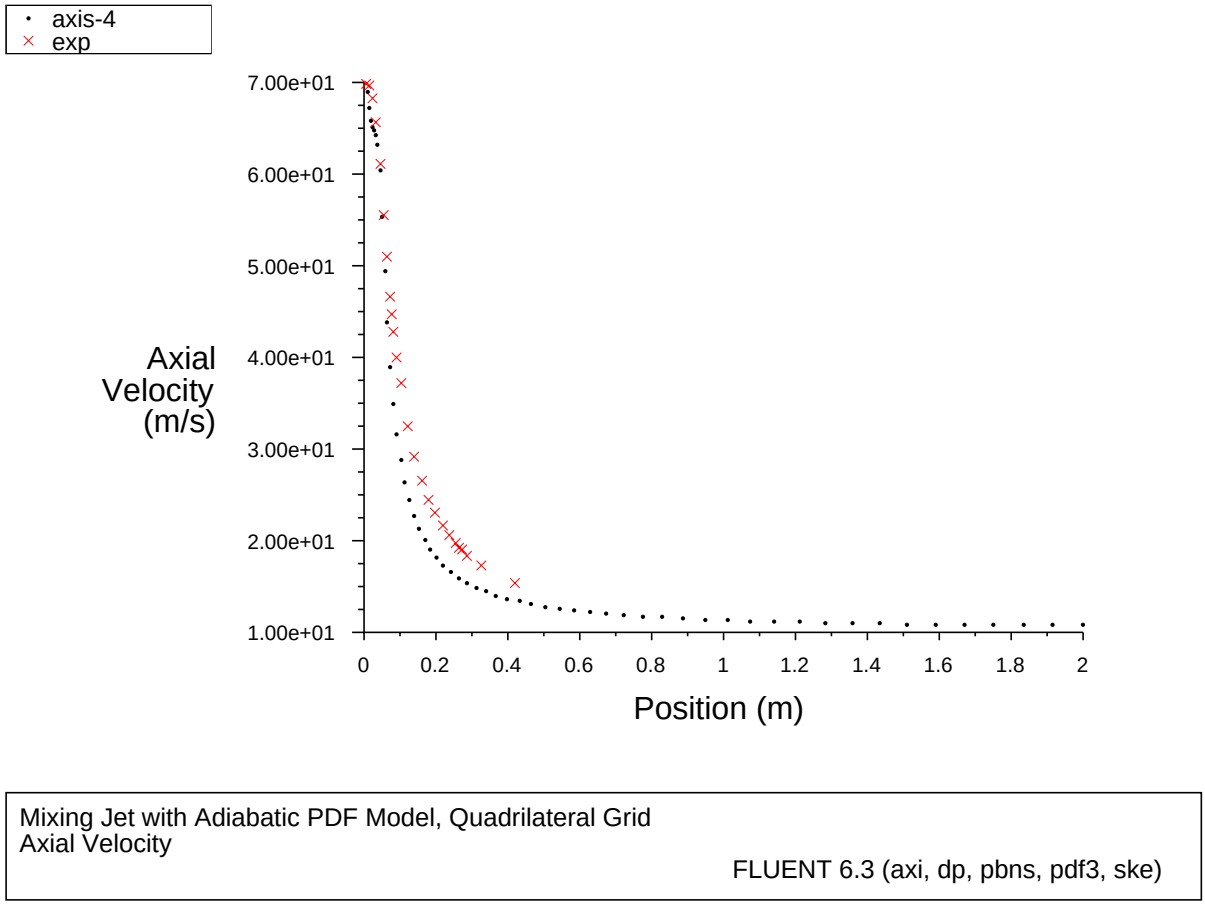

Figure 7.4.5: Axial Velocity along the Symmetry Axis (Mixture Fraction/PDF Model, Quadrilateral Mesh)

© Fluent Inc. August 8, 2006

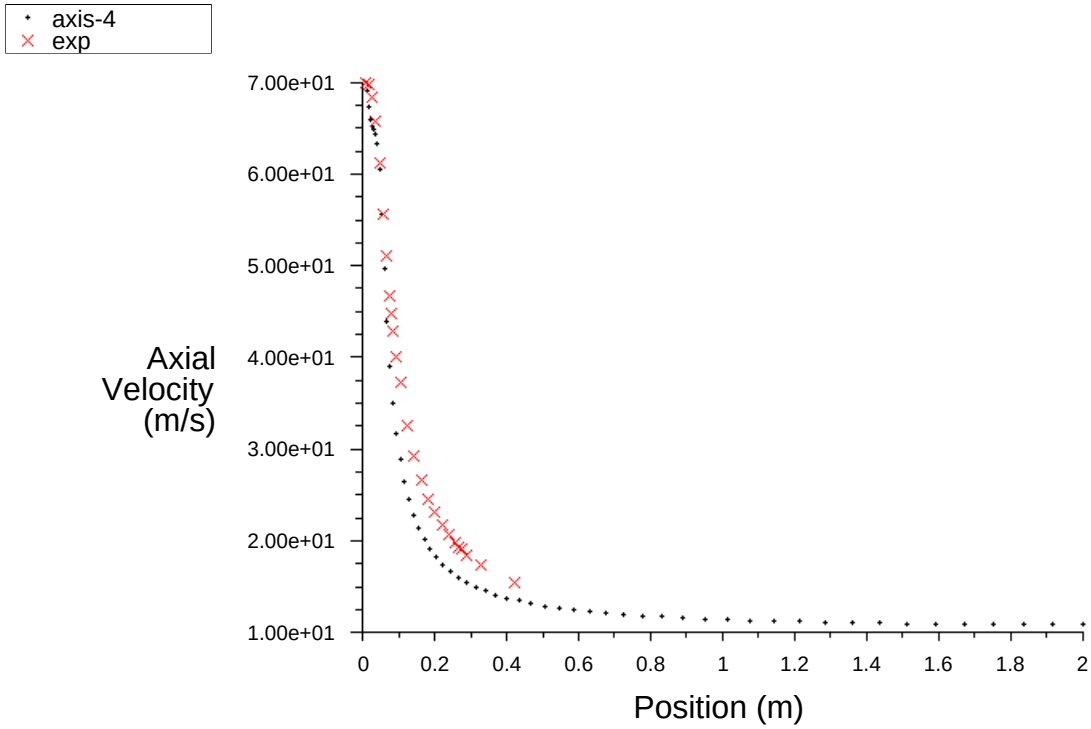

Mixing Jet with Non-Reacting Species, Quadrilateral Grid
Axial Velocity
FLUENT 6.3 (axi, dp, pbns, spe, ske)

Figure 7.4.6: Axial Velocity along the Symmetry Axis (Non-Reacting Species Transport Model, Quadrilateral Mesh)

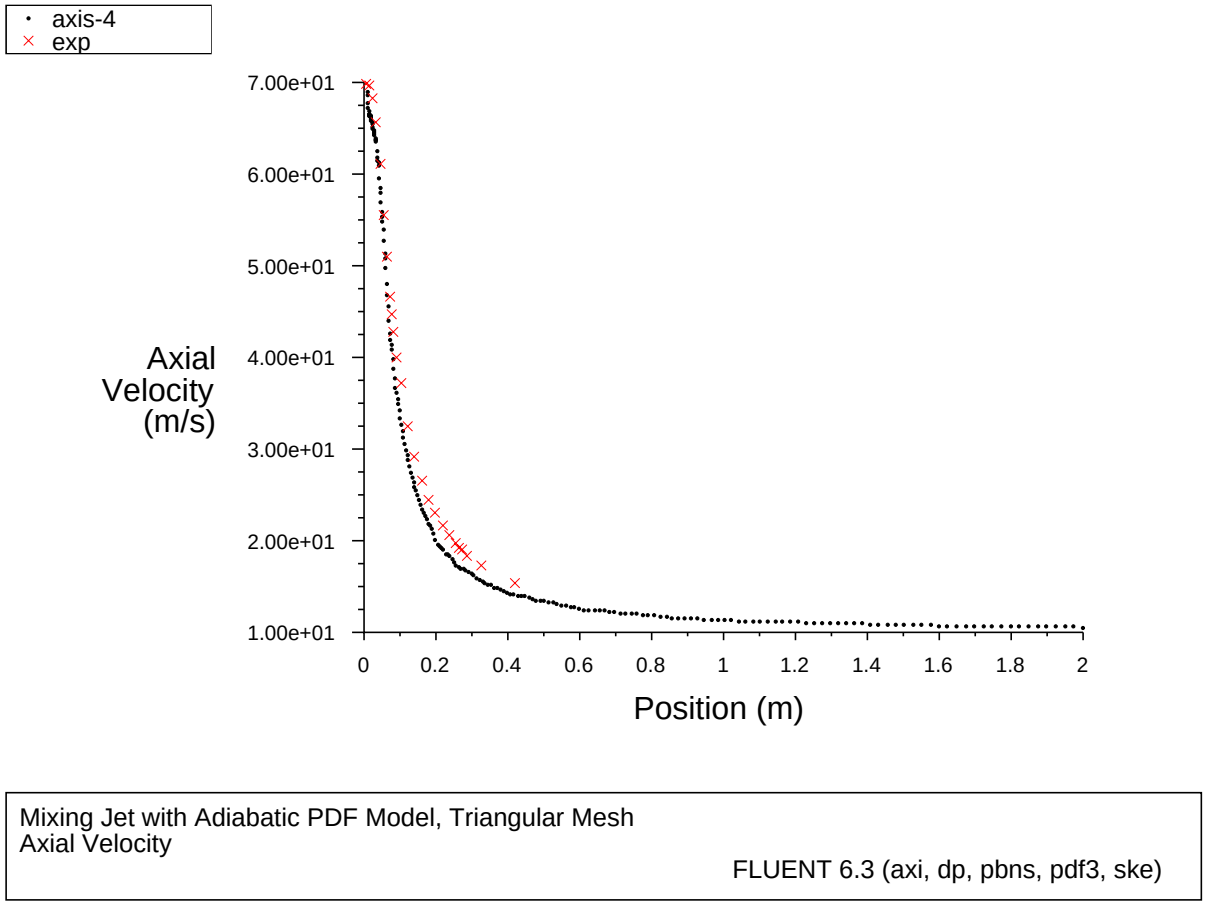

Figure 7.4.7: Axial Velocity along the Symmetry Axis (Mixture Fraction/PDF Model, Triangular Mesh)

© Fluent Inc. August 8, 2006

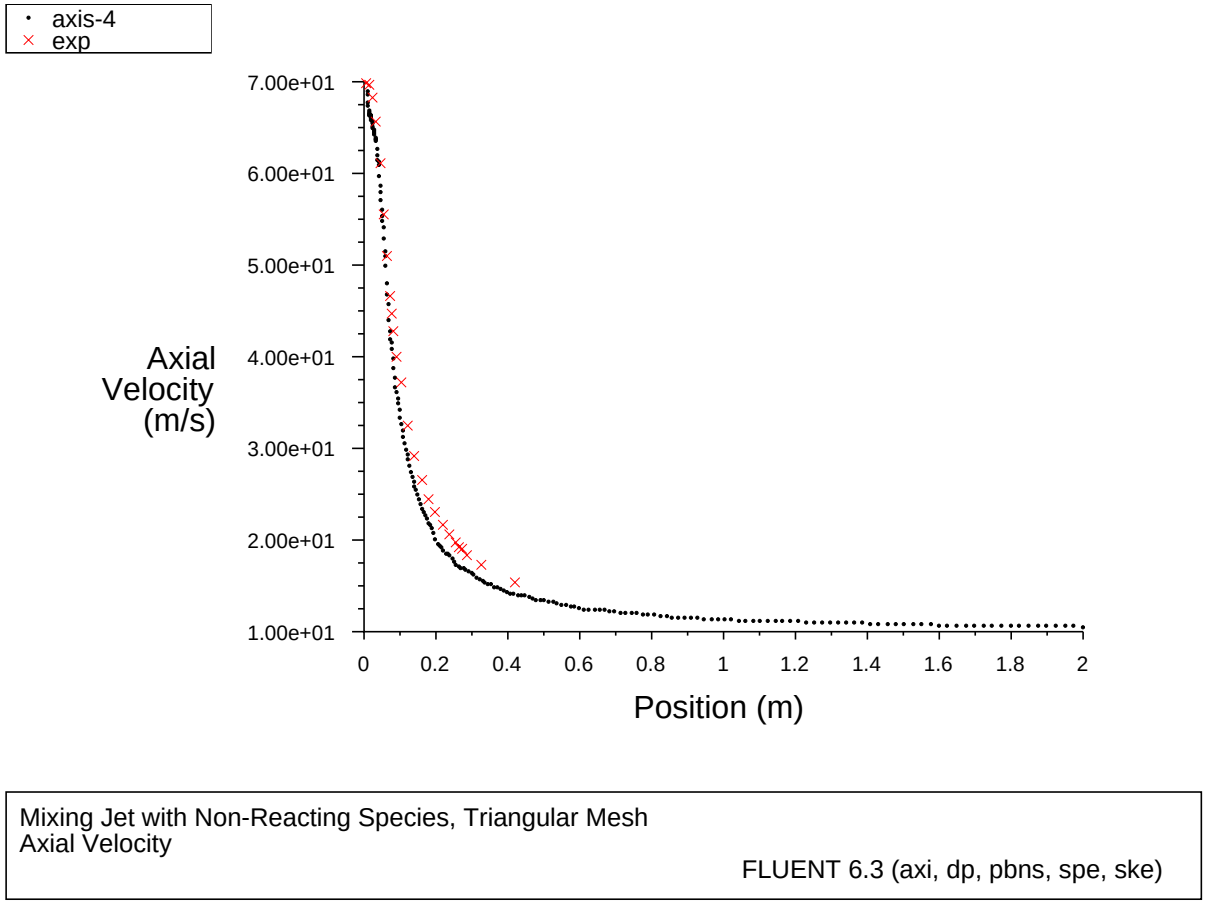

Figure 7.4.8: Axial Velocity along the Symmetry Axis (Non-Reacting Species Transport Model, Triangular Mesh)

© Fluent Inc. August 8, 2006

Validation 8. Non-Premixed Hydrogen/Air Flame

8.1 Purpose

The purpose of this validation is to compare FLUENT's predictions for the density and the axial velocity along the jet axis with the experimental data of [1]. The test uses the Finite-Rate/Eddy-Dissipation model and the Non-Premixed Combustion model with a quadrilateral mesh and a triangular mesh.

8.2 Problem Description

The flow considered is a hydrogen-argon turbulent round jet flowing in a coaxial air flow. The problem is axisymmetric. The air tunnel has a length $L = 2$ m and a diameter $D = 0.3385$ m. The inner diameter of the jet tube exit is $d = 5.2$ mm, and the outer diameter is $d' = 9.525$ mm. Figure 8.2.1 shows the geometry of the problem.

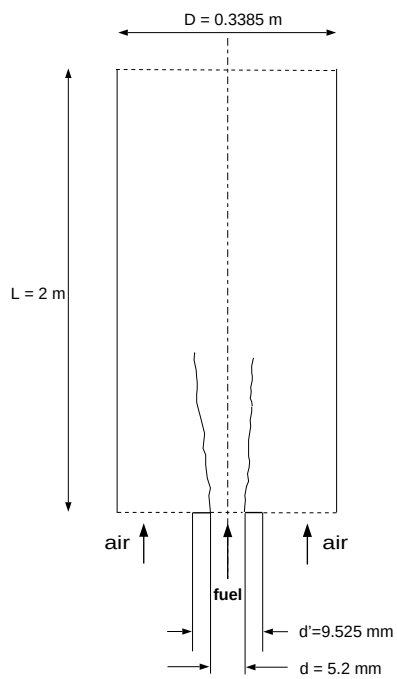

Figure 8.2.1: Problem Description

8.3 References

1. Strahle, W.C. and Lekoudis, S.G., *Evaluation of Data on Simple Turbulent Reacting Flows*, AFOSR TR-85 0880, School of Aerospace Engineering, Georgia Institute of Technology, Atlanta, GA.

8.4 Results

Figures compare FLUENT's results with the experimental data (density and axial velocity) as measured along the symmetry axis of the tunnel, downstream of the injector. The density drops downstream of the injector where the hydrogen is burnt. Further downstream, the density increases with the diffusion of the products.

8.4.1 Validation-Specific Information

Solver:	FLUENT 2d, axisymmetric
Version:	6.3.11
Solution Files:	1. `pdf_quad.cas`, `pdf_quad.dat` (+ `hydrogen.pdf`)
	2. `pdf_tri.cas`, `pdf_tri.dat` (+ `hydrogen.pdf`)
	3. `mag_quad.cas`, `mag_quad.dat`
	4. `mag_tri.cas`, `mag_tri.dat`

These solution files are available from the Fluent Inc. User Services Center as described in the Introduction.

© Fluent Inc. August 8, 2006

8.4.2 Plot Data

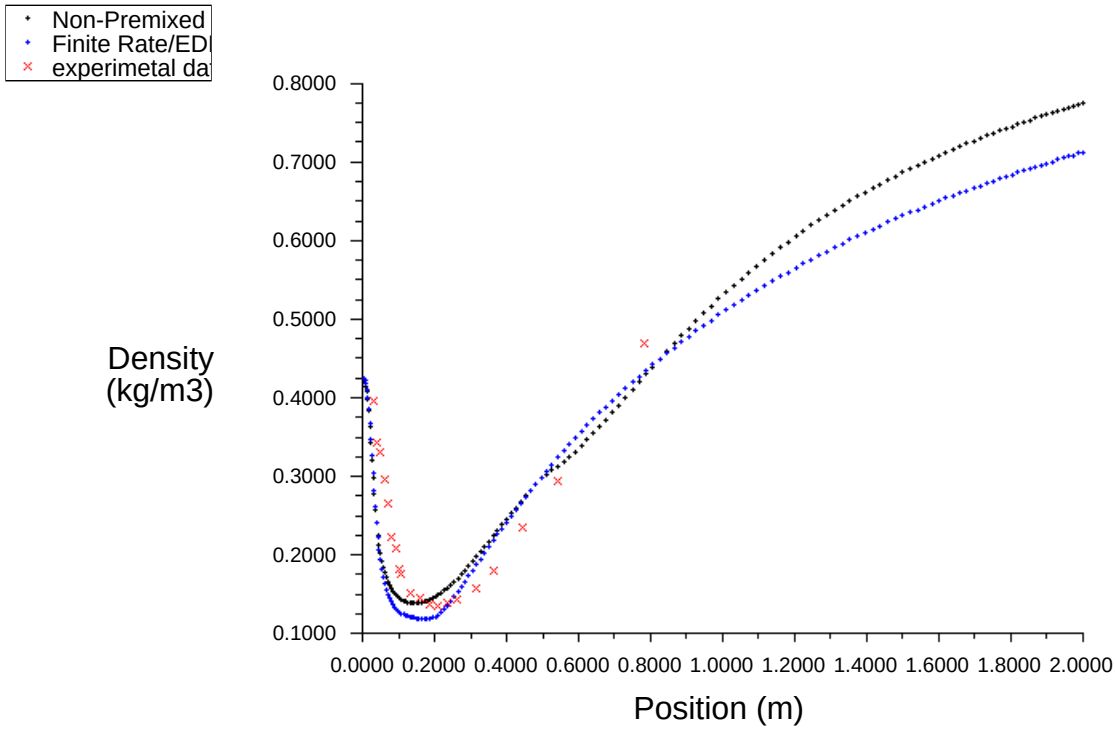

Hydrogen/Air Flame, Quad Grid
Density

FLUENT 6.3 (axi, dp, pbns, spe, ske)

Figure 8.4.1: Density along the Axis (Quadrilateral Grid)

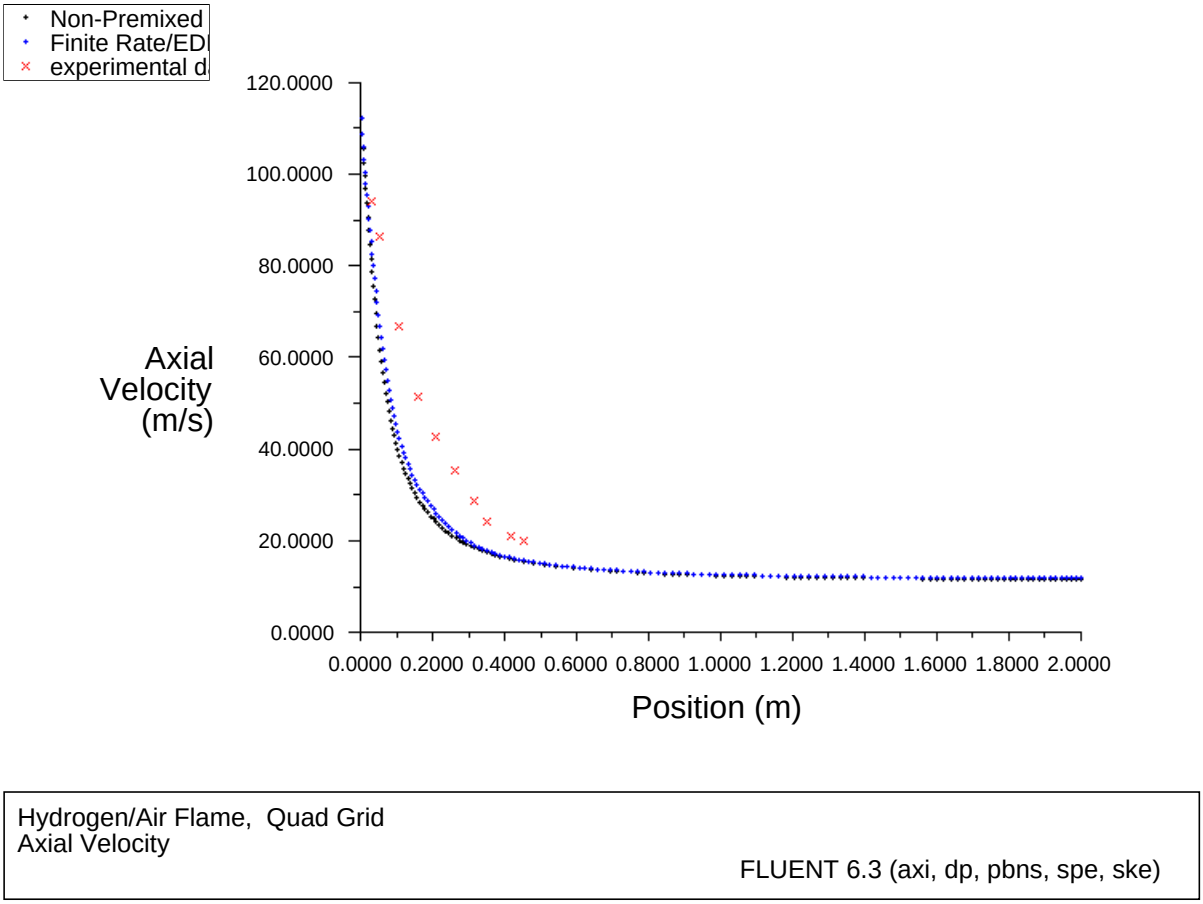

Figure 8.4.2: Axial Velocity along the Axis (Quadrilateral Grid)

© Fluent Inc. August 8, 2006

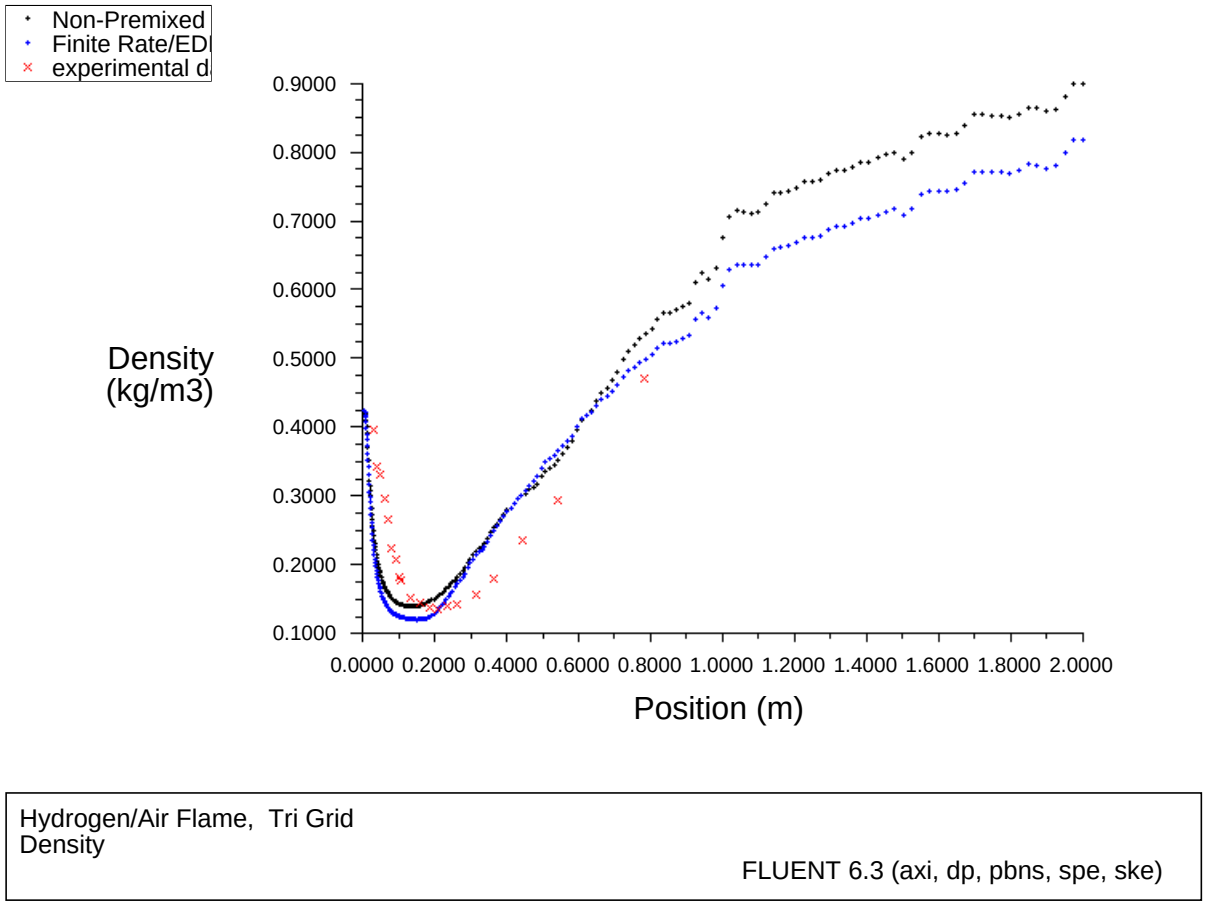

Figure 8.4.3: Density along the Axis (Triangular Grid)

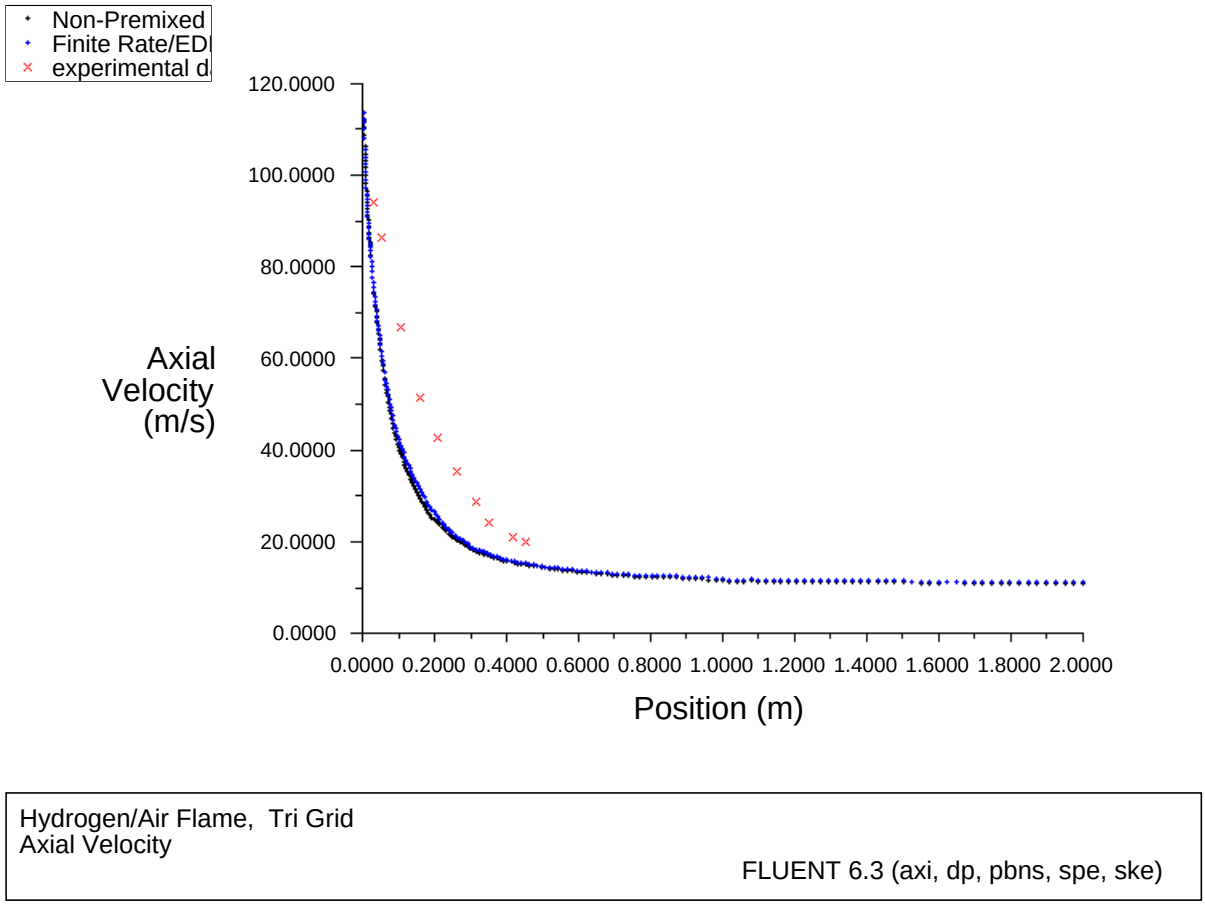

Figure 8.4.4: Axial Velocity along the Axis (Triangular Grid)

© Fluent Inc. August 8, 2006

Validation 9. Flow through an Engine Inlet Valve

9.1 Purpose

The purpose of this test is to compare the FLUENT prediction of the local velocity field against experimental data of Chen et al. [1].

9.2 Problem Description

A flow in an idealized engine cylinder with a straight inlet port and a valve lift of 10 mm (the distance from the top of the cylinder to the bottom of the valve) is examined in this case. The length of the cylinder is chosen to be large enough that it will not affect the flow in the cylinder. The configuration of the inlet port, valve, and cylinder is shown in Figure 9.2.1.

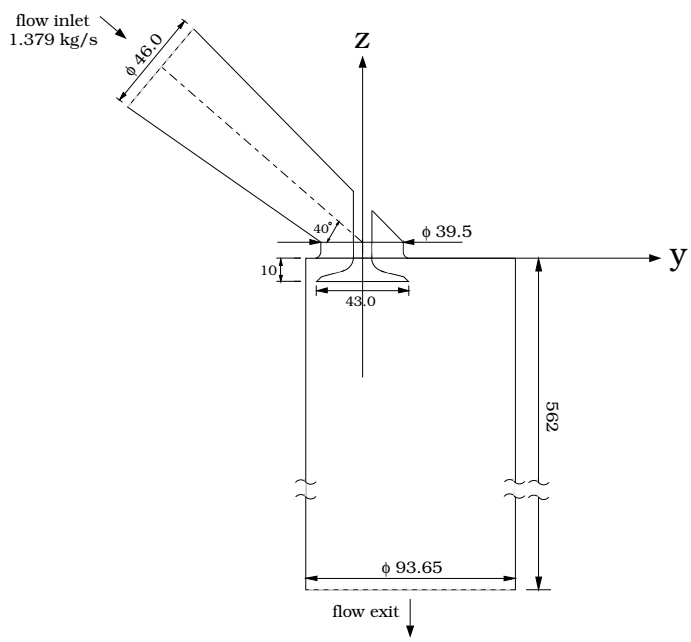

Figure 9.2.1: Problem Description (all dimensions in millimeters)

9.3 References

1. Chen, A., Lee, K.C., Yianneskis, M., and Ganti, G., Velocity Characteristics of Steady Flow Through a Straight Generic Inlet Port, *International Journal for Numerical Methods in Fluids*, 21:571–590, 1995.

9.4 Results

Figures compare FLUENT's results with the experimental data (z component of velocity at different heights). All the characteristics of the flow (the angle of the inlet jet, the vortices at the far right and the far left side of the cylinder, and the little vortex to the left of the valve) are correctly predicted by FLUENT.

9.4.1 Validation-Specific Information

Solver:	FLUENT 3d
Version:	6.3.11
Solution Files:	1. `valve10_r1.cas`, `valve10_r1.dat` - 1st order discretization
	2. `valve10_r2.cas`, `valve10_r2.dat` - 2nd order discretization
	3. `valve10_r3.cas`, `valve10_r3.dat` - adaption

These solution files are available from the Fluent Inc. User Services Center as described in the Introduction.

© Fluent Inc. August 8, 2006

9.4.2 Plot Data

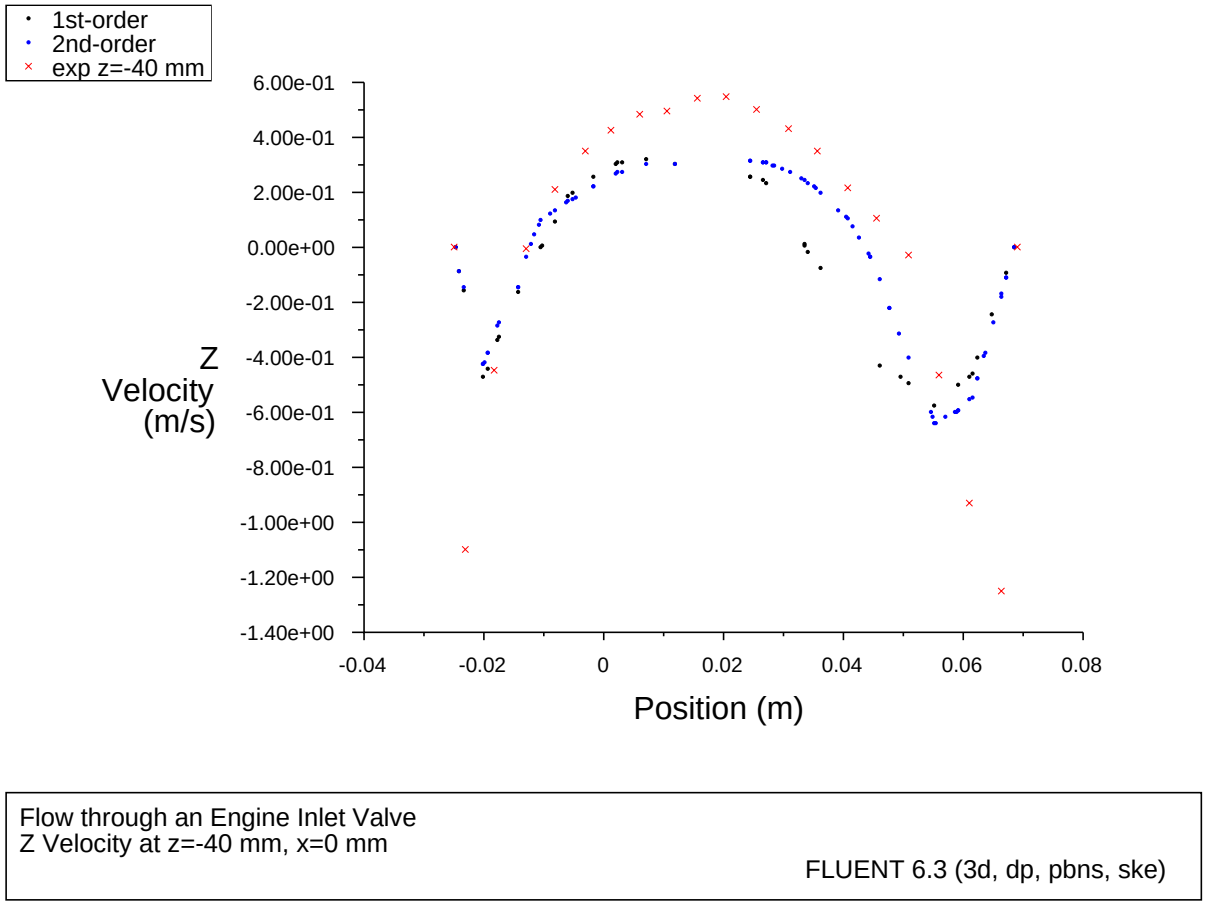

Figure 9.4.1: z-Velocity Components at $z = -40$ mm

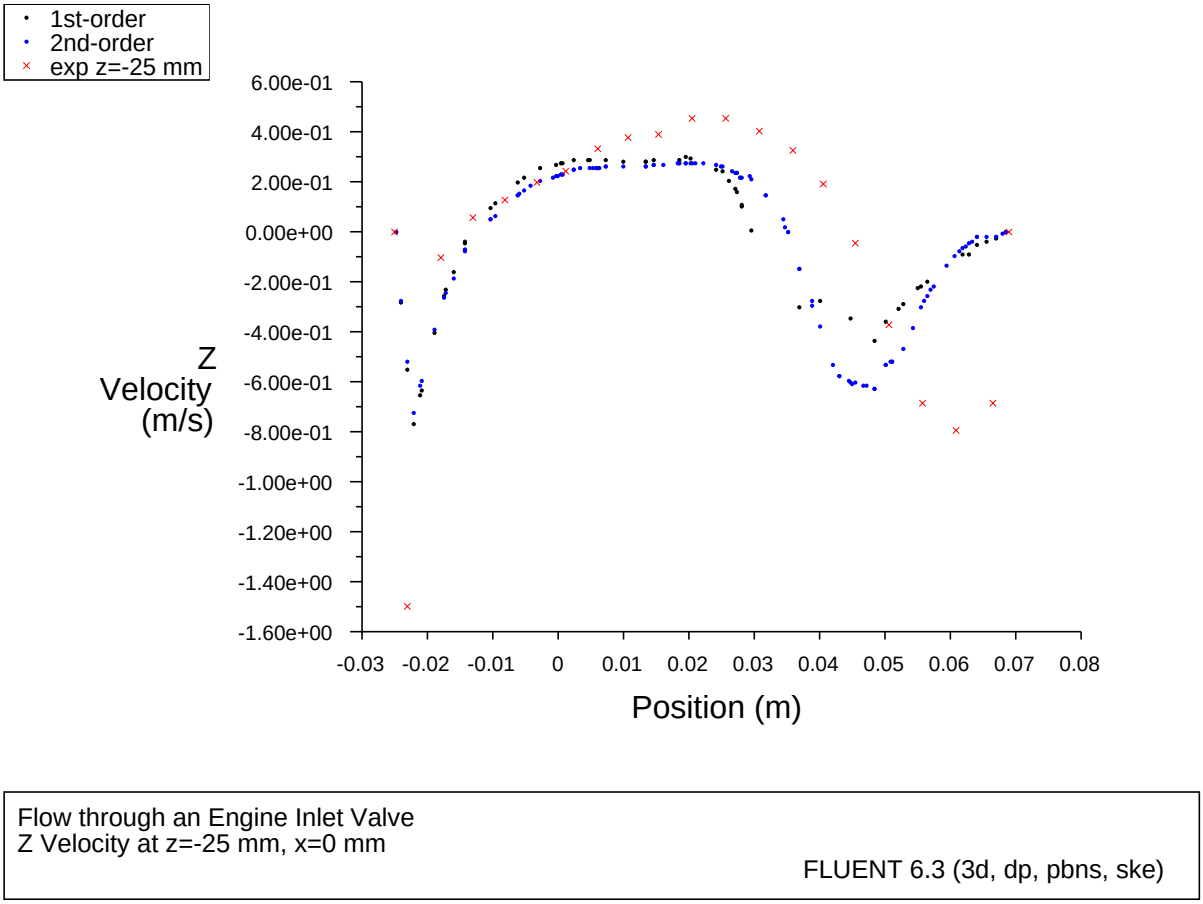

Figure 9.4.2: z-Velocity Components at $z = -25$ mm

© Fluent Inc. August 8, 2006

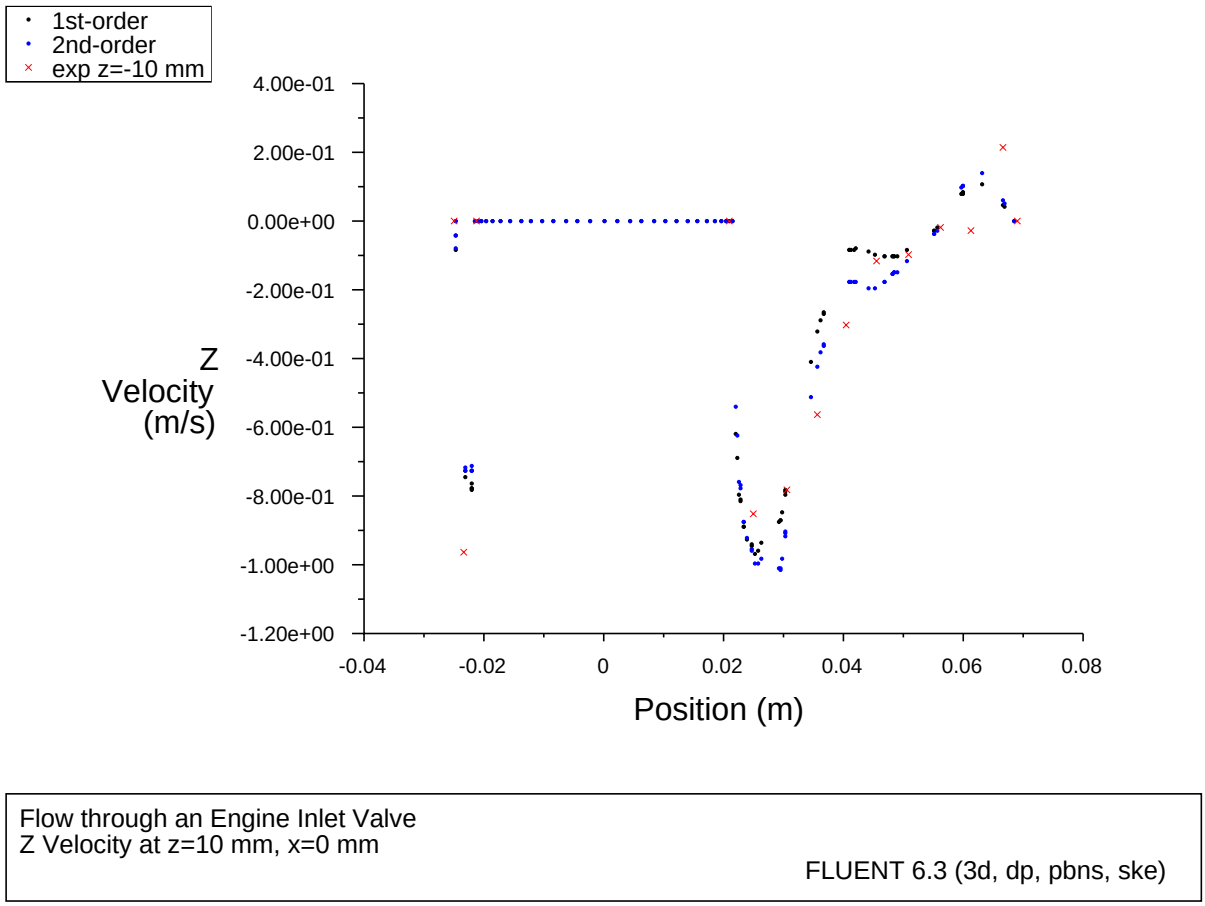

Figure 9.4.3: z-Velocity Components at $z = -10$ mm

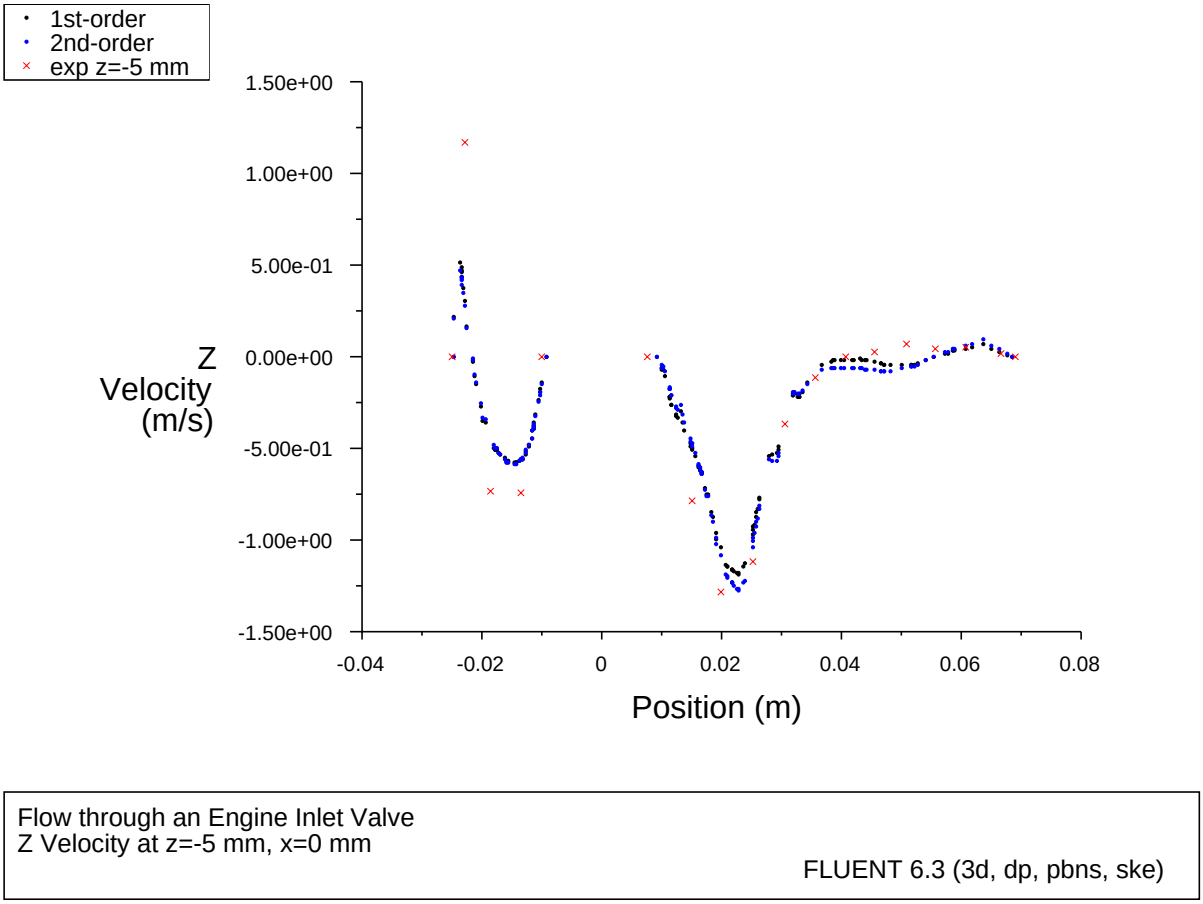

Figure 9.4.4: z-Velocity Components at $z = -5$ mm

© Fluent Inc. August 8, 2006

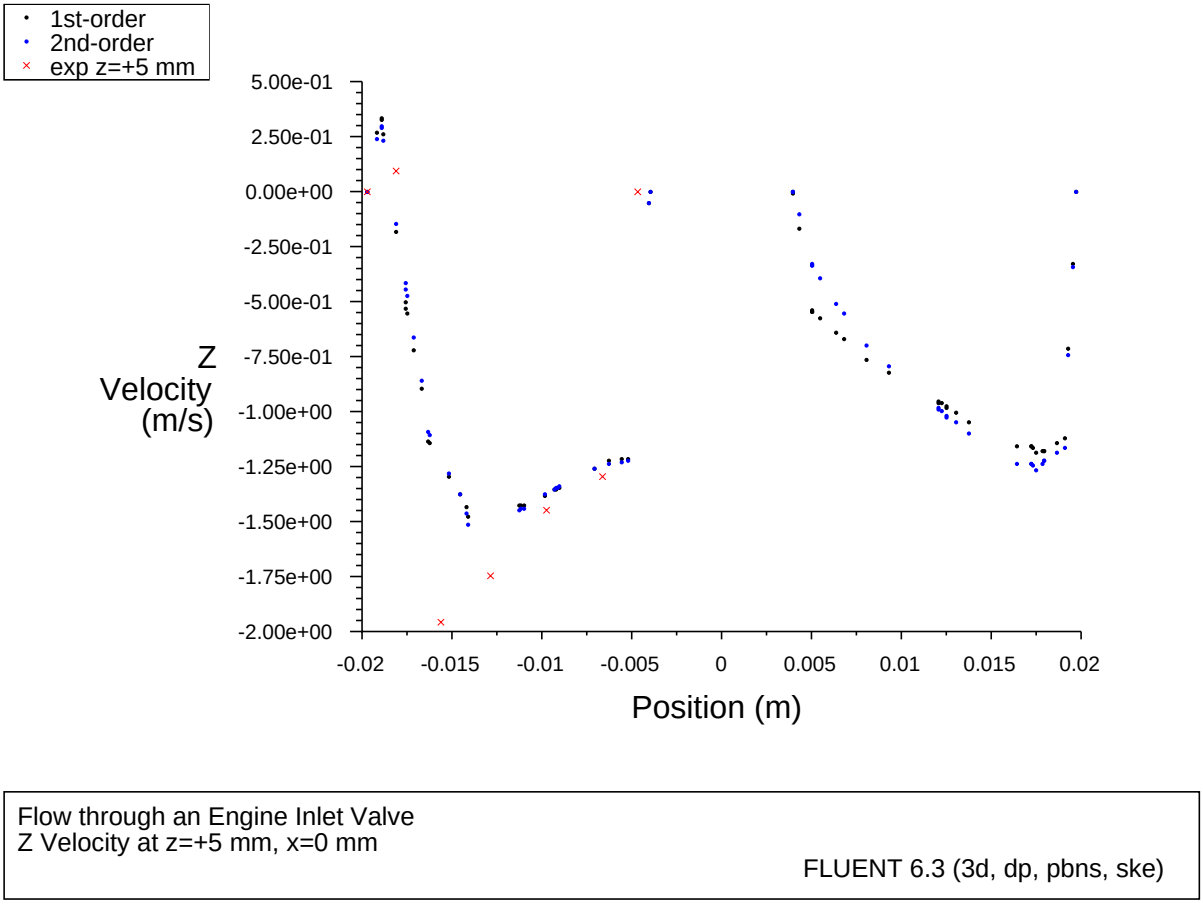

Figure 9.4.5: z-Velocity Components at $z = +5$ mm

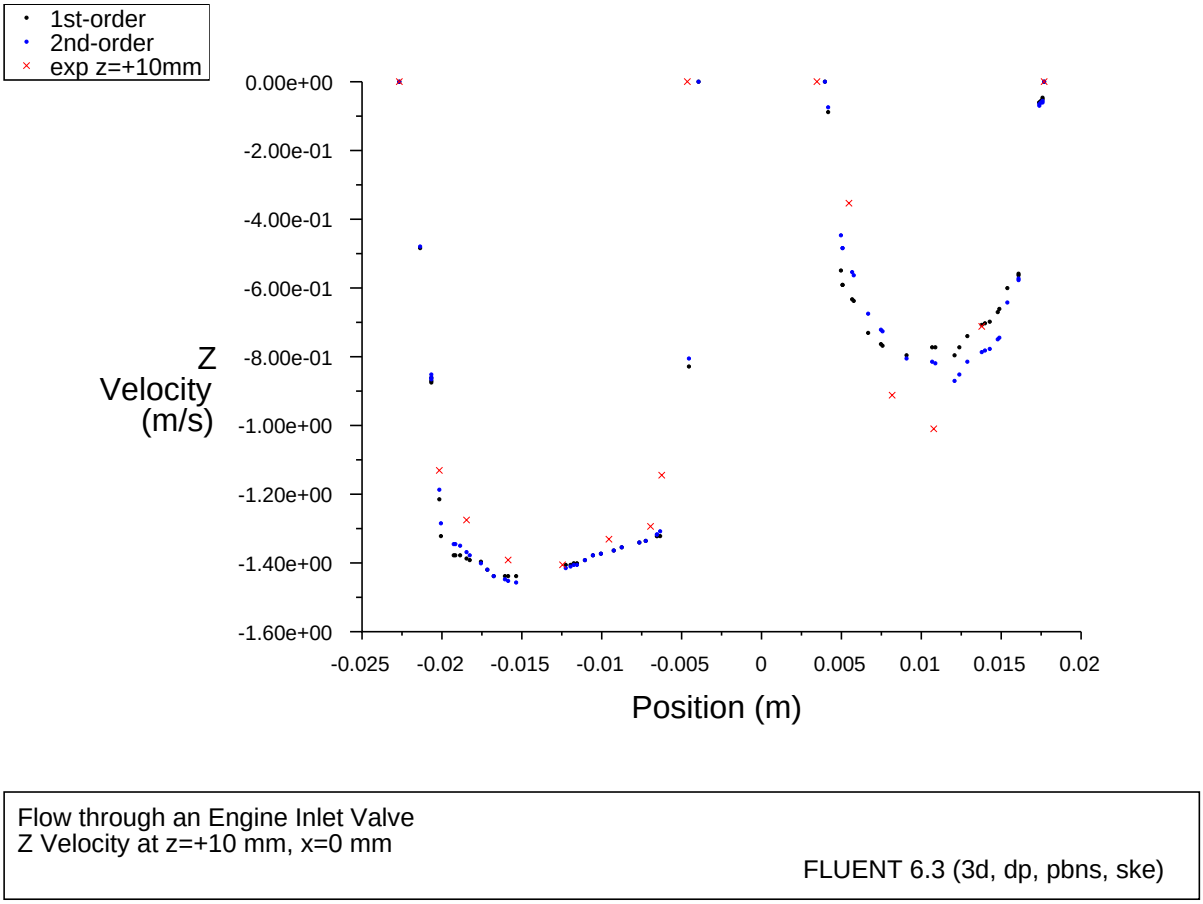

Figure 9.4.6: z-Velocity Components at $z = +10$ mm

© Fluent Inc. August 8, 2006

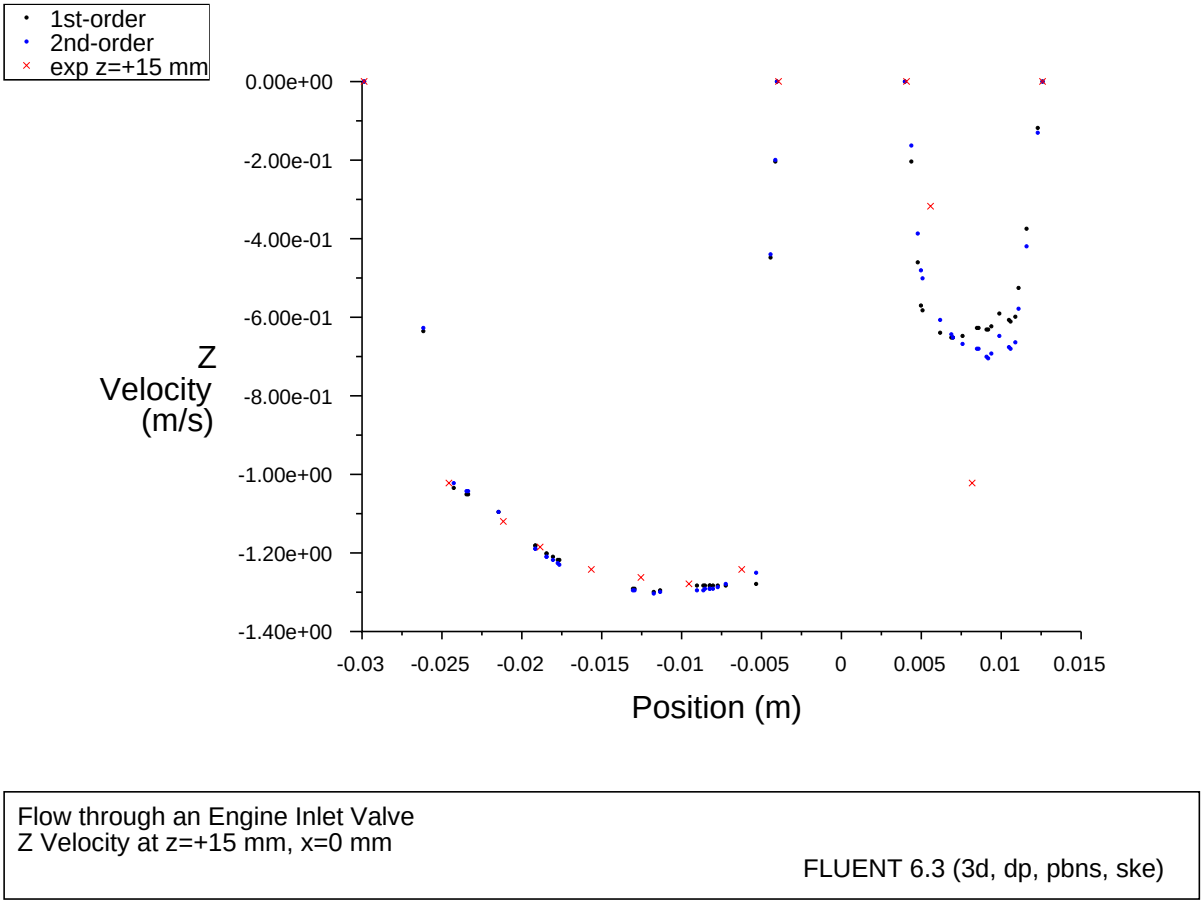

Figure 9.4.7: z-Velocity Components at $z = +15$ mm

© Fluent Inc. August 8, 2006

Validation 10. Turbulent Flow in a Transition Duct

10.1 Purpose

The purpose of this test is to assess the ability of FLUENT to reproduce the complicated three-dimensional features of a flow in a circular to rectangular transition duct. FLUENT predictions for the following quantities are compared with the experimental data of Davis and Gessner [1]:

1. Distribution of pressure coefficient, C_p, and skin friction coefficient, C_f, at two different cross-sections along the duct wall as a function of the non-dimensional girth length
2. Distribution of static pressure coefficient along the centerline

10.2 Problem Description

The problem under consideration involves a flow through a circular-to-rectangular transition duct having the same inlet and outlet cross-sectional areas. The curvature of the duct walls induces a strong pressure-driven crossflow that develops into a counter-rotating vortex pair near the short side walls of the duct. This vortex pair significantly distorts both the primary mean velocity and the Reynolds stress fields. Taking into account the symmetry of the flow field, only one fourth of the duct is modeled (as shown in Figure 10.2.1). Station 5 and Station 6 are the cross-sections at $x/\rho = 4$ and $x/\rho = 8$, respectively, where ρ is the inlet radius and x is the axial direction ($x/\rho = -1$ at the inlet, and $x/\rho = 16$ at the outlet).

10.3 References

1. Davis, D.O., and Gessner, F.B., Experimental Investigation of Turbulent Flow Through a Circular-to-Rectangular Transition Duct, *AIAA Journal*, 30(2):367–375, 1992.

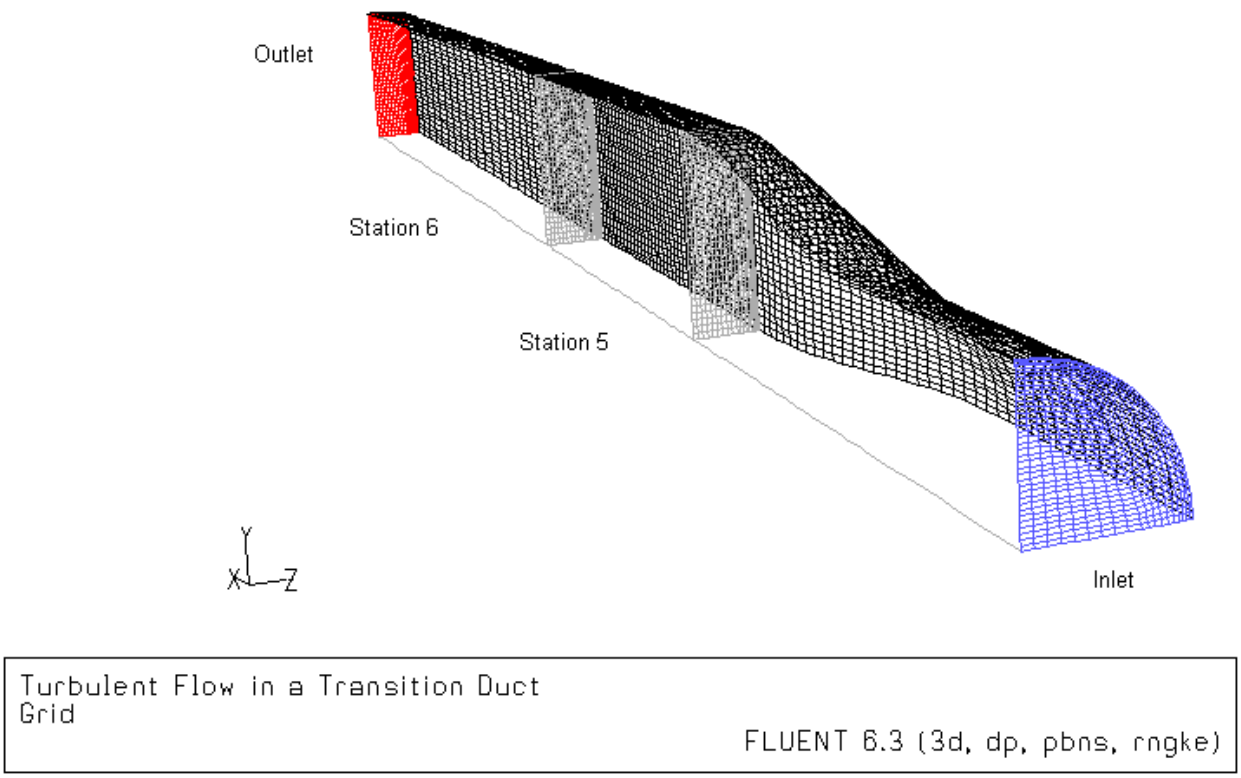

Figure 10.2.1: Problem Grid

© Fluent Inc. August 8, 2006

10.4 Results

Figures show comparison of the following profiles for all three turbulence models:

1. Pressure coefficient, C_p, and skin friction coefficient, C_f, at two different cross-sections along the duct wall as a function of the non-dimensional girth length.

   In the XY plots, the data is plotted against projected quarter of the duct boundary, where a position of 0 m corresponds to the center of the longer side of the duct, and a position of 1 m corresponds to the center of the shorter side.

2. Static pressure coefficient along the centerline.

10.4.1 Validation-Specific Information

Solver:	FLUENT 3d, 3ddp
Version:	6.3.11
Solution Files:	1. `hex_std-ke_r1.cas`, `hex_std-ke_r1.dat` - Standard k-ε
	2. `hex_rng-ke_r2.cas`, `hex_rng-ke_r2.dat` - RNG k-ε
	3. `hex_rsm_r3.cas`, `hex_rsm_r3.dat` - RSM

These solution files are available from the Fluent Inc. User Services Center as described in the Introduction.

10.4.2 Plot Data

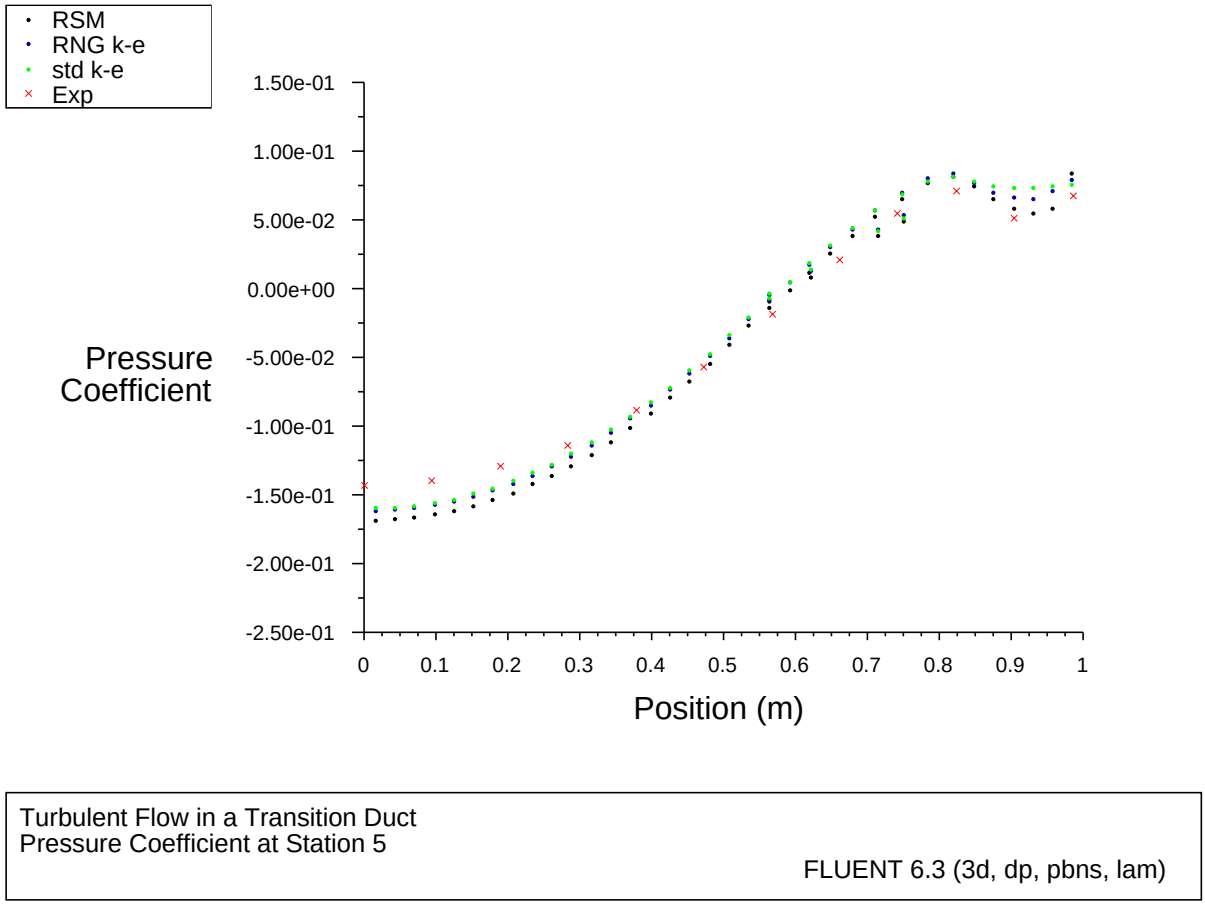

Figure 10.4.1: Comparison of Wall Pressure Coefficient at Station 5

© Fluent Inc. August 8, 2006

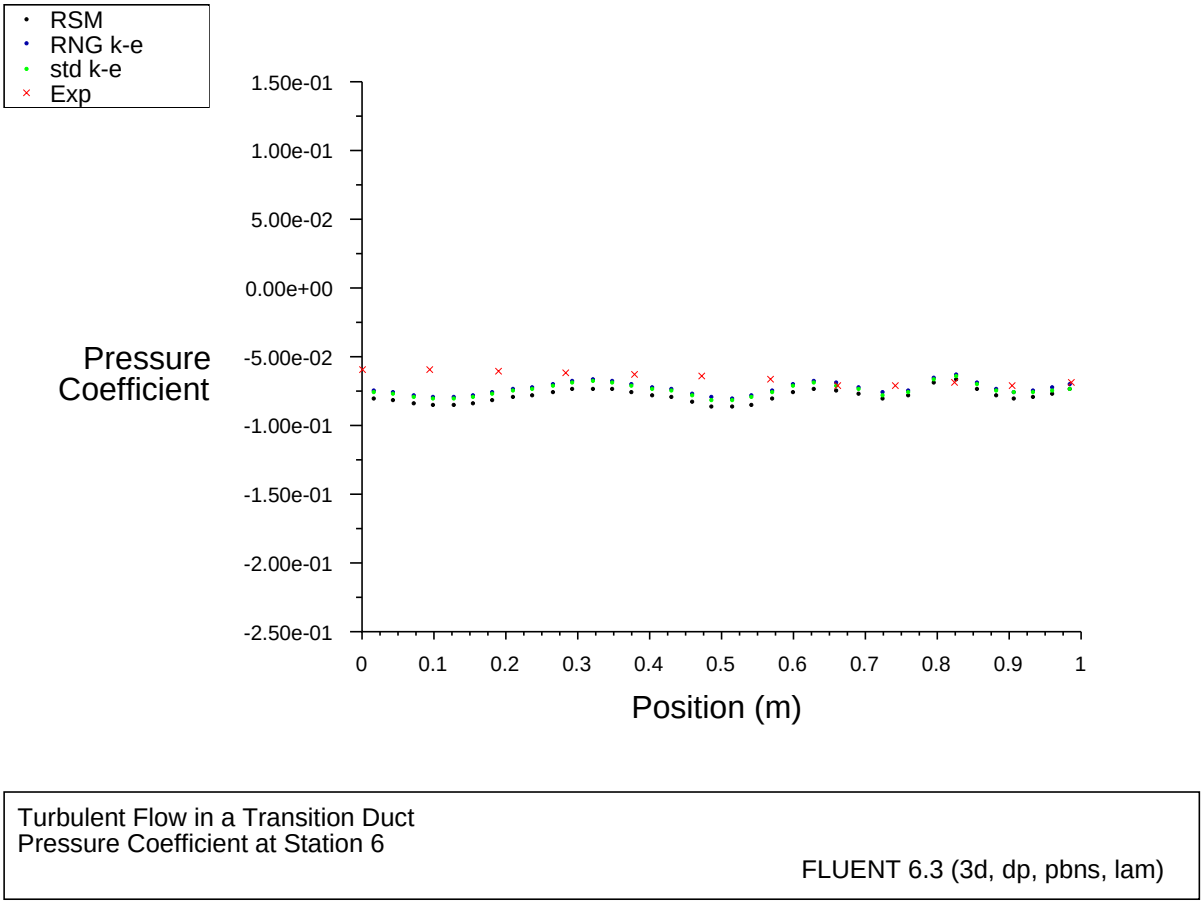

Figure 10.4.2: Comparison of Wall Pressure Coefficient at Station 6

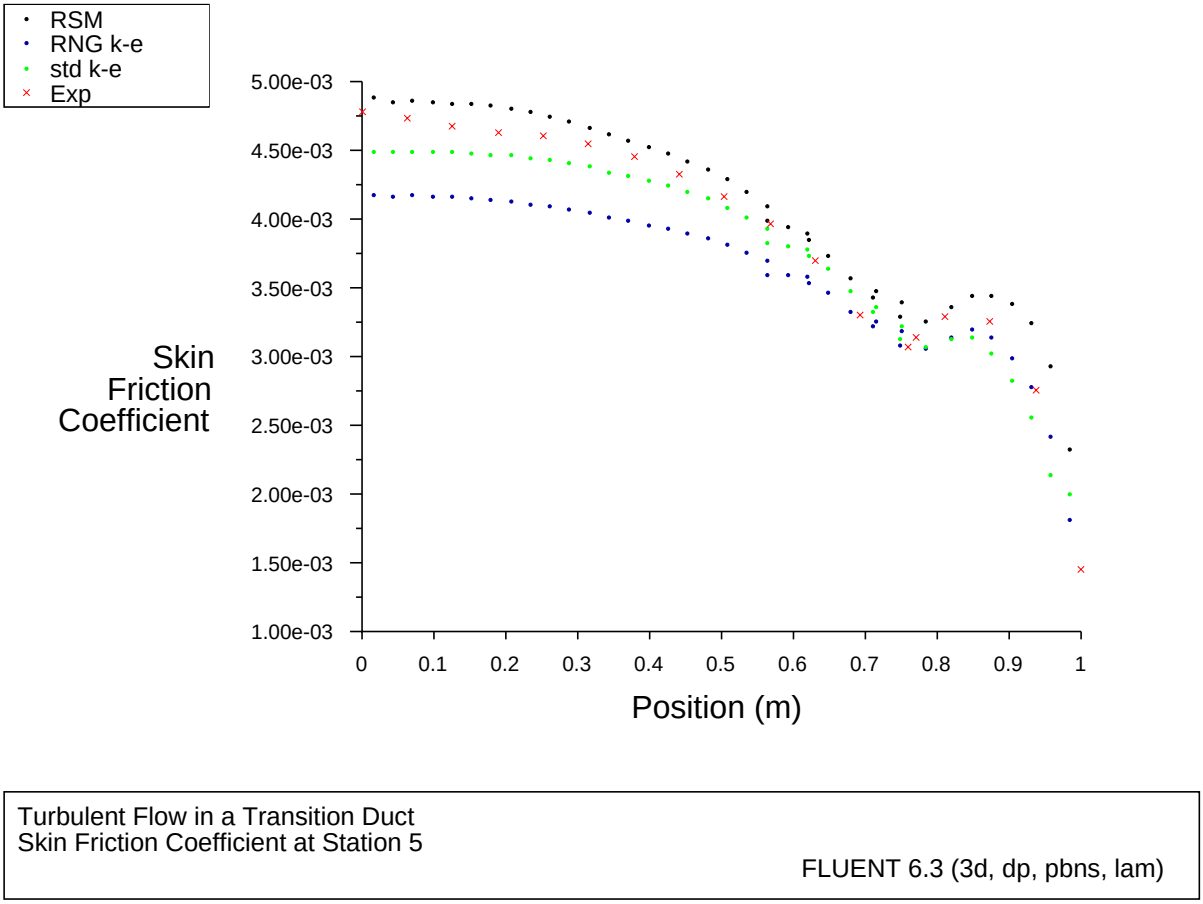

Figure 10.4.3: Comparison of Skin Friction Coefficient at Station 5

© Fluent Inc. August 8, 2006

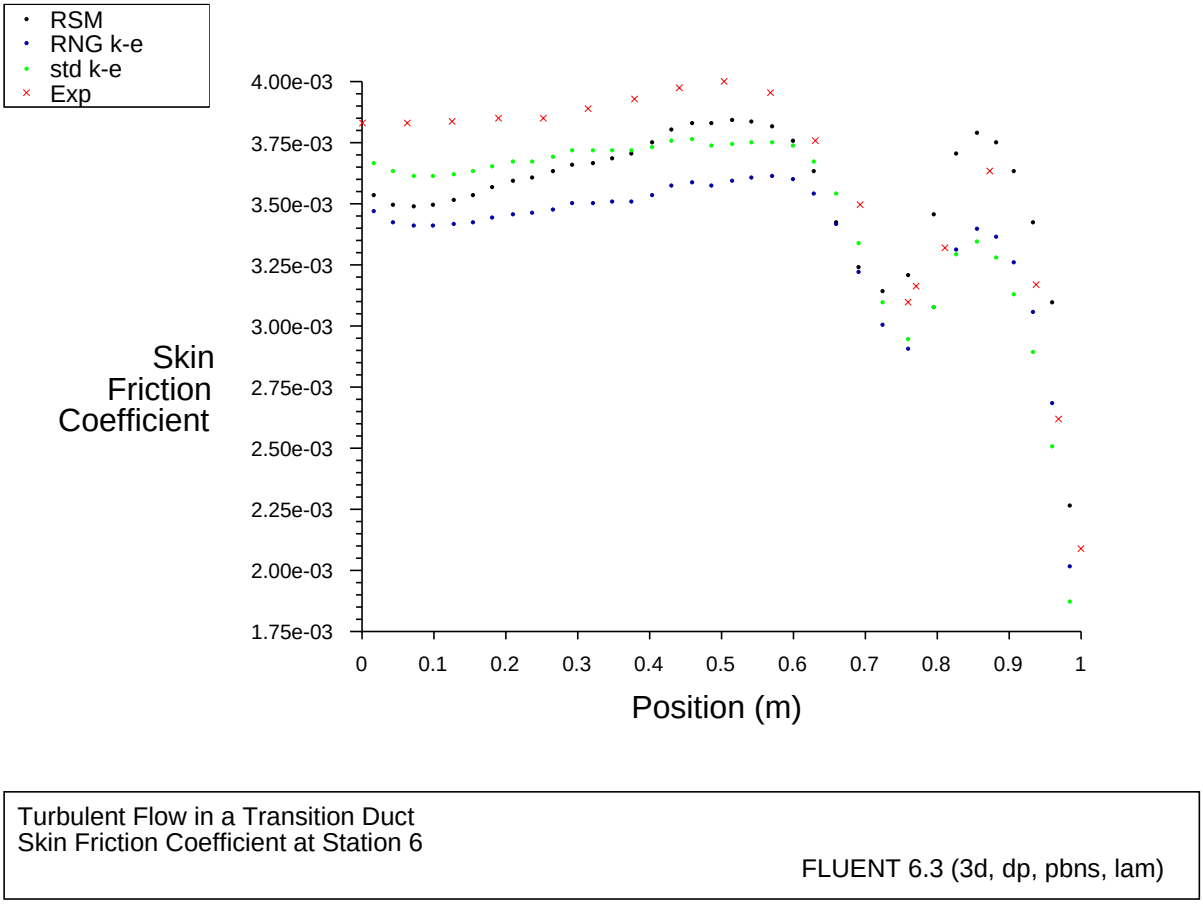

Figure 10.4.4: Comparison of Skin Friction Coefficient at Station 6

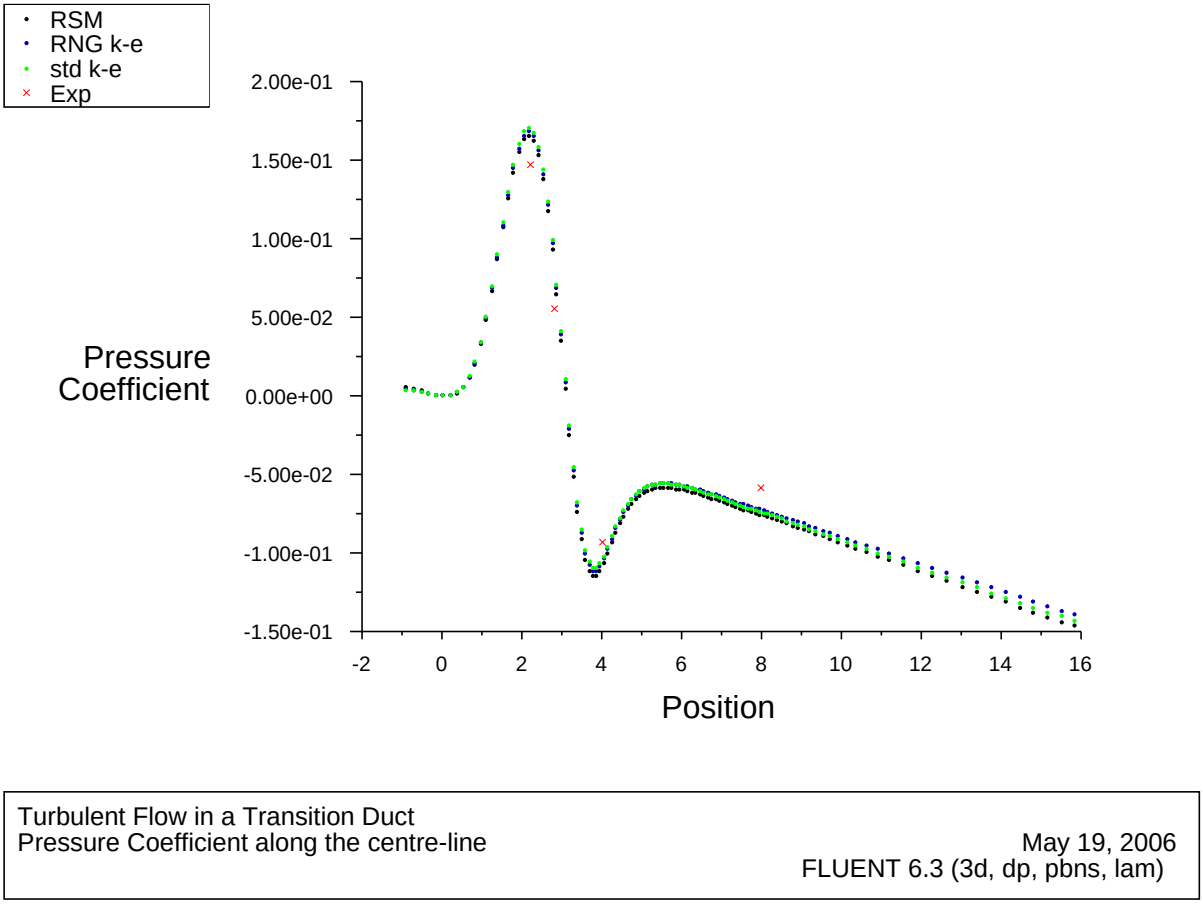

Figure 10.4.5: Comparison of Pressure Coefficient Along the Centerline

© Fluent Inc. August 8, 2006

Validation 11. Transonic Flow Over an RAE 2822 Airfoil

11.1 Purpose

The purpose of this validation is to compare the predictions of FLUENT with the experimental data of Cook et al. [1] for flow over an RAE 2822 airfoil. The quantities examined are:

1. Static pressure coefficient, C_p.
2. Lift and drag coefficients.
3. Shock position on the airfoil.

11.2 Problem Description

The problem under consideration involves flow over an RAE 2822 airfoil at a free-stream Mach number of 0.73. The angle of attack is 3.19 degrees, which corresponds to case 9 in the experimental data of Cook et al. [1]. Since the calculations were done in free-stream conditions, the angle of attack has been modified to account for the wind-tunnel wall effects. An angle of attack equal to 2.79 degrees was used in the calculations, as suggested by Coakley [2].

The geometry of the RAE 2822 airfoil is shown in Figure 11.2.1. It is a thick airfoil with a chord length, c, of 1.00 m and a maximum thickness, d, of 0.121 m. The domain extends $55c$ from the airfoil, so that the presence of the airfoil is not felt at the outer boundary.

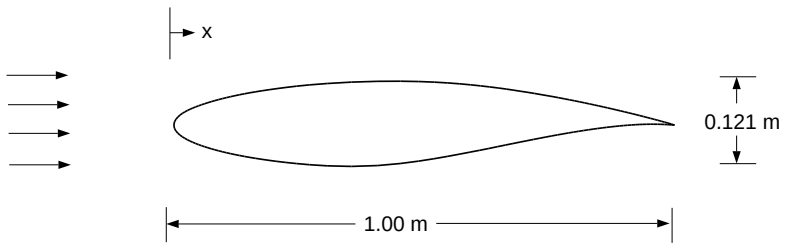

Mach Number = 0.73
Re = 6.5 x 10^6
Angle of Attack = 2.79 degrees
Static Pressure = 43765 Pa
Inlet Temperature = 300 K
Turbulent Intensity = 0.05%
Turbulent Viscosity Ratio = 10

Figure 11.2.1: Geometry of the RAE 2822 Airfoil

© Fluent Inc. August 8, 2006

11.3 References

1. Cook, P.H., McDonald, M.A., and Firmin, M.C.P., *AEROFOIL RAE 2822 Pressure Distribution and Boundary Layer and Wake Measurements*, AGARD Advisory Report No. 138, 1979.

2. Thomas J. Coakley., Numerical Simulation of Viscous Transonic Airfoil Flows, AIAA 25th Aerospace Sciences Meeting, 1987.

11.4 Results

A comparison of FLUENT's predictions of the static pressure coefficient C_p with experimental data has been done for a hybrid and a quadrilateral mesh. In general, FLUENT's predictions agree well with the experimental data.

The shock location over the airfoil is quantified as the location where the top surface pressure coefficient increases rapidly. Table 11.4.1 compares the numerical predictions of the shock location, the lift coefficients, and the drag coefficients with the experimental values.

Table 11.4.1: Comparison of the Predictions of Lift and Drag Coefficients, and Shock Location

Mesh	**Model**	**Lift (C_L)**	**Drag (C_D)**	**Shock (x/c)**
	Experiment	0.803	0.0168	0.52
Hybrid	Realizable k-ϵ	0.825	0.0181	0.52
	SST k-ω	0.781	0.0164	0.50
	Spalart-Allmaras	0.815	0.0171	0.52
Quadrilateral	Realizable k-ϵ	0.828	0.0181	0.52
	SST k-ω	0.782	0.0163	0.50
	Spalart-Allmaras	0.817	0.0170	0.52

From Table 11.4.1, the predicted shock locations and lift coefficients are predicted within 4% of the experimental results, and the drag coefficients are predicted within 8% of the experimental results for all six runs.

11.4.1 Validation-Specific Information

Solver:	FLUENT 2ddp
Version:	6.3.19
Solution Files:	1. `rae_hybrid_rke_nb.cas`, `rae_hybrid_rke_nb.dat` 2. `rae_hybrid_sst_nb.cas`, `rae_hybrid_sst_nb.dat` 3. `rae_hybrid_sa_nb.cas`, `rae_hybrid_sa_nb.dat` 4. `rae_quad_rke.cas`, `rae_quad_rke.dat` 5. `rae_quad_sst.cas`, `rae_quad_sst.dat` 6. `rae_quad_sa.cas`, `rae_quad_sa.dat`

These solution files are available from the Fluent Inc. User Services Center as described in the Introduction.

© Fluent Inc. August 8, 2006

11.4.2 Plot Data

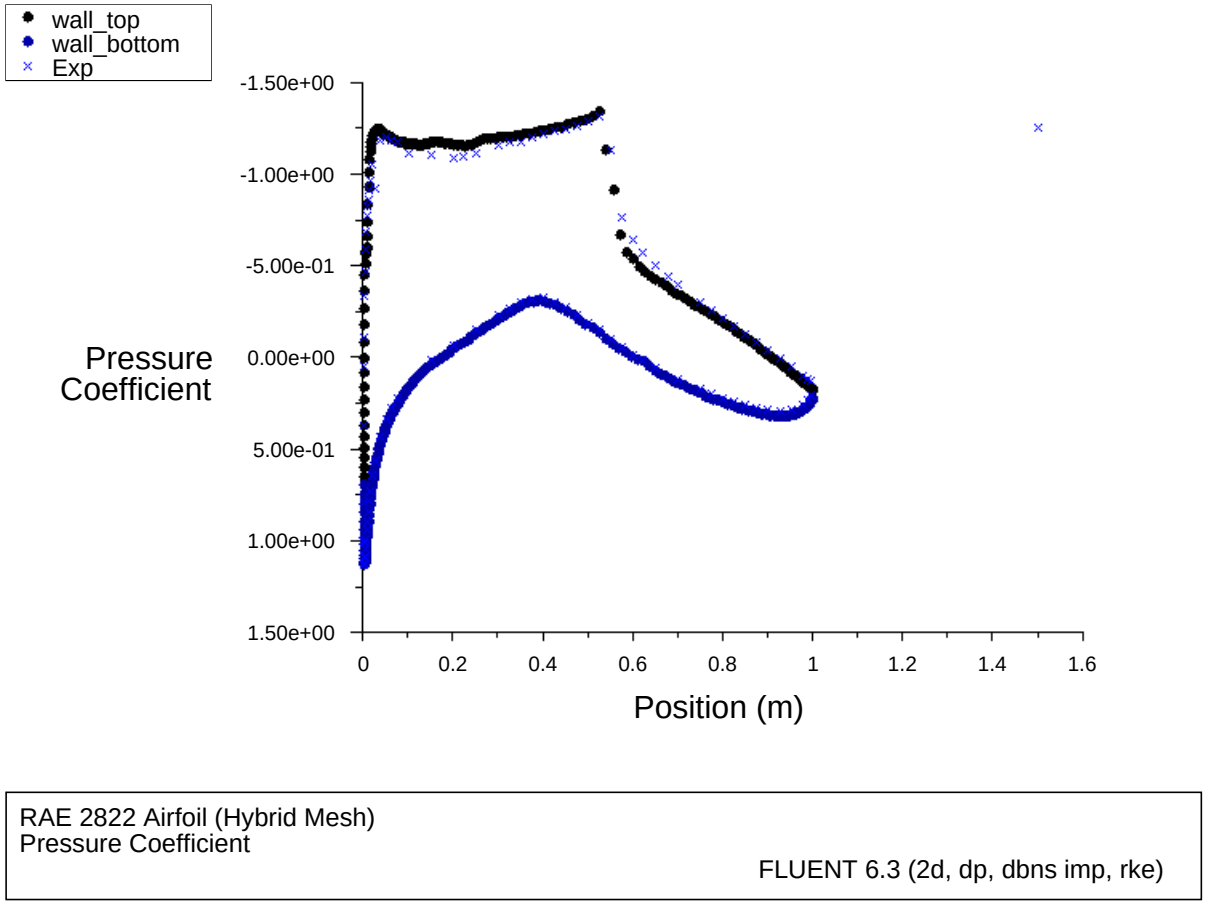

Figure 11.4.1: Comparison of FLUENT's Predictions of the Static Pressure Coefficient C_p With the Experimental Data for the Hybrid Mesh, Realizable k-ϵ Case

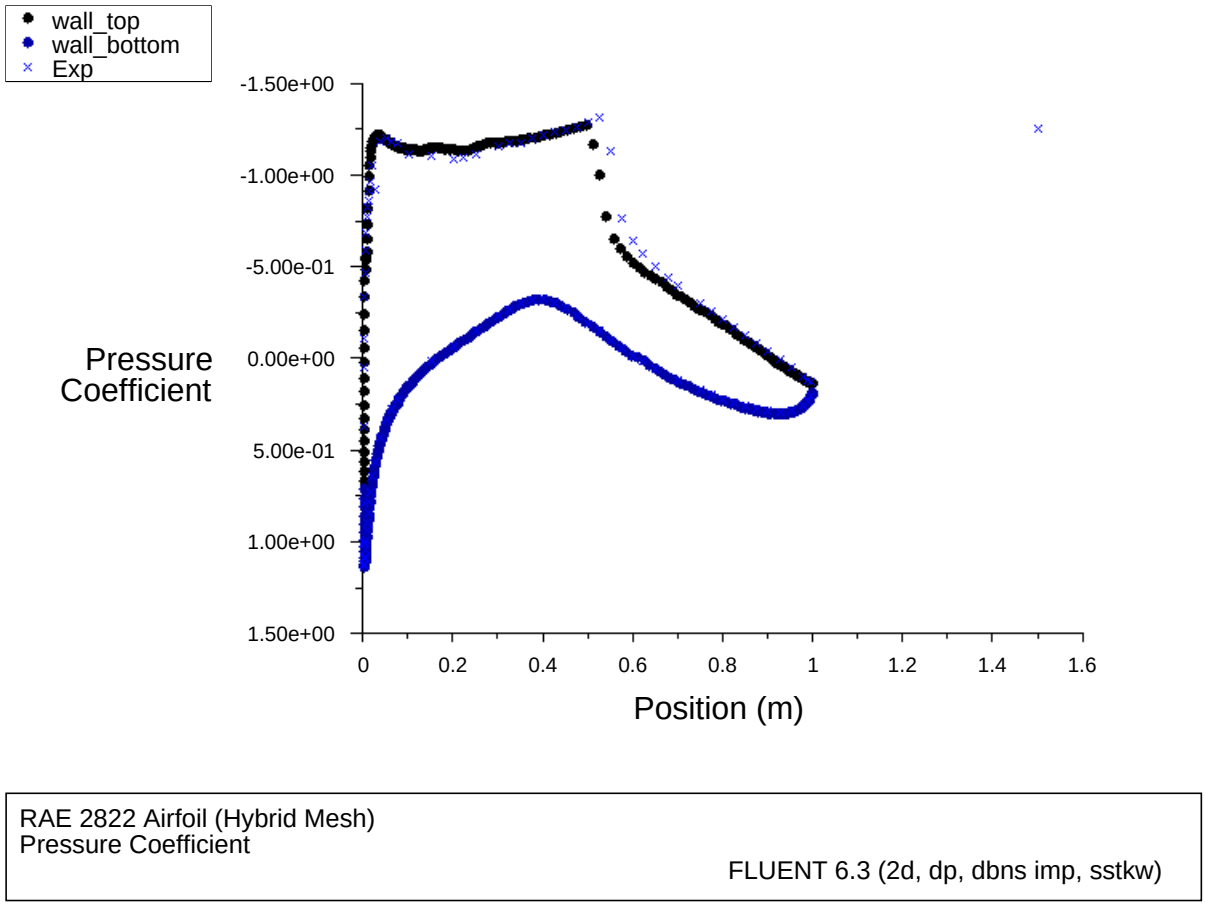

Figure 11.4.2: Comparison of FLUENT's Predictions of the Static Pressure Coefficient C_p With the Experimental Data for the Hybrid Mesh, SST k-ω Case

© Fluent Inc. August 8, 2006

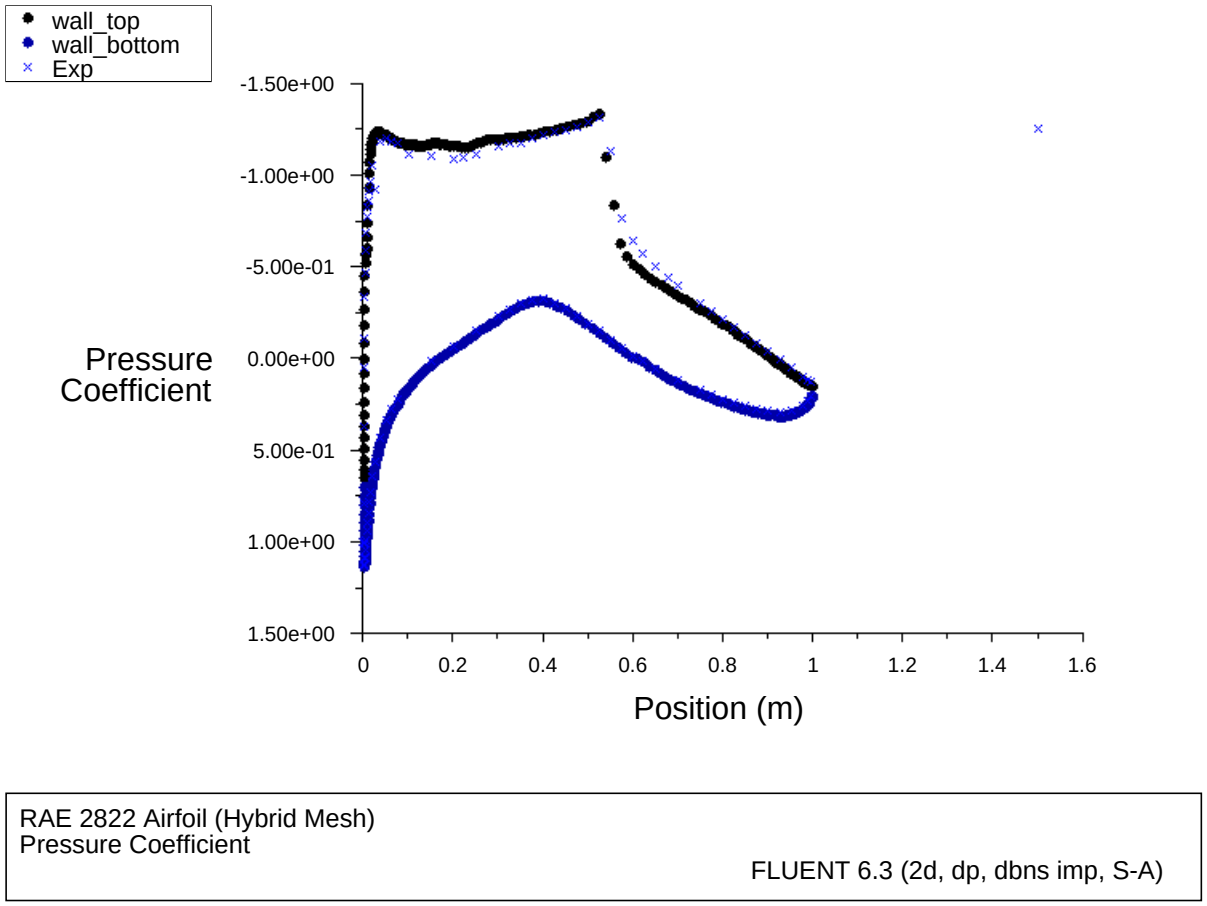

Figure 11.4.3: Comparison of FLUENT's Predictions of the Static Pressure Coefficient C_p With the Experimental Data for the Hybrid Mesh, Spalart-Allmaras Case

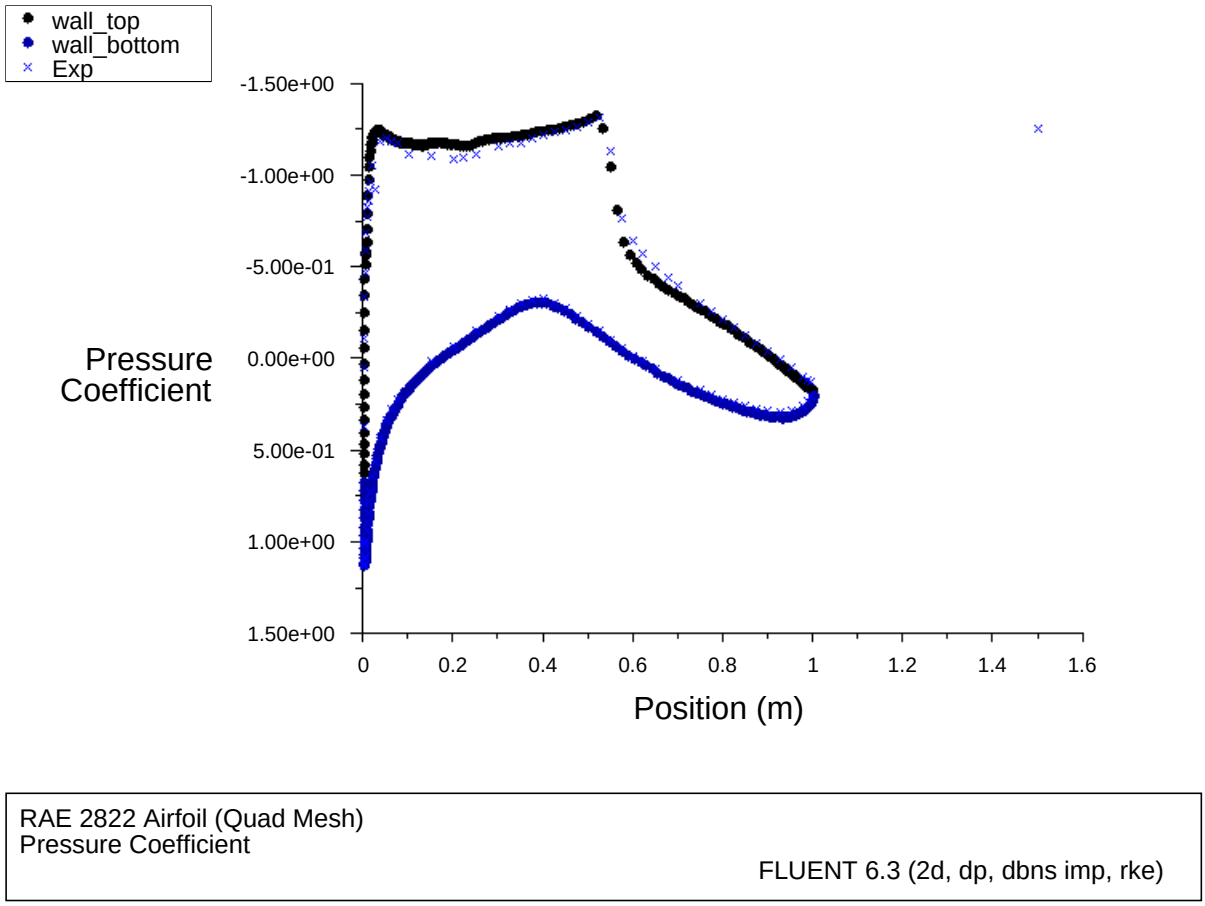

Figure 11.4.4: Comparison of FLUENT's Predictions of the Static Pressure Coefficient C_p With the Experimental Data for the Quadrilateral Mesh, Realizable k-ϵ Case

© Fluent Inc. August 8, 2006

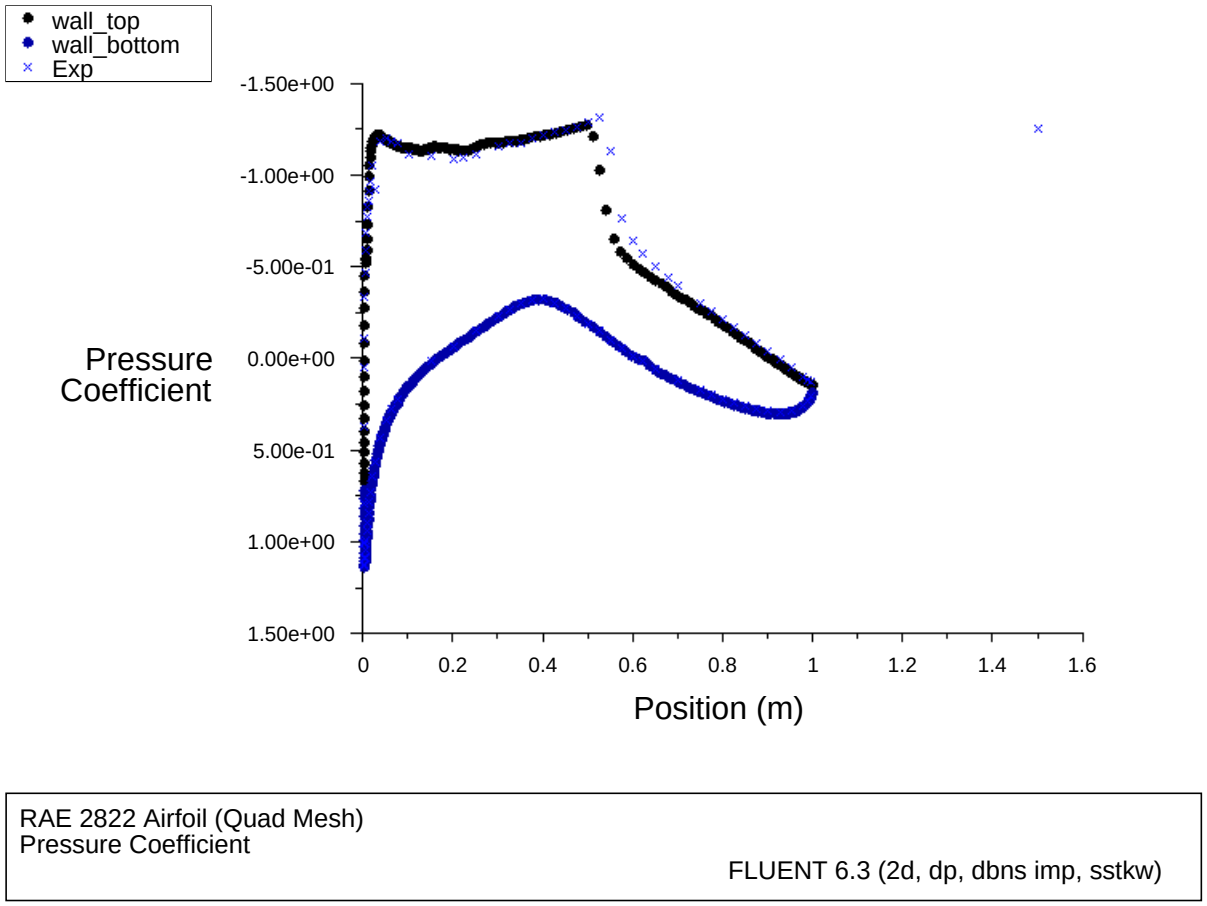

Figure 11.4.5: Comparison of FLUENT's Predictions of the Static Pressure Coefficient C_p With the Experimental Data for the Quadrilateral Mesh, SST k-ω Case

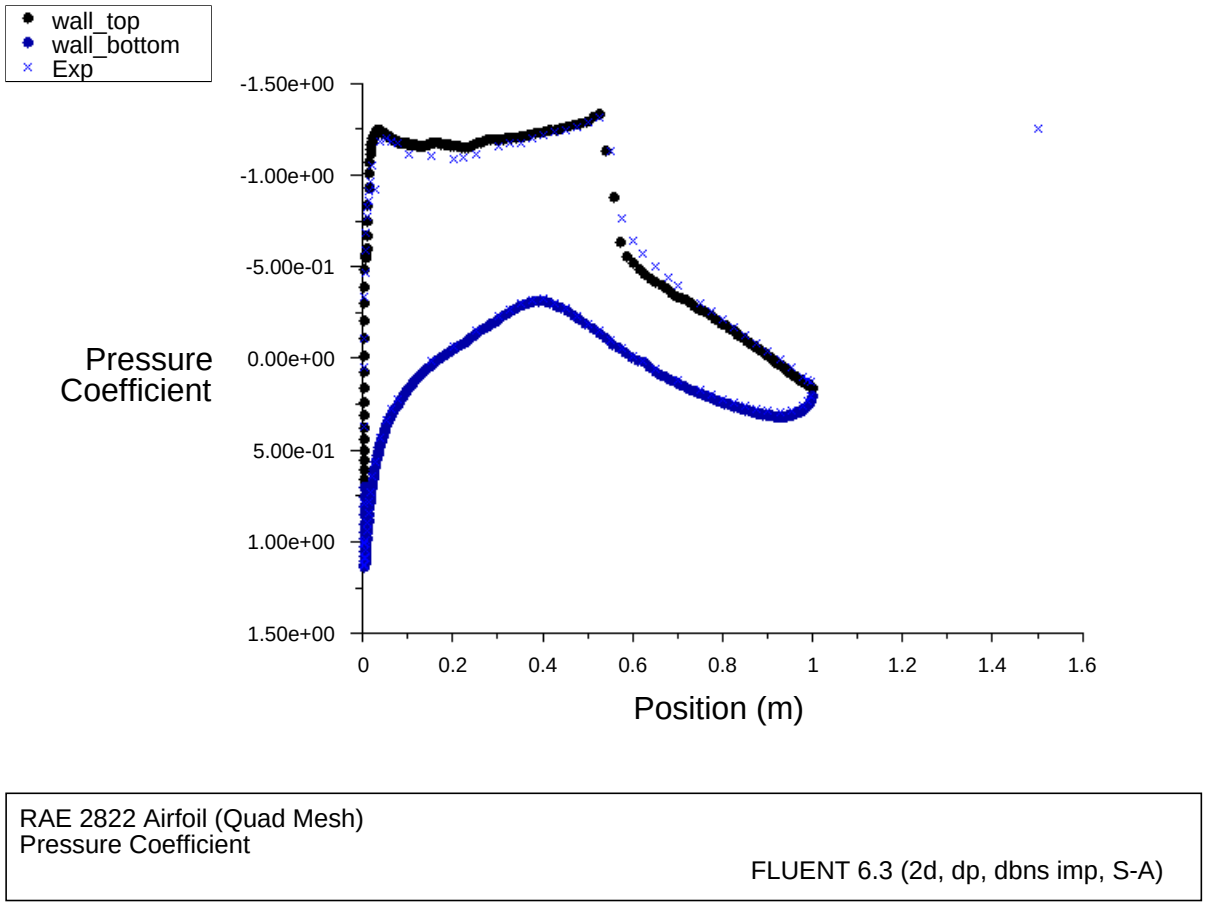

Figure 11.4.6: Comparison of FLUENT's Predictions of the Static Pressure Coefficient (C_p) With the Experimental Data for the Quadrilateral Mesh, Spalart-Allmaras Case

© Fluent Inc. August 8, 2006

Validation 12. Mid-Span Flow Over a Goldman Stator Blade

12.1 Purpose

The purpose of this test is to compare FLUENT's predictions with the experimental data of Goldman et al.[1]. A comparison is also made between the predictions obtained using the Euler equations and the full Navier-Stokes equations.

12.2 Problem Description

In the present test case, flow over a Goldman stator blade at the mid-span is considered. This 2D analysis provides insight into the accuracy of the discretization scheme and FLUENT's ability to predict the complicated flow features typical of turbomachinery applications. The geometry of the domain under consideration is shown in Figure 12.2.1. The inlet and the outlet are located approximately 0.3 m away from the blade's leading and trailing edges, respectively. They are located such that their presence doesn't affect predictions near the blade. The Reynolds number $Re = \rho u h/\mu$ based on the chord length of the blade and the free-stream velocity is $500,000$. Hence the flow is turbulent. The inlet Mach number is approximately 0.2, which implies subsonic flow. Default solver parameters were used in the calculations. The flow field was initialized with the conditions at the inlet. Both the Euler and the full Navier-Stokes equations were used to solve this problem. Moreover, all four solvers available in FLUENT were used: density-based explicit, density-based implicit, pressure-based segregated, and pressure-based coupled.

12.3 References

1. Goldman, L.G., and McLallin, K.L., Cold-Air Annular Cascade Investigation of Aerodynamic Performance of Core-Engine-Cooled Turbine Vanes: I Solid Vane Performance and Facility Description, NASA Technical Memorandum X-3224, April 1977.

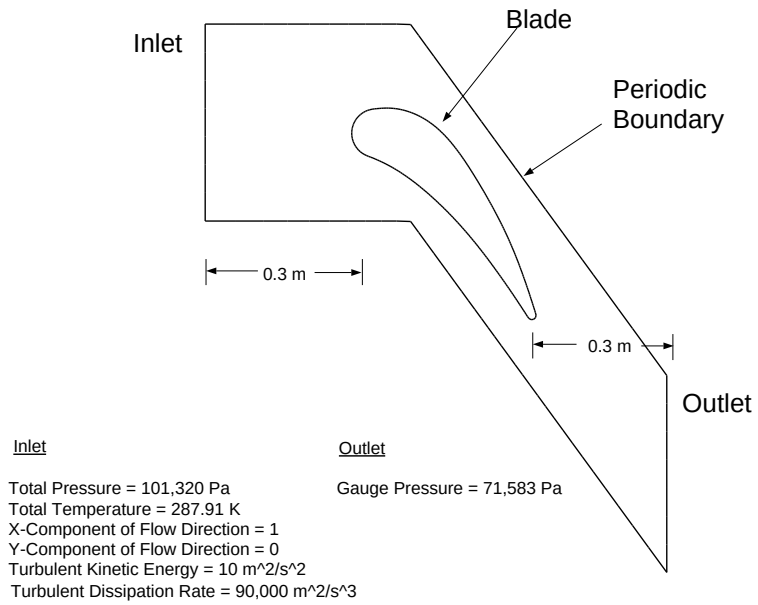

Figure 12.2.1: Geometry of the Goldman Stator Blade

© Fluent Inc. August 8, 2006

12.4 Results

A comparison of the predictions of pressure ratio on the blade (defined as the ratio of static pressure to the inlet total pressure) with the experimental data is shown in Figures 12.4.1 to 12.4.8. FLUENT's predictions of pressure distribution at the mid-span of the blade closely match the experimental data of Goldman et al. [1]. The pressure losses at the mid-span due to the presence of end-wall and fluid viscosity are seen to be negligible.

12.4.1 Validation-Specific Information

Solver:	FLUENT 2ddp
Version:	6.3.13
Solution Files:	1. `ce_inv.cas.gz`, `ce_inv.dat.gz`
	2. `ce_ke.cas.gz`, `ce_ke.dat.gz`
	3. `ci_inv.cas.gz`, `ci_inv.dat.gz`
	4. `ci_ke.cas.gz`, `ci_ke.dat.gz`
	5. `segr_inv.cas.gz`, `segr_inv.dat.gz`
	6. `segr_ke.cas.gz`, `segr_ke.dat.gz`
	7. `pbcs_inv.cas.gz`, `pbcs_inv.dat.gz`
	8. `pbcs_rke.cas.gz`, `pbcs_rke.dat.gz`

These solution files are available from the Fluent Inc. User Services Center as described in the Introduction.

12.4.2 Plot Data

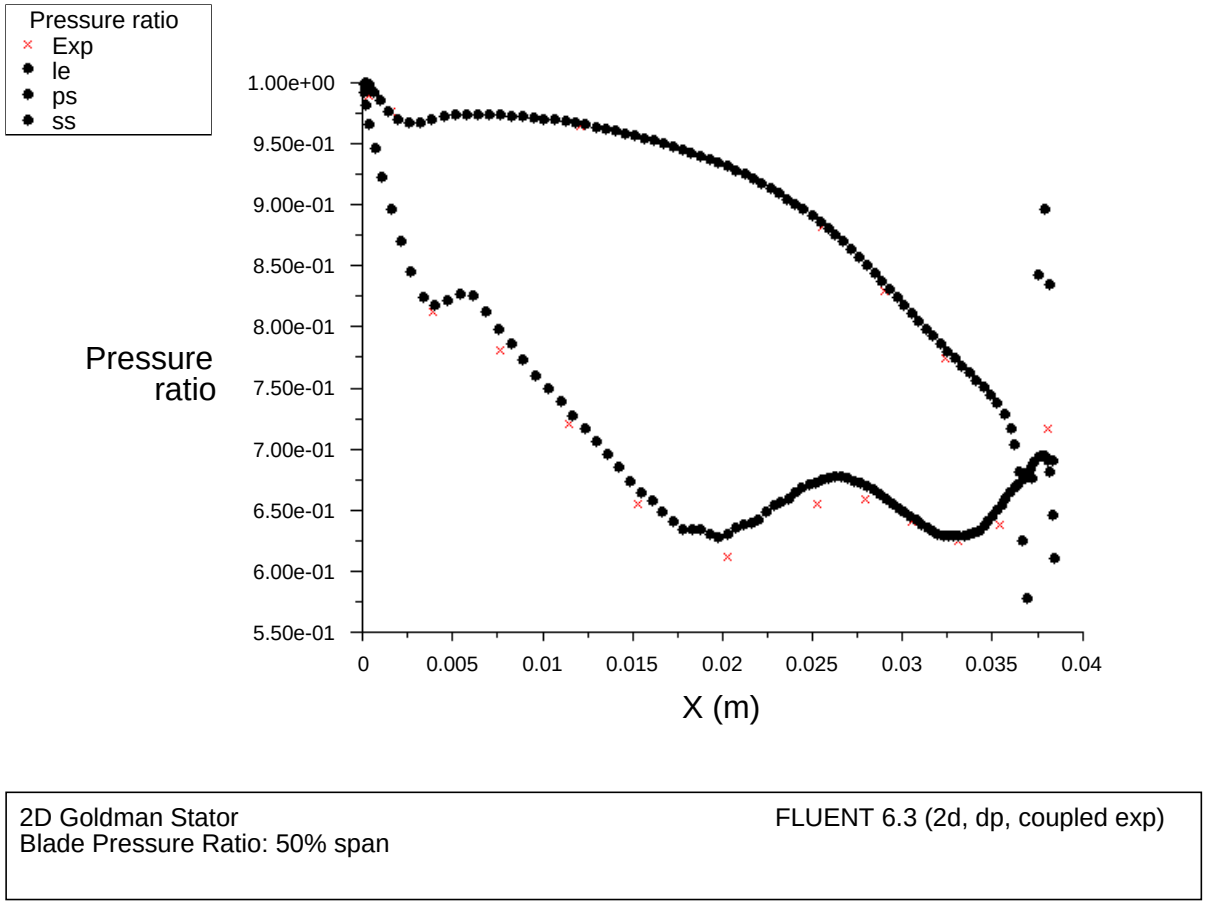

Figure 12.4.1: Pressure Ratio on the Blade (Euler Equations with the Density-Based Explicit Solver)

© Fluent Inc. August 8, 2006

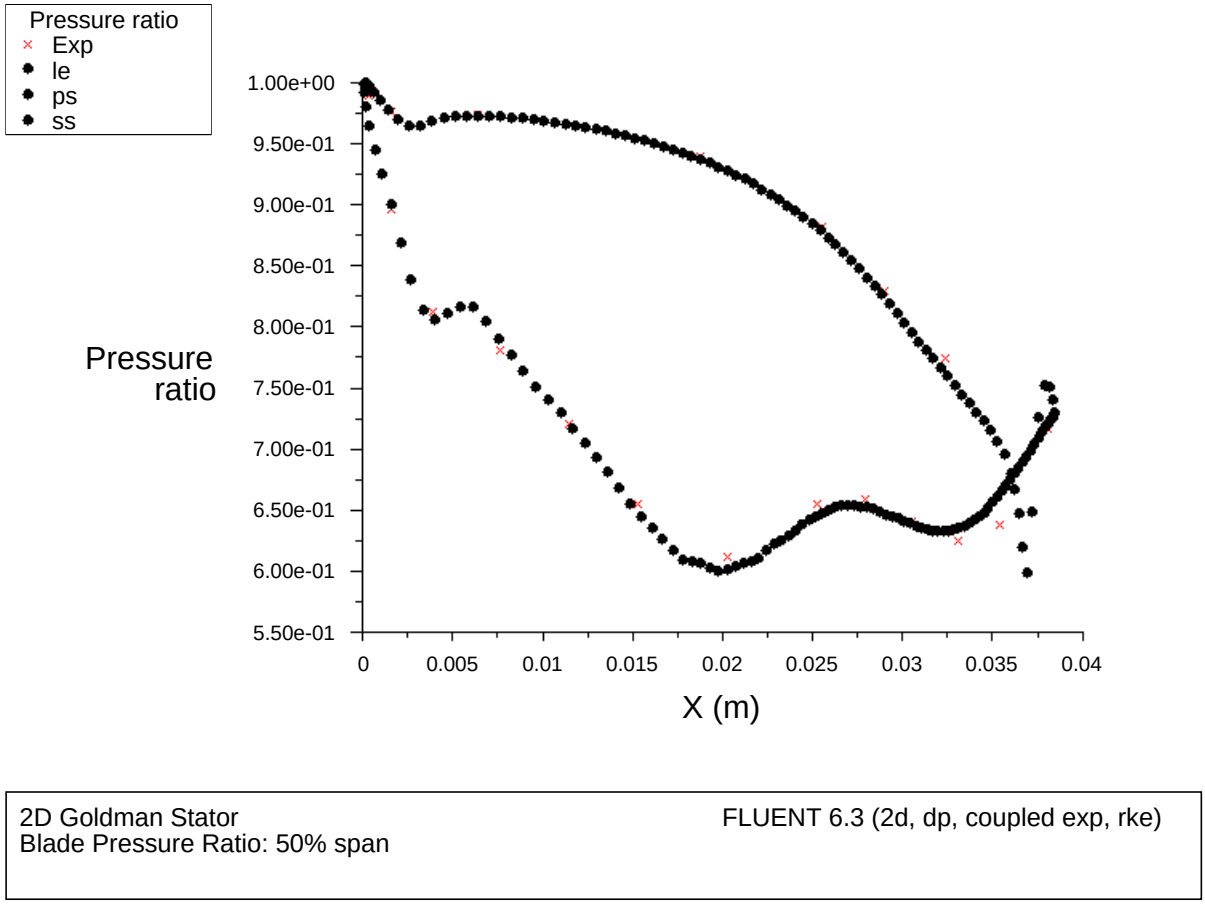

Figure 12.4.2: Pressure Ratio on the Blade (Navier-Stokes Equations with the Density-Based Explicit Solver)

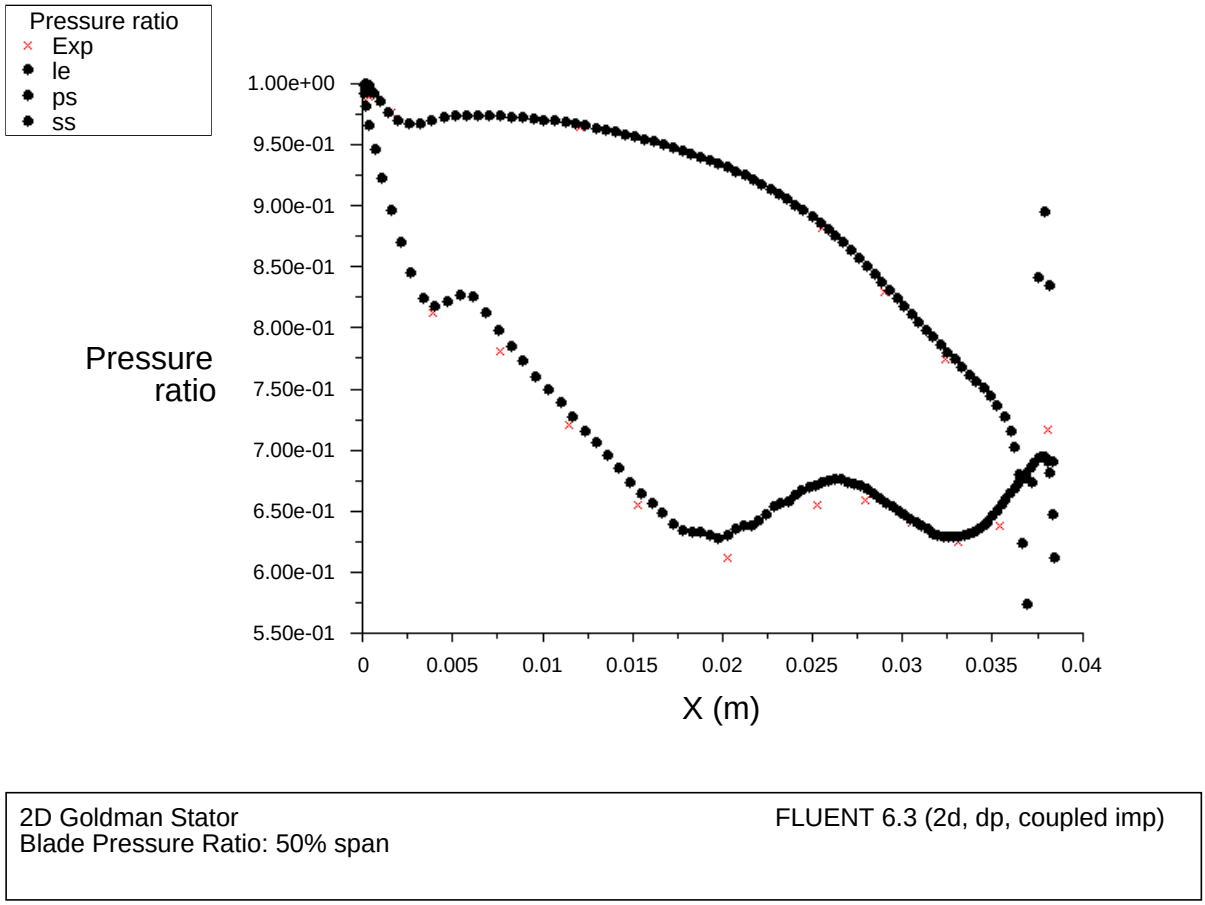

Figure 12.4.3: Pressure Ratio on the Blade (Euler Equations with the Density-Based Implicit Solver)

© Fluent Inc. August 8, 2006

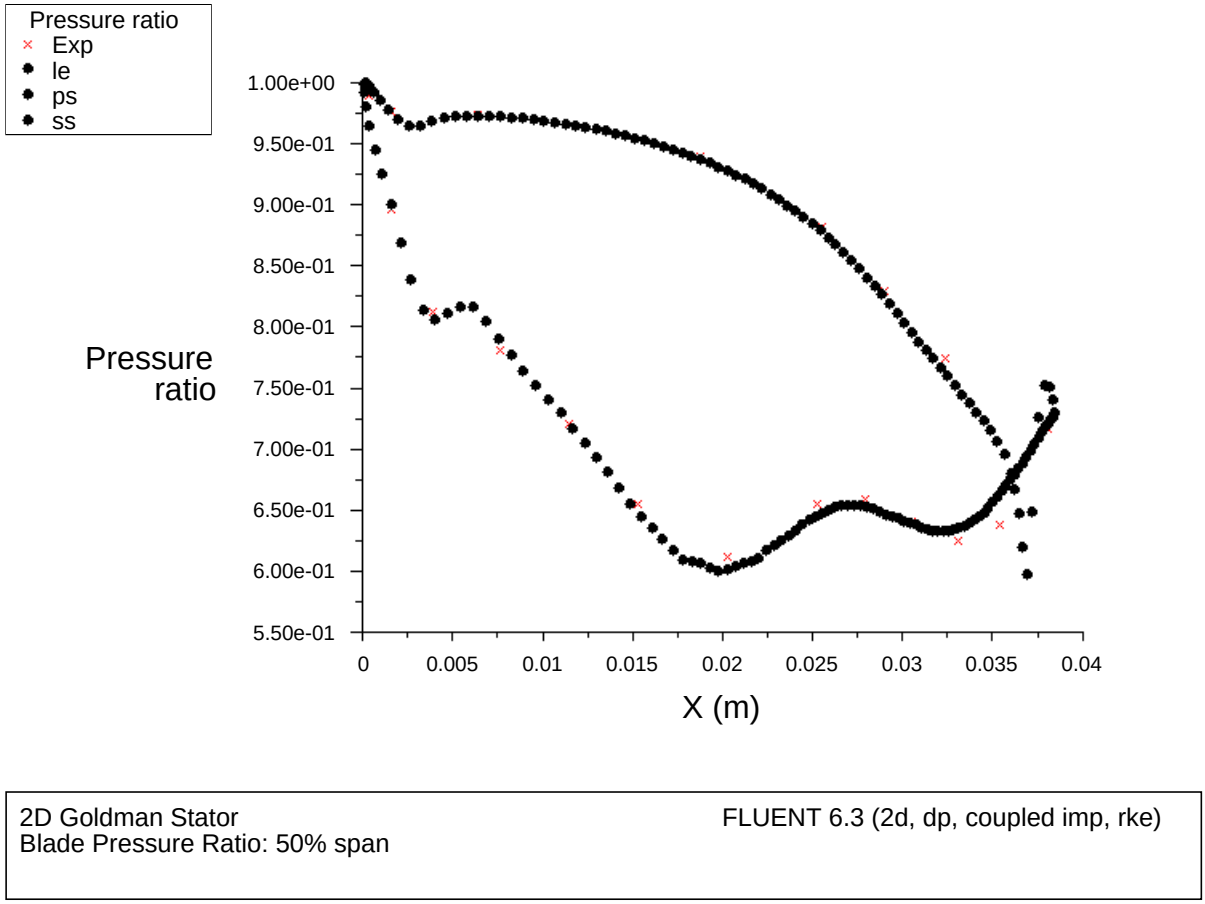

Figure 12.4.4: Pressure Ratio on the Blade (Navier-Stokes Equations with the Density-Based Implicit Solver)

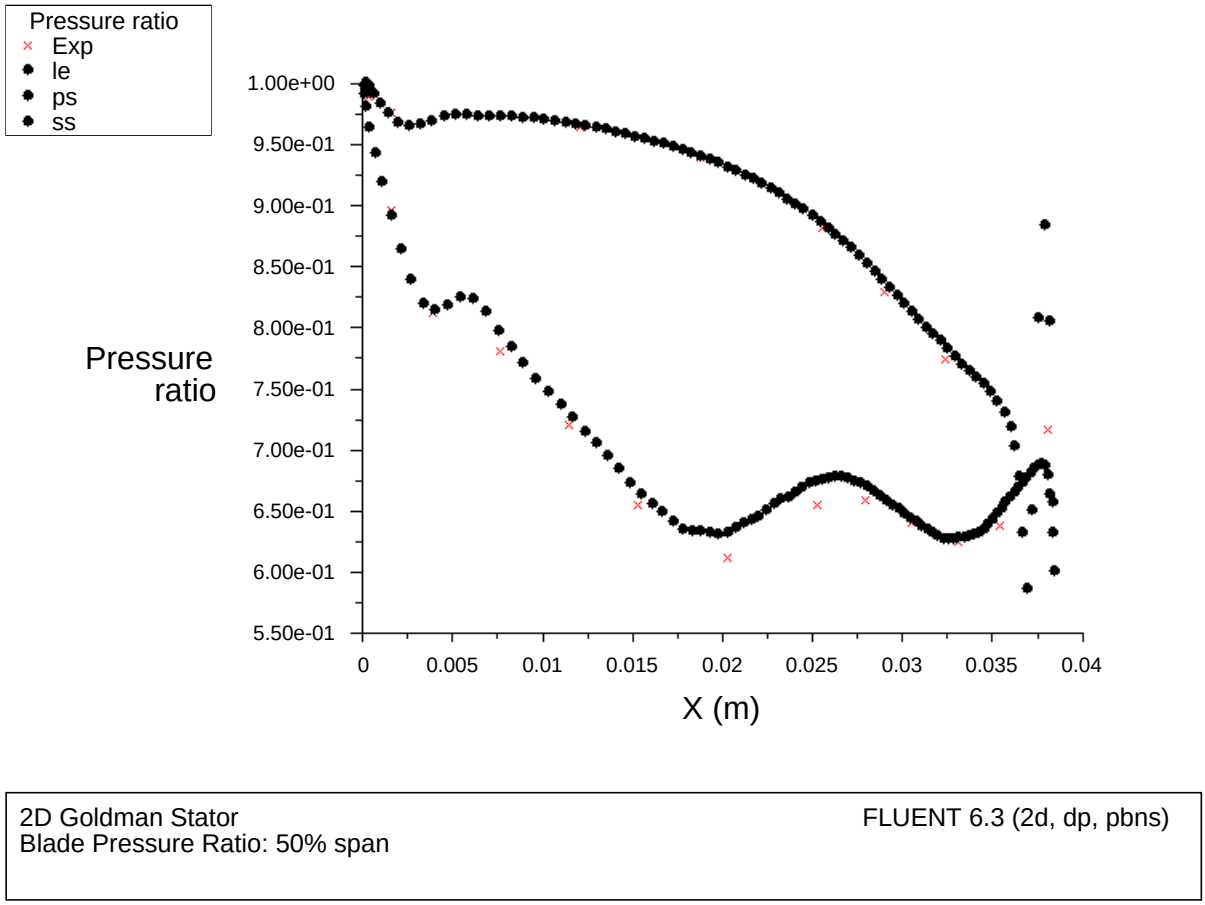

Figure 12.4.5: Pressure Ratio on the Blade (Euler Equations with the Pressure-Based Segregated Solver)

© Fluent Inc. August 8, 2006

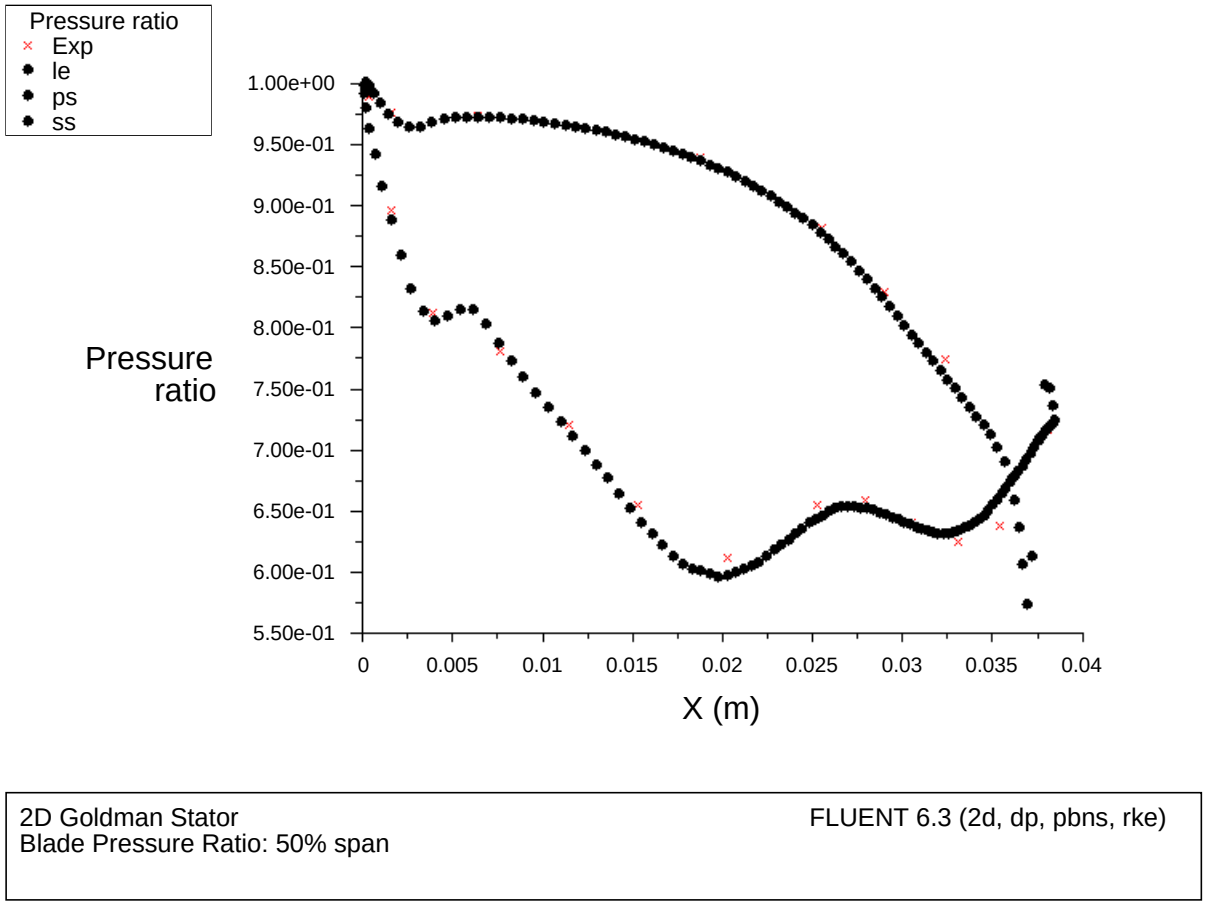

Figure 12.4.6: Pressure Ratio on the Blade (Navier-Stokes Equations with the Pressure-Based Segregated Solver)

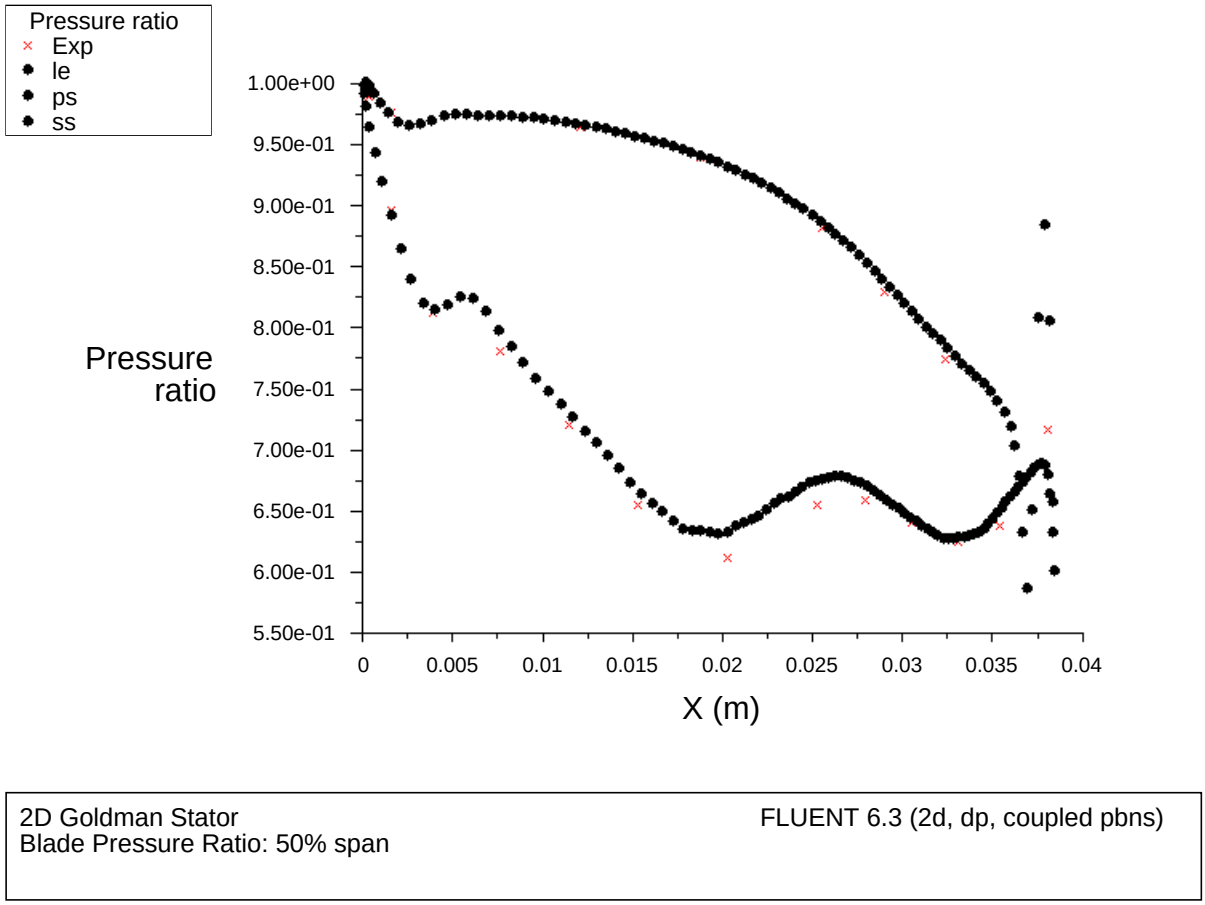

Figure 12.4.7: Pressure Ratio on the Blade (Euler Equations with the Pressure-Based Coupled Solver)

© Fluent Inc. August 8, 2006

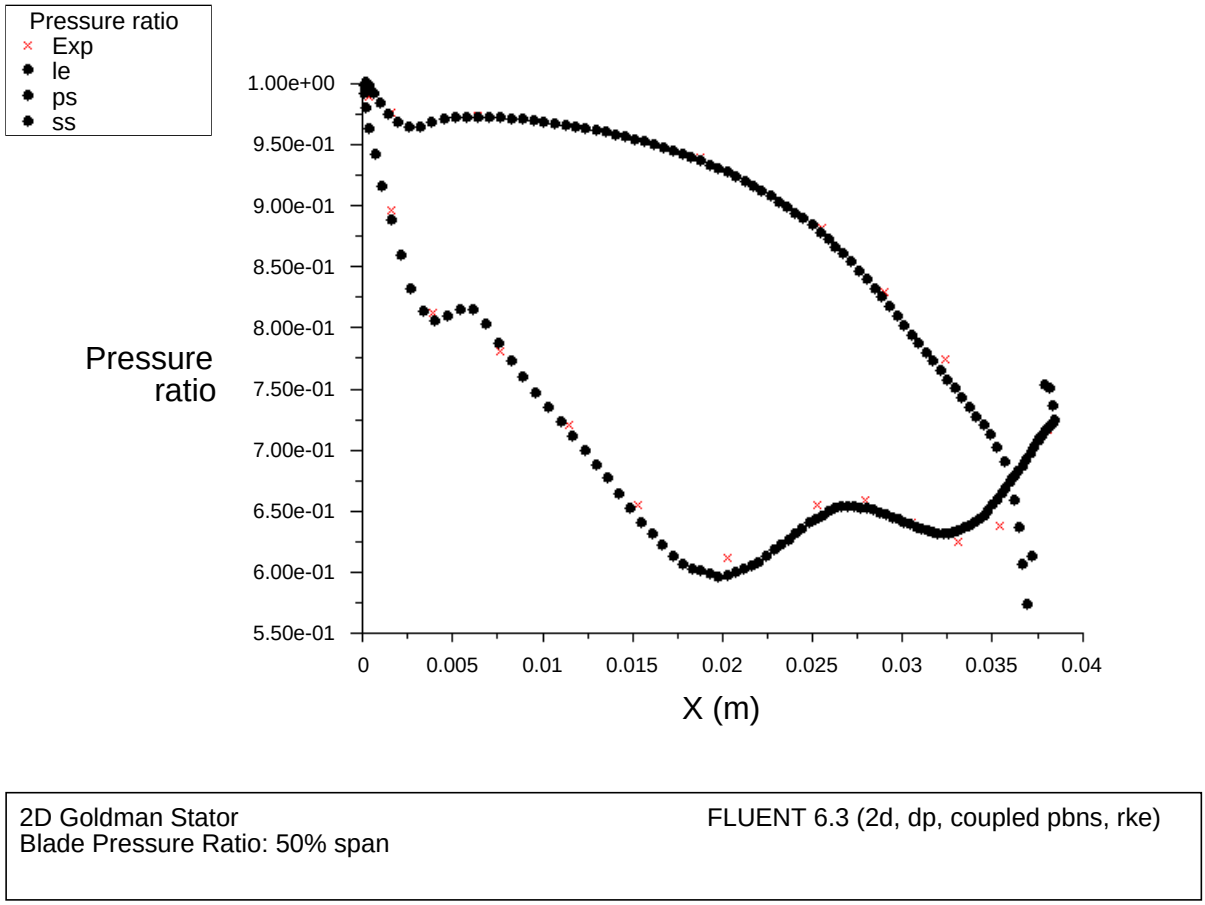

Figure 12.4.8: Pressure Ratio on the Blade (Navier-Stokes Equations with the Pressure-Based Coupled Solver)

© Fluent Inc. August 8, 2006

Validation 13. Compressible Turbulent Mixing Layer

13.1 Purpose

The purpose of this test is to compare FLUENT's predictions of velocity profiles along the mixing layer with the experimental data of Goebel and Dutton [1]. The profiles of turbulent kinetic energy as the mixing layer evolves are also compared with the experimental data.

13.2 Problem Description

Two streams of air are mixed in a rectangular tunnel. The length of the computational domain is chosen such that the local Reynolds number at the exit of the test section, based on the velocity difference between the streams and the mixing layer thickness, is greater than $100,000$, the Reynolds number needed for the complete development of the mixing layer. The geometry of the rectangular tunnel is shown in Figure 13.2.1.

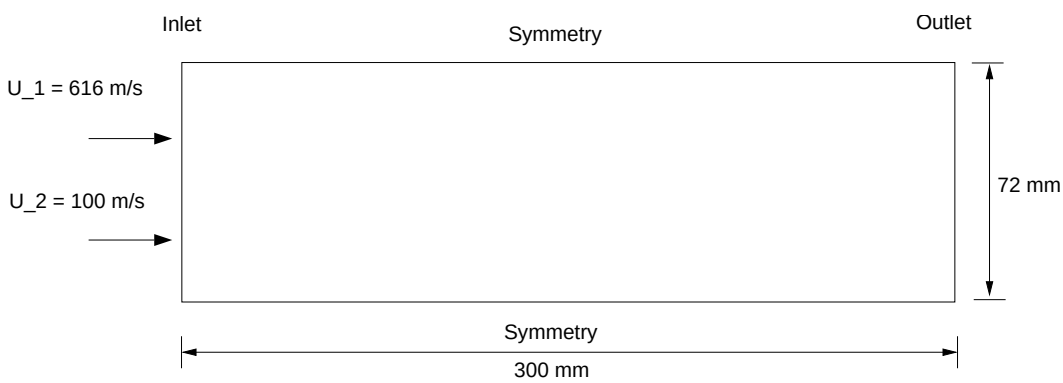

Primary Stream (1)	Secondary Stream (2)
Total Pressure = 487 kPa	Total Pressure = 38 kPa
Static Pressure = 36 kPa	Static Pressure = 36 kPa
Total Temperature = 360 K	Total Temperature = 290 K
Mach Number = 2.35	Mach Number = 0.36
Turbulent Kinetic Energy = 74 m^2/s^2	Turbulent Kinetic Energy = 226 m^2/s^2
Turbulent Dissipation Rate = 62,300 m^2/s^3	Turbulent Dissipation Rate = 332,000 m^2/s^3

Figure 13.2.1: Geometry of the Mixing Layer

13.3 References

1. Goebel, S.G., and Dutton, J.C., Experimental Study of Compressible Turbulent Mixing Layers, *AIAA Journal*, 29(4):538–546, 1991.

13.4 Results

The following figures compare the computed velocity profiles and turbulent kinetic energy with measured data at different axial locations (for all three k-ϵ models). The predictions using the RNG and realizable models are better than the predictions with the standard k-ϵ model.

13.4.1 Validation-Specific Information

Solver:	FLUENT 2d, 2ddp
Version:	6.3.11
Solution Files:	1. `std-ke_r1.cas`, `std-ke_r1.dat` - Standard k-ϵ
	2. `rng-ke_r2.cas`, `rng-ke_r2.dat` - RNG k-ϵ
	3. `rea-ke_r3.cas`, `rea-ke_r3.dat` - Realizable k-ϵ

These solution files are available from the Fluent Inc. User Services Center as described in the Introduction.

© Fluent Inc. August 8, 2006

13.4.2 Plot Data

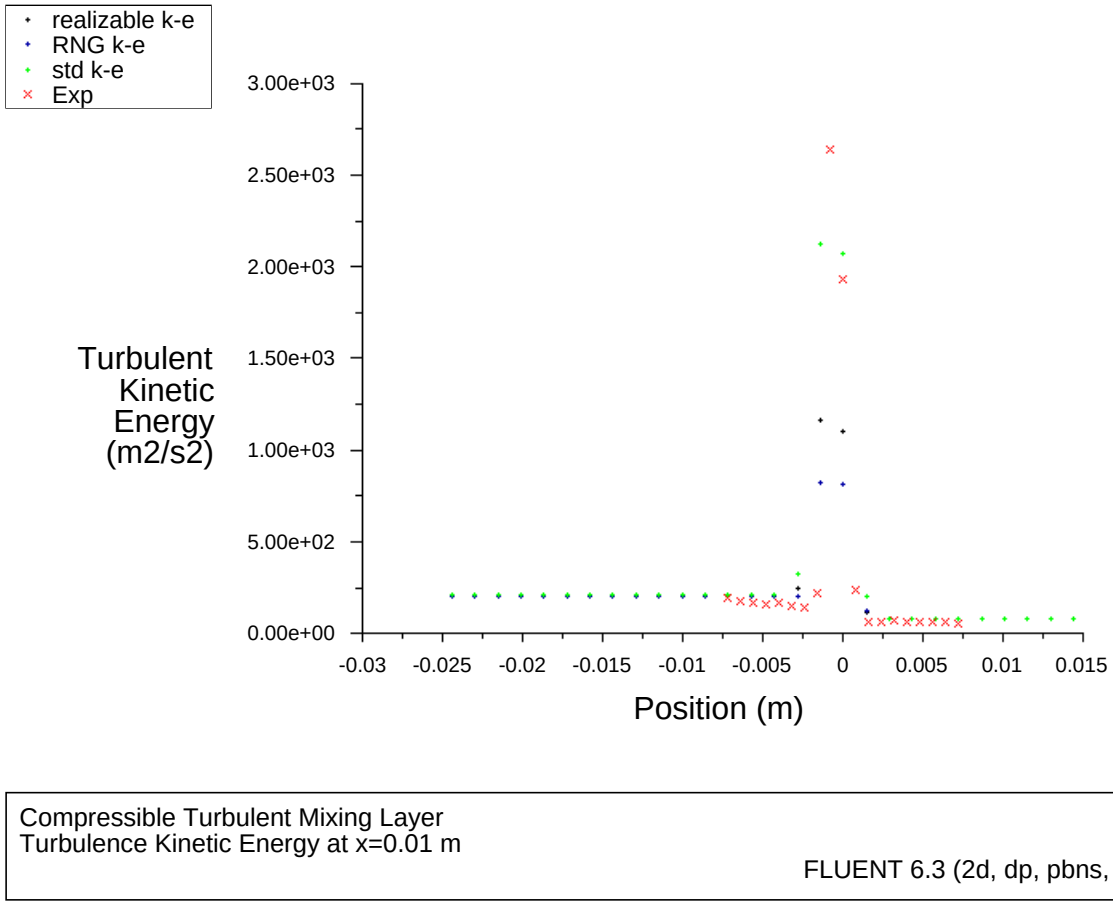

Figure 13.4.1: Turbulent Kinetic Energy at x=10 mm

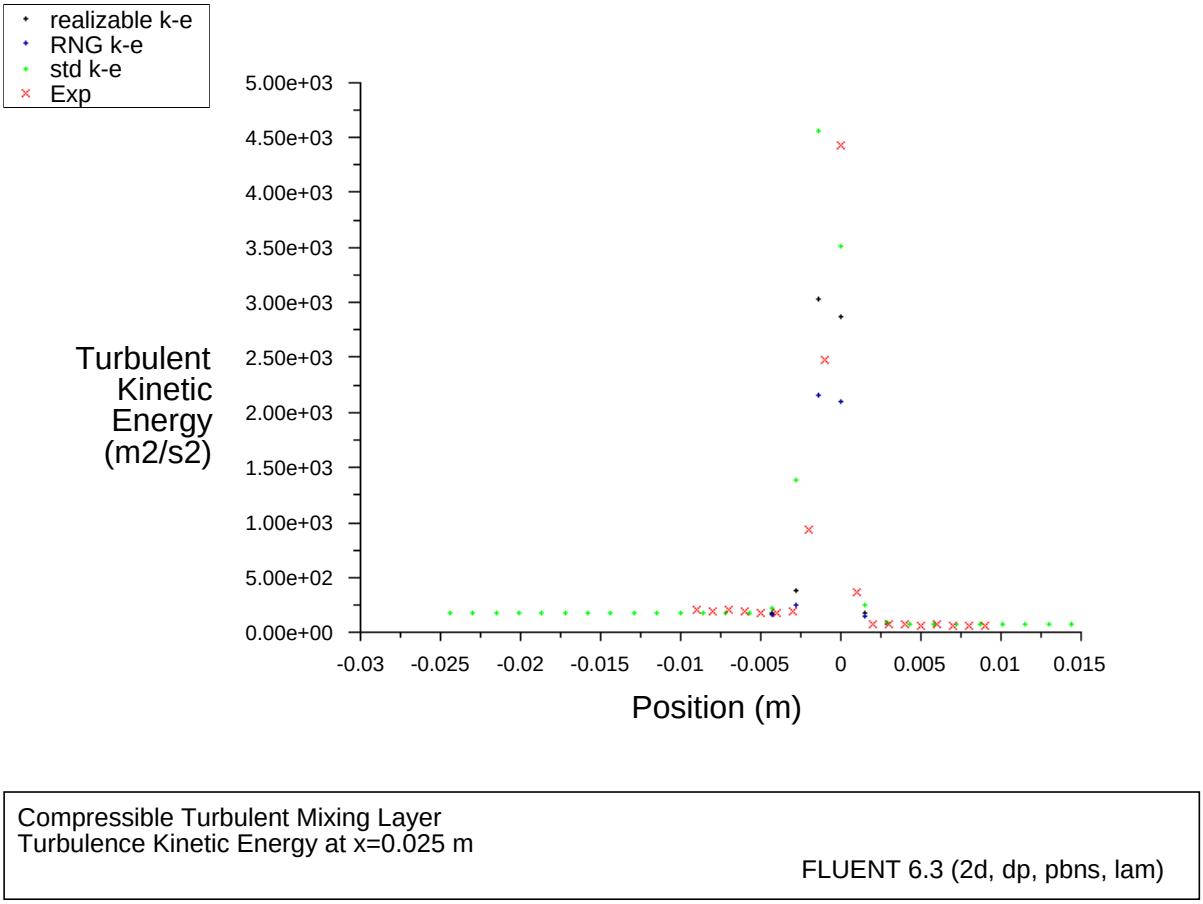

Figure 13.4.2: Turbulent Kinetic Energy at x=25 mm

© Fluent Inc. August 8, 2006

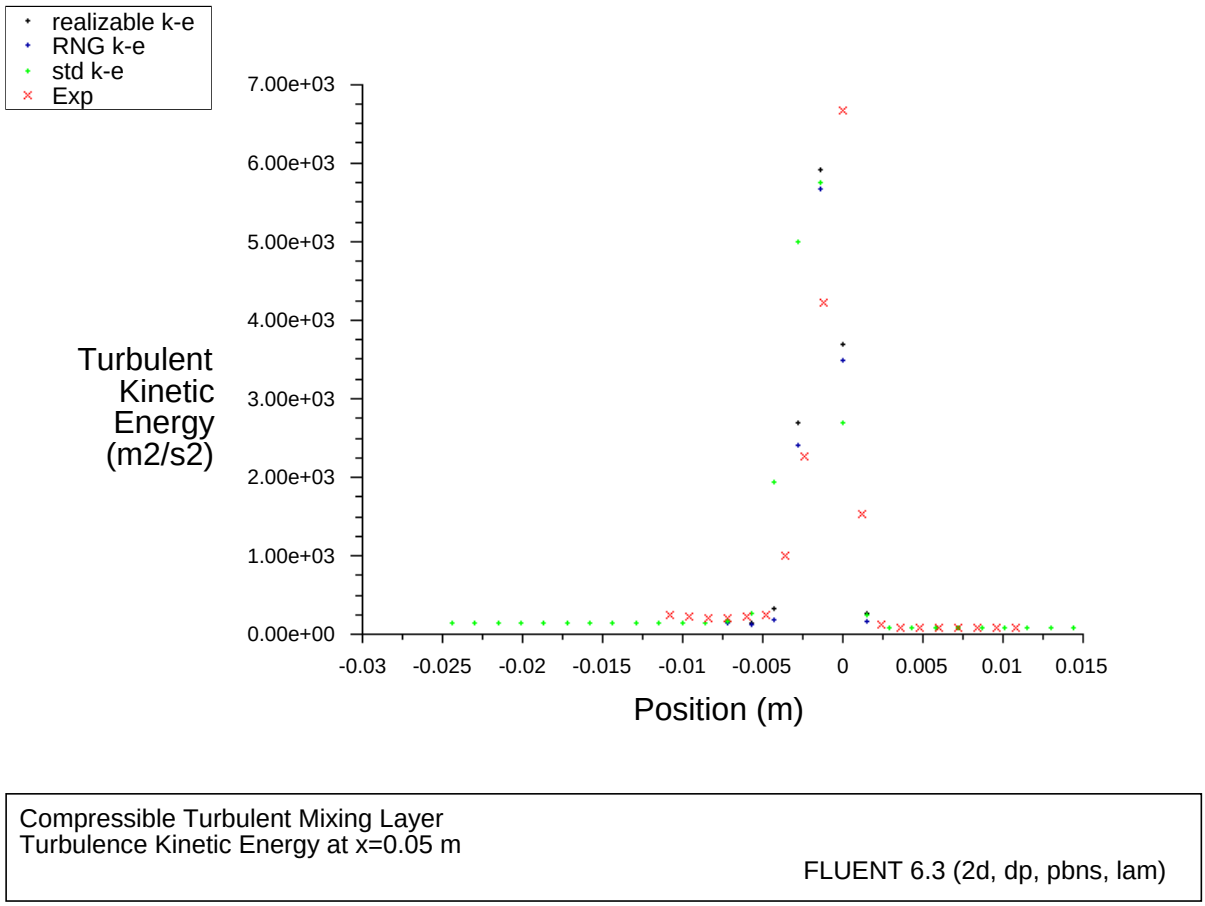

Figure 13.4.3: Turbulent Kinetic Energy at x=50 mm

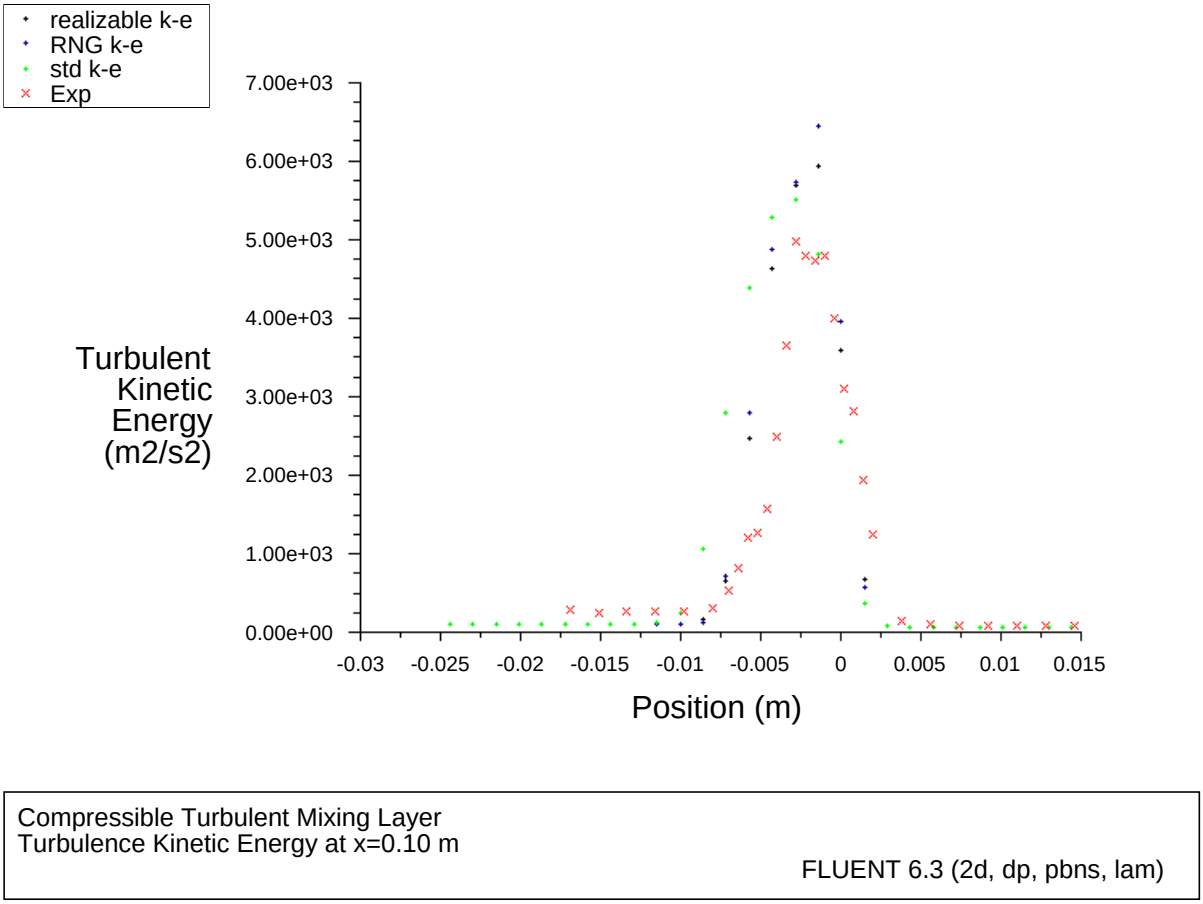

Figure 13.4.4: Turbulent Kinetic Energy at x=100 mm

© Fluent Inc. August 8, 2006

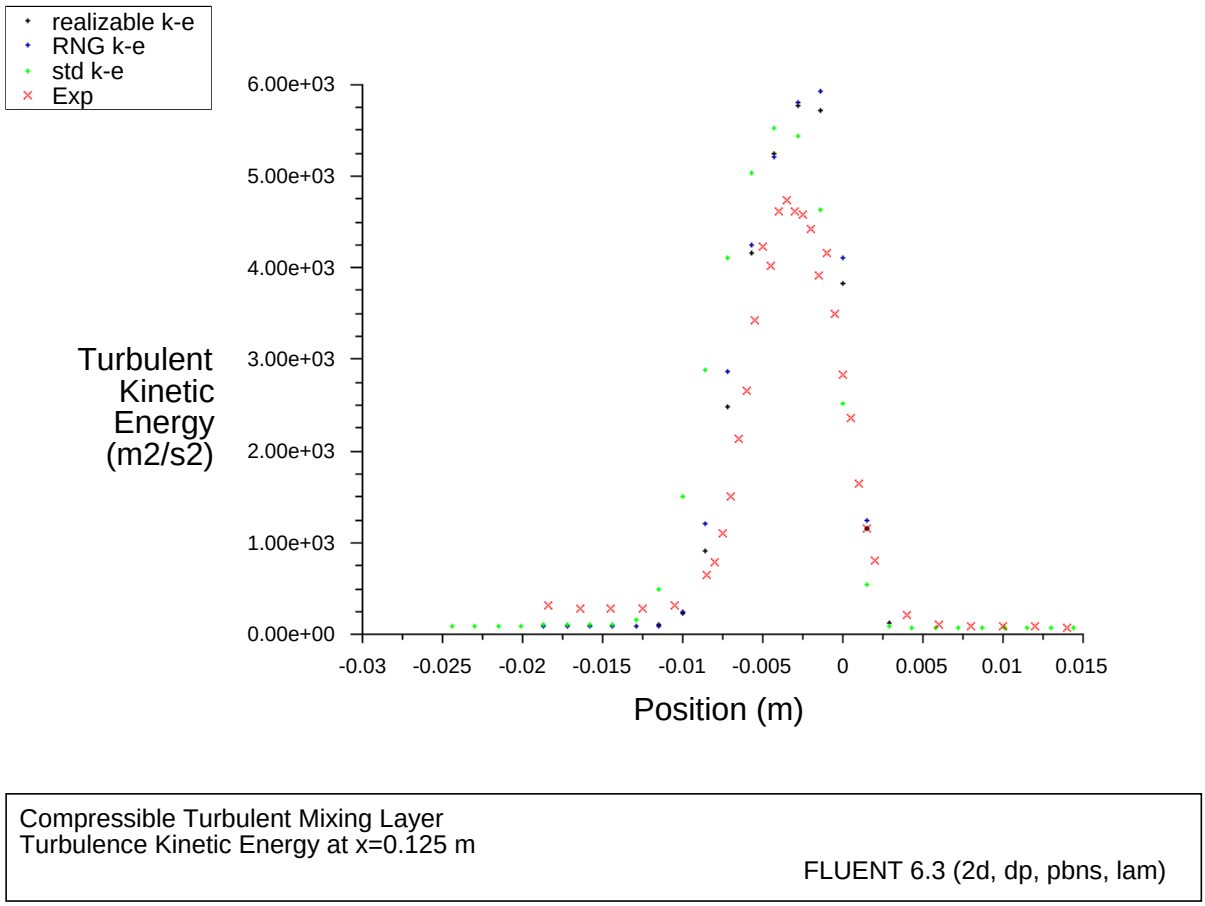

Figure 13.4.5: Turbulent Kinetic Energy at x=125 mm

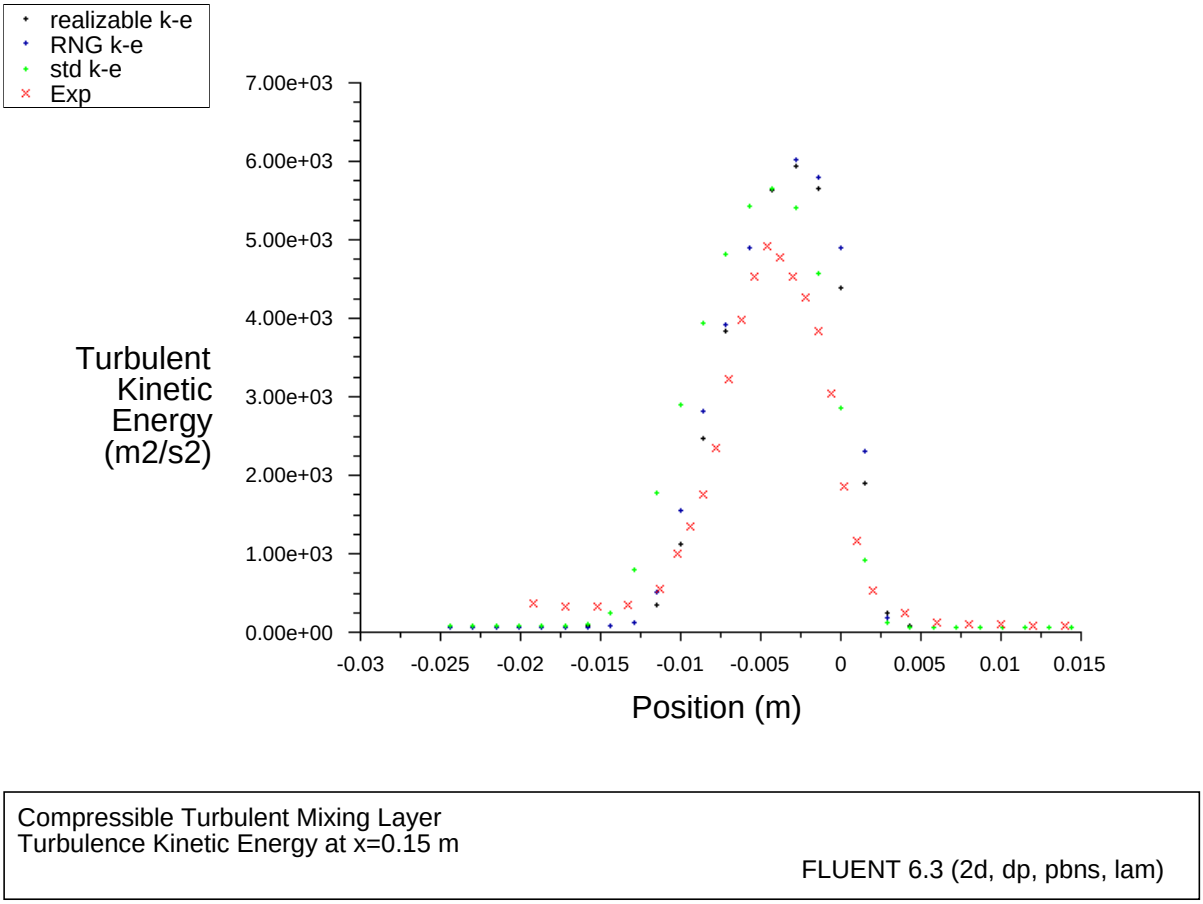

Figure 13.4.6: Turbulent Kinetic Energy at x=150 mm

© Fluent Inc. August 8, 2006

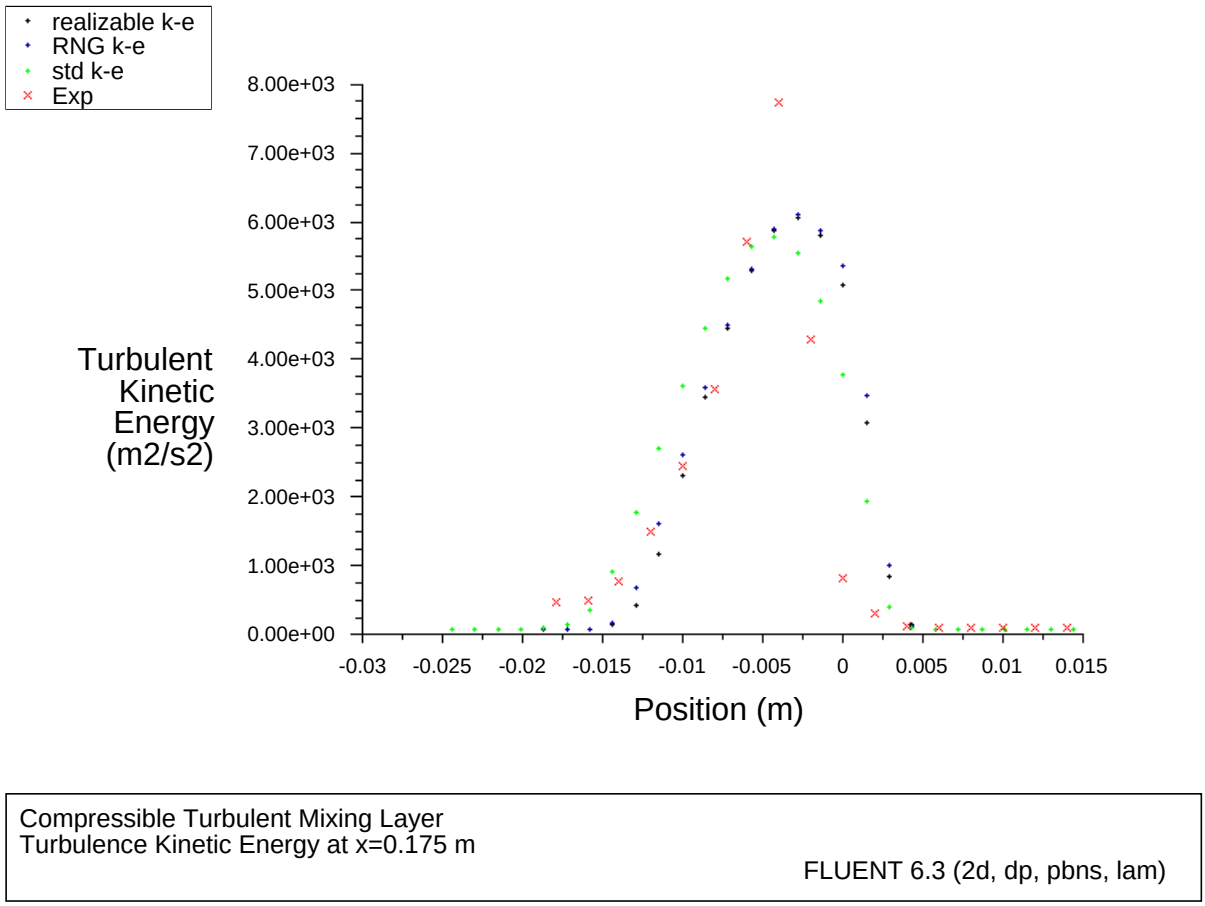

Figure 13.4.7: Turbulent Kinetic Energy at x=175 mm

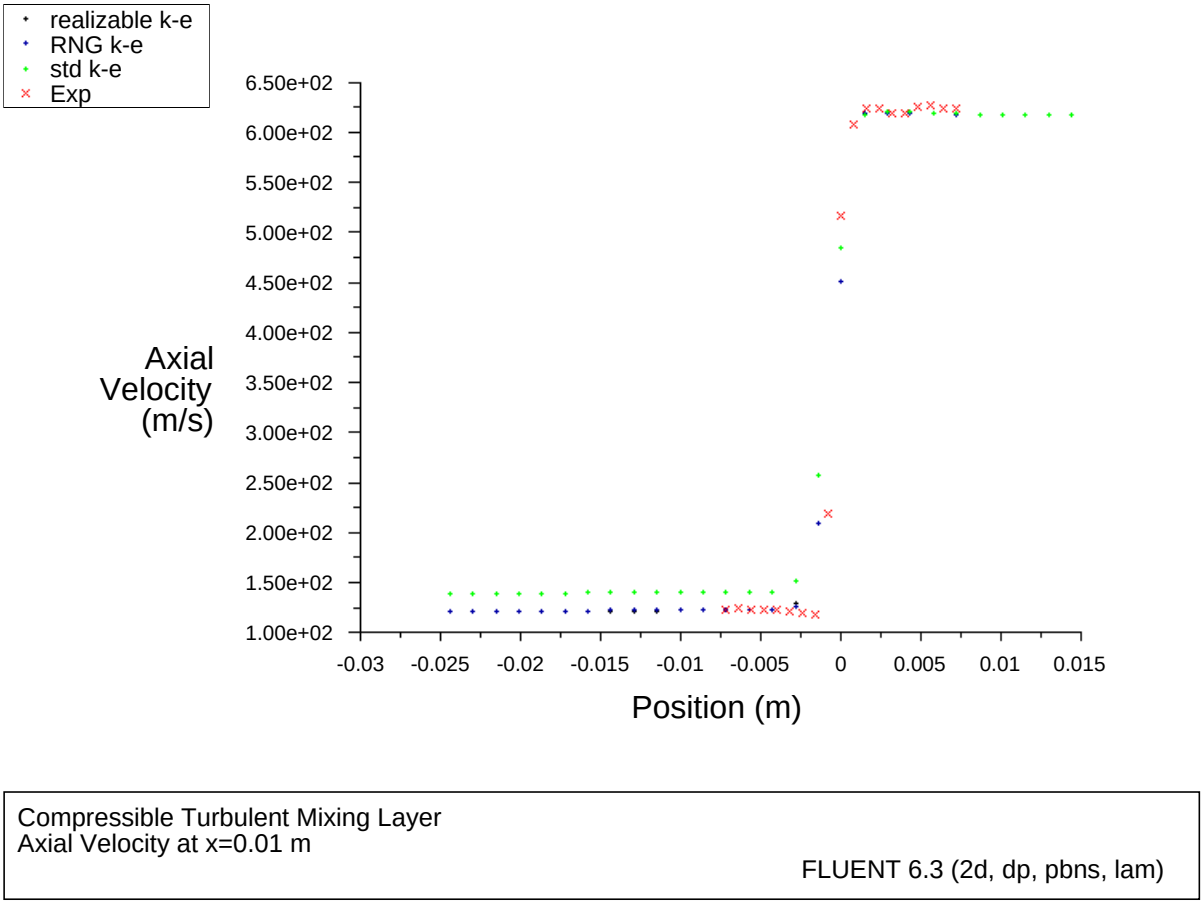

Figure 13.4.8: Axial Velocity Profile at x=10 mm

© Fluent Inc. August 8, 2006

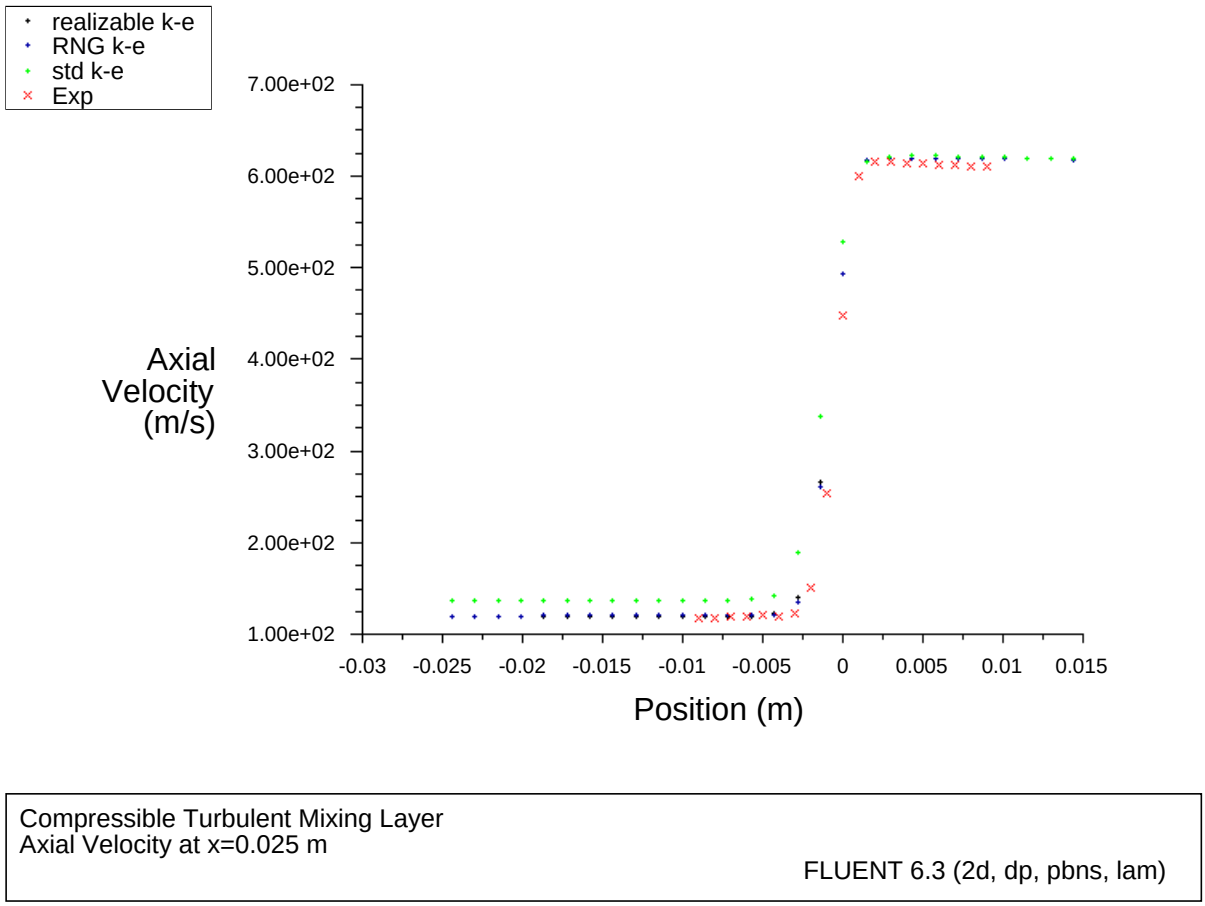

Figure 13.4.9: Axial Velocity Profile at x=25 mm

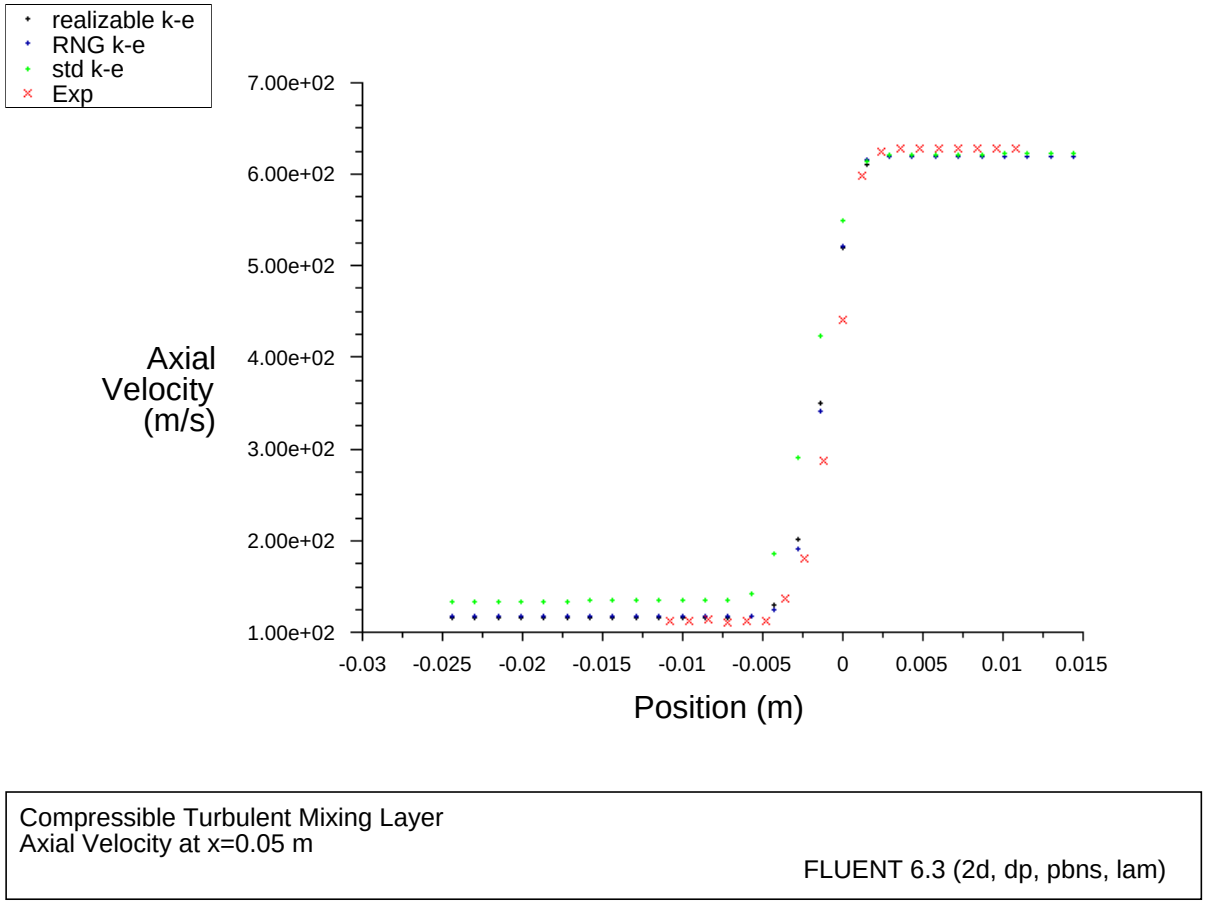

Figure 13.4.10: Axial Velocity Profile at x=50 mm

© Fluent Inc. August 8, 2006

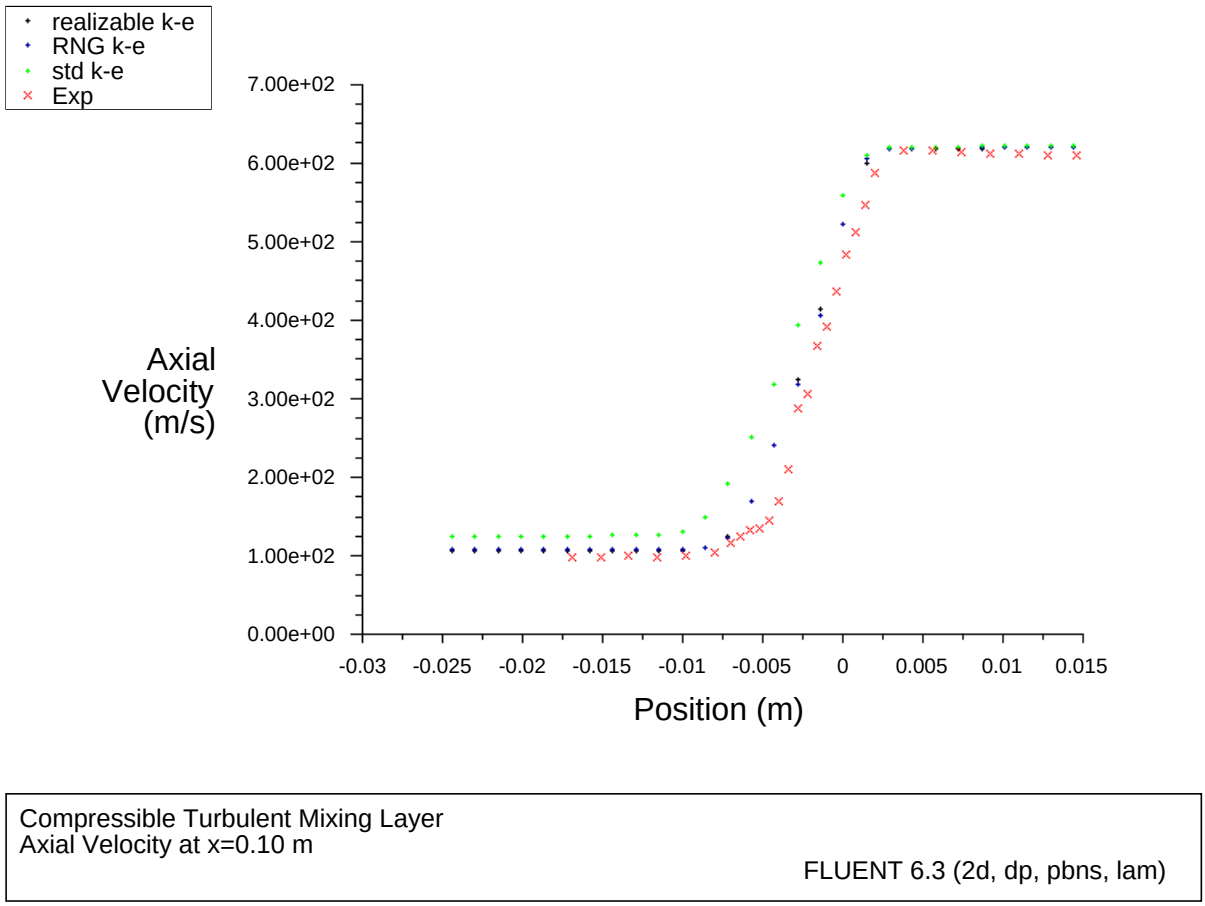

Figure 13.4.11: Axial Velocity Profile at x=100 mm

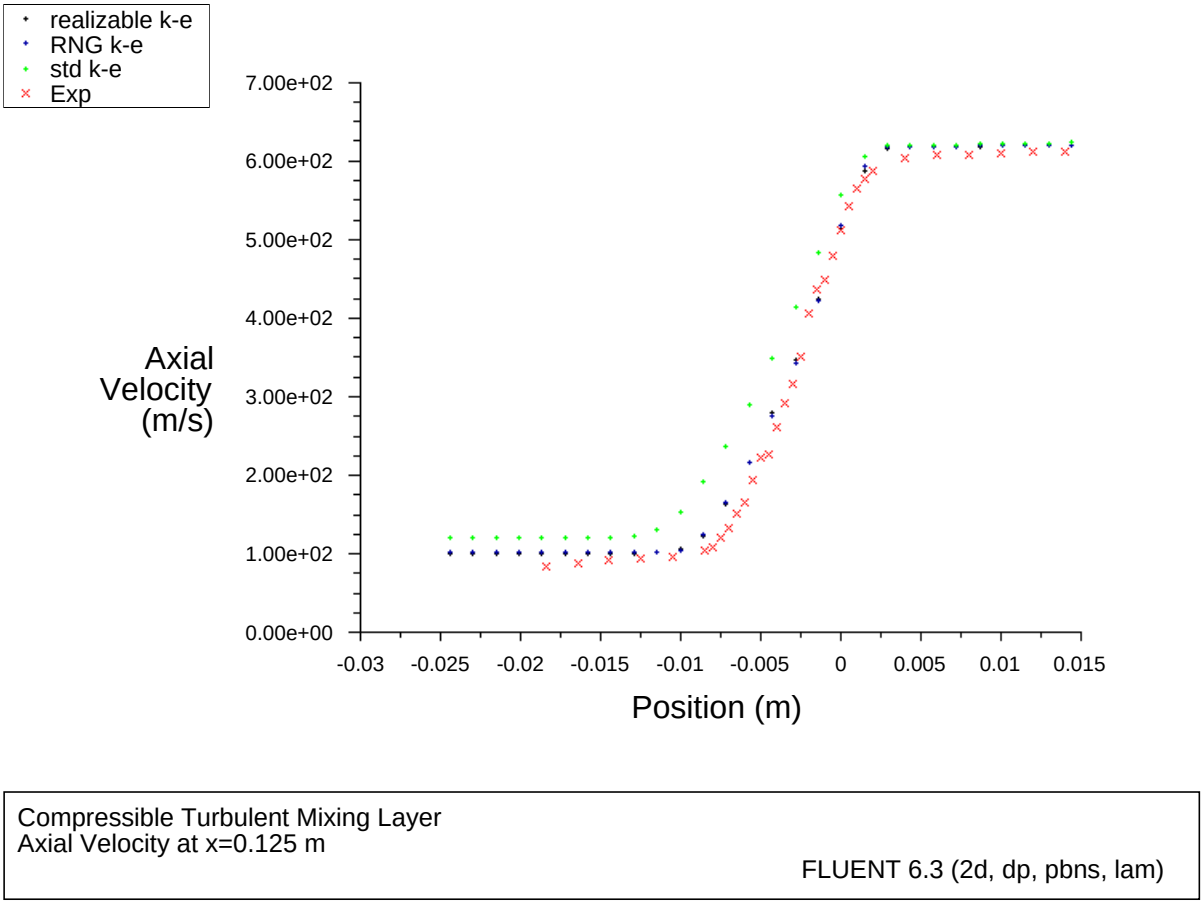

Figure 13.4.12: Axial Velocity Profile at x=125 mm

© Fluent Inc. August 8, 2006

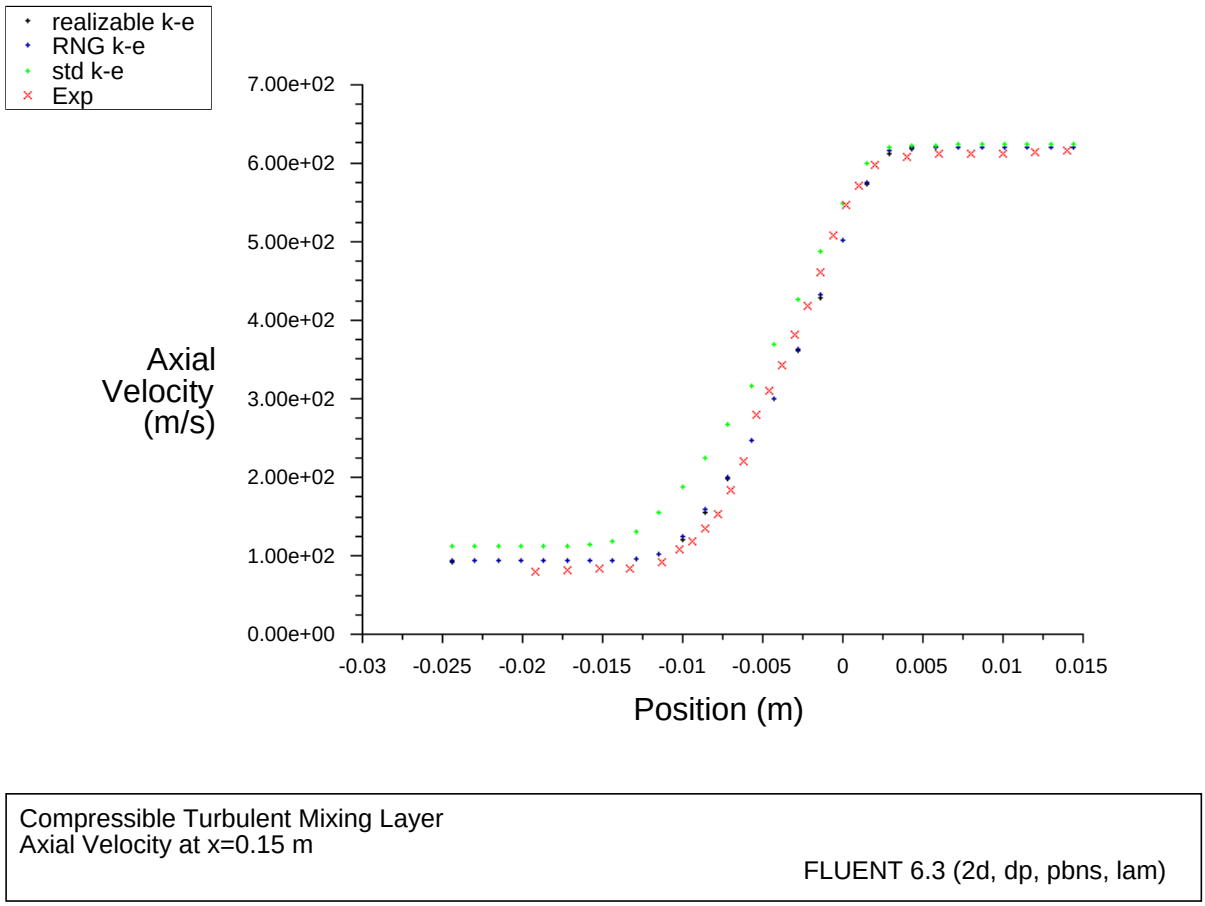

Figure 13.4.13: Axial Velocity Profile at x=150 mm

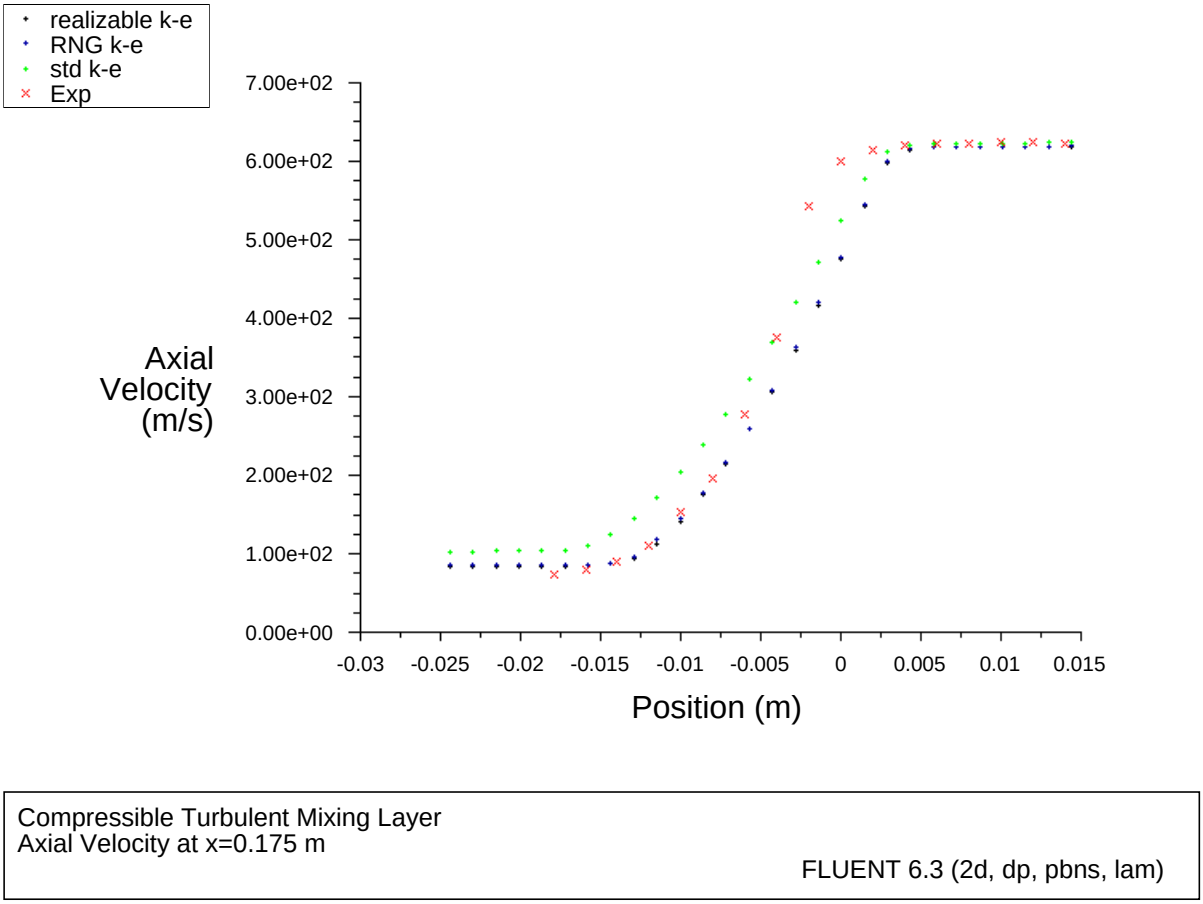

Figure 13.4.14: Axial Velocity Profile at x=175 mm

© Fluent Inc. August 8, 2006

Validation 14. Reflecting Shock Waves

14.1 Purpose

The purpose of this test is to validate FLUENT's ability to predict reflecting shock waves and their effect on wall pressure distribution and heat transfer.

14.2 Problem Description

The flow is considered to be two-dimensional, because the span of the experimental outlet is considerably larger than the height. Both geometries are shown in Figures 14.2.1 and 14.2.2. The flow enters the exhaust section at a Mach number of 1.66. In each case, the cowl wall opposite the afterbody angles initially upward. This is followed by a wedge, inducing a shock that reflects off of the afterbody.

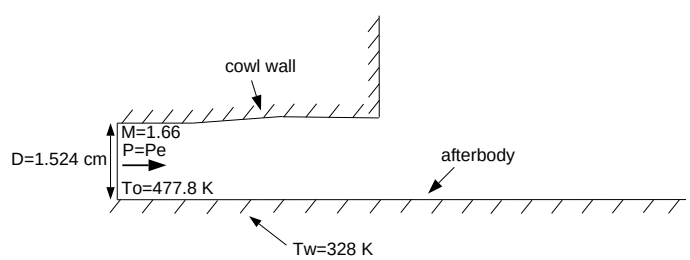

Figure 14.2.1: Problem Description: 0-Degree Afterbody

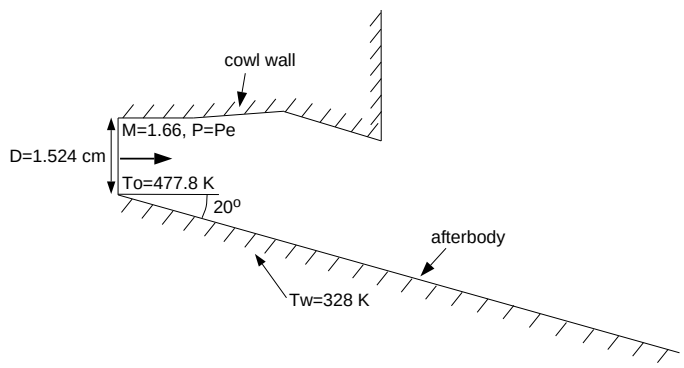

Figure 14.2.2: Problem Description: 20-Degree Afterbody

14.3 References

1. Hopkins, H. B., Konopka, W., and Leng, J. *Validation of scramjet exhaust simulation technique at Mach 6.* NASA Contractor Report 3003, 1979.

14.4 Results

Figure 14.4.1 compares pressure ratio as a function of horizontal distance for the three different meshes and for the experimental results [1]. All are in excellent agreement. Pressure is normalized by the entrance value, P_e.

Figure 14.4.3 compares the heat transfer rate for the three 0-degree meshes with the experimental values. Agreement is good for all of the cases, especially for the quadrilateral and hybrid meshes.

Figures 14.4.2 and 14.4.4 show the pressure and heat transfer distributions for the 20-degree configuration and the comparison with the experiment. Because the impinging shock wave is not as strong as in the 0-degree case, no mesh adaption is required for this case.

© Fluent Inc. August 8, 2006

14.4.1 Validation-Specific Information

Solver:	FLUENT 2d
Version:	6.3.15
Solution Files:	1. `scram0hyb_adapt_r3.cas`, `scram0hyb_adapt_r3.dat`
	2. `scram0quad_adapt_r1.cas`, `scram0quad_adapt_r1.dat`
	3. `scram0tri_adapt_r4.cas`, `scram0tri_adapt_r4.dat`
	4. `scram20quad_r2.cas`, `scram20quad_r2.dat`

These solution files are available from the Fluent Inc. User Services Center as described in the Introduction.

14.4.2 Plot Data

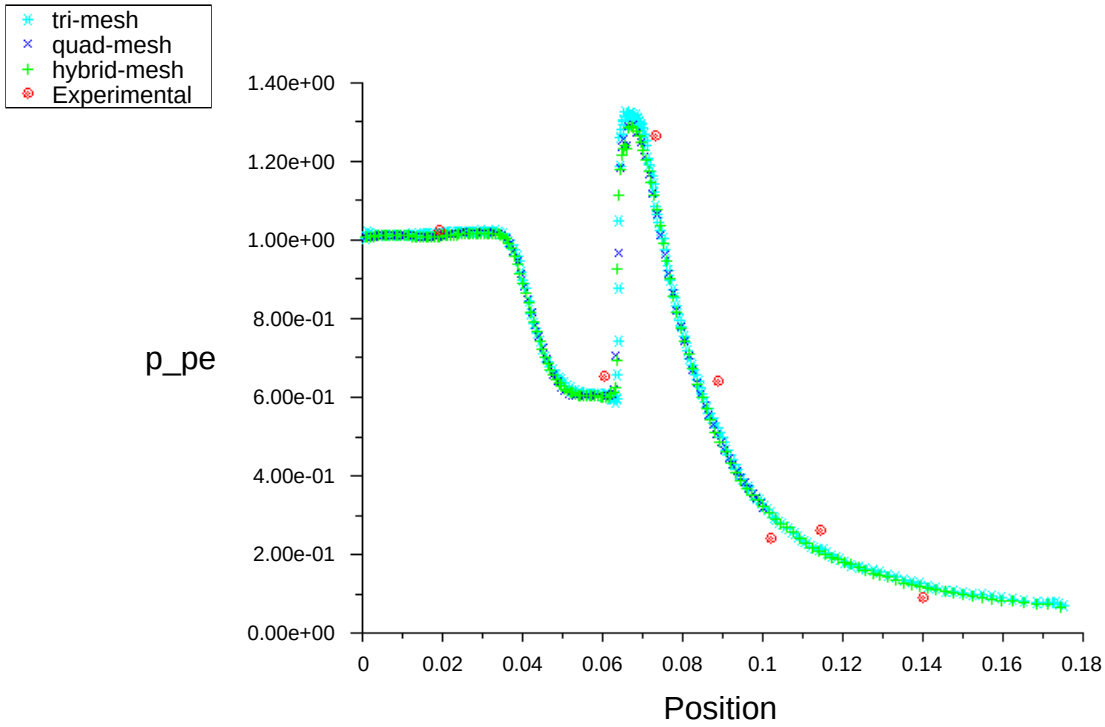

Reflecting shock waves, 0-Degree Afterbody
p_pe
Adapted Quad,Tri and Hybrid Meshes FLUENT 6.3 (2d, dp, pbns, lam)

Figure 14.4.1: Normalized Pressure as a Function of Horizontal Distance for the Three 0-Degree Afterbody Mesh Configurations and for the Hopkins et al. [1] Results

© Fluent Inc. August 8, 2006

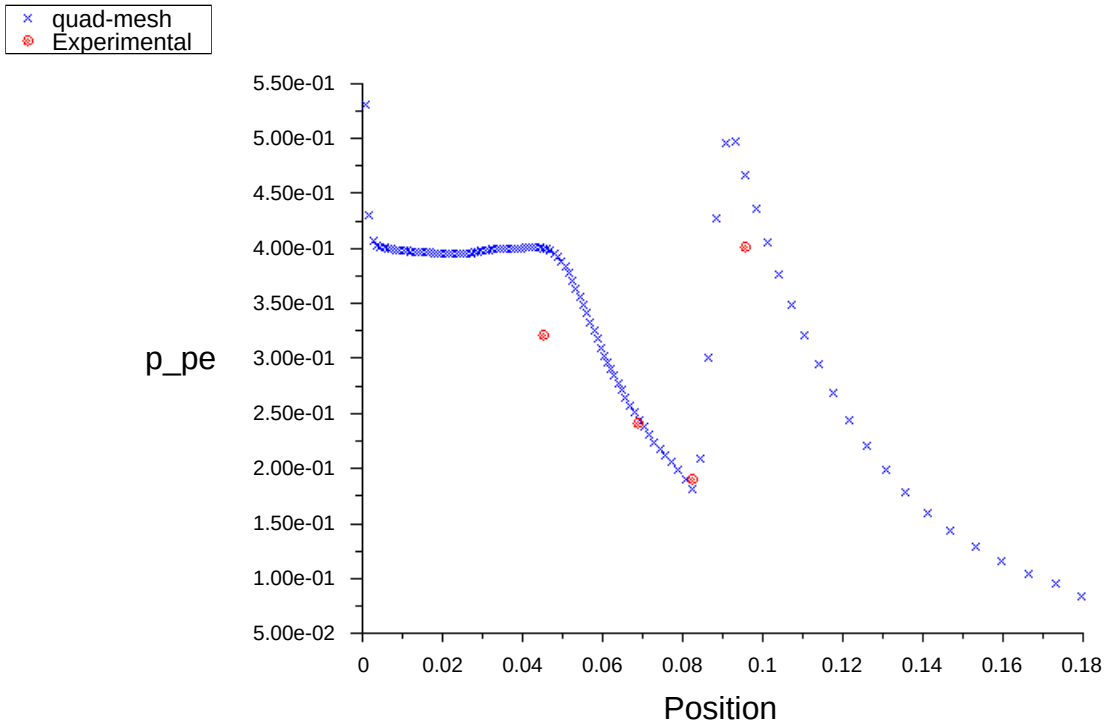

Reflecting shock waves, 20-Degree Afterbody
p_pe
Adapted Quad Mesh FLUENT 6.3 (2d, dp, pbns, lam)

Figure 14.4.2: Normalized Pressure as a Function of Horizontal Distance for the 20-Degree Afterbody and for the Hopkins et al. [1] Results

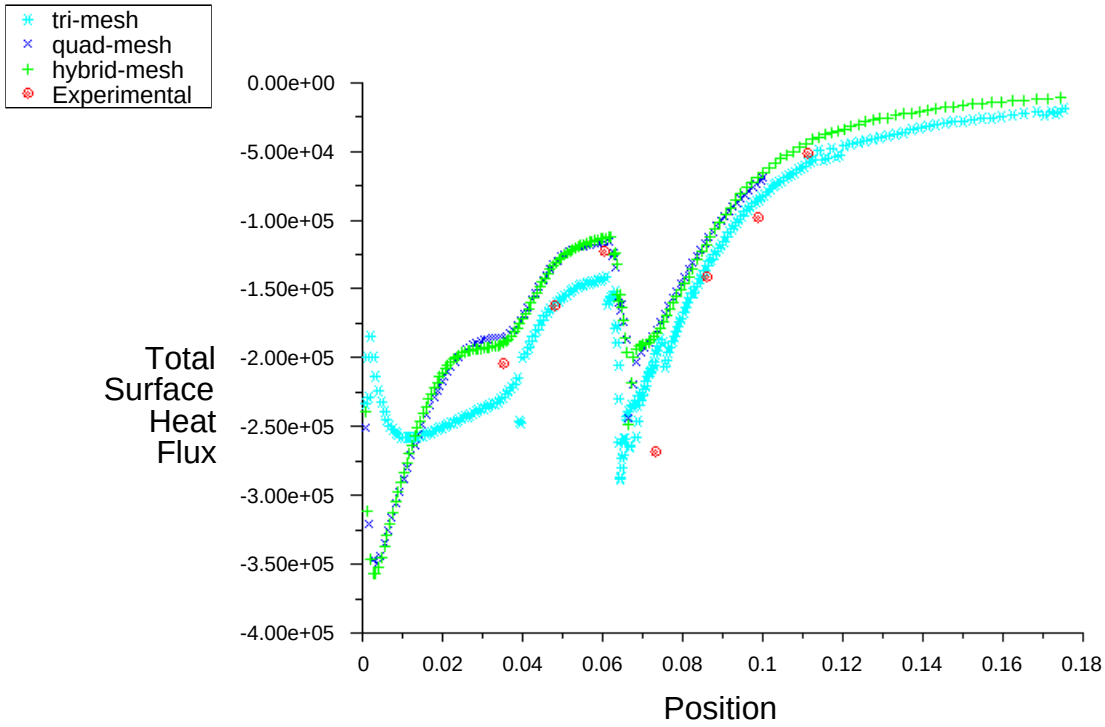

Reflecting shock waves, 0-Degree Afterbody
Total Surface Heat Flux(W/m2)
Adapted Quad,Tri and Hybrid Meshes FLUENT 6.3 (2d, dp, pbns, lam)

Figure 14.4.3: Heat Transfer Rate as a Function of Horizontal Distance for the Three 0-Degree Afterbody Mesh Configurations and for the Hopkins et al. [1] Results

© Fluent Inc. August 8, 2006

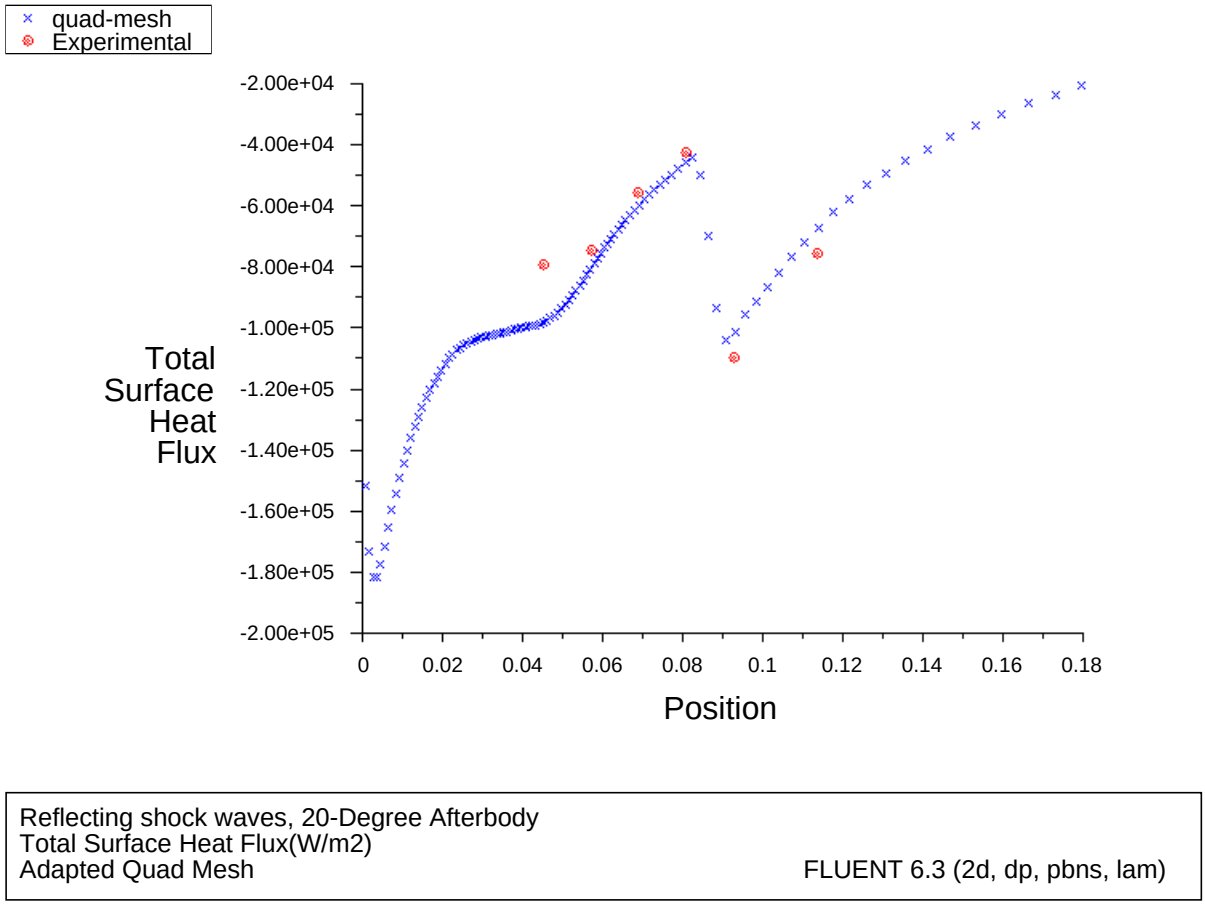

Figure 14.4.4: Heat Transfer Rate as a Function of Horizontal Distance for 20-Degree Afterbody and for the Hopkins et al. [1] Results

© Fluent Inc. August 8, 2006

Validation 15. Turbulent Bubbly Flows

15.1 Purpose

This validation compares FLUENT's predictions of void fraction and axial velocity for bubbly flow in a vertical pipe with experimental data [1,2,3,4,5]. It uses the Eulerian multiphase model with the standard k-ϵ turbulence model.

15.2 Problem Description

The flow considered is an upward, co-current air-water bubbly flow in a vertical, circular pipe under normal conditions. The pipe has a length $L = 2.5$ m and a diameter of $d = 5.7$ cm. Figure 15.2.1 shows the geometry of the problem.

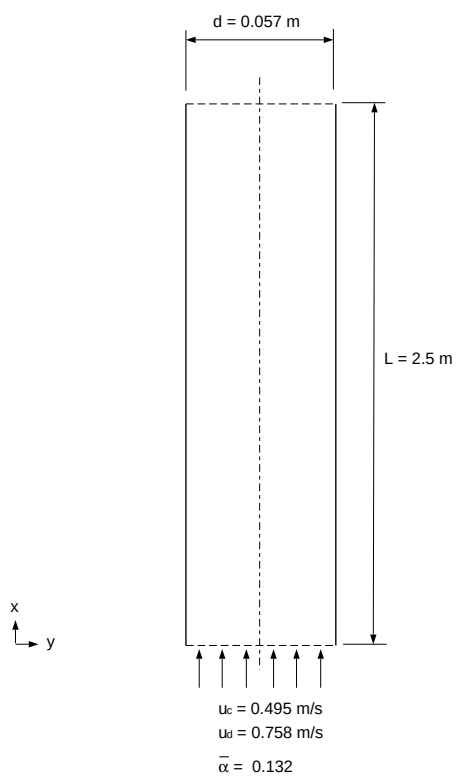

Figure 15.2.1: Problem Description

15.3 References

1. Moraga, F. J., Bonetto, R.T. and Lahey, R. T. 1999 Lateral forces on spheres in turbulent uniform shear flow. *Int. J.Multiphase Flow* 25, 1321-2372.

2. Wang, S. K., Lee, S. J., Jones, O.C. and Lahey, R. T. 1987 3-D turbulence structure and phase distribution measurements in bubbly two-phase flows. *Int. Multiphase Flow* 13 3, 327-343.

3. A. Troshko, V. Ivanov, S. Vasques, *Implementation of a General Lift Coefficient in the CFD Model of Turbulent Bubbly Flows*,Fluent Inc., Lebanon, NH.

4. Troshko, A. A. 2000 Two-equation, multidimensional model of turbulence in bubbly flows, PhD. dissertation, Texas A&M University.

5. R. Clift, J. R. Grace and M.E. Weber, *Bubbles, drops and particles*, Academic Press, 1978.

15.4 Results

Figures 15.4.1 and 15.4.2 show the comparison between experimental and FLUENT's data for the continuous-phase axial velocity and the dispersed-phase volume fraction radial profiles. Note that simulation results at $x = 26$, 35 and 44 d were essentially the same due to the fully-developed nature of the flow at those downstream locations. There is a good agreement for the velocity, and excellent agreement for the dispersed-phase volume fraction. Inviscid lift is predominant in the outer layer, pushing bubbles toward the wall, while vortex shedding lift dominates the inner layer, driving bubbles from the wall.

Near the wall, liquid film between the bubble and the wall moves slower than the liquid at the free-stream side of the bubble. This velocity gradient is due to the no-slip condition at the wall, creating a pressure difference driving bubbles from the wall.

15.4.1 Validation-Specific Information

Solver:	FLUENT 2d
Version:	6.3.11
Solution Files:	`liftch-drag-disp-ke.cas`, `liftch-drag-disp-ke.dat`

These solution files are available from the Fluent Inc. User Services Center as described in the Introduction.

© Fluent Inc. August 8, 2006

15.4.2 Plot Data

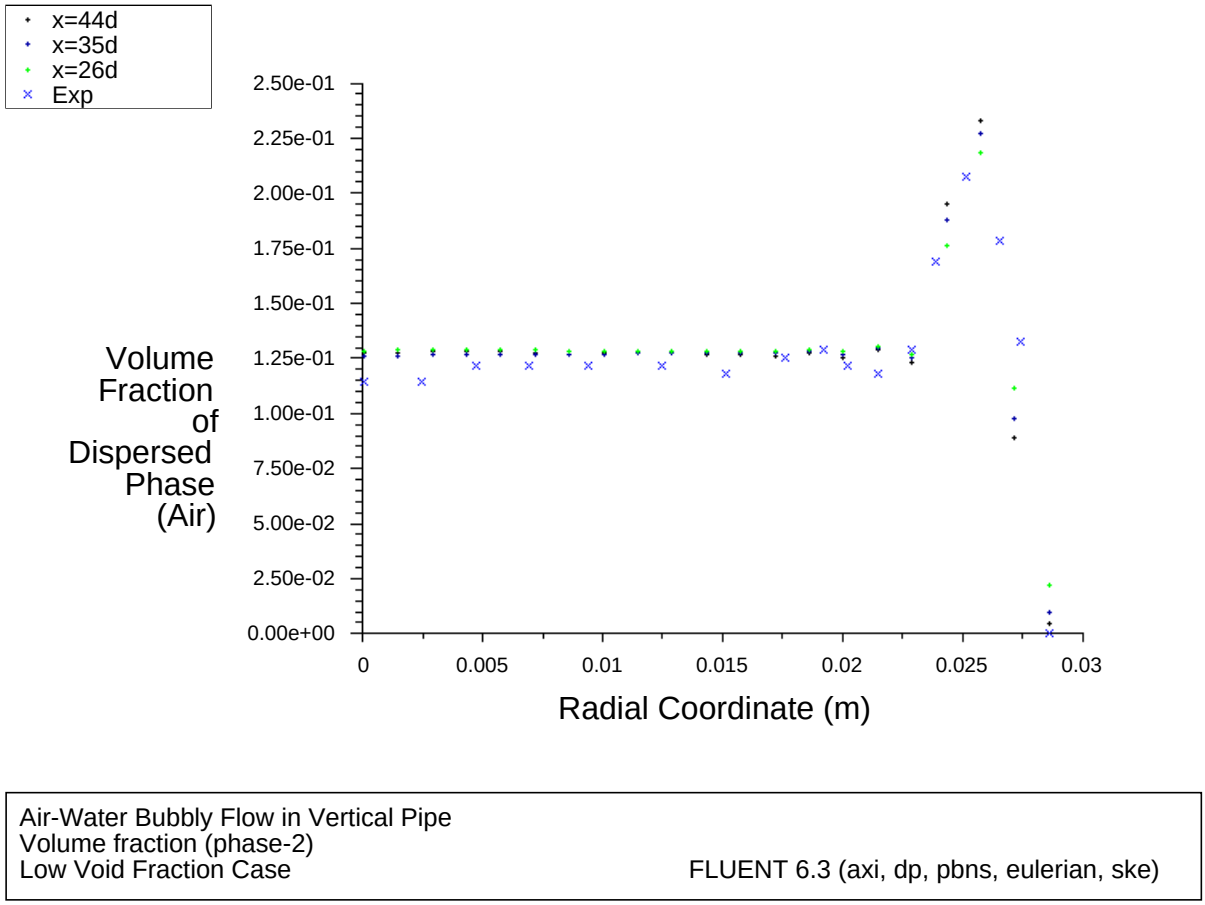

Figure 15.4.1: Radial Profile of Dispersed Phase Volume Fraction (Air)

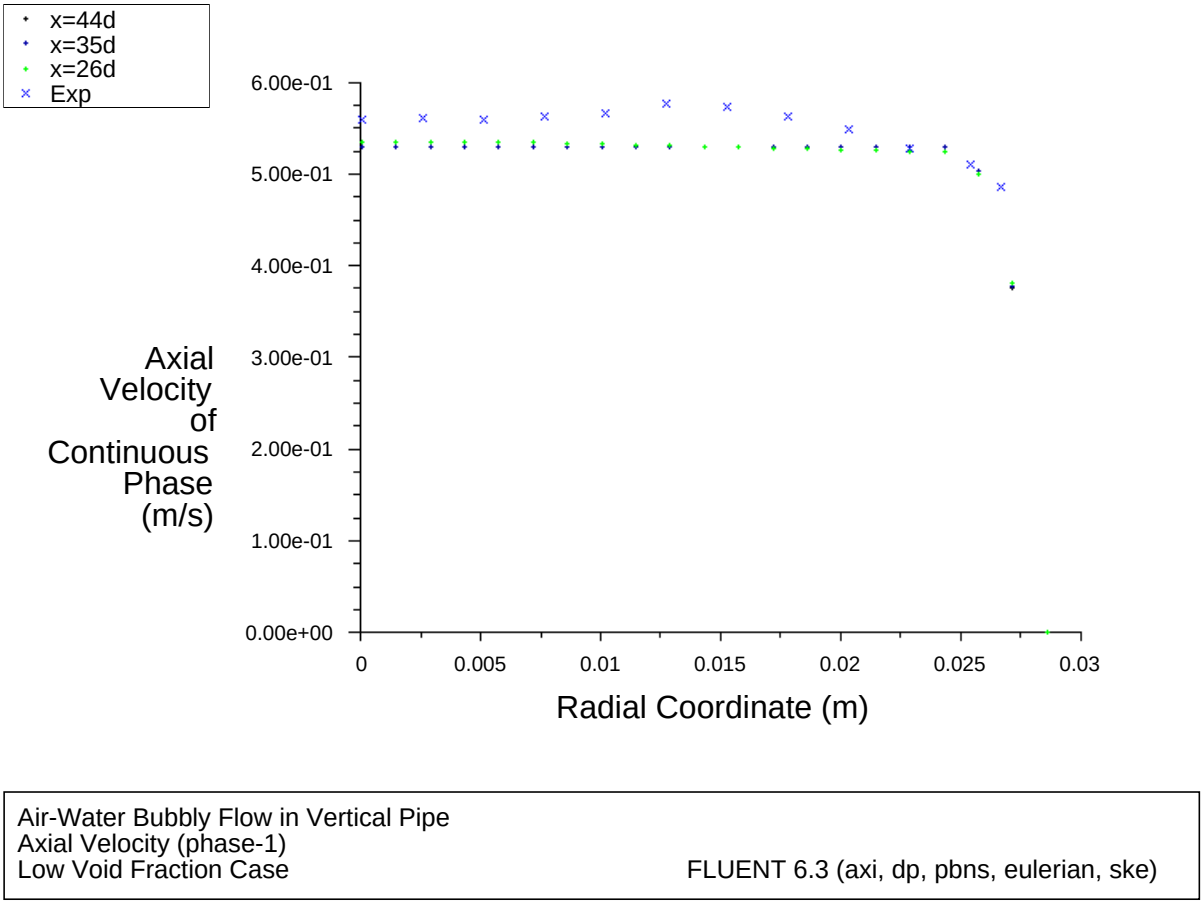

Figure 15.4.2: Radial Profile of Continuous Phase Axial Velocity (Water)

© Fluent Inc. August 8, 2006

Validation 16. Adiabatic Compression and Expansion Inside an Idealized 2D In-Cylinder Engine

16.1 Purpose

This validation compares FLUENT's predictions for an idealized 2D in-cylinder engine simulating an adiabatic process against analytical data from isentropic thermodynamic relations. Two different methods are used to model the deforming mesh: dynamic layering and spring-based smoothing with local remeshing.

16.2 Problem Description

A simplified 2D in-cylinder geometry is used, consisting of a 10m x 8m box. The bottom surface represents the piston head. The piston moves up from the bottom dead center (BDC) position, corresponding to a crank shaft angle of 180 degrees, slowly compressing the fluid adiabatically until the volume decreases to 2m x 8m. Once it reaches the top dead center (TDC) position, corresponding to a crank shaft angle of 360 degrees, the piston moves back downward to the initial position, to complete the cycle (see Figures 16.2.1 and 16.2.2).

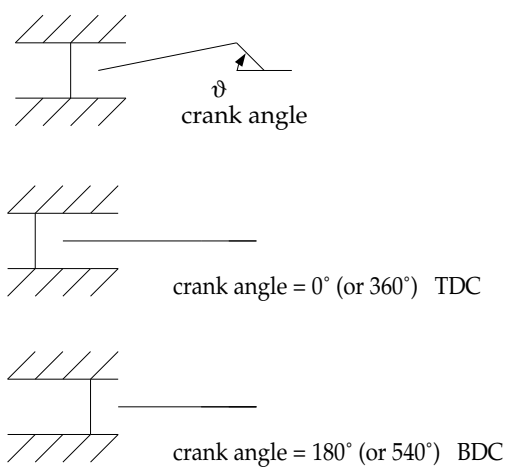

Figure 16.2.1: Problem Specification

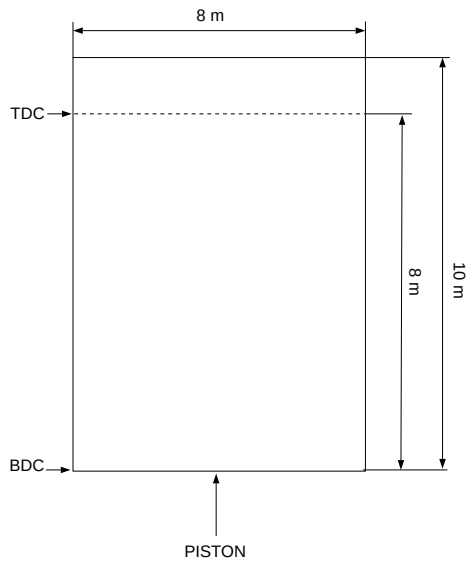

Figure 16.2.2: Problem Geometry

16.3 Results

FLUENT results were compared with analytical data from isentropic thermodynamic relations. Pressure and temperature values were obtained through the following expressions:

$$\frac{T_2}{T_1} = \left(\frac{V_1}{V_2}\right)^{\gamma-1} \tag{16.3-1}$$

$$\frac{P_2}{P_1} = \left(\frac{V_1}{V_2}\right)^{\gamma} \tag{16.3-2}$$

where P_1 is the pressure at the volume V_1 and temperature T_1, P_2 is the pressure at the volume $V2$ and temperature T_2 and γ is the specific heat ratio.

Figures 16.3.1 and 16.3.2 compare the temperature and pressure of FLUENT results against the analytical data, showing an excellent match of the values for both the layering methods, dynamic layering, and the spring-based smoothing method with local remeshing for the dynamic mesh motion.

© Fluent Inc. August 8, 2006

16.3.1 Validation-Specific Information

Solver:	FLUENT 2d
Version:	6.3.11
Solution Files:	1. `poly_2d_layer.cas`, `poly_2d_layer.dat`
	2. `poly_2d_remesh.cas`, `poly_2d_remesh.dat`

These solution files are available from the Fluent Inc. User Services Center as described in the Introduction.

16.3.2 Plot Data

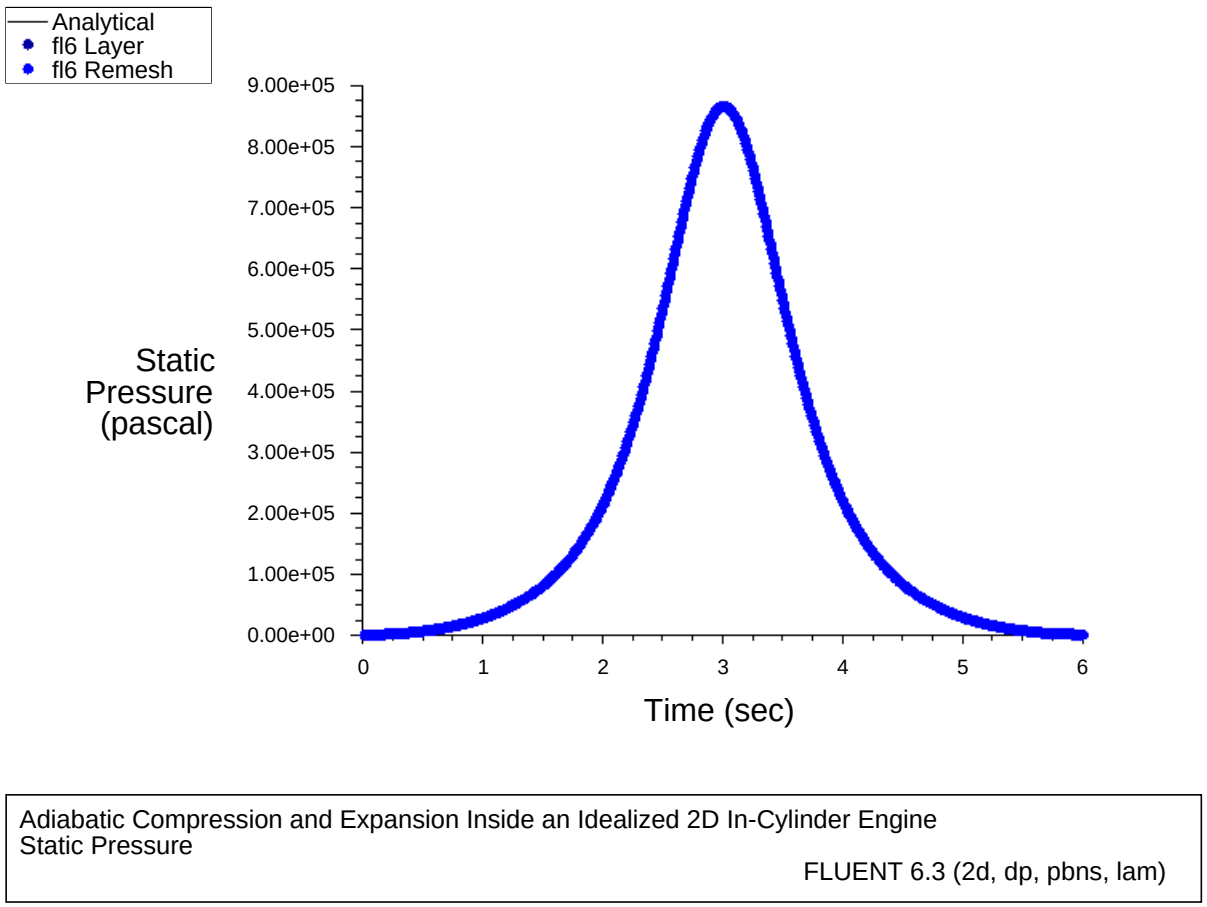

Figure 16.3.1: Static Pressure in the Chamber Area During One Piston Cycle

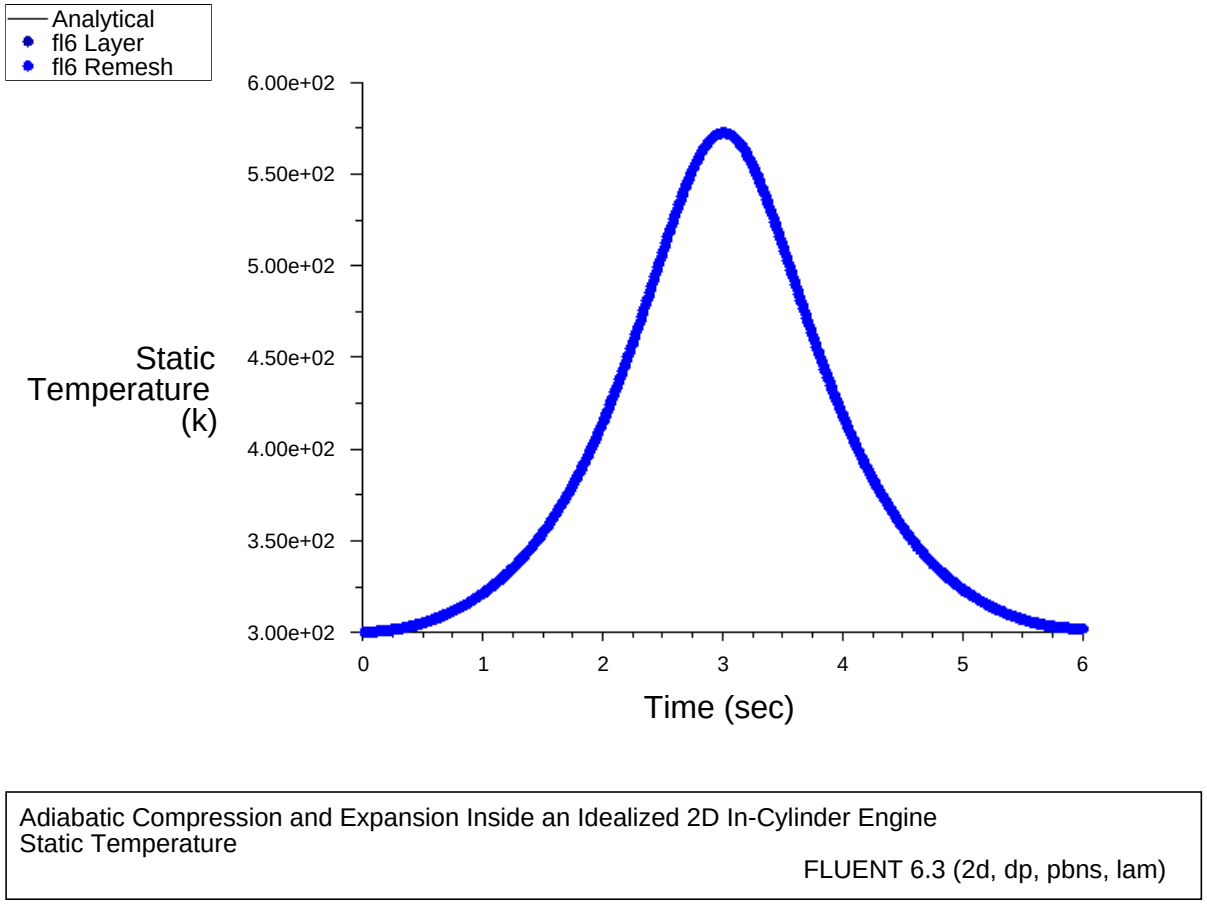

Figure 16.3.2: Static Temperature in the Chamber Area During One Piston Cycle

© Fluent Inc. August 8, 2006

Validation 17. Cavitation Over a Sharp-Edged Orifice

17.1 Purpose

The purpose of this test is to validate the capability of the cavitation model when applied to a cavitating flow. The strength of the cavitation depends on the inlet pressure. When the inlet pressure is small, the cavitation number is large, and the flow is weakly cavitating. For larger inlet pressures, the cavitation number is smaller, which in turn results in a strongly cavitating flow.

Fourteen (14) test cases were prepared with the inlet total pressure ranging from 1.9×10^5 to 4×10^8 Pa. The computed discharge coefficients were compared with the experimental correlation by Nurick [1].

17.2 Problem Description

A 2D axisymmetric sharp-edged orifice is considered, as shown in Figure 17.2.1. Its geometric parameters are $R/r = 2.86$ and $L/r = 7.94$, where R, r, and L denote the inlet radius, orifice radius, and orifice length, respectively. The flow is assumed to be turbulent, and the standard $k-\varepsilon$ model is employed. The specified boundary conditions are the total pressure P_o at the inlet, which varies from 1.9×10^5 to 4×10^8 Pa, and the static pressure $P_{exit} = 95000$ Pa at the exit.

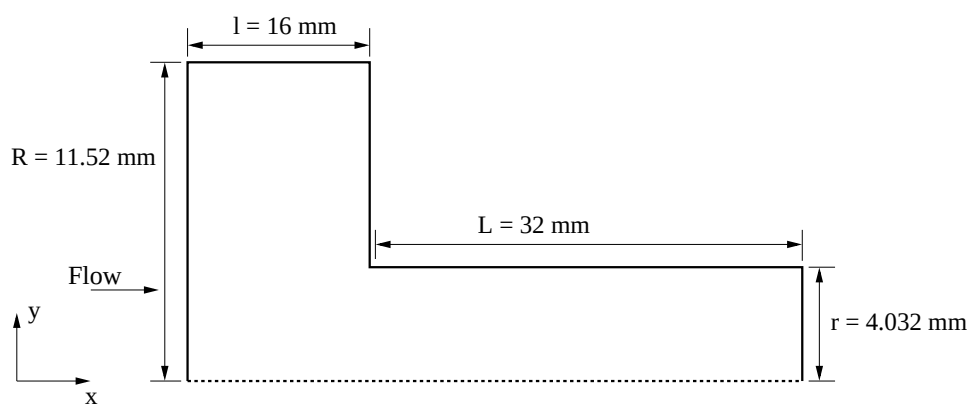

Figure 17.2.1: Problem Description

17.3 References

1. W.H. Nurick, Orifice Cavitation and its Effects on Spray Mixing, *Journal of Fluids Engineering*, Vol. 98, 1976.

17.4 Results

Experimental data is available in the form of discharge coefficient versus cavitation number, where the discharge coefficient is defined as $\dot{m}/\dot{m}_i$, $\dot{m}$ is the computed mass flow rate, and $\dot{m}_i$ is the ideal mass flow rate through the orifice. The ideal mass flow rate through the orifice is computed as $\dot{m}_i = A\sqrt{2\rho(P_o - P_{exit})}$, where A is the cross-sectional area of the orifice, $A = \pi r^2$, ρ is the density, and P_o and P_{exit} are the inlet pressure and the exit pressure, respectively. FLUENT shows excellent agreement with the experimental measurements.

17.4.1 Validation-Specific Information

Solver:	FLUENT 2d
Version:	6.3.11
Solution Files:	1. `1.9bar_n_1.cas`, `1.9bar_n_1.dat`
	2. `2bar_n_1.cas`, `2bar_n_1.dat`
	3. `2.25bar_n_1.cas`, `2.25bar_n_1.dat`
	4. `2.5bar_n_1.cas`, `2.5bar_n_1.dat`
	5. `3bar_n_1.cas`, `3bar_n_1.dat`
	6. `3.75bar_n_1.cas`, `3.75bar_n_1.dat`
	7. `5bar_n_1.cas`, `5bar_n_1.dat`
	8. `10bar_n_1.cas`, `10bar_n_1.dat`
	9. `50bar_n_1.cas`, `50bar_n_1.dat`
	10. `100bar_n_1.cas`, `100bar_n_1.dat`
	11. `500bar_n_1.cas`, `500bar_n_1.dat`
	12. `1000bar_n_1.cas`, `1000bar_n_1.dat`
	13. `2500bar_n_1.cas`, `2500bar_n_1.dat`
	14. `4000bar_n_1.cas`, `4000bar_n_1.dat`

These solution files are available from the Fluent Inc. User Services Center as described in the Introduction.

© Fluent Inc. August 8, 2006

17.4.2 Plot Data

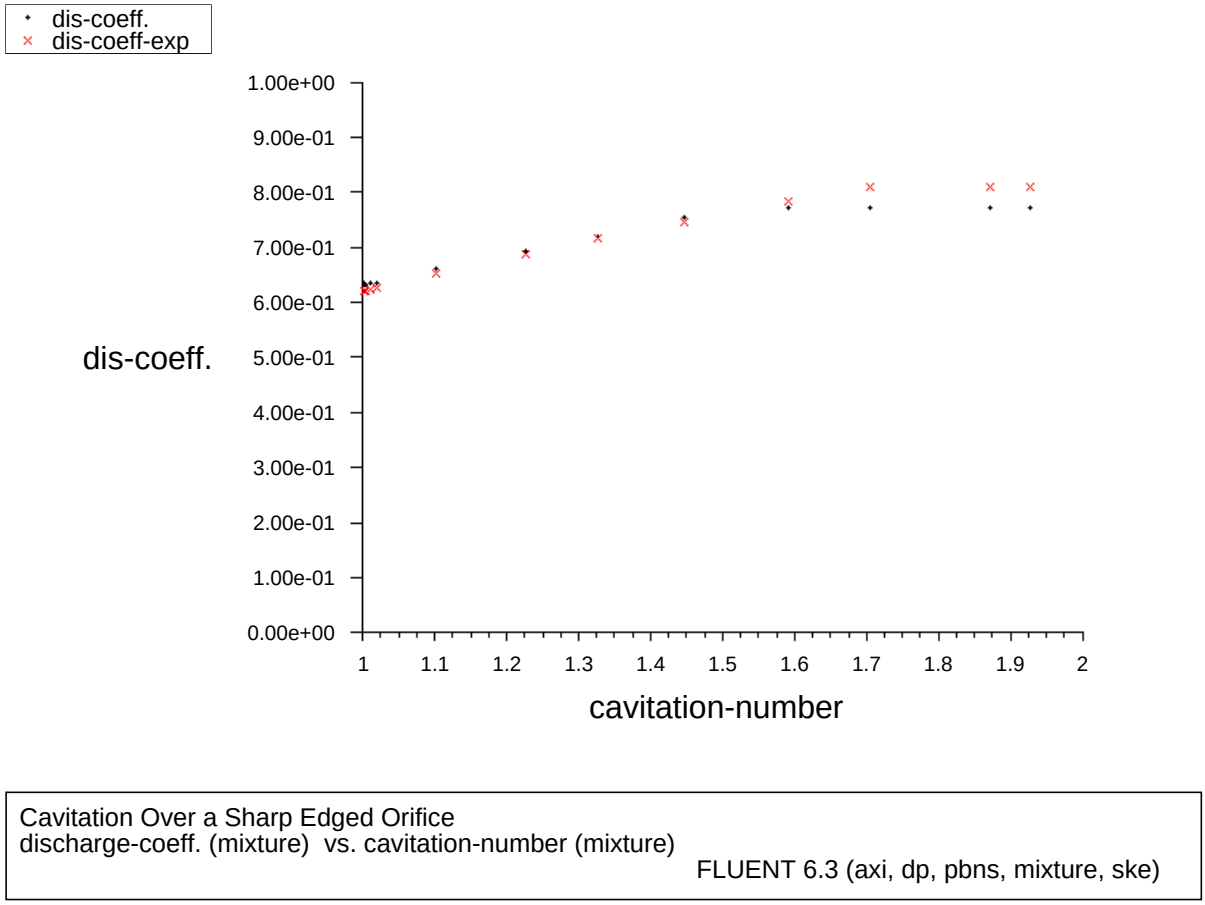

Figure 17.4.1: Comparison of FLUENT Prediction of Discharge Coefficient Versus Cavitation Number with Experimental Data

© Fluent Inc. August 8, 2006

Validation 18. Oscillating Laminar Flow Around a Circular Cylinder

18.1 Purpose

The purpose of this test is to validate FLUENT's ability to predict the frequency of periodically shed vortices behind a circular cylinder using the iterative and non-iterative time advancement schemes. The present calculations are confined to the low-Reynolds-number regime ($Re = 100$), which encompasses unsteady asymmetric flow. The results obtained using the different non-iterative time advancement (NITA) schemes (NITA with PISO and NITA with Fractional Step) are compared to the iterative time advancement (ITA) scheme and to experimental data [1,2].

18.2 Problem Description

An infinitely long circular cylinder of diameter $D = 2.0\ m$ is placed in an otherwise undisturbed uniform crossflow ($U_\infty = 1.0\ m/s$) as shown in Figure 18.2.1. The lateral boundary and the exit boundary in the far wake are placed at $5D$ and $20D$ from the center of the circular cylinder, respectively.

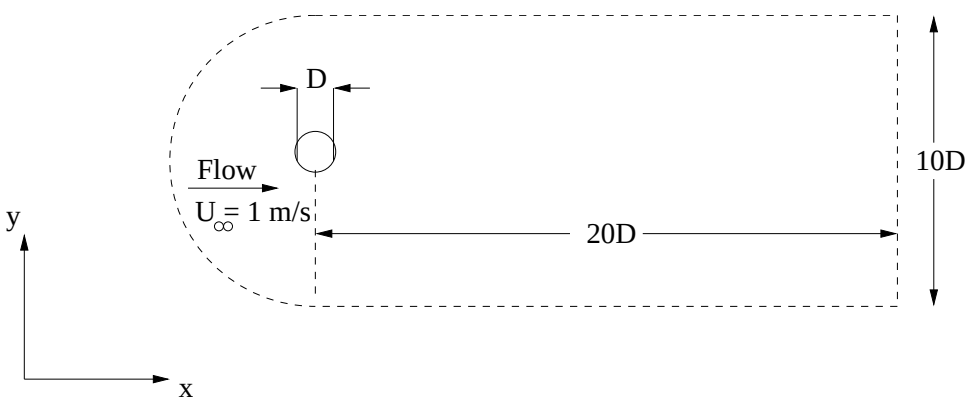

Figure 18.2.1: Problem Description

18.3 References

1. Coutanceau, M. and Defaye, J.R., Circular Cylinder Wake Configurations - A Flow Visualization Survey, Appl. Mech. Rev., 44(6), June 1991.

2. Braza, M., Chassaing, P., and Minh, H.H., Numerical Study and Physical Analysis of the Pressure and Velocity Fields in the Near Wake of a Circular Cylinder, J. Fluid Mech., 165:79-130, 1986.

18.4 Results

The flow seems to demonstrate periodic shedding of vortices downstream of the cylinder. To quantify the periodicity of the flow, the time history of the y velocity, situated at a point that is 1 m behind the cylinder in the near wake, is presented. Also an FFT analysis of the lift coefficient on the cylinder wall is presented to determine the frequency of oscillations. The Strouhal number corresponding to the maximum magnitude of oscillations with different solver schemes are summarized in Table 18.4.1.

Table 18.4.1: Predicted Strouhal Number Using Different Solver Schemes

Method	**Strouhal Number**
Experimental Value	0.165
ITA	0.173
NITA + PISO	0.173
NITA + Fractional Step	0.173

From experimental data, we have a Strouhal number of 0.165. The Formula for the Strouhal number is

$$S = (N * D)/V_\infty \tag{18.4-1}$$

where N is the frequency, D is the diameter of the cylinder, and V_∞ is the freestream velocity. Solving Equation 18.4-1 for the experimental frequency, we get $N = 0.0825s^{-1}$. Computational results yield a frequency of $N = 0.0865s^{-1}$, which are within 5% of the experimental value. Furthermore, the ITA and NITA schemes gave nearly identical solutions.

© Fluent Inc. August 8, 2006

18.4.1 Validation-Specific Information

Solver:	FLUENT 2d
Version:	6.3.11
Solution Files:	1. `cylin_iter.cas`, `cylin_iter.dat`
	2. `cylin_NITA_FS.cas`, `cylin_NITA_FS.dat`
	3. `cylin_NITA_PISO.cas`, `cylin_NITA_PISO.dat`

These solution files are available from the Fluent Inc. User Services Center as described in the Introduction.

18.4.2 Plot Data

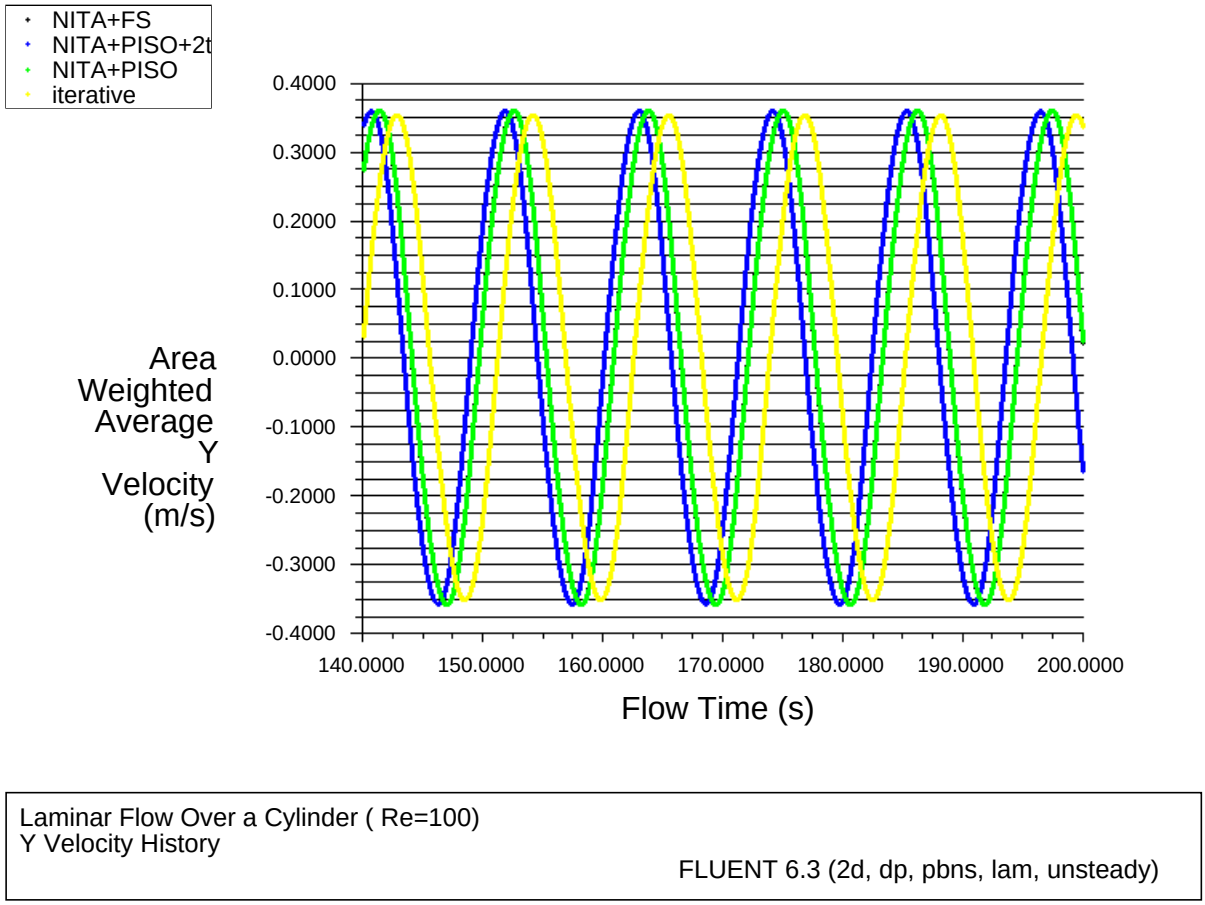

Figure 18.4.1: Comparison of Monitor of y Velocity at History Point Between Iterative Solver and Different NITA Schemes

© Fluent Inc. August 8, 2006

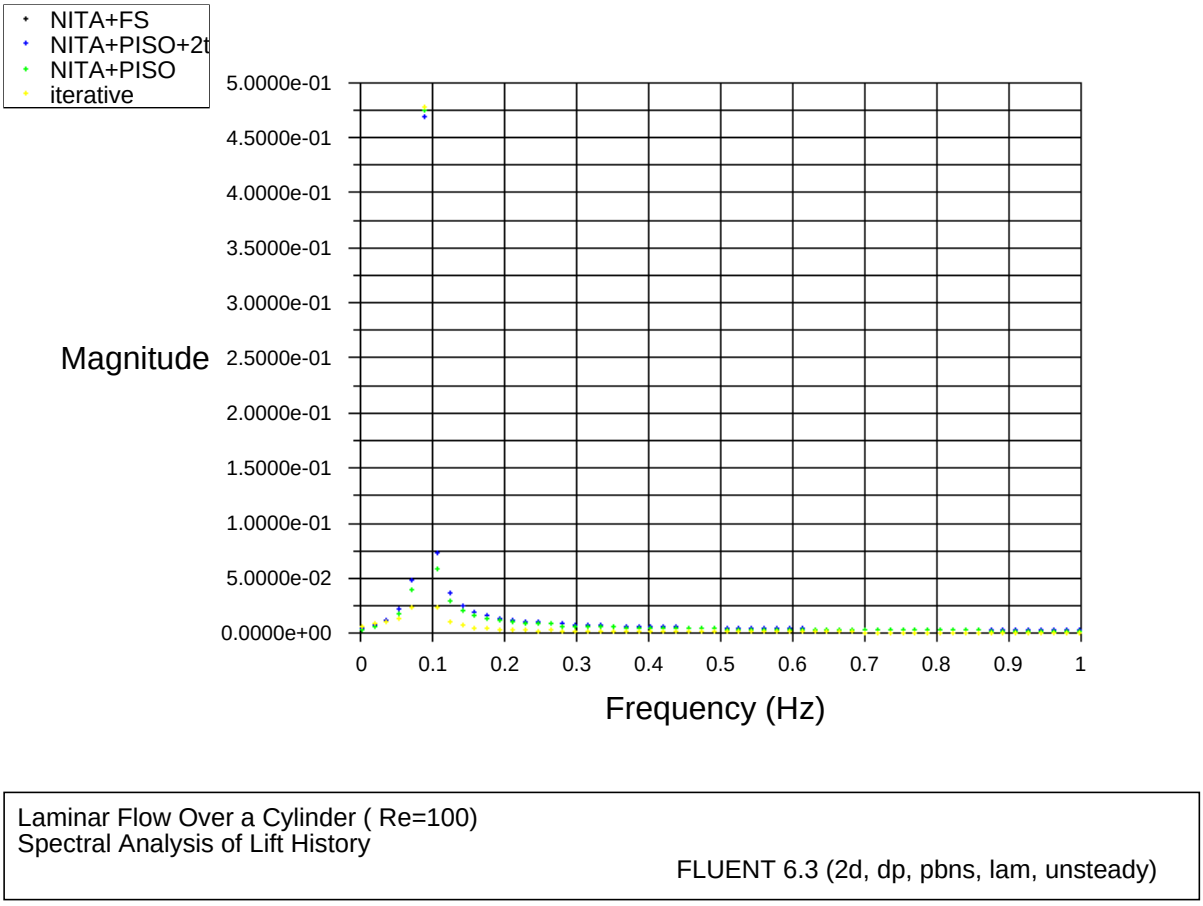

Figure 18.4.2: Comparison of FFT Analysis of Monitor of Lift Coefficient on the Cylinder Wall Between Iterative Solver and Different NITA Schemes

© Fluent Inc. August 8, 2006

Validation 19. Rotation of Two Immiscible Liquids

19.1 Purpose

The purpose of this test is to validate FLUENT's Volume of Fluid (VOF) model for rotational flow of immiscible liquids. FLUENT's predictions of swirl velocity and displacement of the interface between the liquids are in close agreement with the experimental data of Sugimoto and Iguchi [1].

19.2 Problem Description

A vertical cylindrical vessel containing immiscible silicone oil and water is initially at rest. The silicone oil layer rests on top of the water due to its lower density. The top of the cylindrical vessel is sealed. The vessel is set into rotation with a constant angular velocity, ω. The diameter and height of the vessel are 46 mm and 120 mm, respectively. The following equations are definitions of the dimensionless parameters:

$$Re_\omega = R(\frac{\omega}{\nu_w})^{\frac{1}{2}} \tag{19.2-1}$$

$$VR = \frac{V_w}{V_{so}} \tag{19.2-2}$$

where, R is the radius of the vessel, ω is the angular velocity of the vessel, ν_w is the kinematic viscosity of water, V_w is the volume of water, V_{so} is the volume of silicone oil, Re_ω is the rotation Reynolds number, and VR is the volume ratio.

Dimensionless swirl velocity is defined as $V_{sw}/(R\omega)$, where V_{sw} is the swirl velocity of water, and R and ω are the radius of the cylinder and the angular velocity of the cylindrical vessel, respectively.

Development of the flow field as a function of time, and the behavior of the interface between the two liquids are numerically studied using the VOF model. A geometric reconstruction scheme is used for the entire unsteady run. Due to the symmetrical nature of the flow, a 2D axisymmetric calculation is performed.

19.3 References

1. Sugimoto, T. and Iguchi, M., Behavior of Immiscible Two Liquid Layers Contained in Cylindrical Vessel Suddenly Set in Rotation, ISIJ Int., 42, pp. 338-343, 2002.

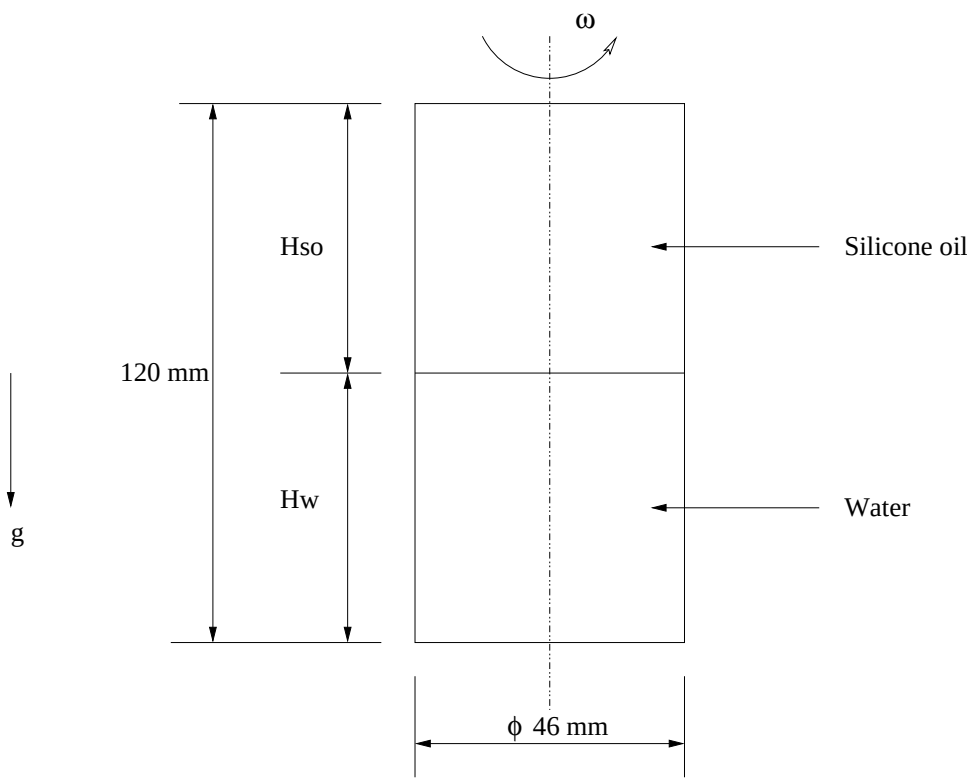

Figure 19.2.1: Problem Description

© Fluent Inc. August 8, 2006

19.4 Results

Experimental data is available in the form of

1. Dimensionless swirl velocity of water vs. time.
2. Vertical displacement of the interface h vs. time.

Dimensionless swirl velocity is defined as

$$\frac{V_{sw}}{R\omega}$$

where V_{sw} is the swirl velocity of water, and the displacement, h, of the interface on the axis of the vessel is calculated from the initial horizontal interfacial plane. Time histories of dimensionless swirl velocities of water are compared with experimental results for a $Re_\omega = 35.6$ and a VR of 0.5. The axial (x) and radial (r) coordinates of the locations, where the profiles are computed, are shown in Figures 19.4.3, 19.4.2, 19.4.1, and 19.4.4. The axial distance is measured from the bottom of the cylinder. For $Re_\omega = 74.9$ and VR=1, the variation of the interface height, h, with time is measured from the intermediate data files. Results show strong agreement with experimental results.

19.4.1 Validation-Specific Information

Solver:	FLUENT 2ddp
Version:	6.3.15
Solution Files:	1. `Rew35.6_VR0.5-swirl_t80.cas`, `Rew35.6_VR0.5-swirl_t80.dat` (for $Re_\omega = 35.6$ and VR=0.5, final solution at 80 sec)
	2. `Rew74.9_VR1-Interface_t60.cas`, `Rew74.9_VR1-Interface_t60.dat` (for $Re_\omega = 74.9$ and VR=1, final solution at 60 sec)

These solution files are available from the Fluent Inc. User Services Center as described in the Introduction.

19.4.2 Plot Data

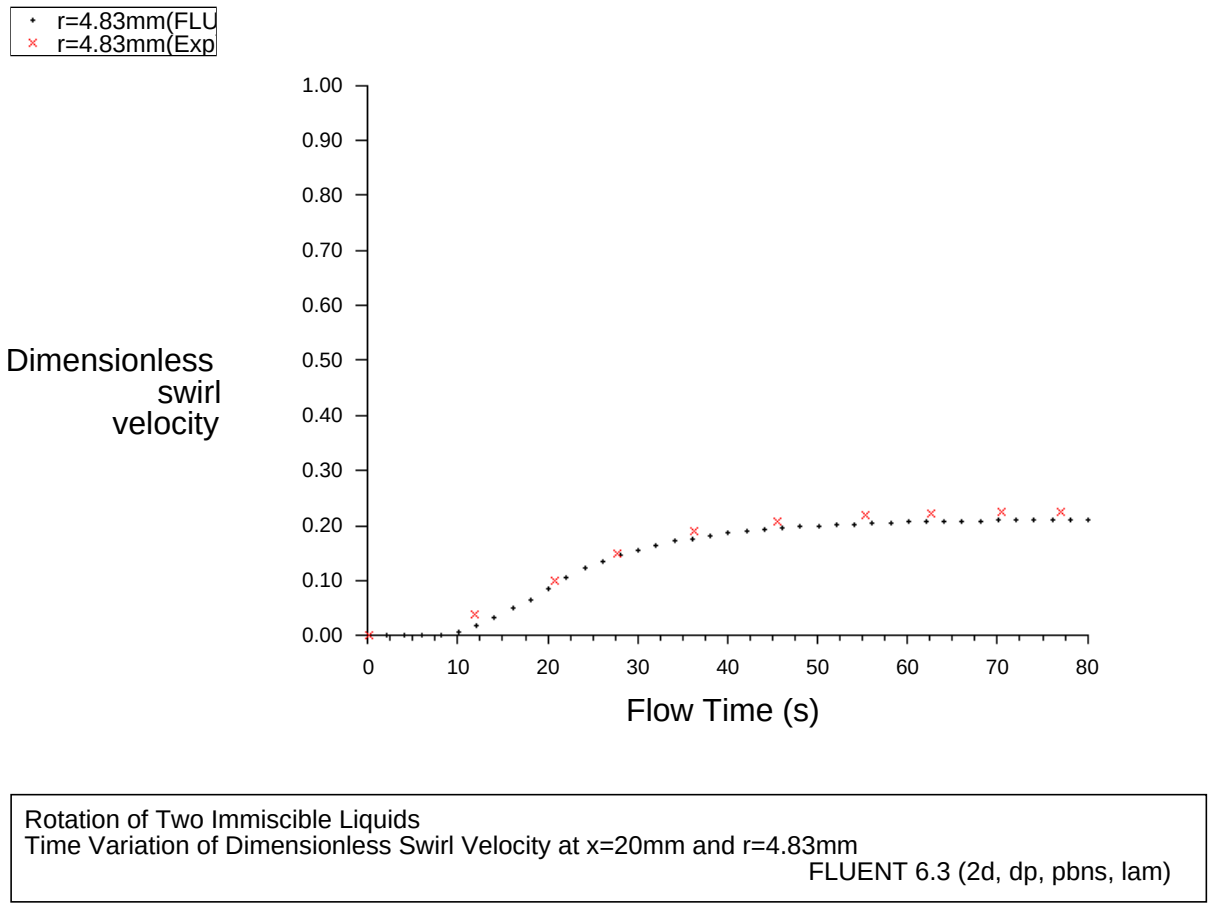

Figure 19.4.1: Time Variation of Dimensionless Swirl Velocity at $x = 20$ mm and $r = 4.83$ mm for $Re_\omega = 35.6$ and $VR = 0.5$

© Fluent Inc. August 8, 2006

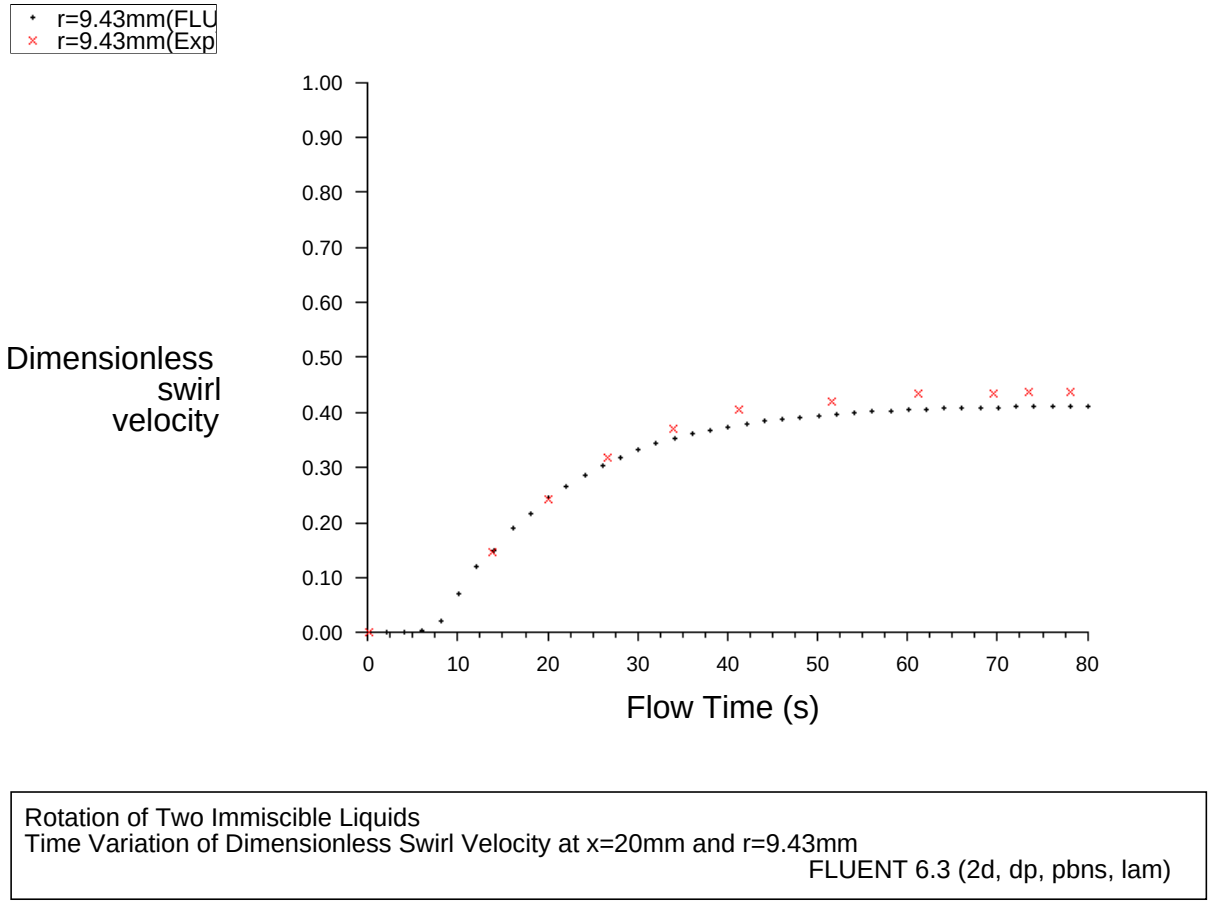

Figure 19.4.2: Time Variation of Dimensionless Swirl Velocity at $x = 20$ mm and $r = 9.43$ mm for $Re_\omega = 35.6$ and $VR = 0.5$

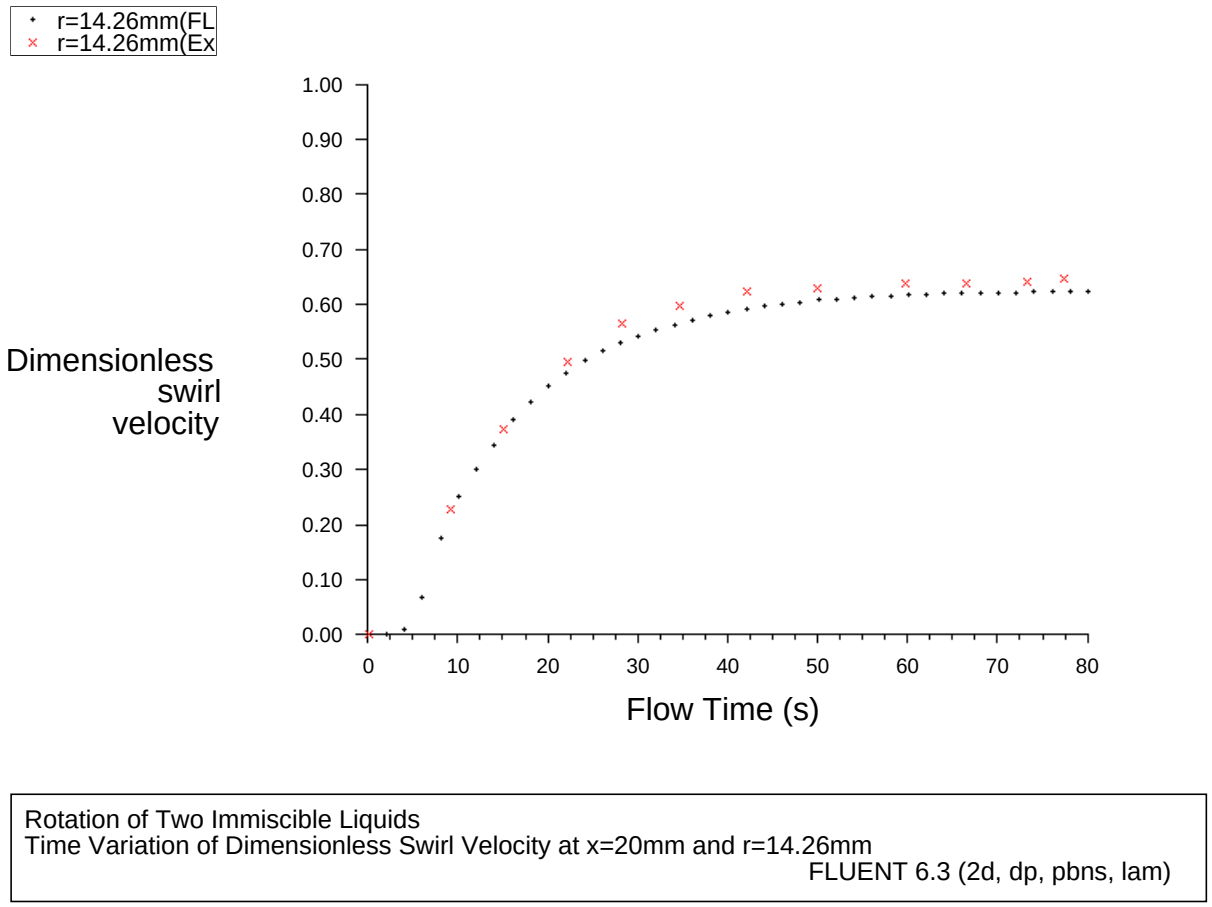

Figure 19.4.3: Time Variation of Dimensionless Swirl Velocity at $x = 20$ mm and $r = 14.26$ mm for $Re_\omega = 35.6$ and $VR = 0.5$

© Fluent Inc. August 8, 2006

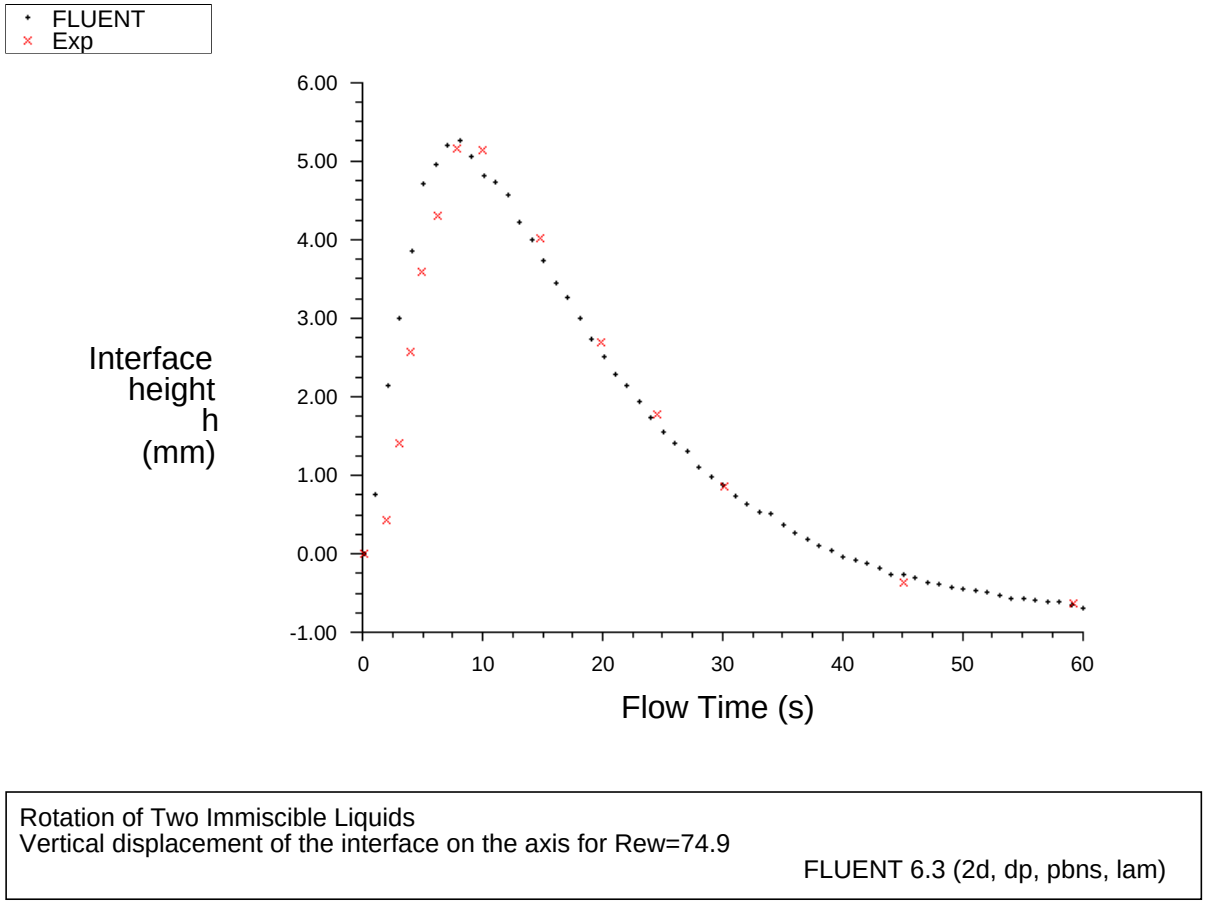

Figure 19.4.4: Vertical Displacement of the Interface on the Axis for $Re_\omega = 74.9$ and $VR = 1.0$

© Fluent Inc. August 8, 2006

Validation 20. Polyhedral and Tetrahedral Mesh Accuracy

20.1 Purpose

The purpose of this test is to validate the accuracy of second-order discretization schemes for the pressure-based solver, with tetrahedral and polyhedral meshes.

20.2 Problem Description

The laminar incompressible flow in a 3D driven cavity is solved at Reynolds number = 1000. A half domain is modeled with height = 1m, length = 1m and breadth = 0.5m, using symmetry boundary conditions. The top of the domain is modeled using a moving boundary condition. The flow is solved with second-order discretization schemes for pressure and momentum and SIMPLE coupling method.

20.3 References

1. Roache, P. J., *Verification and Validation in Computational Science and Engineering*, Hermosa Publishers, Albuquerque, New Mexico, 1998.

2. Wirogo, S., *Flux Corrected Method: An accurate approach to fluid flow modeling*, Ph.D thesis, Iowa State University, Ames, Iowa, 1997.

20.4 Results

The problem is solved for five sets of tetrahedral and polyhedral meshes, with increasing mesh density. A baseline is established for the velocity distribution along a line at the center of the symmetry plane and perpendicular to the direction of flow by obtaining a solution on a very fine, uniform mesh comprised of 500,000 hexahedral cells. This baseline is used to calculate the percent relative L2 norm (a measurement of error) for the velocity results of each of the tetrahedral and polyhedral meshes.

A logarithmic plot is then generated that shows how the L2 norm results change for each of the mesh types as the cell count increases (see Figure 20.4.4). Such a plot makes it possible to visually compare the difference in the cell count of polyhedral meshes and tetrahedral meshes for the same level of accuracy. Also plotted are points that demonstrate how the error drops off for first- and second-order accurate solutions. For 3D meshes, a first-order accurate solution can be represented by $y = x^{(-1/3)}$ and a second-order accurate solution can be represented by $y = x^{(-2/3)}$, where x is the cell count.

The second-order accuracy of the pressure-based segregated solver is validated by comparing the slopes of the polyhedral and tetrahedral plots to the slopes of the first- and second-order accurate solution plots. The results show that both mesh types exhibit second-order accuracy, as the error drop-off of each mesh type more closely corresponds to the slope of the second-order plot rather than the first-order plot.

20.4.1 Validation-Specific Information

Serial Number	Tetrahedral Mesh Cell Count	Tetrahedral Mesh Face Count	Polyhedral Mesh Cell Count	Polyhedral Mesh Face Count
1	12290	25658	2621	17224
2	29000	59808	5787	38608
3	57789	118427	11114	74858
4	241041	489263	43839	299647
5	1592404	3213634	279894	1930755

Solver: FLUENT 3ddp
Version: 6.3.11
Solution Files: Tetrahedral Meshes

1. `drv-cav-tet-1.cas.gz`, `drv-cav-tet-1.dat.gz`
2. `drv-cav-tet-2.cas.gz`, `drv-cav-tet-2.dat.gz`
3. `drv-cav-tet-3.cas.gz`, `drv-cav-tet-3.dat.gz`
4. `drv-cav-tet-4.cas.gz`, `drv-cav-tet-4.dat.gz`
5. `drv-cav-tet-5.cas.gz`, `drv-cav-tet-5.dat.gz`

Polyhedral Meshes

1. `drv-cav-poly-1.cas.gz`, `drv-cav-poly-1.dat.gz`
2. `drv-cav-poly-2.cas.gz`, `drv-cav-poly-2.dat.gz`
3. `drv-cav-poly-3.cas.gz`, `drv-cav-poly-3.dat.gz`
4. `drv-cav-poly-4.cas.gz`, `drv-cav-poly-4.dat.gz`
5. `drv-cav-poly-5.cas.gz`, `drv-cav-poly-5.dat.gz`

These solution files are available from the Fluent Inc. User Services Center as described in the Introduction.

© Fluent Inc. August 8, 2006

20.4.2 Plot Data

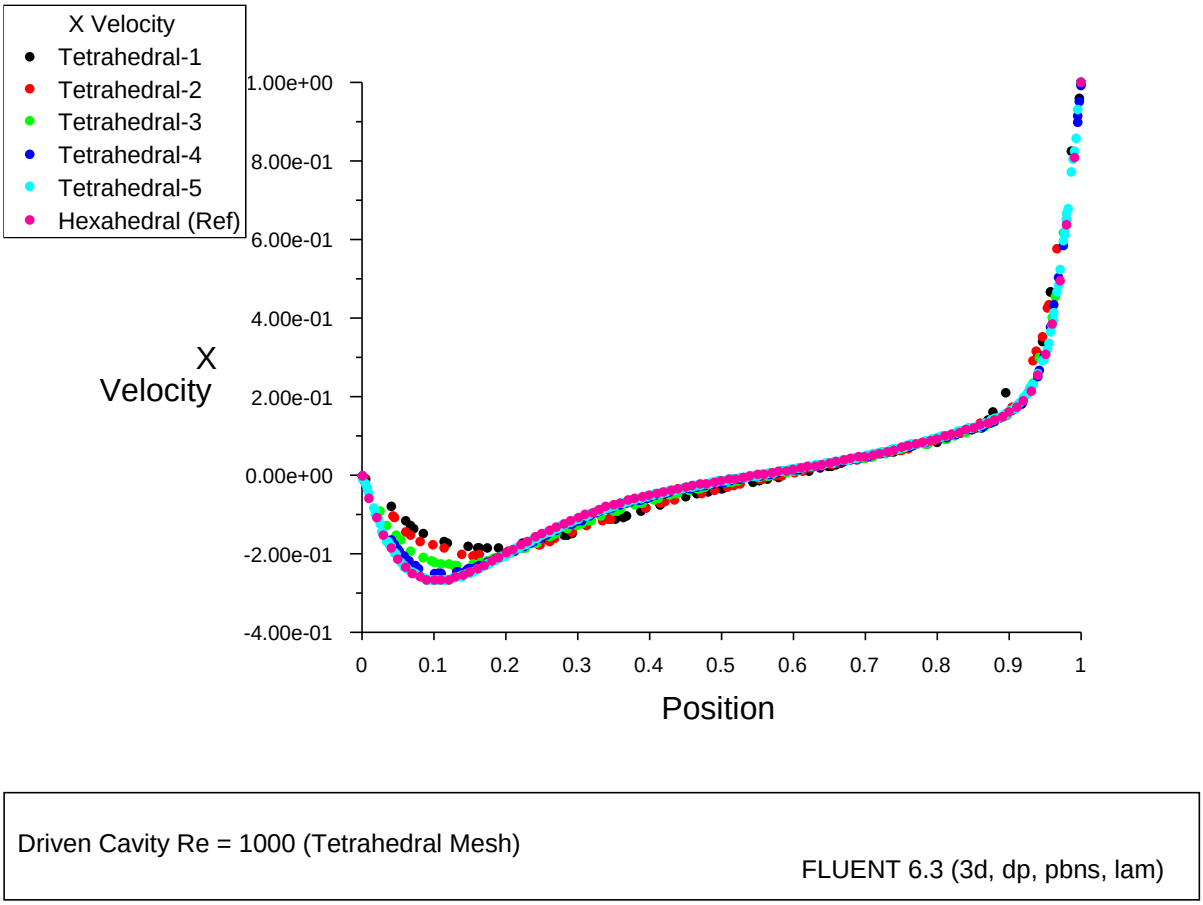

Figure 20.4.1: Velocity Distribution for Tetrahedral Meshes

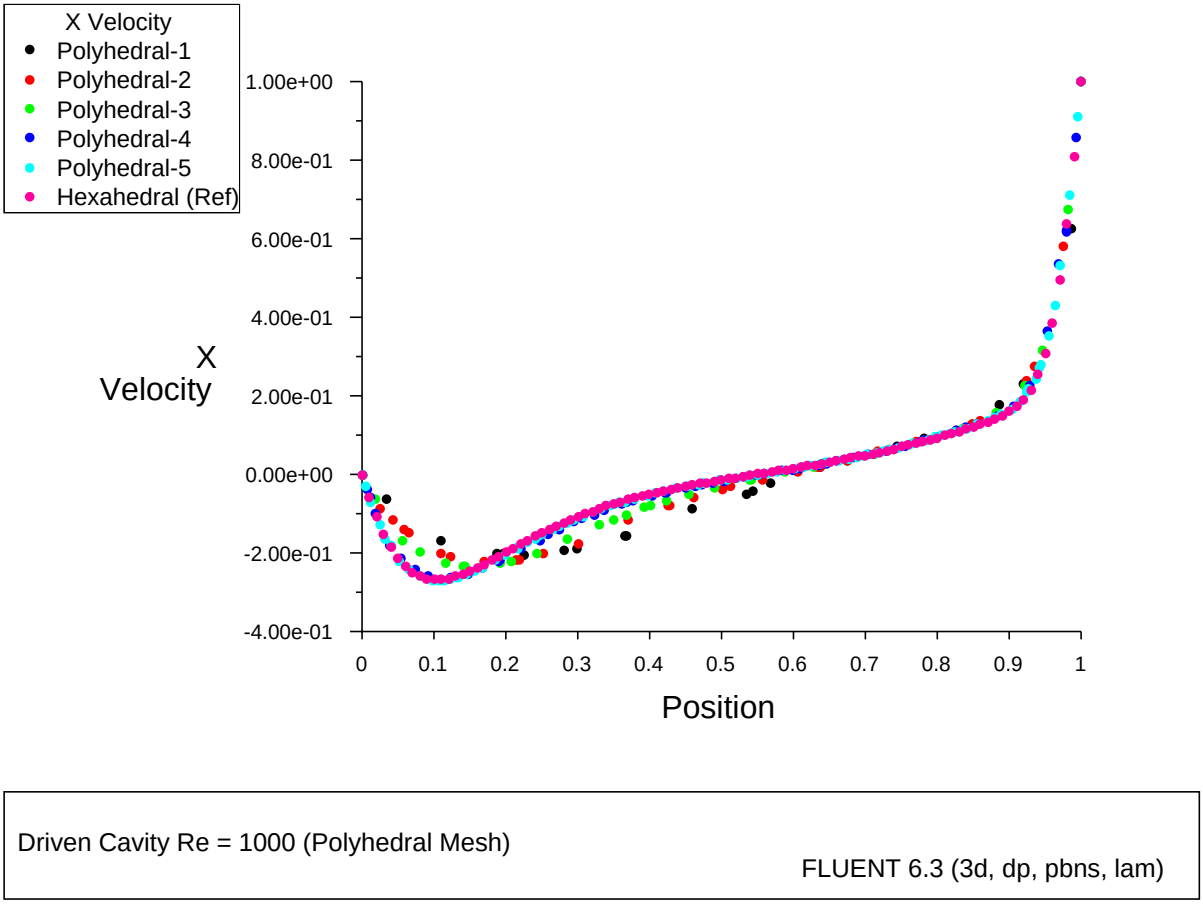

Figure 20.4.2: Velocity Distribution for Polyhedral Meshes

© Fluent Inc. August 8, 2006

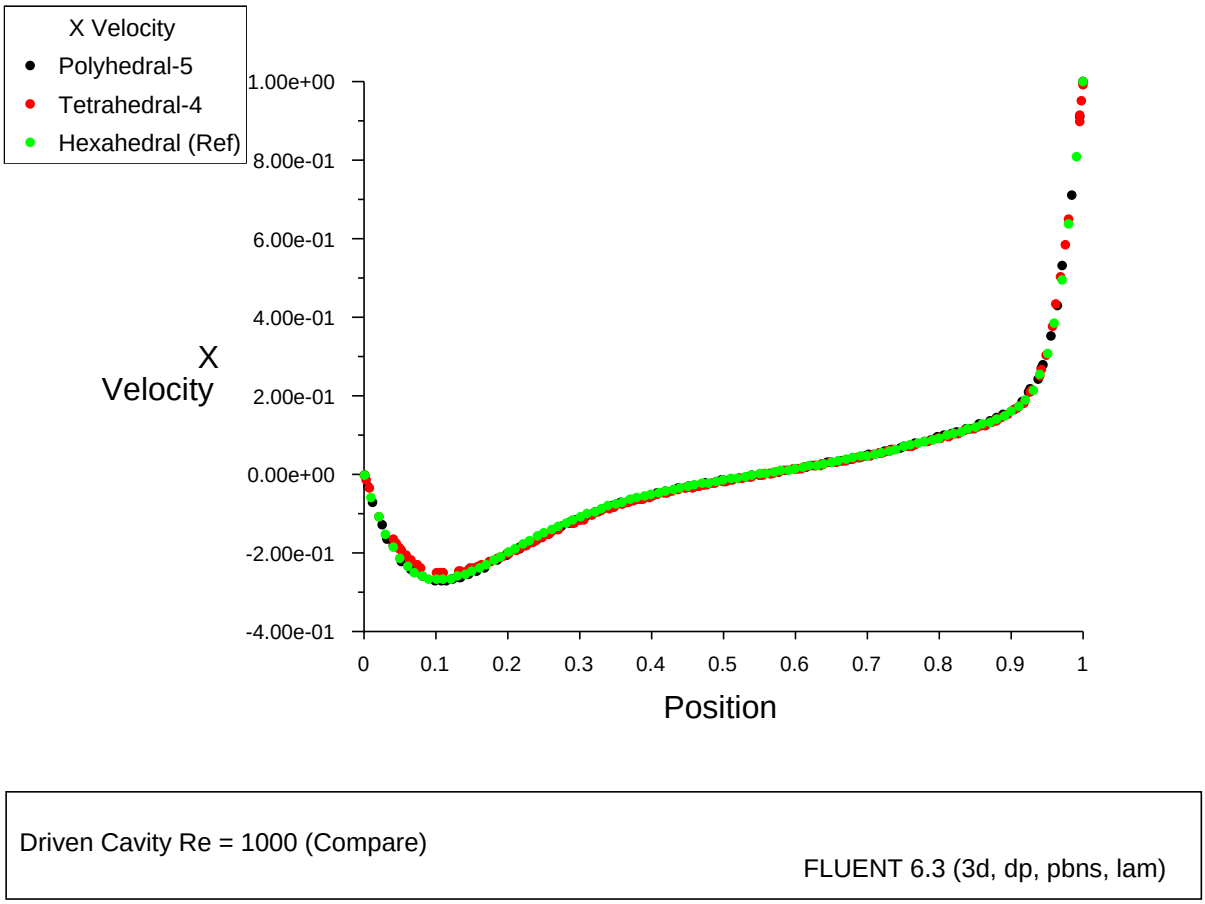

Figure 20.4.3: Comparison of Velocity Distributions by Mesh Type

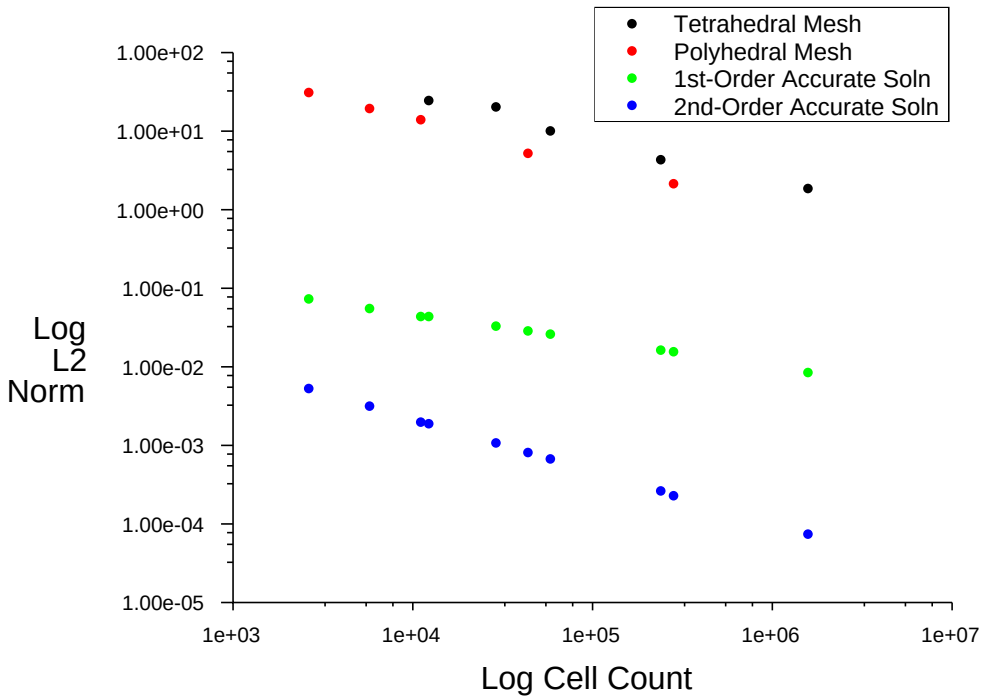

Driven Cavity Re = 1000 (Accuracy Comparison)

FLUENT 6.3 (3d, dp, pbns, lam)

Figure 20.4.4: Accuracy Comparison

© Fluent Inc. August 8, 2006